Contribution to the modelisation and failure prognosis in a synchrone permanent magnet motor

Riham Ginzarly

Normandie Université

THÈSE

Pour obtenir le diplôme de doctorat

Spécialité Automatique et traitement du signal

Préparée au sein de l'Université de Rouen Normandie

Contribution à la modélisation et au pronostic des défaillances d'une machine synchrone à aimants permanents

Présentée et soutenue par
Riham GINZARLY

Thèse soutenue publiquement le 26/09/2019 devant le jury composé de		
M. / Farid MEIBODY-TABAR	Professeur à l'Université de Lorraine, Nancy	Rapporteur
M. / Mohand DJEZIRI	MCF-HDR à Aix-Marseille Université, Marseille	Rapporteur
M. / Paul HONEINE	Professeur à l'Université de Rouen, Rouen	Examinateur
Mme / Khadija EL-KADRI BENKARA	MCF à l'Université de Technologie de Compiègne, Compiègne	Examinatrice
M. / Nazih MOUBAYED	Professeur à l'Université Libanaise, Tripoli, Liban	Codirecteur de thèse
M. / Ghaleb HOBLOS	EC-HDR à l'ESIGELEC, Rouen	Directeur de thèse

Thèse dirigée par M. Ghaleb HOBLOS, laboratoire IRSEEM
et codirigée par M. Nazih MOUBAYED, laboratoire CRSI

UNIVERSITÉ DE ROUEN NORMANDIE

MIIS

irseem

My trust in God never fails…

Acknowledgements

Dreams always come true with God blessings, hardworking, support of beloved ones and good people.

I express my sincere gratitude to my dear supervisors Dr Ghaleb Hoblos and Dr Nazih Moubayed; your guidance and support was always there for me. You are the godfather of this achievement.

Dad, Mum, my sister and brothers, you are my backbone. You were always there to care, love and support.

My beloved husband, no words can express my appreciation for you being always by my side and believing in me. My lovely daughter who always complains that I care about the laptop more than anything else, I adore you my sweetheart.

I would like to thank also Ghina Hassan, a hard worker and fresh engineer for her help in the inverter modeling and closed loop system; and, Dr Saadallah Halimi for his interest and help.

Because of you all, this report is completed and a bright phase of my life manifest.

Abstract

Due to the accelerating pace of environmental concerns and fear from conventional source of energy depletion, researches are working on finding renewable energy sources of power for different axes of life. Transportation sector intervenes in this field and introduces hybrid electric vehicles. Many complains had been mentioned concerning the fault detection and identification in the vehicle to ensure its safety, reliability and availability. Diagnosis couldn't overcome all those concerns, researches shift toward prognosis where the manufacturing sector is urged to integrate fault prognosis in the vehicle's electrical powertrain.

In this thesis, prognosis of the vehicle's electrical machine is treated using Hidden Markov Model after modeling the electrical machine using finite element method. Permanent magnet machines are preferable in this application. The modeling of the machine is a combination of electromagnetic, thermal and vibration finite element model. The considered faults are demagnetization, turn to turn short circuit and eccentricity.

Keywords – hybrid electric vehicle, electrical machine, permanent magnet machine, finite element model, prognosis, hidden Markov model, remaining useful life, demagnetization, turn to turn short circuit, eccentricity.

Table of Contents

Acknowledgements 5
Abstract 7
Table of Contents 9
List of figures 13
List of tables 19
List of publications 21
Abbreviations 23
Symbols 25
General Introduction 27
Chapter 1: Literature review 31
1.1 Introduction 31
1.2 Hybrid electric vehicles (HEV) 31
1.3 Electrical machines used in HEVs 34
1.3.1 Types of electrical machines used in HEV 34
1.3.2 The importance of electrical machine prognosis in HEVs 36
1.3.3 Permanent magnet machine 37
1.4 Faults in electric machine 39
1.4.1 Different type of faults in electrical machines 39
1.4.2 Useful monitored parameters for fault detection 40
1.4.3 Fault severity in permanent magnet machine 44
1.5 Prognosis 45
1.5.1 Prognostic strategy and condition base monitoring 45
1.5.2 Prognostic methods 47
1.5.3 Prognostic techniques 48
1.5.4 Prognosis in Hybrid electric vehicles and its electric machine 59
1.6 Finite Element Method and electrical machine 61
1.7 Conclusion 61

Chapter 2: Finite element model 63
2.1 Introduction 63
2.2 Electromagnetic FEM 63
2.2.1 Static current fed model 66
2.2.2 Static voltage fed model 70
2.2.3 Dynamic Time Stepping FEM 72
2.3 Thermal finite element model 75
2.3.1 Thermal model equations and specification 77
2.3.2 Thermal model outcomes (Steady state analysis) 79
2.3.3 Thermal model outcomes (Transient analysis) 80
2.4 Vibration finite element model 83
2.5 Integration of faults in FEM 87
2.5.1 Demagnetization fault 88
2.5.2 Turn to turn short circuit fault 91
2.5.3 Eccentricity 94
2.6 Analytical analysis versus finite element Analysis 97
2.7 Conclusion 98
Chapter 3: Dynamic variable aspect for fault identification and detection 101
3.1 Introduction 101
3.2 Classical signal parameters and features 101
3.2.1 Statistical parameters 101
3.2.2 Spectral characteristics 104
3.3 Identify useful measured parameters for fault identification 104
3.3.1 Outcome of electromagnetic FEM 104
3.3.2 Outcomes of Thermal FEM model 110
3.3.3 Outcomes of Vibration FEM model 125
3.4 Priority between parameters' indicators for fault detection and localization 139
3.5 Signature table for fault detection and localization 140
3.6 Conclusion 141
Chapter 4: Prognostic Approach-Hidden Markov Model (HMM) 143

4.1 Introduction 143
4.2 Hidden Markov Model (HMM) 143
4.2.1 HMM strategy 143
4.2.2 HMM: technical concept and model formulation 144
4.2.3 The HMM of our application 150
4.3 Remaining useful life (RUL) 156
4.3.1 Aging of PMM's components 157
4.3.2 Estimation strategy of RUL calculation using thermal FEM in the case of turn to turn short circuit 166
4.3.3 Estimation strategy of RUL calculation in the case of crack in the magnet 168
4.5 Conclusion 176
Chapter 5: Closed loop system analysis 177
5.1 Introduction 177
5.2 The inverter modeling 177
5.2.1 HEV's main power electronics elements 178
5.2.2 Power Inverter Modeling 179
5.2.3 Switched state-space model and equations 180
5.2.4 Inverter Design Parameters 182
5.2.5 Generation of control systems 182
5.3 Fault interaction between the inverter and the electric machine 184
5.3.1 Faults in the inverter 184
5.3.2 Threshold value of the inverter 187
5.3.3 Impact of machine performance on VSI 189
5.3.4 Impact of VSI's faults on PMM 193
5.4 Vector control for the PMSM 198
5.5 Features extracted from closed loop system data sets 204
5.6 Impact of closed loop system on the prognostic model 211
5.7 Conclusion 215
General conclusion 217
Appendix A: DIFFERENCE BETWEEN RTD AND THERMOCOUPLE SENSOR 219

Reference.. 221

List of figures

Figure 1: Components of a hybrid electric car 32
Figure 2: The components of series HEV architecture 33
Figure 3: The components of parallel HEV architecture 34
Figure 4: Surface mounted permanent magnet topology 38
Figure 5: Interior permanent magnet topology 38
Figure 6: Measured parameters versus failures 42
Figure 7: prognostic strategy 47
Figure 8: Prognostic methods and techniques 49
Figure 9: Laminated sheet of SPMM 65
Figure 10: Two poles section of the SPMM's laminated sheet 65
Figure 11: Sub-domain or finite element 66
Figure 12: Current fed FEM 67
Figure 13: Flow of flux lines in the machine with zero current in the phases 69
Figure 14: SPMM's air gap flux density with zero current in the phases 69
Figure 15: SPMM's air gap flux density coming from stator contribution only 69
Figure 16: Flux lines (stator contribution) 69
Figure 17: Distribution of total flux density inside the machine in Tesla 70
Figure 18: : Total flux lines in the SPMM 70
Figure 19: Total air gap flux density of the SPMM 70
Figure 20: Voltage fed FEM 71
Figure 21: Air gap flux density (Voltage fed model) 72
Figure 22: Flux lines (Voltage fed model) 72
Figure 23: Block diagram of Time Stepping FEM 73
Figure 24: : Flux lines at 4 different moments during the rotation from 0 to 30 degree (Healthy machine) 75
Figure 25: Block diagram of the thermal steady state analysis 78
Figure 26: Block diagram of the thermal transient analysis 78
Figure 27: Distribution of temperature in the healthy PMM at Steady state 79
Figure 28: Temperature along radial line 80
Figure 29: Distribution of temperature in the laminated sheet at t= 5000, 10000, 15000 and 20000 seconds 81
Figure 30: Distribution of temperature in the laminated sheet at t=25000 81
Figure 31: : Transient temperature on the top edge of the magnet 82
Figure 32: Variation of temperature function of time in the first slot 82
Figure 33: Transient temperature on the outer boundary of the Permanent magnet machine 83
Figure 34: Stator's iron part of the laminated sheet 86
Figure 35: Distribution of electromagnetic forces in the air gap 86
Figure 36: Zoom figure 35 86
Figure 37: Vibration on the periphery of the SPMM 87
Figure 38: : Stator's displacement in mm (Healthy machine) 87
Figure 39: Crack in the magnet of pole 1 89
Figure 40: Flux focusing due to the crack 89

Figure 41: Air gap flux density for 1 and 3 mm crack 89
Figure 42: Distribution of temperature (°C) in the machine (Healthy case) 90
Figure 43: Distribution of temperature (°C) in the machine (in the case of crack) 90
Figure 44: Vibration of the machine's stator in mm (in the case of crack) 91
Figure 45: flow of flux lines in the machine with one turn short circuited 93
Figure 46: air gap flux density with one turn short circuited 93
Figure 47: distribution of flux density inside the machine with one turn short circuited 93
Figure 48: Distribution of temperature (°C) in the machine (in the case of short circuit turn in one slot) . 94
Figure 49: Vibration of the machine's stator in mm (in the case of short circuit turn in one slot) 94
Figure 50: flux lines in the machine with 10% eccentricity fault 95
Figure 51: air gap flux density with 10% eccentricity fault 95
Figure 52: distribution of flux density inside the machine with 10% eccentricity fault 96
Figure 53: Distribution of temperature (°C) in the machine (in the case of 10% eccentricity fault) 96
Figure 54: Vibration of the machine's stator in mm (in the case of 10% eccentricity fault) 97
Figure 55: Air gap flux density using FEM and Analytical method 98
Figure 56: air gap flux density with 1 mm crack in the magnet of the first pole 98
Figure 57: FEM's outcomes 99
Figure 58: Air Gap Flux Density in time domain (Healthy machine) 106
Figure 59: Air Gap Flux Density in time domain (Machine with 1 mm crack) 106
Figure 60: Air Gap Flux Density in time domain (Machine with 10 % eccentricity fault) 106
Figure 61: Air Gap Flux Density in time domain (Machine with turn to turn short circuit fault) 106
Figure 62: Torque versus time for the different states of the machine 107
Figure 63: Spectral power density of the torque 109
Figure 64: Fourier transformation of torque 110
Figure 65: laminated sheet of the PMM with turn to turn fault integrated 111
Figure 66: Equivalent circuit of turn to turn short circuit at phase A 112
Figure 67: Distribution of temperature in the machine when a turn to turn short circuit occur in slot 1.. 112
Figure 68: Boundary temperature in healthy case 113
Figure 69: : Boundary temperature with turn to turn fault in the first slot (Phase A) 113
Figure 70: Location of temperature sensor 114
Figure 71: Sensor temperature for healthy machine and machine with turn to turn short circuit in slot 1115
Figure 72: Sensor temperature for healthy machine and machine with turn to turn short circuit in slot 1115
Figure 73: Sensor temperature for turn to turn short circuit in each slot 116
Figure 74: Zoom of figure 73 116
Figure 75: Sensor temperature for 1 mm crack in one magnet a time 116
Figure 76: Sensor temperature for machine with 10 % eccentricity faults 117
Figure 77: Sensor temperature for healthy machine, machine with eccentricity fault and machine with crack in the magnet 117
Figure 78: Peak to peak values of temperature data sets 118
Figure 79: Mean values of temperature data sets 118
Figure 80: RMS values of temperature data sets 119
Figure 81: Kurtosis values of temperature data sets 119
Figure 82: Skewness values of temperature data sets 119
Figure 83: Shape factor values of temperature data sets 119

Figure 84: Pulse factor values of temperature data sets 119
Figure 85: Crest factor values of temperature data sets 119
Figure 86: Standard deviation values of temperature data sets 120
Figure 87: Variance values of temperature data sets 120
Figure 88: Spectral power density of temperature data sets (zoomed view on the right) 123
Figure 89: Fourier transformation of the collected temperature data for all the machine states 124
Figure 90: Zoom of figure 89 125
Figure 91: Vibration at machine's periphery in Healthy and demagnetization case 126
Figure 92: Vibration at machine's periphery in Healthy and eccentricity case 127
Figure 93: Vibration at machine's periphery in Healthy and turn to turn short circuit case 127
Figure 94: Vibration in time domain, Healthy machine 128
Figure 95: : Zoom figure 94 128
Figure 96: Vibration in time domain, Machine with eccentricity fault 129
Figure 97: Zoom figure 95 129
Figure 98: Vibration in time domain, Machine with demagnetization fault 129
Figure 99: Zoom figure 98 130
Figure 100: Vibration in time domain, machine with turn to turn short circuit in one slot 130
Figure 101: Zoom figure 100 131
Figure 102: Vibration in time domain when a crack is integrated in one of the machine's magnet 131
Figure 103: Vibration for the case of turn to turn short circuit in slot 1, 4 and 7 132
Figure 104: Zoomed view of figure 103 132
Figure 105: Peak to peak values of vibration data sets 133
Figure 106: Mean values of vibration data sets 133
Figure 107: RMS values of vibration data sets 133
Figure 108: Kurtosis values of vibration data sets 133
Figure 109: Skewness values of vibration data sets 134
Figure 110: Shape factor values of vibration data sets 134
Figure 111: Pulse factor values of vibration data sets 134
Figure 112: Crest values of vibration data sets 134
Figure 113: Standard deviation values of vibration data sets 134
Figure 114: Variance values of vibration data sets 134
Figure 115: Spectral power density of vibration in case of healthy machine and machine with eccentricity fault (zoomed view on the right) 137
Figure 116: Spectral power density of vibration in case of healthy machine and machine with crack in one magnet (zoomed view on the right) 137
Figure 117: Spectral power density of vibration in case of healthy machine and machine with turn to turn short circuit (zoomed view on the right) 138
Figure 118: Fourier transformation of vibration (zoomed view on the right) 139
Figure 119: the prognostic strategy 144
Figure 120: Trellis Diagram 146
Figure 121: Viterbi diagram 149
Figure 122: Block diagram combining HMM, Viterbi algorithm, observations and states 150
Figure 123: Trellis diagram example 151
Figure 124: Multi level trellis diagram 153

Figure 125: Example of Viterbi algorithm..... 156
Figure 126: Aging graph of windings insulation..... 159
Figure 127: % Br versus operating hours 161
Figure 128: magnet's flux loss versus time at different temperatures 162
Figure 129: Distribution of flux density in the machine after 1 year, 5 years, 10 years and 14 years of aging 163
Figure 130: The change in air gap flux density with magnet aging (100 °C) 164
Figure 131: The change in air gap flux density with magnet aging (150 °C) 164
Figure 132: Torque with magnet aging at 100 and 150 degree of operation 166
Figure 133: RUL calculation in the case of turn to turn short circuit 167
Figure 134: Illustrative example for RUL calculation..... 168
Figure 135: Meshed laminated sheet with 4 mm crack in the magnet 173
Figure 136: Air gap flux density in the case of 4 mm crack in the magnet 173
Figure 137: Vibration detected by the sensor in the case of 4 mm crack in the magnet 174
Figure 138: RUL calculation in the case of demagnetization fault 174
Figure 139: illustrative example of RUL calculation in the case of demagnetization..... 175
Figure 140: Global block diagram of the prognostic approach..... 176
Figure 141: Main electric power train architecture for HEV [117]..... 178
Figure 142: Standard two level three phase voltage source inverter..... 179
Figure 143: schematic of the power inverter 180
Figure 144: SVPWM conduction mode: electrical measurements..... 182
Figure 145: SVPWM conduction mode: normalized harmonics of output voltage 183
Figure 146: Rates of possible failures in power electronics of the inverter..... 184
Figure 147: Typical power electronics package structure 185
Figure 148: Lifetime of IGBT versus junction temperature 191
Figure 149: electrical measurements and harmonic spectrum of output voltage during IGBT1 short-circuit faulty..... 194
Figure 150: Electrical measurements when IGBT1 open-circuit (left) and IGBT2 open circuit (right) . 195
Figure 151: harmonic spectrum of output voltage in single open circuit fault 195
Figure 152: Electrical measurements in open leg faulty..... 197
Figure 153: Direct torque control for PMSM 199
Figure 154: Block diagram of DTC strategy 200
Figure 155: Block diagram of closed loop combined model 201
Figure 156: ΔTorque in case of 1 mm crack (Open and Closed loop) 202
Figure 157: ΔDisplacement in case of 1 mm crack (Open and Closed loop) 202
Figure 158: ΔTemperature in case of 1 mm crack (Open and Closed loop)..... 203
Figure 159: Instantaneous current in phase A in case of 1 mm crack (Open and Closed loop)..... 203
Figure 160: The high envelope of the signals in figure 159 204
Figure 161: Torque of closed loop system of healthy machine and machine with 1 mm crack 205
Figure 162: Temperature of closed loop system of healthy machine and machine with 1 mm crack (Zoom in at the right)..... 205
Figure 163: Vibration of closed loop system of healthy machine and machine with 1 mm crack (Zoom in at the right)..... 206
Figure 164: Torque spectral power density, closed loop, of healthy machine and machine with 1 mm crack 207

Figure 165: Temperature spectral power density, closed loop, of healthy machine and machine with 1 mm crack 207
Figure 166: Vibration spectral power density, closed loop, of healthy machine and machine with 1 mm crack 208
Figure 167: Fourier transformation of torque, Closed loop system 209
Figure 168: Fourier transformation of temperature, Closed loop system 209
Figure 169: Fourier transformation of temperature, Closed loop system 210
Figure 170: Viterbi algorithm for the open loop system 213
Figure 171: Viterbi algorithm for the closed loop system 214
Figure 172: Diagram illustrating the prognostic approach in the case of closed loop system with 1 mm crack in one magnet 214

List of tables

TABLE 1: : HYBRID CLASSIFICATION [17] 31
TABLE 2: PERCENTAGE OF FAULT OCCURRENCE 42
TABLE 3: SOME THRESHOLD VALUES OF MEASURED PARAMETERS 43
TABLE 4: CLASSIFICATION OF FAULTY COMPONENTS 45
TABLE 5: : DESCRIPTION OF PROGNOSTIC APPROACHES 49
TABLE 6: : MACHINE'S SPECIFICATIONS AND PARAMETERS 63
TABLE 7: PHYSICAL AND THERMAL CHARACTERISTICS OF MACHINE'S MATERIAL 79
TABLE 8: MATERIAL CHARACTERISTICS NEEDED FOR VIBRATION MODEL 84
TABLE 9: CURRENT VERSUS NUMBER OF SHORT CIRCUITED TURNS 92
TABLE 10: STATISTICAL FEATURES OF TORQUE SIGNAL 108
TABLE 11: AVERAGE SPECTRAL POWER DENSITY OF TORQUE 109
TABLE 12: AVERAGE TORQUE FOR THE DIFFERENT STATES OF THE MACHINE 110
TABLE 13: : AVERAGE SENSOR TEMPERATURE FOR DIFFERENT MACHINE STATE 121
TABLE 14: : AVERAGE SPECTRAL POWER DENSITY OF TEMPERATURE 124
TABLE 15: MACHINE VIBRATION FOR DIFFERENT TYPES OF FAULT 135
TABLE 16: AVERAGE SPECTRAL POWER DENSITY OF DISPLACEMENT 138
TABLE 17: : PERCENTAGE OF PARAMETER DEVIATION FOR DIFFERENT TYPES OF FAULT 139
TABLE 18: SIGNATURE TABLE FOR FAULT DETECTION AND LOCALIZATION 141
TABLE 19: PERCENTAGE OF FAULT OCCURRENCE IN THE ELECTRICAL MACHINE 154
TABLE 20: : VARIATION OF COIL'S RESISTANCE DUE TO AGING 158
TABLE 21: NDFEB TEMPERATURE RELATED PARAMETERS 160
TABLE 22: EFFECT OF MAGNET AGING ON ITS BR AND HC 161
TABLE 23: IMPACT OF MAGNET AGING ON BR AND HC WHEN THE OPERATING TEMPERATURE IS 150 CELSIUS 162
TABLE 24: IMPACT OF MAGNET AGING OVER YEARS AT TEMPERATURES 100 AND 150 CELSIUS 165
TABLE 25: SVPWM: SIMULATIONS RESULTS 183
TABLE 26: ENVIRONMENTAL CONDITIONS AND OPERATIONAL REQUIREMENTS 186
TABLE 27: MEASUREMENTS RESULTS UNDER NORMAL OPERATION 189
TABLE 28: MEASUREMENTS RESULTS WITH DEMAGNETIZATION FAULT 190
TABLE 29: MEASUREMENTS RESULTS WITH TURN TO TURN SHORT CIRCUIT FAULT 191
TABLE 30: MEASUREMENTS RESULTS UNDER ECCENTRICITY FAULT 192
TABLE 31: DEGRADATION OF TEMPERATURE AND VIBRATION FROM THE MACHINE TO THE INVERTER 192
TABLE 32: MEASUREMENTS RESULTS IN IGBT1 SHORT-CIRCUIT FAULT 194
TABLE 33: RESULTS WHEN IGBT1 OR IGBT2 IS OPEN-CIRCUITED 196
TABLE 34: MEASUREMENTS RESULTS WHEN PHASE A IS OPEN 197
TABLE 35: COMPARISON BETWEE MEASUREMENTS OF CLOSED LOOP AND OPEN LOOP SYSTEM-CASE OF CRACK IN THE MAGNET 204
TABLE 36: STATISTICAL FEATURES OF CLOSED LOOP DATA SETS 206
TABLE 37: AVERAGE SPECTRAL POWER DENSITY OF TORQUE 208

TABLE 38: COMPARISON BETWEEN THE EFFECTIVENESS OF DATA FEATURES ON FAULT DETECTION IN OPEN LOOP AND CLOSED LOOP SYSTEM 210
TABLE 39: PERCENTAGE DIFFERENCE IN MACHINE'S PARAMETERS IN THE CASE OF OPEN LOOP AND CLOSED LOOP SYSTEM 211

List of publications

Riham GINZARLY, Ghaleb HOBLOS, Nazih MOUBAYED, "Faults in Hybrid Electric Vehicles' Permanent Magnet Machines", TAEECE2015 conference, Lebanon.

Riham GINZARLY, Ghaleb HOBLOS, Nazih MOUBAYED, "Decision on Prognosis approaches of Hybrid Electric Vehicles' electrical machines", TAEECE2015 conference, Lebanon.

Riham GINZARLY, Kawthar ALAMEH, Ghaleb HOBLOS, Nazih MOUBAYED, "Numerical versus analytical techniques for healthy and faulty surface permanent magnet machine", EECEA2016 conference, Lebanon.

Kawthar, ALAMEH, **Riham GINZARLY,** Ghaleb HOBLOS, Georges BARAKAT, "Fault Detection and Identification Approach for Brushless Direct Current (DC) Motors based on Vibration Signal Analysis", 3rd Conference on Control and Fault-Tolerant Systems, Systol'16, September 7–9, 2016.

Riham GINZARLY, Ghaleb HOBLOS, Nazih MOUBAYED, "Severity faults classification in hybrid electric vehicles' permanent magnet machines for prognostic purposes", International Journal of Computer Aided Engineering and Technology, 2017.

Riham GINZARLY, Ghaleb HOBLOS, Nazih MOUBAYED, "Electromagnetic and vibration finite element model for early fault detection in permanent magnet machine", 10th IFAC Symposium on Fault Detection, Supervision and Safety of Technical Processes (SafeProcess 2018), Warsaw, Poland, August 29-31, 2018.

Riham GINZARLY, Ghaleb HOBLOS, Nazih MOUBAYED, "Localizing Turn to Turn Short Circuit in HEV's Machine Using Thermal Finite Element Model", IEEE International Multidisciplinary Conference on Engineering Technology (IMCET), 2018

Riham GINZARLY, Ghaleb HOBLOS, Nazih MOUBAYED, "Hidden Markov Model Based Failure Prognosis for Permanent Magnet Synchronous Machine", ACD European Workshop on Advanced Control and Diagnosis, 2019.

Riham GINZARLY, Ghaleb HOBLOS, Nazih MOUBAYED, **"**From Modeling to Failure Prognosis of Permanent Magnet Synchronous Machine", applied sciences journal (submitted)

Abbreviations

AC	Alternative Current
CSI	Current Source Inverter
DC	Direct Current
DTC	Direct Torque Control
FOC	Field Oriented Control
HEV	Hybrid Electric Vehicle
IGBT	Insulated Gate Bipolar Transistor
IPMM	Interior Permanent Magnet Machine
KCL	Kirchhoff's Current Law
KVL	Kirchhoff's Voltage Law
OC	Open Circuit
PMSM	Permanent Magnet Synchronous Machine
PF	Power Factor
RTG	Resistance To Ground
RMS	Root Mean Square
SC	Short Circuit
SPMM	Surface Permanent Magnet Machine
SPWM	Sinusoidal Pulse Width Modulation
SVM	Space Vector Modulation
SVPWM	Space Vector Pulse Width Modulation
THD	Total Harmonic Distortion
VSI	Voltage Source Inverter
Ctt	Circuit
PM	Permanent Magnet
HMM	Hidden Markov Model
CM	Condition Monitoring
NdFeB	Neodymium Iron Boron
RUL	Remaining Useful life
TM	Transition Matrix
EM	Emission Matrix
OFD	Offline Database
CB	Circuit Breaker
PP	Peak to peak
RMS	Root mean square
Ku	Kurtosis
Sk	Skewness
SF	Shape factor
PF	Pulse factor
CF	Crest factor

SD	Standard deviation
V	Variance
APS	Average power spectral
AFC	Amplitude of frequency component

Symbols

Br	Remanence Flux Density
Hc	Coercive Force
Tc	Curie Temperature
T˚C	Temperature in Celsius
w	Angular frequency
σ	electrical conductivity
Θ	Angle depending on the sense of magnetization of the magnet
v	Reluctivity
A	Vector Potential
{Ic}	The circuit current vector
{Es}	The bar voltage vector
[D]	The bar connection matrix
[Ωb]	The bar cross sectional area diagonal matrix
[zext]	The circuit external impedance diagonal matrix
{vs}	The circuit voltage vector
Vb	Voltage across rotor's bar (the equivalent of the magnets)
l	Axial length of the machine
V	Linear rotor's speed
t	Time
I	Current in each conductor
Vc	Voltage across series coils (stator's coil)
db	Diagonal matrix with entries of + 1 or -1, indicating the polarity of each bar in the coil
Lext	Coils' equivalent inductance
Rext	Coils 'equivalent resistance
Rs	Series conductor's equivalent resistance
Ls	parallel conductor's equivalent inductance
m	Rotor's mass
x	Rotor's position
λ	Damping factor (in synchronous machine this value is almost zero)
Fem	Electromagnetic force
Fext	Externally-applied mechanical force (load).
ρ	Material density, kg/m^3
Cp	The specific heat, J/kg.K
tz	The thickness model
k	Thermal conductivity, W/m.K
Qd	Heat source, $watt/m^2$
Ta	Ambient temperature
hc	Convection coefficient, $W/m^2.K$
ϵ	Emissivity of the face
σ	Stefan-Boltzmann constant, W/m^2K^4
[M]	Mass matrix

[C]	Damping matrix
[K]	Stiffness matrix
Te	Tension
G	Modulus of elasticity
R0	Initial value of the resistor in ohms
ΔR	Increase in resistance of the resistor operating at temperature T for a time t, in ohms.
EOLselected	End of life selected
a	Depth of the crack
W	The radial length of the magnet
J	Average current density
Ki	Parameter describing current dependency of switching losses
Kf	Slot's filling factor
Kv	Parameter describing voltage dependency of switching losses
L	Filter inductor
m	Modulation index
mr	Modulation ratio
R	Resistive load
Rl	ESR of filter inductor
RON	Switch internal resistance
RCE	IGBT on-state resistance
RF	Diode on-state resistance
S	Heat transfer area
{T0, Ta, Tb}	Dwell time
Ts	Sampling period
{VA, VB, VC}	Three phase voltages at load level
{Van, Vbn, Vcn}	Three phase voltages at inverter level
{Sa, Sb, Sc}	Inverter switching signal
{VT1 to VT6}	Collector-emitter voltages of the six IGBTs
Vdc	DC link voltage
VCE0	IGBT threshold voltage of the on-state characteristics
VF0	Diode threshold voltage of the on-state characteristics
Vib	Vibration value
Vref	Reference DC voltage, to which switching losses in datasheet correlate
Ws	Actual stator flux amplitude
Ws_ref	Reference stator flux amplitude
Ys	Rotor position

General Introduction

Taking a look on the history of automobile, the concept has started in 1769 where the first steam powered automobile for passenger transportation had been created by Nicolas-Joseph Cugnot. In 1808, Francois Isaac de Rivaz introduces the first automobile driven by an internal combustion engine fueled by hydrogen. As the extraction of fuel increases worldwide, the gasoline powered combustion engine had been produced; this innovation was manifested by Siegfried Marcus in 1870. Excessive work and research had been conducted by Marcus for over 15 years; he introduced the two and four cycle combustion engine. His work is the main influencer of the nowadays conventional cars. He is the one who introduced steering, clutch and brake to the automobile structure. After that, Nicolaus Otto invented the four stroke gasoline combustion engine and Rudolf Diesel invented the four stroke diesel engine [1].

In 1838, renewal concepts start to strike the automotive industrial field where hydrogen fuel cell was developed by Christian Friedrich Schonbein and in 1859 the lead acid battery was introduced by Anyos Jedic as source of power for vehicles [2].

Although chemical and electric sources of power were introduced for automobile application, combustion engine remained the first choice to empower cars. In 1885, Benz started its first production. In 1913, Ford started its mass production [3].

Nowadays, automobile transportation is in a crisis due to the high price of gasoline. In the future, the crises will worsen unprecedentedly. The supply of oil will diminish widely. Moreover, the dilemma of the environment arises, where the need to reduce emissions has become a must. Climate change has turned out to be a very powerful motivator for researches to head toward energy efficiency and emission reduction goals.
According to the yearly consumption of oil and gas, studies state that oil will run out in 2052 and gas will run out in 2060 [1].

The environmental factor makes the need to reduce emissions of greenhouse gases (GHGs), mainly carbon dioxide (CO2), a necessity. The Intergovernmental Panel on Climate Change (IPCC) assesses that CO2 emissions should be reduced up to 85% by 2050 in order to limit global temperature rise to less than 2.4 C□ [2].
Accordingly, the only envisaged solution is to switch to green energy.

In the field of transportation, electric vehicles (EV) and Hybrid Electric Vehicles (HEV) are a good alternative for conventional vehicles. however, HEVs earned a highest popularity over EVs due to their problems linked to their battery capacity, reliability and lifecycle. This is why, the idea of combining conventional technology with environmental friendly technology is more salable.

HEVs are becoming widely spread due to the predicted lack of fuel in addition to the pollution caused by the conventional vehicles. To overcome pollution and since it is expected that the lack of fuel will increase, it is assessed that the production and use of HEVs will increase in the coming years and divert the situation [3].

The invention of HEV firstly started in 1901 with Porsche. However, it didn't became widely spread and used until 1997 where Toyota launched its first HEV. After that, in 1999, Honda commenced its HEV production [4].

HEVs on the market span from micro, mild, to full hybrid. A micro hybrid has a very small machine compared to the gasoline engine. A mild hybrid has a Machine with power about 15%–25% the power of the engine. A full hybrid has a Machine with power about 40%–50% the power of the engine. Mild hybrids are the most popular due to their low price in comparison to the conventional vehicles [5] [6].

The main concern of HEVs is their reliability and availability; hence, assuring the health and proper operation of HEVs is a mission.
HEV contains many components; one of them is the electrical machine. Any type of electrical machine can be used in HEVs. However, the most used in the industry are induction machine and permanent magnet machine. Permanent Magnet Machine (PMM) is always preferable; due to its high power density and efficiency, robust construction and low weight [7] [8].
Many researches had focused on the diagnosis of the different elements in the HEV, the evolution in the field drives us to the prognosis, to predict the fault before it occurs. The aim of this thesis is to apply prognosis on HEV's electrical machine to ensure its proper health and operation.
To figure out the importance of electrical machine prognosis in a hybrid electric vehicle over other components, researchers are going to examine the relative cost of the electrical machine with respect to the cost of the whole system.

Most manufactured HEVs are mild-hybrid vehicle having the parallel topology using permanent magnet or induction machine where the electric Machine has 15%–25% of the engine power. In general, the power rating of the electrical machine in a mid-size HEV is between 10KW and 20KW. Examining the cost of electric Machines in $/KW leads us to the fact that the cost of permanent magnet machine is 15% higher than the cost of induction machine. Moreover, when a permanent magnet machine is used in the hybrid electric vehicle, the cost of the electrical machine is 30% that of the overall traction system in the vehicle [9] [10].
Executing prognostic analysis and studies for electric machines in HEVs are very important and justified, knowing their high cost with respect to the cost of the whole system.

Prognosis will help in predicting the coming fault before the relative component fails. It will also help in regulating the maintenance schedule and in predicting the remaining useful life of the machine.
In all cases, prognostic studies are very beneficial in saving money.

Author in [15] states that, in HEV application, a forward-looking diagnosis and prognosis technologies are required to promptly sense and isolate faults in network-embedded automotive systems so that proactive corrective maintenance actions can be taken to evade failures and increase the availability of the vehicle.
Due to the importance of electrical machines health state in HEVs, a survey will be presented on the available prognostic techniques that may be applied to assure an optimal and convenient operation of electrical machines in hybrid electric vehicle.

A decision on the best prognostic technique to be applied is elaborated. It has been agreed to adopt Hidden Markov Model (HMM). Hidden Markov Model is a Data-driven prognostic approach since it efforts to derive models directly from collected Condition Monitoring (CM) data; they get predictive output directly in terms of CM data. It's a stochastic signal model [11].

To decide the types of fault that need to be detected in the permanent magnet machine a review of the litterature on the different types of fault that may occur in the electrical machine is elaborated and the useful parameters that should be examined and measured to detect the presence of each type of fault are illustrated.
The faults are classified according to their level of severity; a case study is conducted where it is shown that demagnetization of magnet is the most sever fault; taking into consideration the relative cost of magnet and the percentage occurrence of demagnetization. The other types of faults that will be encountered are: turn to turn short circuit and eccentricity [12].

An experimental prototype containing the permanent magnet machine where faults are easily integrated and measured data are progressively collected is not available. Hence, the need for an accurate machine model arises. Electromagnetic, thermal and vibration finite element model is built at normal operation of the machine, and when different types of faults are integrated. The measured collected data will be torque, temperature and vibration also at normal operation and in the case of fault. This data will be inputs of the HMM.

A strategy will be developed to detect the presence of fault at its early stage. The remaining useful life of the relevant machine's components will be calculated accordingly and a prognostic decision will be elaborated.

Chapter one will present a general literature review on hybrid electric vehicles (HEV), the electrical machines used in HEVs, the different types of electrical machine used in such application and the most preferable type of electrical machine. Then, the different type of faults that may occur in those electrical machines will be presented, the useful monitoring parameters that are useful for those different types of faults will be identified and a fault severity index for PMM will be formulated. Moreover, a survey will enumerate all the prognostic techniques that can be applied on this application after a briefing on prognostic strategy and condition monitoring concept.

In chapter two, the Electromagnetic, thermal and vibration finite element model of the permanent magnet machine will be presented. The electromagnetic FEM will encounter static current fed, static voltage fed and dynamic time stepping FEM. The output of the electromagnetic model is vector potential that will be used to generate air gap flux density and torque. The steady state and transient thermal FEM will be generated. The outcome of the thermal model is the distribution of temperature in the whole machine. The outcome of the vibration FEM is the displacement of the machine. The model will be investigated at normal operation and when a fault is integrated. The considered types of faults are: demagnetization, turn to turn short circuit and eccentricity.
A confrontation between analytical and numerical method for electromagnetic machine modeling will be demonstrated.

Chapter three will emphasis fault indicators where useful measured parameters for fault identification will be identified and useful features from the measured parameters will be extracted.

Torque, temperature and vibration signal will be elaborated for the healthy and faulty states of the machine. Priority between parameters as indicators for fault detection and localization will be highlighted. At this stage, we will discuss sensor selection and localization.

In chapter four, the strategy of the adopted prognostic approach which is HMM will be explained. The technical aspect of the method will be presented and the prognostic model will be formulated. HMM will be applied to detect and localize small scale faults where a systematic strategy is developed. The aging of machine's equipment, specially the sensitive ones that are the stator's coil and the permanent magnet, is a very important matter for RUL calculation.
An estimation strategy for remaining useful life (RUL) calculation will be presented and discussed for those mentioned machine's components.

Till chapter four, the system in an open loop configuration where the considered electric source is a pure sinusoidal three phase supply. Closed loop configuration is very important, it is adopted by all available vehicle systems. Hence, such configuration will be built for our model where the input of the machine's FEM will come from the modeled inverter. This will be illustrated in chapter five and six.

In chapter five a model of the inverter will be elaborated. A brief on the main HEV's power electronic elements, power inverter modeling, switched state space model and governing equation, inverter design parameters and signal generation will be presented. Fault interaction between the inverter and the machine is an important matter in the HEV; this will be encountered in this chapter after enumerating the faults that may occur in the inverter and their relevant threshold parameter values. After that, the direct oriented closed loop control system for the SPMM will be presented; the impact of this closed loop system on the machine's dynamic parameters (torque, temperature and vibration) will be approached, the influence of this closed loop on the prognostic model will be offered.

To sum up, this thesis will bring several innovative contributions. First, the developed interactive electromagnetic, thermal and dynamic finite element model for permanent magnet machine used in hybrid electric vehicle. Second, the developed data base signal that will be the input of the prognostic model. Third, the prognostic Hidden Markov Model where the remaining useful life of the machine in the case of fault will be calculated, for open and closed loop system. Fourth, the model coupling the inverter and the electric machine where fault interaction between those two main elements will be discussed and examined in the electromagnetic, thermal and vibration field.

Chapter 1: Literature review

1.1 Introduction

In this chapter we will present a general literature review on hybrid electric vehicles, types of electric machine used in this application and types of fault that may occur in the machine. An approach to classify machine's faults in terms of severity is conducted. A survey on the available prognostic techniques that may be used for an electric machine is demonstrated. A general view on the hierarchy strategy of prognosis is illustrated.

1.2 Hybrid electric vehicles (HEV)

Hybrid Electrical Vehicle (HEV) is a combination between the conventional internal combustion system and an electric propulsion system.
Hybrids on the market span from micro, mild, to full hybridness. Micro hybrid has a small motor compared to the gasoline engine. Mild hybrid has a motor with power about 15%–25% that of the engine. Full hybrid has a motor with power about 40%–50% the power of the engine. [16]

TABLE 1: : HYBRID CLASSIFICATION [17]

	Power rating (KW)	**Voltage level (V)**	**Energy saving (%)**	**Price rise (%)**
Micro-Hybrid	2.5	12	5-10	3
Mild-Hybrid	10-20	100-200	20-30	20-30
Full-Hybrid	30-50	200-300	30-50	30-40

Mild hybrids are the most popular due to its low price compared with the conventional vehicles.
Hybrid vehicles can also be divided into diesel/electric and gasoline/electric HEVs. Diesel/electric vehicle is better fuel economy and reduces emissions more than gasoline/electric vehicle. But, the diesel engine is more expensive. Plus, its torque is usually high at fewer revolutions per minute (rpm), which does not match the motor torque as well as a gasoline engine does. This leads that the electric part of the diesel/electrical vehicle is more expensive also.
Making the diesel/electrical vehicles affordable is an important goal for many researches.

The components that deliver torque from the engine to the drive wheels is called "Powertrain". Powertrain is the torque converter (automatic transmissions), transmission, driveshaft, differential, and axle shafts.
In earlier times, automatic transmissions have been inferior to manual transmissions regarding their efficiency.

Nowadays, automatic transmissions compete manual transmissions due to the increase in the range of speeds. Most automatic vehicles have six speed. Some luxury ones offer eight speed; accordingly, the number of manual transmissions decreased from 23% in 1975 to only 8% in 2006. [16]

The electric vehicle has an electric motor/generator which allows regenerative braking for an EV. Regenerative braking returns a portion of the kinetic energy of HEV motion to charge the battery.

A typical hybrid-electric vehicle propulsion system consists of:

- an internal combustion engine (ICE)
- one or more electrical energy carriers (e.g. batteries, super-capacitors)
- Electric machines
- Power electronics
- Control system
- Transmission and various driveline linkages

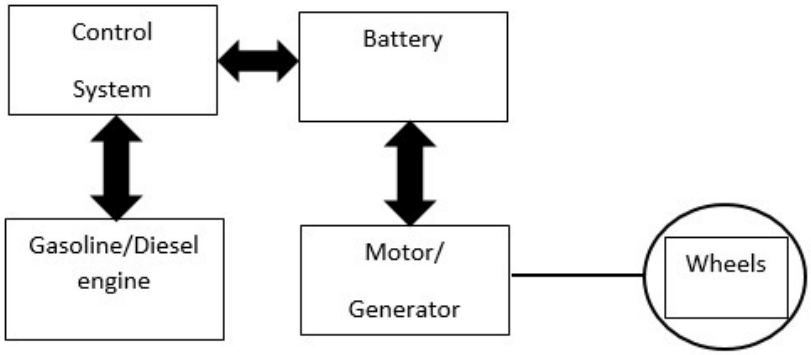

Figure 1: Components of a hybrid electric car

There are several ways to combine these elements. The general main categories of these combinations are[18] [19]:

Series Hybrids: in the series configuration, the HEV has only two shafts that are not connected. Hence, the engine can run at an optimum rpm and regulate its settings to enssure minimum fuel consumption and minimum emissions. The engine and generator can be located anywhere. The tractive power is supplied directly by one or more electric machines, hence, transmission is not needed. The electric generator drives the engine in an efficient operating region to charge the electrical energy storage system also. The capacity of the generator plus the battery maximum power and the power of the M/G machine must be equal the total power of the HEV.
Note that the battery deliver DC electrical current while the electrical machine usually deliver AC electrical current. The direction of the current flow changes as the operating mode changes

between accelerating mode, normal operating mode, battery charging mode and regenerative braking mode. The power electronics converts back and forth between DC and AC [20].
One disadvantage of the series HEV is its relative high weight.
Operating modes:

- At accelerating mode, the battery and the generator tend to supply power.
- At normal operating mode, the power is extracted from the engine only. The engine can operate on its ideal operating line for minimum fuel consumption since the generator can deliver the required power at different rpm.
- At battery charging mode, Part of the generator output goes to the battery through the power electronics and part goes to the electric machine (M/G) working in motor mode.
- At regenerative braking mode, the electric machine (M/G) operates in the generator mode where energy are extracted from the vehicle motion and electric power is generated. In this mode, the engine can be turned off.

Series hybrid vehicle architectures are typically used in heavy-duty vehicles such as trucks and locomotives.

Figure 2 shows the components of the series HEV architecture.

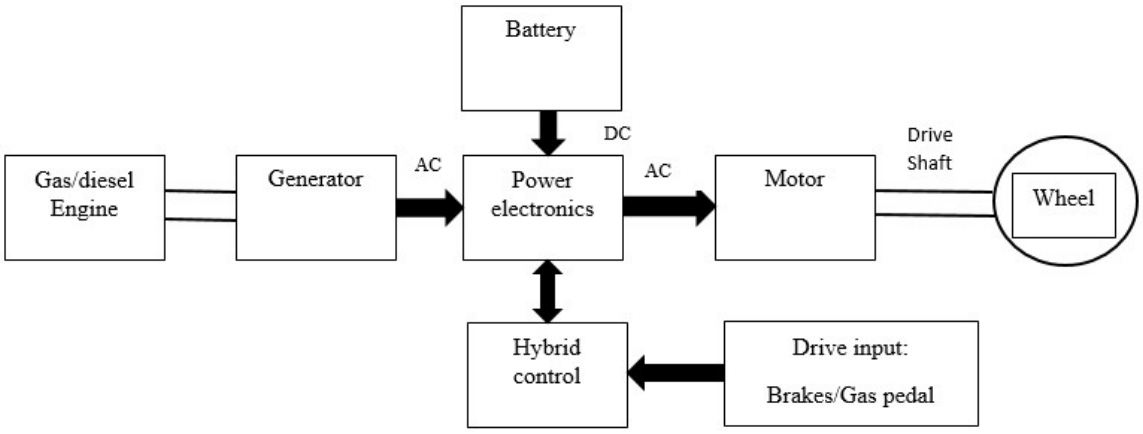

Figure 2: The components of series HEV architecture

Parallel Hybrids: In the parallel HEV configuration, the tractive power is supplied by a proper combination of the engine and the electric machine where there is a mechanical connection between the electric machine (M/G) and the drive wheel and between the engine and the drive wheel. To match engine speed with drive shaft speed, a gearbox is integrated. The engine runs only if the vehicle is moving and if the SOC of the battery is not low. The parallel hybrid can respond to the demand for large, near instantaneous changes in either torque or power. In contrast, the series hybrid is slower. The fast response is an advantage in traffic [21].
Parallel HEV configuration has many other advantages. Heavy component like generator do not exist. Plus, it has the ability to operate with engine alone, electric motor only, or with both motor and engine supplying torque. The use of three-shaft emission leads to the use of three-way gearbox. This mechanical connection makes the choice of the location of the engine limited.

Operating mode:

- At accelerating mode, maximum power is needed. The battery feed power into the M/G set in M-mode and the engine torque is routed through and adjusted by the transmission. They are both engaged through the three-way gear.
- At normal mode operation, the power is generated from the engine alone. The controller adjusts the ratio of the gear for minimum fuel consumption.
- At electric-only mode, the engine is off. The power is generated from the battery alone. The torque created by the M/G in M mode is transmitted by the shaft to the three-way gear.
- At the regenerative braking mode, like electric-only mode, the engine is off. But, the flow of power is the reverse of the electric only mode.

The parallel type of hybrid electric vehicle is the most manufactured type, nowadays [22].

Figure 3 shows the components of the parallel HEV architecture.

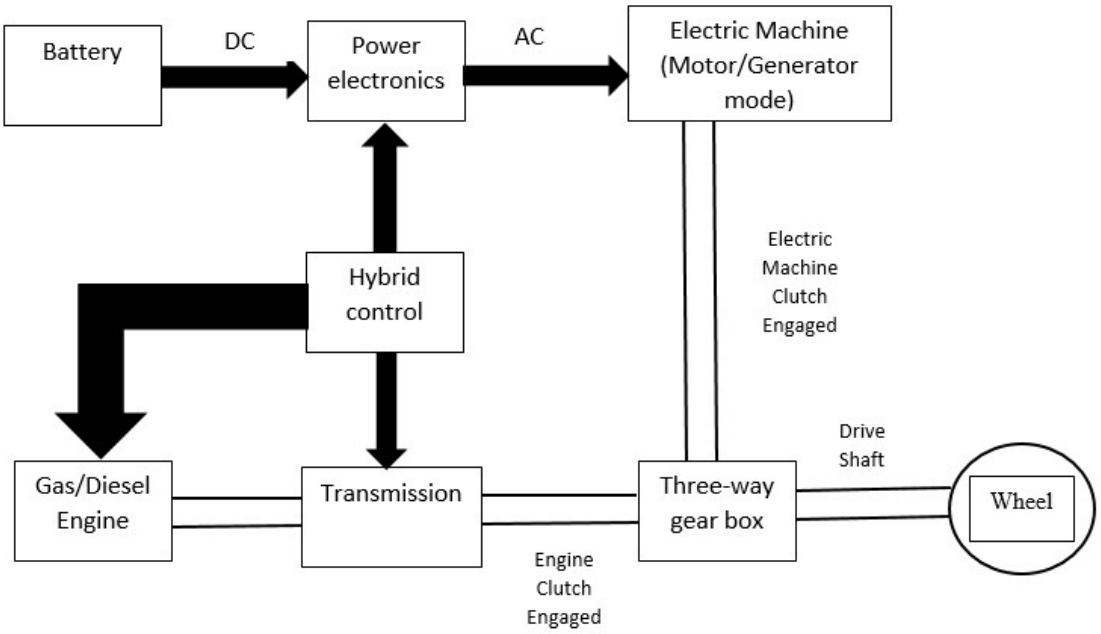

Figure 3: The components of parallel HEV architecture

Mixed Hybrids: Mixed designs that encounter the advantages of the series and the parallel configuration. It offers more flexibility than series or parallel design.

1.3 Electrical machines used in HEVs

1.3.1 Types of electrical machines used in HEV

The fundamental requirement for traction motors used in electric vehicles is to generate propulsion torque over a wide speed range [23]. Several topologies of electrical machines can be used to meet

the requirements of hybrid electric vehicle applications [1]. Over the last decade, we can see that several types of electric machines were used in hybrid electric vehicles: the direct current machine (DC), the induction machine (IM), the permanent magnet excited synchronous machine (PMSM) and the switched reluctance machine (SRM). Switched reluctance is still less widespread. However, the most commonly used types of machine are Permanent Magnet Machine (PMM) and Induction Machine (IM).
HEVs commonly available in the market have a nominal power of 30 kW, a nominal speed of 3000 rpm and a nominal line voltage of 400 V.
Each type of machine has its advantages and disadvantages when used in HEVs application.

DC machine

- Advantages: it can be connected directly to the battery, hence, no complex power electronic s are required. It also has a relative low cost and simple controllability, especially for small rated powers.
- Disadvantages: it has low reliability and high maintenance cost due to the presence of commutators and brushes. It's large and more expensive than other types of machine. It also has a moderate power density and low efficiency. Most losses of the DC machine persist in the rotor, which makes it necessary to add a complex cooling system at high power and restricts the overload capacity.

Induction machine (IM)

- Advantages: compared to the DC machine, squirrel-cage Induction machines have higher power density and higher efficiency. IM provides a wide speed range while conserving its efficiency.
- Disadvantages: it has high copper losses which increase the heat in the rotor; hence, a cooling is required which limits the overload capacity. To decrease the magnetization current, a very small air gap is needed which increase its production cost.

Permanent magnet synchronous machine (PMSM)

- Advantages: it has high energy density due to the presence of magnet in the rotor where small piece of magnet can generate high magnetic field. It has high efficiency since no excitation current is required. Most of its losses are iron losses that occur in the stator, so, only simple cooling is required.
- Disadvantages: its major disadvantage is its high cost due to the relative high cost of rare-earth magnets like Samarium Cobalt and Neodymium. Its efficiency decreases at high speeds due to high stator current. The magnet is very delicate, when using it we should take care about the operating temperature; high temperature causes demagnetization.

Due to their advantages, PMSM is the most suitable machines for HEVs. Furthermore, decreasing magnet costs, nowadays, will decrease the total cost of the machine since the magnet is the most expensive part of it.

Switched reluctance machine (SRM)

- Advantages: compared to the IM, SRM has higher power density and higher efficiency due to the absence of rotor copper losses. It has a simple construction: without rotor winding, with concentrated stator windings; therefore, a better thermal characteristic. It is robust and

it has a relative low volume. In addition, it is cost-effective in production and has low-maintenance [24].

- Disadvantages: it has high acoustic noise radiation, high torque ripples at low speed and a complicated control. For those reasons, until now, only few prototypes of HEVs used the SRM.

The choice of the machine to be used in HEVs depends on its type and its requirements. For example, in series HEVs, IM are advantageous due to their wide speed range and low cost. Whereas, in parallel HEVs where the gearbox controls the speed, the PMSM is recommended since it has high efficiency at low speeds.
Several topologies of permanent magnet machine are available: internal permanent magnet motor, surface mounted permanent magnet motor and axial flux permanent magnet motor.

1.3.2 The importance of electrical machine prognosis in HEVs

Hybrid electric vehicles, being series or parallel, have many components. Hence, an axiomatic question is asked: Why executing a prognosis for electrical machines, rather than another component? What is its importance?
To recognize the importance of electrical machine prognosis in a hybrid electric vehicle, we are going to compare between its cost and the cost of the other component in the system.
In general, the power rating of the electrical motor in a mid-size HEV is between 50 Kw and 100 Kw. According to [25], the cost of electrical machines per power rating is around 40$/KW. A 50 Kw AC induction motor costs 40-60$/KW; a 53Kw brushless permanent magnet (BPM) machine costs 115$/KW. Those numbers are true if the number of purchased units is 1000 units per year minimum. For a single unit purchase, the cost is higher.
The cost of AC induction controller of ratings 50-10 Kw is 14-19 $/Kw, and, the cost of BPM motor having the same rating is 10-14 $/Kw.
Paper [25] also gives idea about the entire cost of the drive system where a drive system containing a brushless permanent magnet motor of rating 50 Kw costs 115$/Kw and that containing an AC induction motor of the same rate costs is 40-60$/Kw.
In general, when brushless permanent magnet machine (BPM) is used, it is assumed that one-third of the system cost is that of the machine, where the cost of BPM machine is 15% higher than the AC induction machine costs and this is due to the high relative cost of permanent magnet. Executing prognostic analysis and studies for electric machines in HEVs are very important and justified, knowing their high cost with respect to the cost of the whole system.
When a failure occurs in the electrical machine, two options pop up: we can repair the failure part in the machine but in this case, we should analyze and know the cause of this failure and solve it to prevent the fail occurring again. Alternatively, we can replace the entire machine by a new one.
The prognostic study is responsible of selecting the appropriate decision.

Before we move to the prognostic models, the selection of the used electric machine and the implementation of its model should be executed.

1.3.3 Permanent magnet machine

Most manufactured hybrid electric vehicles have the parallel configuration. Almost all parallel hybrid electric vehicles use permanent magnet machine. Therefore, the selected electric machine to be investigated in this study is the permanent magnet machine (PMM) [26].
The use of permanent magnets in construction of electrical machines brings many benefits:

- High efficiency and high torque density because of the absence of excitation losses.
- Higher air gap flux density compared the other type of electric machines hence better dynamic performance
- Simple construction and less maintenance compared with other types of electric machines with coils in the rotor or with need of slip ring.
- Low ventilation requirements since there is no copper losses in the rotor.
- When using a low cost magnet, like ferrite, the price of the permanent magnet machine will be lower than its analogous.
- No electrical energy is absorbed for field excitation since the magnet is responsible for the rotor's field.
- Permanent magnet machine is environment friendly since it does not require slip rings and brushes.

Although permanent magnet machine has many advantages, it has few disadvantages that should be noted:

- The healthy performance of magnets is directly related to its operating temperature, hence, the risk of demagnetization always exists caused by an increase of the temperature inside the machine.
- PMM cannot be controlled field current.
- When rare earth magnet is used, the cost of the PMM is high.

The configuration of PMM consists of a set of permanent magnets located at rotor level. The most commonly used magnets are the alloys of neodymium iron boron (NdFeB), samarium cobalt (SmCo5) and ferrite.
The topology or the shape of PMM's rotor was a cause of dilemma for many researchers and was investigated in many papers. Several topologies and configurations are available; the most popular topologies of PMM are: the surface mounted permanent magnet machine and the interior permanent magnet machine [27].

Surface permanent magnet machine

In surface mounted configuration, the magnets are normally glued to the rotor surface, as shown in figure 4, making it easy to be built. It is used for low speed applications because of the limitation that the magnets will fly apart during high-speed operations [28].
Surface mounted permanent magnet machine has radial field where the direction of flux lines is along the radius of the machine.
The electromagnetic traveling field that will be produced in the rotor will pass through the air gap and crosses the stator teeth where a small amount of it, only, traverses radially the stator slots that contain conductor materials. We note that the stator teeth are the iron part existing between two consecutive slots.

Due to its isotropic rotor, the d- and q-axis inductances are identical and the saliency ratio is 1. Therefore, no reluctance torque befalls.

Figure 4: Surface mounted permanent magnet topology

The advantages of this topology is the simplicity of its design and its relative cost. However, it has limitation concerning the selection of magnet type where only neodymium iron boron (NdFeB) can be used in surface permanent magnet machine [29].

Interior permanent magnet machine

In interior permanent magnet (IPM) machine topology, the magnets are incorporated in the rotor core as shown in figure 5.

Figure 5: Interior permanent magnet topology

Setting the magnets inside the rotor improves the mechanical strength and magnetic protection. This topology is suitable for high-speed application. By appropriate positioning of the permanent magnets, the saliency ratio ξ of the IPM is varied accordingly. It is considered to have saliency with q axis inductance greater than the d axis inductance. An IPM motor exhibits both magnetic and reluctance torque [30].

IPM has axial field where the direction of the flux lines is perpendicular to the radius of the machine [31].

Interior magnet rotor design has many advantages:

- It has a better mechanical strength.
- It can reach its maximum energy product (BH_{max}) at a lower operation point.
- It has a reduced air gap length.
- This configuration presents a good reliability for high speed applications.
- It has a high flux focusing.

Interior permanent magnet can be constructed in different topologies. Paper [32] states three topologies: V-shape IPM, W-shape IPM and segmented IPM. A finite element analysis is investigated where they conclude that V-shape interior permanent magnet topology is the most

suitable for electric vehicle applications due to its good flux-weakening performance and wide constant-power operating range.

1.4 Faults in electric machine

1.4.1 Different type of faults in electrical machines

In general, as any other type of electric machine, faults that may occur in permanent magnet machine can be electrical or mechanical. The main difference is in the rotor where there exist pieces of permanent magnets instead of windings or bars.

- Bearing fault

The bearings are normally divided into two types: ball bearings and roller bearings. Typical failures of bearings are flaking, seizing, race factor, retainer failure, rust, wear, fatigue, roughening, brinelling, smearing, and creeping. There are several causes for these failures. Some are unavoidable; the others are avoidable since they are caused by improper installation, improper lubrication or improper handling [33].

- Stator fault

Failures in the stator are mainly failures in the windings. This type of failure is due to failure in the insulation of the winding wire [34]. Phase to phase or phase to ground short circuit may also occur. The causes of winding insulation failures are: high temperature, defects in stator core, loose connection at winding's terminals, contamination due to oil, moisture and dirt, short circuit, electrical discharges, leakage in cooling system [35].

- Rotor fault

Demagnetization is a serious problem in permanent magnet machines. Demagnetization means losing the magnet of its strength [36]. This does not, always, mean the deterioration of the magnet. Many are the causes of demagnetization:
- Loads that Require Starting Torque and Reaction
- Magnetic Fields in Opposite Directions
- Some Magnets Corrode
- Turn to Turn Short Circuit
- High Temperature
- Cracks in The Magnet

- Shaft fault

The main factors that contribute in the shaft fail are: environmental like corrosion and wear, electrical like overload, mechanical like fatigue and thermal like temperature gradients and rotor bowing [37].

- Eccentricity

Eccentricity can be static if the air gap length is not constant around the rotor, dynamic if the center of the rotor and the center of the stator do not coincide [38].

The common causes of electric motor failures are: overheating, overload, power supply abnormalities, environmental condition like humidity, chemical abrasive substances in the air and high altitude operation, contamination, improper lubrication and unusual mechanical loads
Researches have proved that reducing those strains increase the life cycle of electric machines [39].

1.4.2 Useful monitored parameters for fault detection

To predict the presence of faults or failures in the different components of electrical machines one should choose dynamic and measurable parameters that change when a defect occurs. In the following a brief description of a set of useful measured parameters in electric machines [40] [41] [42]:

- Flux monitoring: normal flux shape is sinusoidal. In the presence of certain faults, this sinusoidal shape varies. Such monitoring is useful to detect faults like rotor eccentricity. This may be done by inserting coils in stator slot or installing coil around the shaft. Although this is an effective monitoring method, it's not very practical to insert coils in an existing machine or even a new one which limit its use in industrial applications [43].
- Vibration monitoring: vibration is a common symptom for several motor failures. It can be monitored by non-invasive transducers. However, in some types of faults, like eccentricity, this type of monitoring is not practical since installing such transducers on the back core of the stator is difficult; it is not accurate since at high static eccentricity, dynamic eccentricity is also generated and this detection is not assured by vibration monitoring.
- Stator current monitoring: this parameter is also a common symptom for different types of faults. It can be easily implemented by connecting a current transformer and visualized the current spectrum. The analysis of the spectrum may need to be done in time or frequency domain; it depends on the application.
- Thermal monitoring: electrical machines have a maximum permissible operating ambient temperature and internal temperature to assure proper operation. Overheating in an electrical machine can be caused by high ambient temperature, improper ventilation, and overcurrent. Monitoring the temperature is easy by temperature sensors, but this will make the system more complicated and expensive. Monitoring the temperature can be detected by monitoring the resistance in one winding, minimum since the internal resistance in a coil changes with temperature [44].
- Acoustic noise monitoring: contact between rolling elements generates noise waves of very small energy but with high detectable frequency. Those waves can be easily detected by piezoelectric or capacitive transducer. Other faults like flux disturbances caused by magnet defects also generate abnormal noises.
- Speed fluctuation monitoring: it is the monitoring of the rotation period; when the period is not constant, a fault is detected. Rotor faults, vibrations, air gap eccentricity, rotor asymmetry, damaged bearings/couplings and shaft misalignment are all faults that can be detected with this type of monitoring. However, in applications like vehicles,

this fluctuation may be a load requirement; hence, during monitoring, load fluctuation and fault fluctuation should be distinguished.

- Power monitoring: monitoring the power gives a general idea about the state of the electrical machine. Under fault conditions, the efficiency will decrease.
- Air gap torque monitoring: this torque is different than the mechanical torque measured at the shaft. Air gap torque is a very important parameter to detect the presence of shorted stator winding. This parameter combines the effects of flux linkages and currents. It is sensitive to winding faults and unbalance voltages. The methods for air gap torque measurement are: search coils, partial coils of main windings, and Hall-effect generators [45]. The tools for air gap torque measurements are simple; it requires air gap flux and current measurements. The measurement can be done during the operation of the machine and it takes small time to be achieved [46].
- Lubricant monitoring: the aim of this monitoring is to detect the presence of impurities in lubricants. Impurities like metals, fibers and dust are harmful for bearing, shaft and gear. Electrical conductance of the lubricant is a good parameter to detect the presence of impurities in it. Clear lubricants have low electrical conductance; impure lubricants have higher electrical conductance. Moreover, the analysis should detect over or under lubrication. This can be done by monitoring the oil pressure near valves or measuring the thickness of oil film at a certain critical point. This measurement can be determined through a piezoelectric sensor for example, or by means of ultrasonic technique [47].
- Phase resistance monitoring: measuring the resistance on phases is an important parameter to identify faults like turns short circuit and supply asymmetry. In case of asymmetric supply, the phase to phase resistances are not identical. In case of turns' fault, the resistance of the faulty phase decreases; if the cause of the fault persists, an open circuit occurs and the resistance increases. To measure this resistance, several methods based on vibration and flux induced by fault current were developed. However, the most used methods are based on current and voltage measurements [48].
- Harmonics: harmonics are one of the parameters that help in sensing the existence of faults. For example, dynamic eccentricity and stator winding faults causes changes in stator current harmonics. Dynamic eccentricity also causes changes in air-gap flux harmonics. One of the important parameters to be checked to detect power supply defect is the total harmonic distortion in the current. We note that when harmonics increase, the current increase leading to temperature increase.
- Voltage surge monitoring: fast rise surge causes insulation failure; insulation failure will cause short circuit of winding turns. This surge is usually caused by the switching of the power system switching or by the power electronics devices used in switching like GTOs and IGBTs.
- Electrical discharge monitoring: when a weakness or hole exist in the winding insulation, partial discharge or corona coming from the wire, cause rapid degradation of the insulation and turns short circuit occur. Moreover, the presence of contamination at the surface of the insulation contributes to high surface discharge, leading to winding defect [49].
- Contamination monitoring: the presence of contaminations is harmful for winding insulation, magnet, bearing, shaft and fan. Paper [50] suggests a method called high sensitivity differential current transformer (HSCT) that is based on measuring the

capacitance of the insulation, during operation, to detect the presence of contamination like moisture in the electrical machine.

We remark that many symptoms may be an indication for a single defect. It is useful, to be sure of the occurrence of a fault, to check the presence of more than one symptom, before taking any decision or corrective measure.

The chart in Figure 6 relates the useful measured parameters to the corresponding element of the system [51].

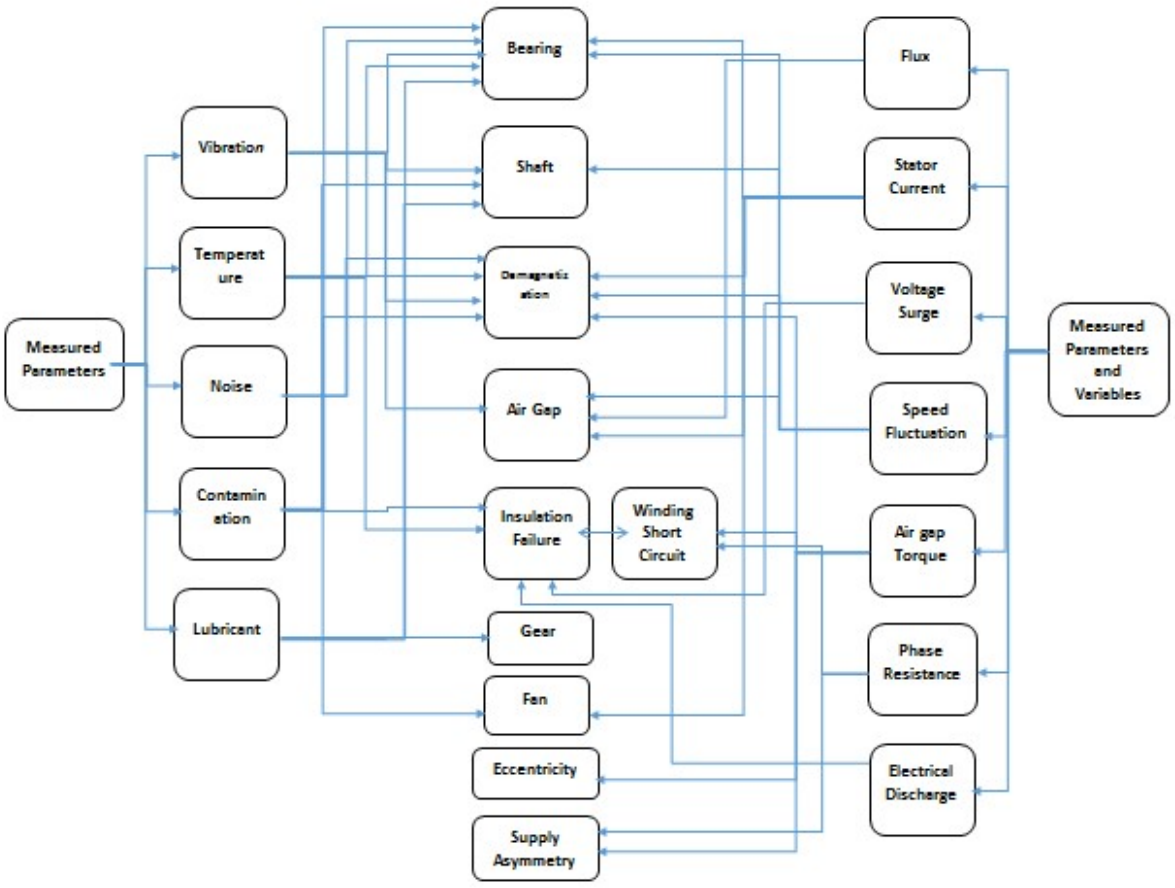

Figure 6: Measured parameters versus failures

Table 2 relates the different types of faults to their percentage of occurrence [52].

TABLE 2: PERCENTAGE OF FAULT OCCURRENCE

Fault type	**Bearing Failure**	**Stator Failure**	**Rotor Failure**	**Shaft Failure**	**Eccentricity failure and others**
% of occurrence	41	37	10	2	10

Table 3 indicates the threshold or permissible parameters, that are measured for prognostic purposes and at which the system is not considered defected.

TABLE 3: SOME THRESHOLD VALUES OF MEASURED PARAMETERS

Measured Parameter	Threshold Value
Vibration	<1.6 rms[(1)]
Stator current	+ 20% of the rated current
Acoustic noise	+3 dB
Speed fluctuation	+- 20% of rated value
Power efficiency	>85%
Voltage	Short period: +- 10% of rated value
	Long period: +- 5% of rated value
Frequency	Small period: +3 to -5% of rated value
	Long period: +- 2% of rated value
Air gap torque ripple	Between -15% and +25% of rated value
Voltage surge	1600 V peak for 0.1 µs
Eccentricity	<10% defect
Static eccentricity	Frequency twice the supply frequency indicates defect
Temperature	At frame level: 40 °C
	At insulation level: 155 °C (Class F)
	At magnet level: Neodymium N45 withstand a temperature of 80°C Neodymium 33 UH withstand a temperature of 180°C
Alignment	The difference between maximum and minimum point: 0.03% Vibrations of double rotor speed frequency indicates misalignment
Harmonics	<3 % of the fundamental
Phase resistance	(10 minutes RTG[(2)]) /(1 minute RTG)=~2
Insulation resistance	>10 MΩ at 25°C This resistance is halved with every 20°C temperature rise
Flux	Under normal conditions, Neodymium will lose only 1% of its flux over 100 years. Hence, a drop of flux > 1% is an indication of demagnetization.

(1) rms: it's the square root of the average of the squared value of the vibration waveform.
(2) RTG: resistance to ground.

1.4.3 Fault severity in permanent magnet machine

Many researches have classify the types of failures, from the most to the less severe, in terms of fault occurrence percentage. However, this is not enough, alone, to classify failures in the order of urgencies. Hence, a novel classification is suggested taken into consideration the percentage of occurrence and the cost of the relative failed component.

In this study, it is considered the worst case; the failed component needs to be replaced.
To do this classification, we define a Fault Severity Factor FSF where:

*FSF = (% price of the relative failed component * % of occurrence of a fault) / (Σ (% price of the relative failed component * % of occurrence of a fault))*

This approach will be applied to the 15 Kw permanent magnet machine.

1) Bearing: According to [53], a machine of rating 10-20 kW has a shaft of diameter 48-60mm. this imply to consider a mid-value of 55 mm. An adequate bearing will cost around 4- 8$.

2) Stator winding: A typical 15 kW permanent magnet machine will have 36 slots, slot area around 200 mm2, a 0.35 filling factor, 235 mm outer diameter of stator, 145 mm outer diameter of rotor, 195 mm axial length.
   Having three phases, the length of cable per phase will be around 50 m with a minimum cross sectional area As=2 mm2. According to the manufacturer, a copper wire for electric motor winding having a cross sectional area between 2 and 6 mm2 cost 8-10$/kg. From the geometry of the laminated sheet, the mass of copper in the winding can be estimated. The density of copper is 8960 kg/m3, hence, the mass of copper in the machine is around 2.7 kg and its cost is around 25 $.

3) Magnet: Interior permanent magnet can be constructed in different topologies. In [54], three topologies are stated: V-shape IPM, W-shape IPM and segmented IPM. A finite element analysis is investigated where it is concluded that W-shape interior permanent magnet topology is the most suitable for electric vehicle applications due to its good flux-weakening performance and wide constant-power operating range.
   Combining information in [55] and [56], the volume of magnet in an interior permanent magnet machine, of rating 15 kW, adopting W-shape topology is around 1.3 kg. The used type of magnet is the Neodymium Iron Boron (NdFeB). In 2013, the cost of NdFeB was 150$/kg. If one only considers the cost of NdFeB as raw material, the cost of 1.3 kg of it will be 195$.

4) Shaft: The shaft of a15 kW machine will have a maximum length of 400 mm. A shaft made of carbon steel having a proper length and diameter will cost around 15 $. It should be noted that this cost is for a single shaft order.

TABLE 4: CLASSIFICATION OF FAULTY COMPONENTS

	Price ($)	**% price of the relative failed component**	**% of occurrence of a fault**	**FSF**
Permanent magnet	195	80.2	10	60.26
Stator winding	25	10.3	37	28.64
Bearing	8	3.3	41	10.17
Shaft	15	6.2	2	0.93
Miscellaneous faults	-	-	10	-

The results illustrated in Table 4 Show that permanent magnet fault detection has the priority over the remaining fault possibilities. We recall that the price of the permanent magnet mentioned in the table do not consider the manufacturing cost of the magnet, which means that its real price is higher.

1.5 Prognosis

1.5.1 Prognostic strategy and condition base monitoring

In general, prognosis assists the present health of a system and predicts its remaining life based on features that effect the gradual degradation in a system's operational competencies. Prognosis techniques are used to advance safety, plan successful work, schedule maintenance, and diminish maintenance costs and down time where [57] states that, in USA, 25 billion US $ are spend in the transportation sector for annual additional maintenance.

We note that maintenance constitutes the followings [58] [59]:

- Periodic inspections to monitor and record of the system performance
- Precautionary maintenance to ensure that the components of the system are well executing their functions through their operation
- Repairing system's components when defect occurs
- Restoration where a major component of the system is replaced by a new one when the service life of the system tends to end

Maintenance strategies can be classified in three types: Breakdown maintenance that occurs to fix a failed element in the system, it needs a large budget; Preventive maintenance that is schedule

and periodic; Predictive maintenance that is directly related to condition based monitoring decision.

Because of prognosis, equipment failure is predicted and unnecessary maintenance activities are avoided. Prognosis is a relatively new field, but it has becoming an important part of Condition-based maintenance (CBM) of systems.
Being a prediction technique, prognosis cannot predict 100% of faults and failures. The lack in prognosis prediction is overcome by diagnosis.

Steps followed when applying Condition Based Monitoring System:

- Step 1: sensors deliver the data to the CBM system.
- Step 2: the signal processor receives this data and conduct it through appropriate CBM featured.
- Step 3: the condition monitor receives this data and compare it to the normal values. If the two magnitudes don't match, alerts are created.
- Step 4: the health assessment module receives data from condition monitoring system, prescribes the health state of the monitored component or system, generate diagnostic histories and advise fault likelihood. It takes into consideration health history, operational status and maintenance history.
- Step 5: Prognosis collect the manipulated data, offers the future health status and the remaining useful life of the component or system.
- Step 6: in the end, the previously collected and treated information is examined, useful remaining life and proper action is generated.

The useful remaining life denotes the portion of normal useful life of the treated system, in years, running from the date of evaluation to the end of its use. Determining the remaining useful life of a system is not simple, many parameters should be prudently deliberated.
In figure 7, the prognostic strategy and its logical sequence for appropriate prognostic decision is illustrated.

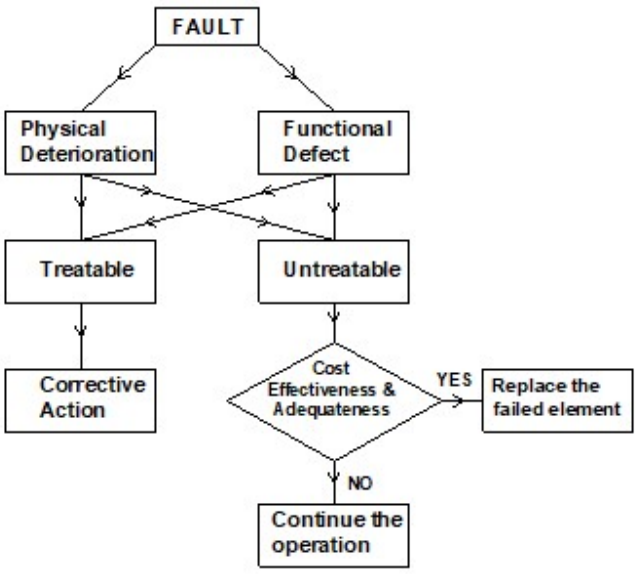

Figure 7: prognostic strategy

There are two types of defects in electric machine: physical defects, like a crack in a piece of magnet; and functional defects, like the presence of impurities in the lubricant. Some of these defects are treatable like a crack in the magnet, and some of them are untreatable like removing impurities from lubricant. When defects are treatable, direct corresponding acts should be taken. Nonetheless, when defects are untreatable, other measures should be considered Operating load based.

When the fault is untreatable, an important question should be asked: is it cost effective and adequate to replace the failed element? If yes, the replacement of the failed element should be done. Otherwise, the prognostic approach should intervene to calculate the remaining useful life of the defected component and make the appropriate decision: stop the system and replace the defected component or, continue the operation of the system.

1.5.2 Prognostic methods

Prognostic methods can be grouped in three main categories: heuristic methods, model based methods and data based methods [9] [11].

Heuristic methods

Earlier, heuristic methods were based on time or frequency processing techniques. Recently, they are based on time and frequency domain information.

It consists of forming a feature vector containing values that designates when the parameters coming from the evaluated system reached a predetermined failure threshold.

Heuristic methods are simple, easy and work well most of the times, however, they do not encounter a theoretical basis that guarantees this wellness without system testing.

Model based method

Model based method is more complex and expensive then heuristic methods. Yet, it overcomes some of the heuristic method drawback.

It is based on the physical understanding of the system where physical models are generated. This can be done at micro or macro level.

At the micro level, the physical models are characterized by series of dynamic equations that outline relationships between the component of the system, the operation and the environment.

At macro-level models, the mathematical model is applied at system level, which defines the relationship between system input variables, system state variables, and system measures variables.

Accordingly, the macro level is a more developed and expended presentation of the system.

Data based methods

Data-driven approaches are based on the collection of data coming from sensors. It is recommended when the understanding of the treated system is incomplete or when the system is complex such that, developing an accurate model is hard and expensive. Therefore, data driven approaches are often faster and cheaper compared to other approaches.

The conventional data-driven methods comprise the use of stochastic models like the autoregressive (AR) model, the bilinear model, the projection pursuit, and the Volterra series expansion. Recently, more interests had focus on more flexible models such as different types of neural networks (NNs) and neural fuzzy (NF) systems.

Data-driven method involves two strategies: modeling cumulative destruction in the system and then extrapolating it out to a damage threshold or learning directly from data the remaining useful life. In our thesis we will took advantage of the first strategy.

The first and the second methods have the advantage of having information about faults that already occurs in previous monitored systems. The third approach has the advantage of not being limited by one general rule; a wide variety of data types can be investigated. The statistical model is very beneficial for new sources of data where analysis, physical models and rules are not yet developed.

Machine prognosis is essential to improve its safety, set its planning missions, schedule its maintenance costs and down time.

1.5.3 Prognostic techniques

Every prognostic method has many prognostic techniques that behooves to it. They are illustrated in figure 8.

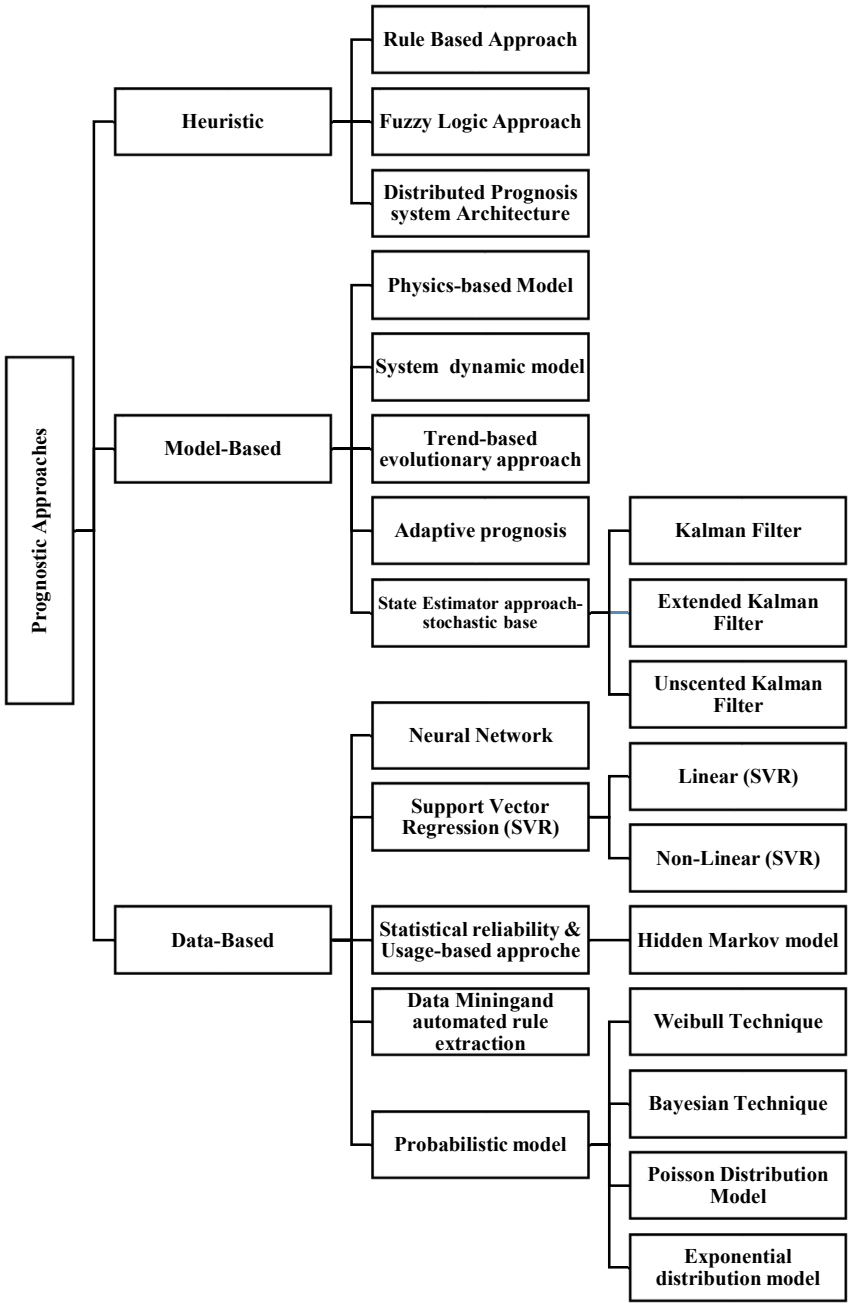

Figure 8: Prognostic methods and techniques

A brief description of each prognostic technique is illustrated in table 6.

TABLE 5: : DESCRIPTION OF PROGNOSTIC APPROACHES

	Prognostic Approach	Description	State equation or representation

Heuristic Approach	Rule Based Approach (Known as expert systems)	It's the simplest artificial intelligent and the most commonly used approach. It's based on using rules to perform a given situation.	It's represented by a set of IF and THEN statements.
	Fuzzy Logic Approach	First step: Identification of fuzzy inputs and assign membership function or set for each one. Second step: form the rule that will govern the sets like AND, OR and NOT. Other relations like implication between sets can be represented using IF and THEN statements Third step: generating the fuzzy output and mapping the inference between input and output spaces	For example: AND: $\mu A \cap B(x) = \min\{\mu A(x), \mu B(x)\}$ OR: $\mu A \cup B(x) = \max\{\mu A(x), \mu B(x)\}$ NOT: $\mu \neg A(x) = 1 - \mu A(x)$ A,B: sets The fuzzy logic approach can be combined with a set of IF and THEN statement.
	Distributed Prognosis system Architecture	It consists of analyzing data architecture through logical hierarchy to ensure the adequate decision and that from the low level of Line replaceable unit, through the system, to the vehicle level. This approach has many advantages: accuracy, optimal results, details of the system are	- Isolate the fault's cause - Understand the propagation of fault effect - Incorporate the results in the prognosis and health management system using hierarchical reasoners. - Recognize the required corrective act

		considered, ability to accommodate different sources of data and identification of wrong data, ability to isolate and evaluate more than one fault.	
Model-Based Approach	Physics-based Model	It's used to understand and represent the progression of failure mode. It calculates the damage as function of the operating condition and evaluates the growing effects with respect to the usage life of the component. The physical based model helps in predicting the remaining useful component life function of defect in related components like strength/stress properties, loading or lubrication conditions for a particular fault. The results of such model are useful in predicting real time failure prognostic.	For example, the fatigue crack propagation model, mainly based on Paris's formula: $$\frac{d\alpha}{dN} = C_{\circ} (\Delta K)^{n}$$ Where: α: length of dominant crack N: running cycles $C_{\circ}$, n: material's constant ΔK: range of stress intensity factor over loading cycle.
	System Dynamic model	This approach is hard to be applied for complex systems. It consists of imagining the model and observing the input of the output of the system to identify the parameters of the system. Accordingly, this model will be an accurate	In [51] a dynamic model of the gear is investigated. First, they calculated the constant parameters of the gear system, which is defined to be a rotational lumped parameter model, like inertias, damping and stiffness. The geometry of the system and the material properties help in calculating those parameters. Then, those parameters are integrated in the adequate equation motion of the system. In the end,

		representation of the system.	simulation is done to generate the dynamic model and existing failures.
	Trend-Based evolutionary approach	It's based on tracing deviations in specific measured parameters from their regular operating condition for several iterations. It's used in systems facing slow degradation type faults. It needs large sensor information. Details and history of the fault condition should be available. Physical model is not required in this approach.	The priori (expected) function of the measured parameter is compared to the updated function.
	Adaptive prognosis	As its name indicates, it's about adapting, or modifying the model to meet the new specifications or current measures.	If a failure occurs at a time $t=t+p\Delta\tau$, the model should be adjusted accordingly to reach optimal prognosis. The failure's model f(t) will optimized to $f(t+p\Delta\tau)$.
	State Estimator approach- stochastic based prognosis	An example is Alpha-Gamma-Beta filter, kalman filter (KF), Extended kalman filter (EKF), Unscented kalman filter (UKF), or any other filters. EKF and UKF are a development of KF. KF can be used only after linearization of the system. EKF has the ability to linearize the system around an operating point or specific state. UKF has an advantage of performing well in	Kalman filter can be described as $x_{k+1}=Ax_k + Bu_k +Gw_k$ $z_k=Hx_k + v_k$ x_k: internal state z_k: measured values w_k: process noise v_k: measurement noise

		non-linear system [17]	
Data-Based Model	Neural Network	The most commonly used data driven technique. They are useful in classification and prediction. It's fast, better than the traditional statistical methods and has the ability to investigate new complex systems. There are many types of Neural networks: artificial neural network, recurrent neural network, recurrent wavelet neural network, neuro-fuzzy network, feed forward neuro network. The Artificial neural network is the mostly used. The accuracy of the results increases when the quantity of available data increases. Neural network can be updated when new data appears.	The Artificial Neural Network is built of a level of input nodes, one or more level of hidden nodes, one level of output nodes and connecting weights. To identify the unknown, the neural network adjusts the weights with recurrent clarifications of inputs and outputs.
	Support Vector Regression (SVR)	This approach as rapidly developed and applied for classification and regression problems. It's suitable for Support vector machine was used to investigate functions like cost, kernel and	

		performance of machine sets. It has an advantage over the neural network approach being less risky, more general, suitable for complex system and robust with nonlinear data.	
		Support Vector Regression-Linear: It consists of recording data x from a large dimensional space and applying the linear regression on it.	$f(xi) =< w, xi > +b$ xi: required pattern w: uncertainty, should have small value b: system's constant
		Support Vector Regression-Non-Linear: The linear SVR is practically limited; the nonlinear SVR overcome this issue, where the required pattern xi is replaced by required function pattern f(xi).	Nonlinear function φ (xi) is integrated in the function f(x). $f(xi) =< w, \varphi(xi) > +b$
	Statistical reliability & Usage-based approach	This approach is simple. It's implemented when no prognostic model exists or no enough information is available due to the lack of sensors. Data are required from the operating system or from the archive (configuration of fault history) and from legacy system, then fit it to a statistical distribution method to identify fault.	The steps of this approach is: [60] Step 1: collect data and divide them into intervals. Step 2: build a statistical model for each interval or group. Step 3: test each interval according to this equation: $ptci = \prod_{j=1}^{k} ptj$ where: ptci is the test case, k is the transition, ptj is the probability of the jth transition. Step 4: measuring the reliability using the following equations:

		Maintenance interval can be generated; an update of those intervals can be made every time new data are available. Later on, the accumulation of information and the inspection of failure rate will lead to build the corresponding algorithm and model. Hidden Markov model is a statistical modeling method.	$R = 1 - \left(\frac{f}{n}\right)$ $\text{MTBF(mean time between failures)} = \frac{n}{f}$ R: reliability F: failures N: number of failed measurements
	Data Mining and automated rule extraction [61]	According to this approach, rules are extracted from input data by the simple examination of this data. Input data must be chosen from fault period categorized samples. It aims to discover pattern in the collected data. The advantages of this method over the neural network: comprehensibility, explanation, validity, learning new features from data examination, the generated output (like binary tree) is done by a simple analysis of data input.	- Collect the data from different sources. The data must be relatively large since the analysis and fault detection will occur on the available data. - Integrate data in one instant set after removing noises. (there is a standard way to represent the data called ARFF file) - Start find a relation between variables prior finding an algorithm to govern the data - Validate the result by making sure that the generated algorithm is applicable to all data, even to the one out of the chosen set at the beginning
	Probabilistic model [62]	It is a very effective method, accurate and precise. It requires less details then	Weibull model: $F(x) = 1 - e^{-\left(\frac{x}{\beta}\right)^{\alpha}}$ (x: any data value, α: shape parameter, β: location parameter)

		model-based techniques since it requires probability density functions found from observed statistical data. Under this approach come the Weibull model, Poisson model, Exponential model and the Bayesian Theory. It's mentioned that the Weibull, Exponential and Poisson models are rugged in failure behavior estimation. However, they are useful when studying a set of identical population (Machines for example) to predict their failure rate. Hence, they may be beneficial for manufacturers that produce a large number of units.	Although this model as used in predicting lifetime of components like bearing; it's not reliable since it generates an average value of this life time. The recommendation is to use condition monitoring of dynamic parameter, like vibration, in this field. Bayesian Technique: It's an expression of condition probability. $P(T|D) = \frac{P(D|T)*P(T)}{P(D)}$ D: data, T: threshold or expected value

Many researches applied prognosis using different methods for different applications.

In [178], a data-driven method founded on data enlarged in simulation to encounter all the probable trends of the degradation process is proposed for MOS Field-Effect Transistor. This data set is used for an offline assessment of the Remaining Useful Life. The strength of this assessment is its capability to be performed online by updating the model parameters using Wiener process. The drift parameter of the Winer process is updated online; its stochastic part is used to simulate several selected degradation trajectories. The efficiency, the accuracy and the wide application scope of the suggested approach is verified by simulated simulation and experimental results.

The author in [179] perform a fault prognosis for wind turbine when multi faults occur. A hybrid method is presented; a physical model is used for structural analysis, sensor placement, and clusters generation in the normal and faulty situations. An original approach expressing the degradation of the model using the principle of geolocation is illustrated. The Remaining Useful

Lifetime is calculated based on the Euclidean distance between normal and faulty clusters, the degradation direction and velocity. Real wind data is used.
Paper [180] also present a hybrid approach for breakage of drive belt. Fault indicators are generated from a dynamic model simulated in the healthy and faulty states; then, those indicators are treated using a data driven method. No prior knowledge of the system is needed to detect fault degradation.
In [181], a data driven prognostic approach is applied on Batch semiconductor manufacturing processes through three steps. First, extracting raw health index from collected data. Second, monotonic profiles are developed by executing variations in the health index using percentile measure. Third, the developed profiles are modelled by gamma process. Those steps are followed by The remaining useful life (RUL) estimation that is elaborated using an aggregate probability density function (pdf) with a confidence interval. The method shows good accuracy where it estimates better the failure system compared with an existing preprocessing method.

The selected prognosis technique to be used in the succeeding work is the data driven model, Hidden Markov Model (HMM). When applying prognosis, examining the impact of several parameters on the health state of the system is recommended. Hence, this technique is designated due to its advantage over the others to achieve this goal.

Hidden Markov Model is a Data-driven prognostic approach since it efforts to derive models directly from collected Condition Monitoring (CM) data; they get predictive output directly in terms of CM data. It's a stochastic signal model. It's a Bayesian estimation problem.

In general, HMM is useful to predict the sequence of state changes in a system, based on the sequence of observations. Hence, it is recommended for systems having a finite internal states that generate a set of external observations. The internal states of the system are invisible for an outward observer. The current state is directly dependent on the immediate previous state; these sequence is called the Markov process.
In paper [95], the author combines Artificial Neural Network (ANN) and hidden Markov model (HMM) and took advantage of their ability to be applied for diagnosis and prognosis. Those two methods are used to extract useful features from the system and elaborate its remaining useful life (RUL). It also declares that HMM is definitely able to estimate unobservable health-states using observable sensor signals or defined features computed by other techniques like ANN. The application treated is turbofan engine where an example on turbine disk is presented. The target of HMM is to compute the remaining useful life of the turbofan.
The author in paper [96] highlight the importance of detecting native and imminent faults in electric machines used in critical applications like hybrid electric vehicles and avionics. It proves that hidden Markov model, used in diagnostics, is useful to be used as prognostics technique. It presents two methods based on Hidden Markov Models for the Predictions of coming faults. They are based on pattern recognition, that is a data-driven approach commonly used in the field of faults detection and diagnostic.
Paper [97] apply prognosis technique to detect electrical faults using hidden Markov model and estimate the remaining useful life of relevant equipment using estimation approach based on the probability of state failure. The observable of the model are time and frequency features extracted from the machine's torque measurement. To train the HMM experimental observation influenced probability densities is used, due to limited available data. The investigated fault is turn to turn

short circuit; it aims to detect the presence and estimate the severity of turn to turn short circuit from the extracted torque features. However, this will not lead to localize the fault and state which coil is short circuited.

The author in [98] state that HMMs is an advantageous method in diagnosis, prognosis and condition monitoring fields. Nowadays, the wide availability of different types of sensors: vibration, temperature, torque… encourage us to apply HMM. It has been noted that HMMs can still be applied even if few training data and little prior knowledge about the system is available. In this paper, the examined data is the current of the electric motor. This measured parameter is used to detect the presence of fault, define the current state of the machine and predict its future state. However, it has been concluded, in the end, that the presence of few data may not be enough to predict the future state of the system correctly.

As examined, most papers applying hidden Markov model for prognosis or diagnosis purposes in applications like electric machines integrates mainly mechanical faults like a crack in the bearing. None has investigated prognosis when faults like turn to turn short circuit, demagnetization or eccentricity is integrated in the machine.

As we know, electric machines can operate properly and at rated power even when there is a couple of winding turns short circuited, a small crack one piece of magnet or an eccentricity fault with small percentage of deviation. The importance of prognosis is to detect this issue and prevent the propagation of theses faults by appropriate condition monitoring, machine supervision and maintenance decision.

The slackness in this matter will deepen the fault where a whole coil may become short circuited, or the small crack may propagate and become a severe one or, the rotor eccentricity deviation evolves. In the other hand, a specific fault, at its early stages, may the cause of other fault generation knowing the interaction between faults inside the machine that is previously discussed.

1.5.4 Prognosis in Hybrid electric vehicles and its electric machine

Due to its importance, prognosis concept started to be used in applications like hybrid electric vehicle and its components.
Machine health prognosis plays a significant role in the dynamic maintenance and decision-making. A proper maintenance schedule ensures system reliability, decrease the frequency of failures, and improve equipment availability. A novel prognostic method called rolling grey forecasting method is presented in [63]. This method takes into consideration influencing factors like operating load to generate an efficient and accurate machine health prediction.

Paper [58] presents a hybrid model-based, data-driven and knowledge-based integrated diagnosis and prognosis structure, and applies it to auto-motive's battery systems and electronic systems.
In [64], a data-driven multi-scale extended Kalman filtering algorithm had been developed. This algorithm tends to estimate important parameters for the battery like its capacity and its state of charge. This will help in the diagnosis and the prognosis of the battery's general behavior.

The paper in [65] states that, in HEV, an advanced diagnosis and prognosis technologies are needed to rapidly sense and isolate faults in network-embedded automotive systems so that proactive corrective maintenance actions can be taken to avoid failures and improve the availability of the vehicle. It discusses an integrated diagnostic and prognostic framework, and applies it to two automotive systems, a Regenerative Braking System (RBS) in hybrid electric vehicles and an Electric Power Generation and Storage (EPGS) system. The method used is the physics-based modeling approach which consists of figuring out the difference between a measured parameter and its expected value when using a mathematical model. A large difference indicates the presence of a fault. The small difference indicates a normal operation with the presence of noise or modeling errors.

A model-based fault diagnosis and prognosis scheme for a vehicle steering system is presented in [66]. The types of faults are classified as unexpected fault, elementary fault, and discontinuous fault. They are detected using the concept of Augmented Global Analytical Redundancy Relations (AGARRs). After distinguishing the type of fault, a pattern is identified to estimate the magnitude of unexpected faults, the characteristic of discontinuous faults, and the degradation performance of elementary faults. A new adaptive hybrid differential evolution (AHDE) algorithm with less control parameters is used to identify the fault. Once degradation behavior of faults is identified, prognosis is carried out to predict the remaining useful life of faulty components.

As we Remarque, in general, prognosis concept is very innovative in HEVs. Few researches had been conducted for the prognosis of the storage element in the system. None had focus on the fault prognosis in the machinery part or the power electronics part of the system.

Prognosis can be applied for any component in the electrical machine [57]:

a) Bearing prognosis
   Bearing is a rotating element presented in every machine. Its failure may be, in some cases, catastrophic. Hence, developing reliable techniques to predict the failure of the rotating element in early stage and ease precautionary maintenance is very important.

Two models are commonly used for bearing modeling:

- Spall Initiation Model that consider bearing dimensions, loads, lubricant quality, and view empirical constants to execute bearing prognosis.
- Spall Progression Model that takes into consideration oil debris, high vibration levels, and elevated temperatures that ultimately lead to bearing failure.
-

b) Gear prognosis

The gear fault is a mechanical fault that can appear as cracked or missing teeth in the gearbox that is coupled to the motor. This type of fault can be identified by monitoring resistance during the short transients where momentary increase in the resistance appears.

For the gear prognosis a model that considers high fidelity stress, fatigue and crack propagation can be elaborated.

c) Rotor asymmetry prognosis

This is manifested by broken rotor bar, cracked magnet or cracked rotor end-rings (depend on the type of electric motor). This fault can be caused by: thermal stress, magnetic stress, residual stresses due to manufacturing problems, dynamic stress… hence, the related model should consider the above parameter.

d) Stator or armature faults prognosis [67]

They are known as phase-to- ground or phase to-phase faults. Prognosis is useful at this stage since it's believed that the fault starts as undetected turn-to-turn faults which, in the end, grow and culminate into severe ones.

This type of fault affects directly the voltage, current and mechanical torque. [17]

In [25], increased resistance in one phase is introduced as an electrical fault at stator stage that occurs due to bad connection between the motor and the controller.

The causes of this type of faults:

- High stator core or winding temperatures.
- Slack core lamination, slot wedges and joints.
- Loose bracing for end winding.
- Contamination due to oil, moisture and dirt.
- Short circuit.
- Electrical discharges.
- Leakage in cooling systems.

e) Eccentricity faults prognosis

This is due to unequal air-gap that exists between the stator and rotor. When becoming large, this type of fault will cause unbalanced radial forces. This will cause stator to rotor rub, which causes damage to the stator and rotor [68].

f) Defective magnet prognosis

Prognosis of magnet will be mainly to prevent demagnetization that may be caused when a crack occurs in the magnet or when the operating temperature of the magnet increases due to a fault in its environment.

g) Insulation failure prognosis
When temperature at insulation level increases, its life cycle decreases. A failure in the winding's insulation will directly cause turn to turn short circuit. hence, insulation failure prognosis is very significant [69].

1.6 Finite Element Method and electrical machine

Hidden Markov Model is data driven prognostic technique. The input of the model will be the data coming from sensors located at different points in the machine. However, a prototype of a permanent magnet machine where we can integrate different types of fault easily to see their impact on sensors measurements, is not available. Hence, choosing the appropriate model for the electric machine was a must.
Due to its accuracy and its detailed representation of the machine; it's physical aspect, electromagnetic, thermal and vibration performance; we modeled the permanent magnet machine using finite element model.
Finite element model is very advantageous for electric machine. It is capable to show the flow of flux lines in the whole machine. Identifying the path of flux lines in the electrical machine and the flux density in the air gap is of high importance to predict the performance and characteristics of this machine where the average air gap flux density is essential to compute torque, power, flux [17]. In the other hand, the determination of flux density in the whole machine is very important specially in the teeth where the flux density should not exceed a certain predefined value, beyond it the core became saturated.
Finite element model is also valuable in displaying the temperature all over the laminated sheet and exhibiting the vibration at any point inside the machine.
The machine is modeled in the healthy case and in the faulty case where faults of small scale are integrated in its laminated sheet. The considered faults are demagnetization, eccentricity and short circuit.
Fictive sensors can be located anywhere inside the machine or at its boundary. The collected data, by those sensors, will be the input database for the prognostic model.
A wide description of the machine's finite element modeling is presented in chapter 2.

1.7 Conclusion

This chapter was a general literature review about hybrid electric vehicles, electric machines used in such application, the different types of fault that may occur in those electric machines and different available prognostic techniques that may be used. The importance of electric machine prognosis has been highlighted. To achieve its goal, electrical machine prognosis should detect defect at an early stage or before it occurs, assess the machine continuously and predict its remaining useful life and its possible failure mode.
The conducted previous work leads us to focus on three types of fault in electric machine: demagnetization, eccentricity and turn to turn short circuit. Faults of small scale will be integrated in the machine. The selected prognostic technique will predict the faulty state of the machine. It will predict its next state where a fault propagation may occur. In the end, it will calculate its remaining useful life.

The selected prognostic technique, hidden markov model, is a data base model. However, a prototype of the permanent magnet machine where we can introduce different types of mechanical and electrical fault and see its impact on different measureable parameters is not available nor easy to manufacture. Hence, we will take advantage of the accuracy of finite element model, build electromagnetic, thermal and vibration model of the machine for different types of fault and collect the needed database for our prognostic approach.

Chapter 2: Finite element model

2.1 Introduction

As we clarified previously, a prototype for the PMM is not available; hence, the model of the machine is needed. It is decided to build the model using finite element analysis which is a widely used numerical model due to its advantages over the analytical method in terms of simplicity and accuracy. The model will be built for undamaged machine and for machine containing tiny fault.
After the literature done concerning the severity of faults befalling in permanent magnet machine, it has been proven that demagnetization has the preference, being the most sever. The other types of fault that will be considered are eccentricity and turn to turn short circuit.
The strategy followed to achieve the prognosis is to model the permanent magnet machine in the healthy state and in the faulty state; then, compare the behavior of the measureable parameters like torque, vibration, temperature…, in the two cases. This approach will let us link the fault, or intuition of fault, to its relative measurable parameters. In other words, monitoring a parameter will let us prevent the occurrence of a fault.
In this chapter we will present extensively the finite element model where the electromagnetic, thermal and vibration finite element model is built for the permanent magnet machine in the cases of normal operation and when a fault is integrated in the machine.
By use of Matlab, the model is elaborated. The software Matlab presents several functions that are useful for finite element analysis.

2.2 Electromagnetic FEM

The electromagnetic model is divided into two parts: static and dynamic. The static can be a current fed model or a voltage fed model.
The specifications and parameters of the selected PMM, including the geometry of the laminated sheet, are illustrated in table 6 [70].
The geometry of the laminated sheet with the distribution of the phases on the slots and magnet's poles are illustrated in Figure 9. A two poles section of the machine's laminated sheet as developed by the used software 'Matlab' is presented in figure 10.

TABLE 6: : MACHINE'S SPECIFICATIONS AND PARAMETERS

SPMM Parameters	**Values**
Machine active length L_S	204.79 mm
Stator core thickness e_{cs}	7.22 mm
Stator outer radius	117.78 mm
Stator inner radius R_s	61.421 mm

Rotor outer radius	54.92 mm
Rotor inner radius	47.71 mm
Nb of slots N_s	36
Slot opening θ_s	4°
Radial tooth length h_t	49.16 mm
Area of slot	281.05 mm^2
Slot filling factor	0.3
Area of winding turn	3.666 mm^2
Nb of turns per phase	13
Air-gap thickness g	2 mm
Radial PM length e_m	4.5 mm
Nb of pole pairs p	6
Magnet opening angle θ_{PM}	20°/30°
Magnet remanence B_r	1.2 T
Magnet Coercive force H_c	955 kA/m
PM Relative permeability μ_r	1.05
Material properties	**Values**
Young Modulus of steel	210 $\mathrm{GN/m^2}$
Mass density of steel	7650 $\mathrm{kg/m^3}$
Poisson ratio of steel	0.3
Young Modulus of copper	9.4 $\mathrm{GN/m^2}$
Mass density of copper	8953 $\mathrm{kg/m^3}$
Poisson ratio of copper	0.35
Conductivity of copper	4.257 $(\Omega.\mathrm{m})^{-1}$

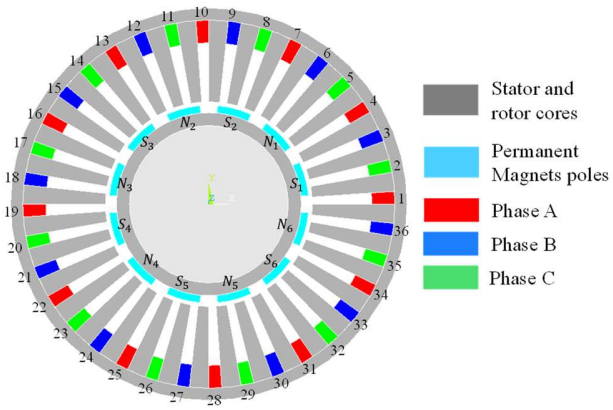

Figure 9: Laminated sheet of SPMM

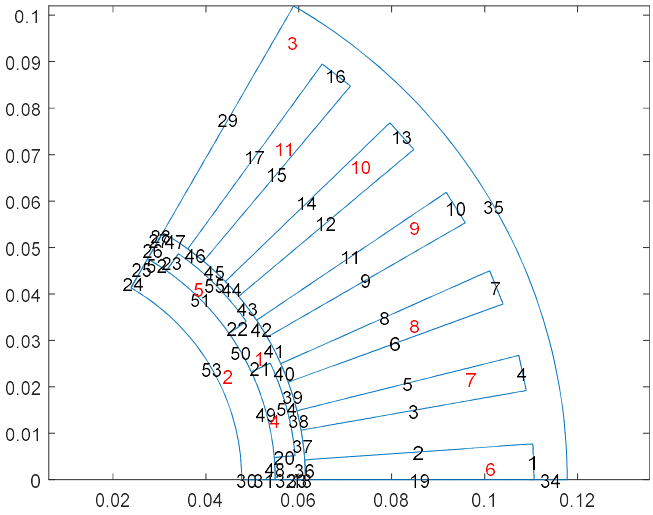

Figure 10: Two poles section of the SPMM's laminated sheet

In figure 10, the red numbers represent the domains of the model. 1 is the air gap. 2 is the iron part of the rotor. 3 is the iron part of the stator. 4 and 5 are the pieces of magnet. 6,7,8,9,10,11 are the slots. The numbers in black are dedicated for the edges of the model.

The input of the model, other than the parameters related to the type of materials forming each part of the machine, is the instantaneous voltage or current at each phase. The voltage and the current are supposed to be sinusoidal expressed in the following equations:

$$Va = Vm * (\cos(w * t)) \quad (1)$$

$$Vb = Vm * \cos((w * t) + \frac{2\pi}{3}) \quad (2)$$

$$Vc = Vm * \cos((w * t) + \frac{4\pi}{3}) \quad (3)$$

$$Ia = Im * \cos((w * t) + alfa) \quad (4)$$

$$Ib = Im * \cos((w * t) + alfa + \frac{2\pi}{3}) \quad (5)$$

$$Ic = Im * \cos((w * t) + alfa + \frac{4\pi}{3}) \quad (6)$$

$frequency = 66.8\ Hz$, $alfa = 0.483\ radians$, $Im = 29.3\ A$, $Vm = 312\ V$.

$w = 2 * \pi * frequency$.

2.2.1 Static current fed model

Finite element analysis is useful for models having complicate geometry and containing several types of materials with different properties.

It consists of dividing the domain subject of analysis into small elements called sub-domains where the differential equation for each domain is built separately. The sub-domain or the finite element can be a triangle or a trapezoid. The triangle finite element is illustrated in figure 11.

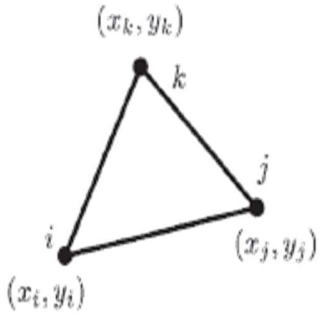

Figure 11: Sub-domain or finite element

Then, the combination of the whole sub-systems forms the governing general system:

$$[S + T] * [A] = [J] \quad (7)$$

[S]: Stiffness matrix (a characteristic matrix of a FEM sub-domain)
[T]: mass matrix
[A]: potential vector
[J]: current density vector

Where: $S = \left(\frac{1}{4*\mu*\Delta}\right) * \begin{pmatrix} b_i^2 + c_i^2 & b_i b_j + c_i c_j & b_i b_k + c_i c_k \\ b_i b_j + c_i c_j & b_j^2 + c_j^2 & b_j b_k + c_j c_k \\ b_i b_k + c_i c_k & b_j b_k + cjc_k & b_k^2 + c_k^2 \end{pmatrix}$

And, $b_i = y_j - y_k; c_i = x_k - x_j$.

$$T = \frac{j * w * \sigma * \Delta}{12} * \begin{bmatrix} 2 & 1 & 1 \\ 1 & 2 & 1 \\ 1 & 1 & 2 \end{bmatrix} \quad (8)$$

w: angular frequency
σ: electrical conductivity
Δ: area of the triangle

The solution of the FEM is the vector potential "A" and the input is the current density "J". In electrical machine analysis, the potential vector in its own is not of big importance, however, it is useful to generate other important parameters like flux density (see equation 9).

$$\nabla \times A = B \quad (9)$$

Figure 12 is a general block diagram representation of the current fed FEM.

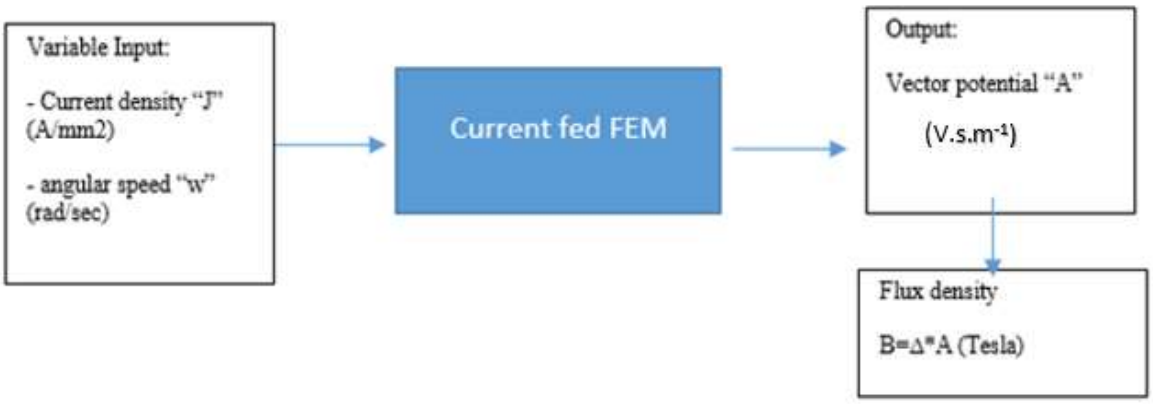

Figure 12: Current fed FEM

To solve properly equation (7) and get unique result, at least the solution (potential A) at one point in the electrical machine should be known or assumed. Hence, boundary conditions are mandatory.

Boundary Condition

Several boundary conditions can be applied in finite element method.

When the potential is specified at a point, we call it Dirichlet boundary condition. When the potential at a point is set to zero, we call it homogeneous Dirichlet boundary condition. When the derivative of the potential, at a point, is constant, we call it Neuman boundary condition. When this constant is zero, we call it homogeneous Neuman boundary condition [71].

In our model, the applied boundary conditions are:

- Homogeneous Dirichlet's boundary condition where the potential is set to zero at the outer boundary of the SPMM. The potential at the upper edge of the slot is also set to zero since this edge is considered as a flux line.
- Newman's boundary condition is also applied since there is symmetry in the laminated sheet and the flow of flux lines in SPMM is repetitive for each two poles. Hence, the finite element analysis can be done for two poles only.

In this section we will mention some notes that are considered in the finite element modeling. First, the electrical machine has similar configuration all through its axial length. Hence, it is common to model the electrical machines in two dimensions instead of three. Second, there is symmetry in the geometry of the machine's laminated sheet where all poles are identical, hence, it is common to model two poles instead of the whole laminated sheet of the machine. These two assumptions and considerations are advantageous because it reduces the size of the stiffness matrix which leads to reduce the time of simulation.

Magnet Modeling in FEM

For the magnet modeling, two main approaches exist, both of them follow the same concept and generates the same results. The first is the magnetization vector approach, the second is the equivalent current sheet approach. Demerdach in [8] has developed and improved the equivalent current sheet method to be applied on magnets having any arbitrary shape. The equivalent current sheet approach consists of replacing the magnet by two thin equivalent conductors representing the magnetic potential of the magnet [72] [73].

The equivalent current at a point of an arbitrary subdomain (triangle) located in the magnet will be:

$$I = \frac{Hc}{2} * (c\cos\theta - b\sin\theta) \tag{10}$$

C and b: are parameters related to the x and y coordinates of the point.
Θ: angle depending on the sense of magnetization of the magnet
Hc: coercive force of the magnet (A/m)

Figure13 shows the flow of flux lines in the laminated sheet when zero current is flowing in the phases. The flux density generated from the contribution of the stator alone is presented in figure 14. The air gap flux density coming from stator contribution is illustrated in figure 15. The flux lines distribution in the machine coming from the contribution of the stator alone is illustrated in figure 16.

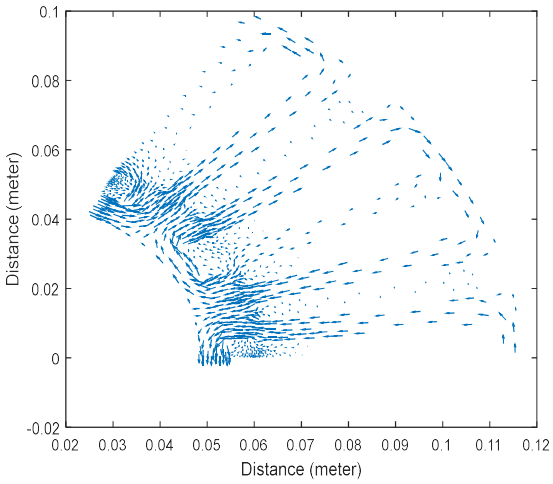

Figure 13: Flow of flux lines in the machine with zero current in the phases

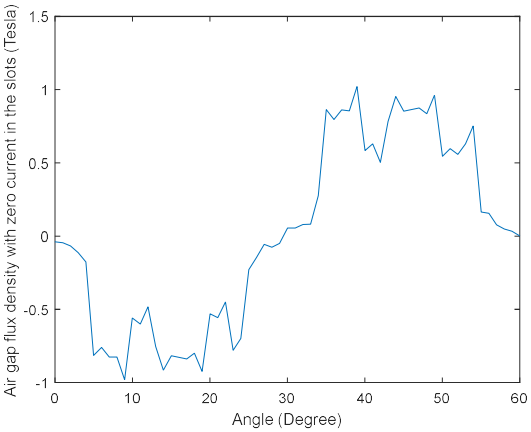

Figure 14: SPMM's air gap flux density with zero current in the phases

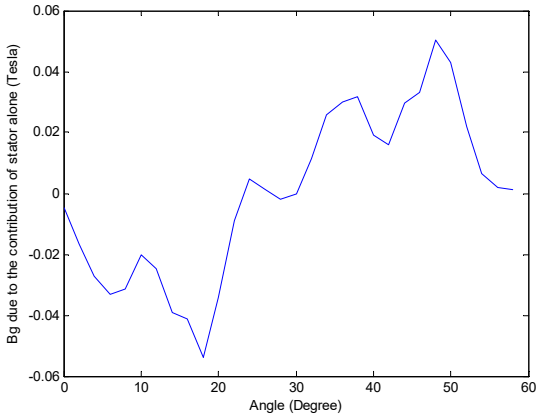

Figure 15: SPMM's air gap flux density coming from stator contribution only

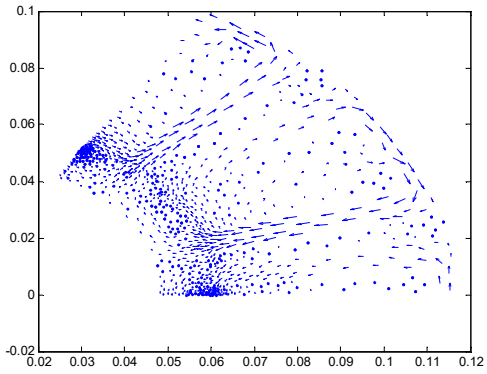

Figure 16: Flux lines (stator contribution)

Figure 17 shows the distribution of the flux density in the laminated sheet where the maximum reached flux density is 1.68 Tesla which is tolerated according to [4]. Figure 18 illustrates the total flow of flux lines inside the machine. Figure 19 represents the total air gap flux density of the machine.

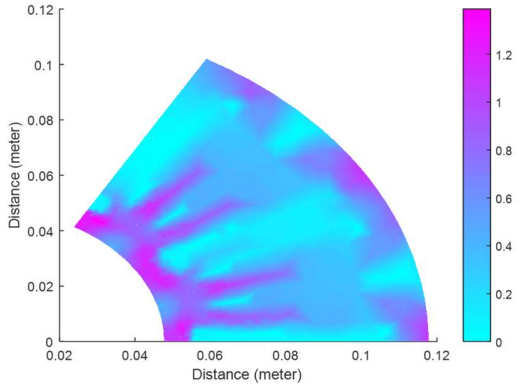

Figure 17: Distribution of total flux density inside the machine in Tesla

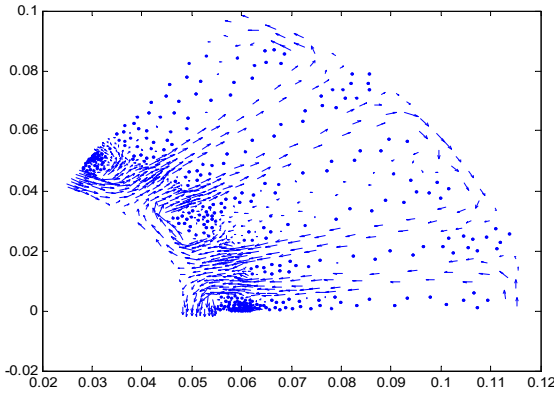

Figure 18: : Total flux lines in the SPMM

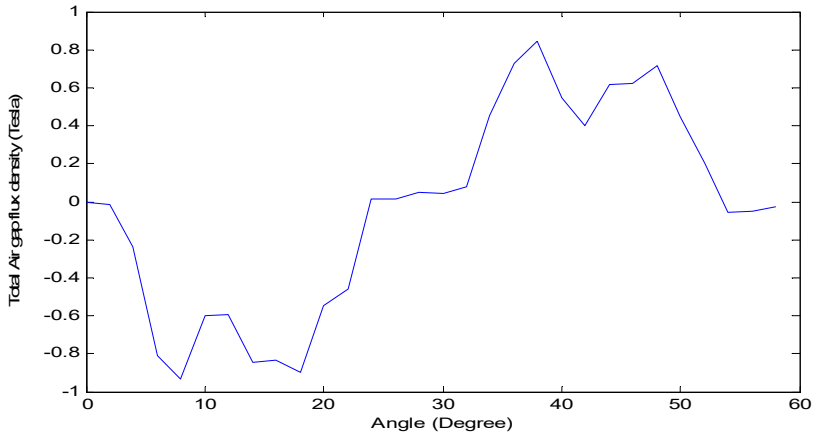

Figure 19: Total air gap flux density of the SPMM

2.2.2 Static voltage fed model

The implementation of a voltage fed finite element model is executed where a results similar to the current fed FEM are generated.

The global system equation of voltage fed finite element model is:

$$\begin{bmatrix} [S]+jw\sigma xy[T] & -jw\sigma z[C] & [0] \\ -jw\sigma z[C]' & jw\sigma z[\Omega b] & -jw[D] \\ [0] & -jw[D] & -jw[Zext] \end{bmatrix} * \begin{bmatrix} A \\ \frac{Es}{jw} \\ \frac{Ic}{jw} \end{bmatrix} = \begin{bmatrix} 0 \\ 0 \\ -Vs \end{bmatrix} \quad (11)$$

{Ic}: the circuit current vector
{Es}: the bar voltage vector

[D]: the bar connection matrix
[Ωb]: the bar cross sectional area diagonal matrix
[C]: the matrix of integration weights used in the area computation
[zext]: the circuit external impedance diagonal matrix
{vs}: the circuit voltage vector.

Figure 20 presents the voltage fed FEM in a block diagram.

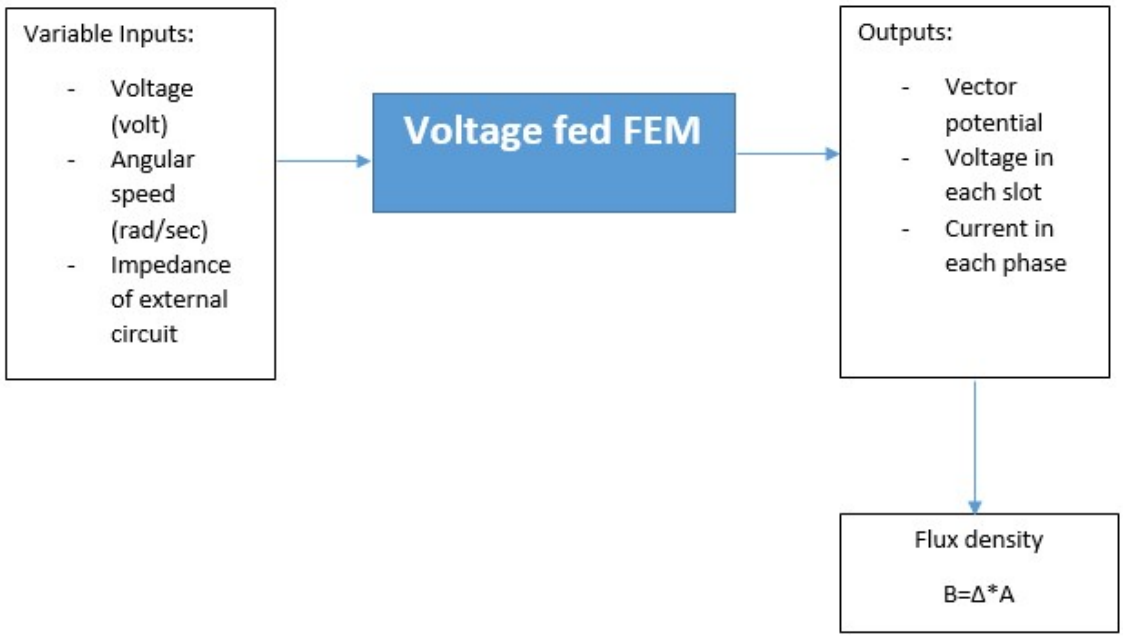

Figure 20: Voltage fed FEM

The simulation of the voltage fed FEM model generates the total air gap flux density in figure 21 and the flow of flux lines in figure 22.

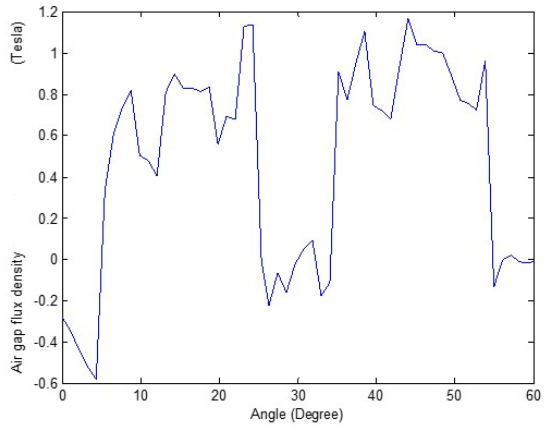

Figure 21: Air gap flux density (Voltage fed model)

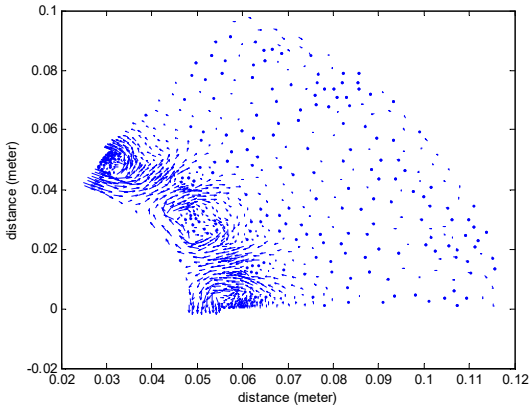

Figure 22: Flux lines (Voltage fed model)

2.2.3 Dynamic Time Stepping FEM

Although static finite element analysis gives a good presentation of the electromagnetic aspect of the machine, the generation of a dynamic model is of big interest.

First, in general, the electrical machine needs to be coupled to an external circuit representing the input supply or source of power; this source is usually time dependent.
Second, the motion of the rotor should be considered in the modeling because of the flux coupling effect between stator and rotor. In other words, when the rotor changes its position, the distribution of flux inside the machine changes.
Third, the final end goal is to apply a real time prognosis scheme. Since the data that will be input for the prognostic model will come from the FEM, this model should be dynamic.
In [72], a time stepping finite element model is presented for induction machine. This model has been manipulated and adapted to be applied for Permanent magnet machine.

The first step in the dynamic FEM is discretization, which converts a continuous physical model into a discrete mathematical model.
The second process is the linearization. The field equation and the acceleration equations are non-linear functions of vector potential A and/or rotor displacement *x*. However, like any non-linear function, when studied for a very small period of time it can be treated as linear. Hence, the field and acceleration equations must be linearized before they can be combined with the other equations of the system in a global matrix equation.

In figure 23, the block diagram of the dynamic model is illustrated.

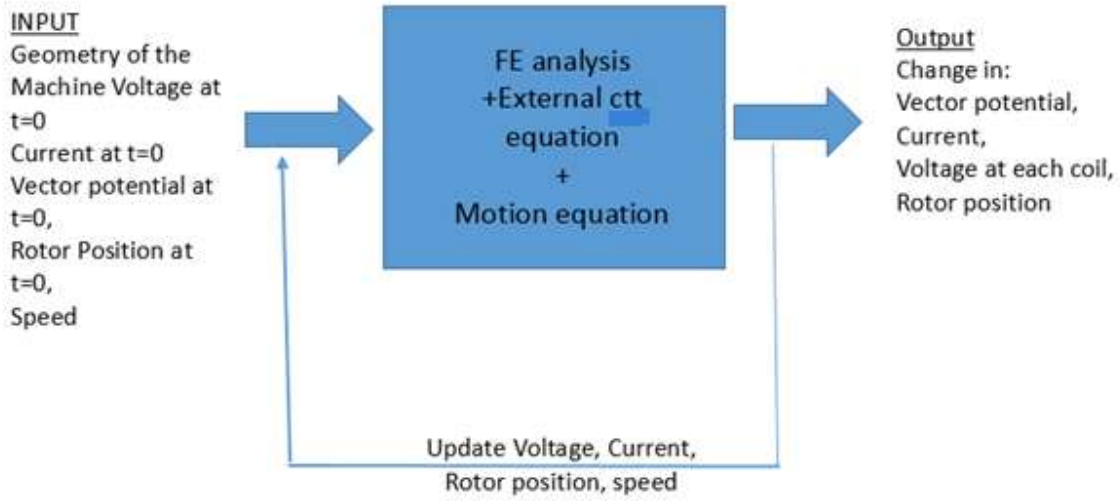

Figure 23: Block diagram of Time Stepping FEM

The governing equations of the system are:

- The time-dependent magnetic diffusion equation

$$\nabla * \nu \nabla * \mathrm{A} = \frac{\sigma \mathrm{Vb}}{\mathrm{l}} - \sigma \frac{\partial A}{\partial t} + \sigma v * \nabla * A \tag{12}$$

- Expression of current in each conductor

$$I \iint \left(\sigma \frac{Vb}{l} - \sigma \frac{\partial A}{\partial t} \right) dx\, dy \tag{13}$$

- Circuit Equation: Series Bar-Coil Equation

$$Vc = \{db\}\{Vb\} + Lext \frac{dIc}{dt} + Rext\ Ic \tag{14}$$

- Circuit Equation: Parallel Coil Equation

$$Vb = Rs\ \{1\}'\{I\} + Ls\{1\}' \left\{\frac{dI}{dt}\right\} + Vc \tag{15}$$

- Mechanical Acceleration Equation

$$m \frac{dv}{dt} + \lambda v = Fem - Fext \tag{16}$$

- Mechanical Velocity Equation

$$v = \frac{dx}{dt} \tag{17}$$

ν: reluctivity
A: vector potential

σ: conductivity
Vb: voltage across rotor's bar (the equivalent of the magnets)
l: axial length of the machine
v: linear rotor's speed
t: time
I: current in each conductor
Vc: voltage across series coils (stator's coil)
db: a diagonal matrix with entries of + 1 or -1, indicating the polarity of each bar in the coil
Lext: coils' equivalent inductance
Rext: coils'equivalent resistance
Rs: parallel conductor's equivalent resistance
Ls: parallel conductor's equivalent inductance
m: rotor's mass
x: rotor's position
λ: damping factor (in synchronous machine this value is almost zero)
Fem: electromagnetic force
Fext: externally-applied mechanical force (load).

After Discretization and Linearization, the global matrix of the system is:

$$\begin{bmatrix} M11 & M12 & 0 & 0 & M15 \\ M12' & M22 & M23 & 0 & 0 \\ 0 & M23' & M33 & M34 & 0 \\ 0 & 0 & M34' & M44 & 0 \\ M15' & 0 & 0 & 0 & M55 \end{bmatrix}^{t+\Delta t}_{k+1} \begin{bmatrix} \Delta A \\ \Delta Vb \\ \Delta I \\ \Delta Vc \\ \Delta x \end{bmatrix} = \begin{bmatrix} N1 \\ N2 \\ N3 \\ N4 \\ N5 \end{bmatrix} \quad (18)$$

The system is solved using Newton Raphson method. For each step of rotation, the Stiffness matrix of the system is updated using this coordinates transformation:

$$xnew = xold * cos\theta - yold * sin\theta \quad (19)$$
$$ynew = yold * cos\theta + xold * sin\theta \quad (20)$$

Θ is the rotating angle of the rotor.

The solution gives the change in the vector potential, voltages, currents and rotor position. Hence, for example, $Anew = Aold + \Delta A$.

To make sure that the solution doesn't diverge, a check should be done after each iteration where a preset tolerated error is taken into consideration. If the solution diverges, this means the step size is not adequate and the model has loss of credibility.

One important issue that assure the accuracy and success of the dynamic model is the time stepping. From the time step we deduce the angle step.

According to [74], the step size Δt is maximum equal to $\frac{1}{20*f}$. And, the minimum integration time is $Tf = N * \Delta t$.

Where N is the sampling point that should be power of 2. However, to guarantee exactitude, the step size is better to be tenth of Δtmax.

The frequency of our system is 66.8 Hz. Δtmax=7.49*10^-4. Δxmin= linear speed * Δt= 24 m/sec * 7.49*10^-4 sec=0.018 m. Rotating step angle= 360*Δx/Rotor Perimeter=~ 10 degree (max).

However, this step of rotation diverged the results radically. Hence, after trial and error the rotation step is settled to 0.9 degree, and the time step of 3.7425e-05 sec.

In each iteration, the generated displacement Δx is compared with the maximum tolerated (calculated) displacement which is(2*pi*0.05942) *(0.9/360) *1.1. (The maximum permissible considered error is 10%).

The simulation is done for 5 revolutions.

A sketches of the rotor's swept in different times of simulation is presented in figure 24.

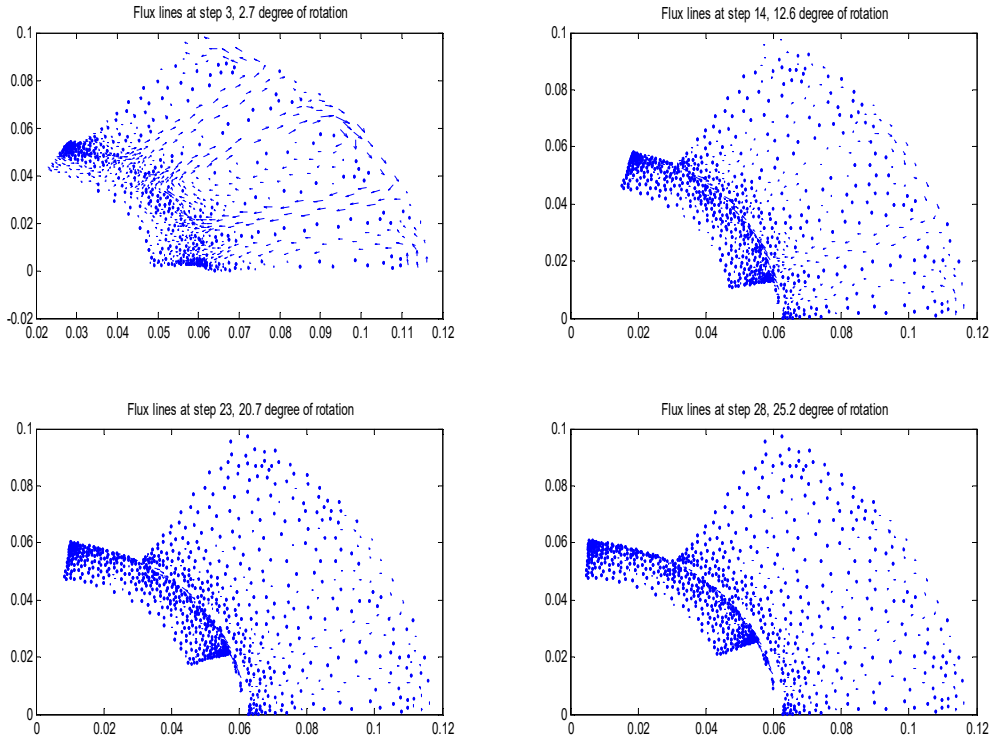

Figure 24: : Flux lines at 4 different moments during the rotation from 0 to 30 degree (Healthy machine)

2.3 Thermal finite element model

Many research papers had taken advantage of the thermal modeling of electrical machine to monitor its state and improve its operation

In [75], the author implemented the thermal model to investigate the cooling phenomena inside the machine and to optimize its geometry versus the selected cooling system. The convection phenomena are represented using empirical dimensionless analysis formulations. A Commercial software package named Motor-CAD is used for this purpose. G. D. Paper [76] states that thermal modeling of electrical machine is very useful to detect any rise of temperature inside the machine; however, many are not recognizing its importance. The aim of this paper is to generate an analytical Thermal model for a permanent magnet machine. Its model is confronted with a finite element thermal model. A review on the different techniques of thermal behavior used for electrical machine is presented in [77]. The mentioned techniques are: lumped parameter thermal model (LPM), finite difference, finite elements and computational fluid dynamics (CFD). Plus, it presented some experimental methods that evaluate precisely and accurately results for machine design and fabrication. This thermal analysis is important to protect the insulation, bearings, permanent magnet, the glue used to attach the magnets and to prevent excessive heating of the surroundings in the case of overload. Paper [78] couples the thermal and the electromagnetic FE model of a power transformer to describe its performance in the case of winding short circuit fault. No papers have encountered the thermal FEM of electrical machine in the aim of detecting the presence of fault at its early stage.

In general, losses in electrical machine are caused by the fundamental components of the stator and rotor currents, hysteresis losses in the iron core, eddy current losses in the conductors, iron core and frame and friction losses. All, can be represented in the thermal model.
In healthy case, the main source of heat inside electrical machine is in the windings, where losses are dissipated as heat.

Due to the difference in temperature inside the machine, heat transfer occurs. In principle, heat transfer occurs from hotter zones to cooler zones.

There are three kinds of heat-transfer mechanisms: conduction, convection and radiation.
Heat conduction is the transfer of heat from one solid to another due to the temperature difference between those two solids.
Heat convection is the transfer of heat by mass motion of a fluid such as air or water when the heated fluid is caused to move away from the source of heat.
Heat radiation is the transfer of heat by the emission of electromagnetic waves which carry energy away from the emitting object [79].

The study of heat transfers in electrical machine and specially in permanent magnet machine is of big interest. First, knowing the sensitivity of magnets toward temperature, we care of avoiding magnet demagnetization [80]. Second, the carbon-fiber sleeve that holds the magnets is also very sensitive to temperature and has restricted limits. Moreover, the insulation of the stator winding has also temperature limit to avoid its deterioration [81].

Convection is the primarily phenomenon that transfers heat out from the machine. This is done by mean of the air gap or between machine's periphery and outward environment. Convection can be natural or forced.

The thermal FEM will be developed for the SPMM in the healthy and faulty case. The target is to detect the presence of fault at its early stage and to identify, later on, the impact of this preliminary fault on the aging of the machine's component; mainly on the permanent magnet and on the winding's insulation.

2.3.1 Thermal model equations and specification

The governing equation of heat transfer for any application is [82]:

$$\rho\ Cp\ tz \frac{\partial T}{\partial t} - k\ tz\ \nabla^2 T = Qd + Qc + Qr \tag{21}$$

ρ: material density, kg/m^3
Cp: the specific heat, J/kg.K
tz: the thickness model
k: thermal conductivity, W/m.K
t: time, sec
T: temperature at a particular x and y location, K
Qd: heat source, watt/m^2

The amount of heat transferred from a surface, per unit area, due to convection is expressed as:

$$Qc = hc * (T - Ta) \tag{22}$$

Ta: ambient temperature
hc: convection coefficient, W/m^2.K

The amount of heat transferred per unit area, due to radiation is expressed as:

$$Qr = \epsilon\ \sigma\ (T^4 - Ta^4) \tag{23}$$

ϵ: emissivity of the face
σ: Stefan-Boltzmann constant, W/m^{2}K^4

The heat general heat equation is a parabolic partial differential equation.
The aim of the thermal analysis is to know the distribution of temperature in all the machine in general, at the magnet level in specific and at the machine's boundary knowing that the maximum allowable temperature for the used magnet is 150 °C.

Both steady state and transient analysis are performed.
In a steady state analysis, we are interested in the final temperature at different points in the laminated sheet of the machine after it has reached an equilibrium state. In this analysis, the element encountering ∂T/∂t in the governing thermal equation is set to zero.

In a transient analysis we are interested in the temperature in the laminated sheet function of time. In this analysis we can know how long does it take the machine to reach an equilibrium temperature.
The block diagrams in figure 25 and 26 shows the input and the output of the steady state and transient thermal analysis.

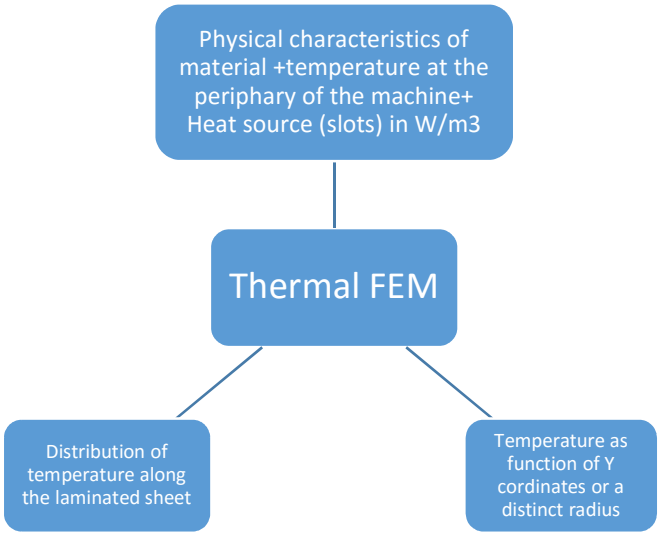

Figure 25: Block diagram of the thermal steady state analysis

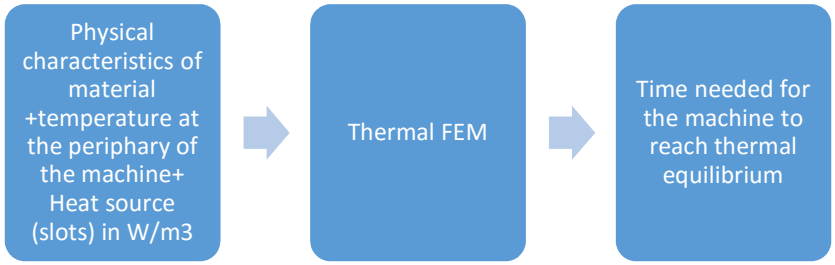

Figure 26: Block diagram of the thermal transient analysis

In the thermal finite element model, we set homogeneous boundary condition where the temperature at the outer periphery of the machine is set to 40°C. (this value will come from the sensor measurement located at the periphery of the machine). We also applied Neuman boundary condition where the flux lines cut the section of the laminated sheet in perpendicular direction.
In table 7, the physical characteristics of the materials constituting the machine are represented.

TABLE 7: PHYSICAL AND THERMAL CHARACTERISTICS OF MACHINE'S MATERIAL

	Thermal conductivity, W/(m-K)	**Density, kg/m^3**	**Specific heat, J/(kg-K)**
Steel	36	7850	490
Copper	400	8960	386
Air	0.02	1.225	1000
Magnet	9	7400	460

The ambient temperature is set to 20°C.
The transfer of heat coming from radiation is not encountered. Only conduction and convection (that has the big interfere in heat exchange) is taken into consideration.
The convection is represented as boundary condition at the outer periphery of the machine.
In the prototype we are using, the thermal protection of the machine starts when the temperature reaches a minimum value of 150°C.

The input of the model, other than the parameters related to the type of materials forming each part of the machine, is the instantaneous power across each coil. We chose to perform the analysis at t=0.09 sec, which is the time needed for the machine to execute one revolution.

2.3.2 Thermal model outcomes (Steady state analysis)

In the following we will show the outcomes of the thermal model and how the results can be represented and expressed in the case of healthy machine.

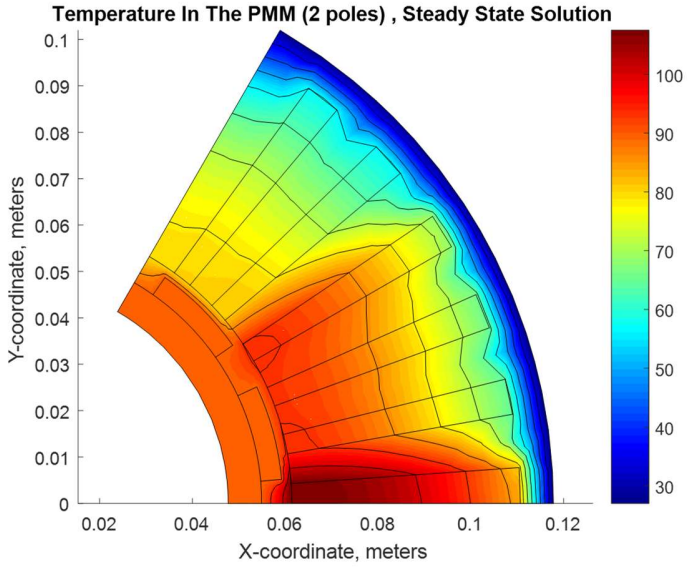

Figure 27: Distribution of temperature in the healthy PMM at Steady state

Figure 27 shows the distribution of temperature inside the electrical machine, in the healthy case. In figure 28, a useful way to represent or visualize the distribution of temperature inside the electrical machine is illustrated. The curve in the figure represents the value of temperature on a selected radial line through the laminated sheet. We chose a line that extends from the center of the machine to its periphery passing by the second piece of magnet.

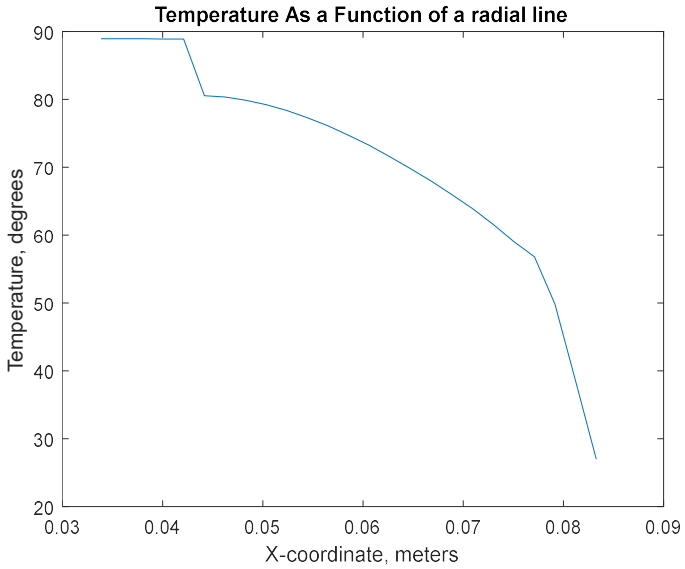

Figure 28: Temperature along radial line

2.3.3 Thermal model outcomes (Transient analysis)

The transient analysis of thermal model generates the change in temperature function of time. It is useful in specifying the time needed for the system to reach the steady state temperature stated in the previous section.
In this analysis, the part of the thermal governing equation that is function of time appears:

$$\rho \, Cp \, tz \frac{\partial T}{\partial t} \tag{24}$$

The initial value of the temperature at t=0 is set to 0. The simulation is done for several interval of time (5000, 10000, 15000, 20000, 25000 seconds). From the results illustrated in the figures 29 and 30, the steady state is reached after 20000 seconds; after this time, the results remain constant.

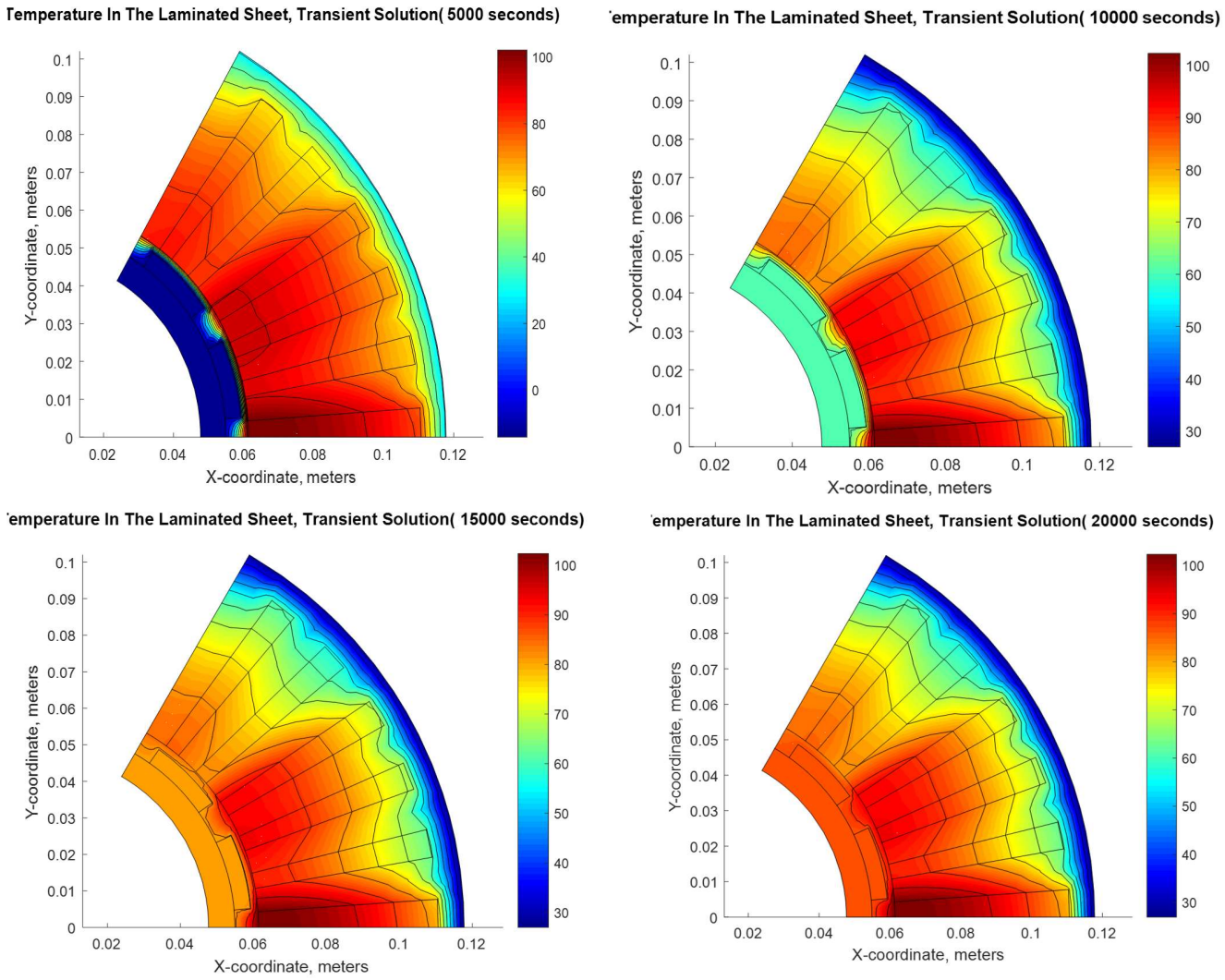

Figure 29: Distribution of temperature in the laminated sheet at t= 5000, 10000, 15000 and 20000 seconds

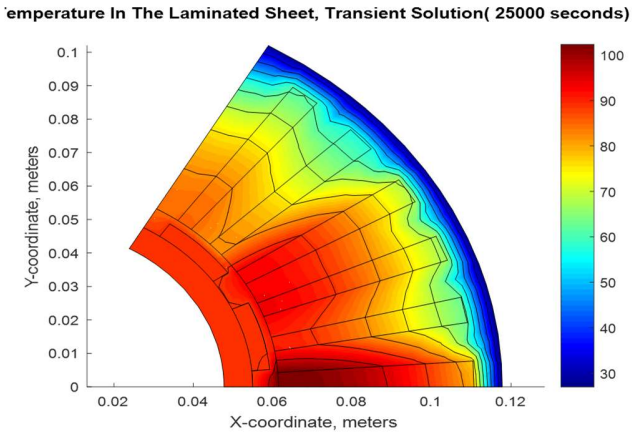

Figure 30: Distribution of temperature in the laminated sheet at t=25000

We remark that the steady state analysis and the transient analysis give the same results concerning the final value of temperature inside the machine.
Focusing on the piece of magnets and the coil's wire (conductor and insulation) inside the machine, we can get the variation of temperature of the targeted element function of time in figure 31 and 32.

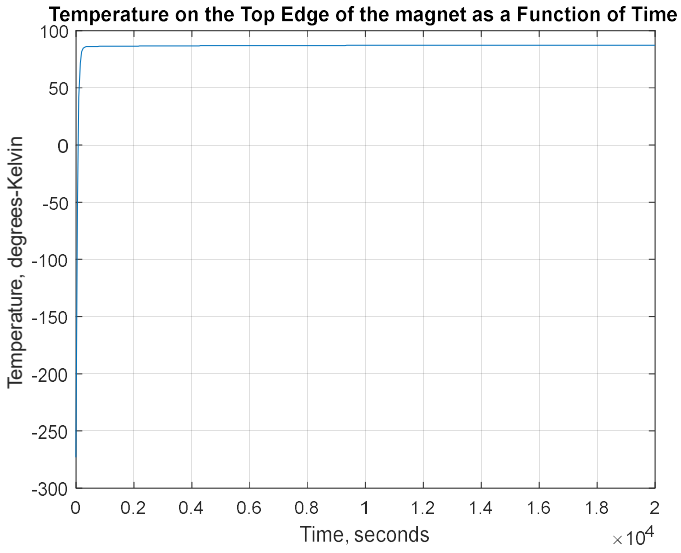

Figure 31: : Transient temperature on the top edge of the magnet

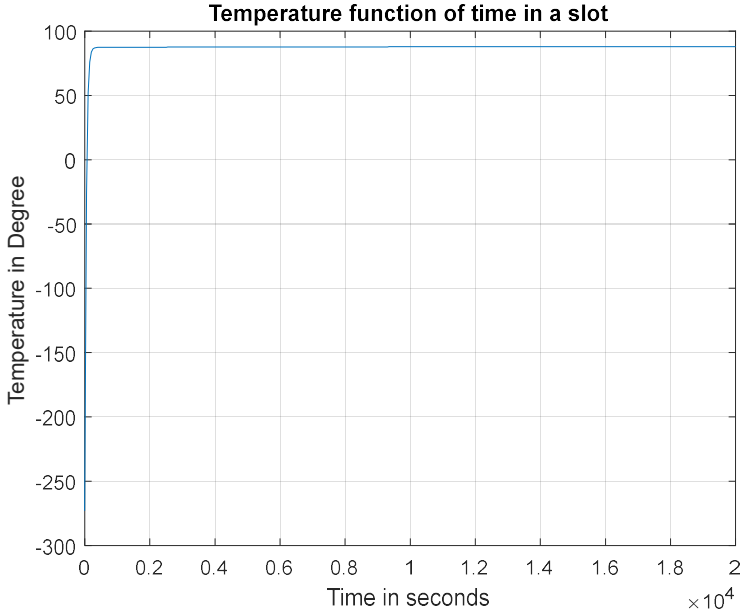

Figure 32: Variation of temperature function of time in the first slot

Figure 33 shows the temperature at a point on the machine's boundary function of time.

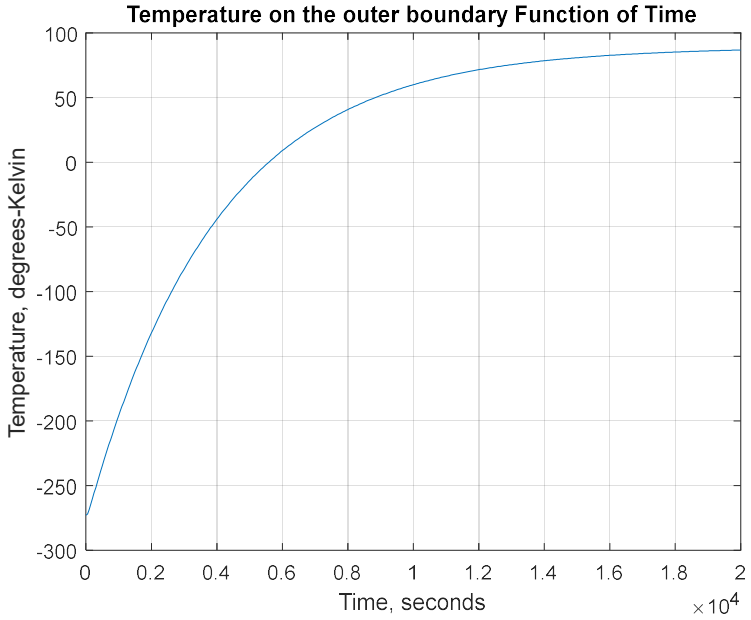

Figure 33: Transient temperature on the outer boundary of the Permanent magnet machine

2.4 Vibration finite element model

There is no analytical model of vibration for complicated geometries, hence, numerical method like finite element method is used to build a vibration model for electrical machines [83] [84].

The nonlinear vibration equation can be expressed as:

$$[M]\{x''(t)\} + [C]\{x'(t)\} + [K]\{x(t)\} = \{F(t)\} \quad (25)$$

[M]: mass matrix
[C]: damping matrix
[K]: stiffness matrix
x(t): displacement vector for each node
x'(t): velocity vector for each node
x''(t): acceleration vector for each node
F(t): load vector, force distribution acting on the stator.

The source of vibration in electrical machine can be classified as: mechanical, aerodynamic and electromagnetic force. The electromagnetic force is the most important having the highest intervention in causing vibration.
The audible sound for human is normally of frequencies between 20 Hz and 20 kHz but responds more to frequencies between 500 Hz and 8 kHz.

The quantity that couples the displacement field and the magnetic field is the vector of magnetic force density f(x,t).

The material characteristics needed for vibration finite element analysis are: modulus of elasticity, density and Poisson's ratio. The modulus of elasticity, the density and Poisson's ratio of the materials used in the permanent magnet machine are enumerated in table 8.

TABLE 8: MATERIAL CHARACTERISTICS NEEDED FOR VIBRATION MODEL

	Modulus of elasticity (10^9 N/m^2, GPa)	**Density (kg/m^3)**	**Poisson's ratio**
Steel	28.8	7850	0.3
Copper	110.3	8960	0.3
Air	0.000142	1.225	0 (air has no elasticity)
Magnet (NdFeB)	150	7400	0.24
Aluminum	66.2	2712	0.35

Wave motion can be: longitudinal (sound waves are examples of longitudinal waves), transversal (vibrating string is an example of transverse wave motion) and torsional.
Wave can be mechanical or electromagnetic. Mechanical wave need elastic medium to propagates; however, electromagnetic wave can propagate in vacuum.

Hyperbolic equation of wave [85]:

$$\rho(x)\frac{\partial^2(u^\circ)}{\partial t^2}(t,x) = Te\frac{\partial^2(u^\circ)}{\partial x^2}(t,x) + f(t,x) \tag{26}$$

ρ: density
Te: tension
f: external force

The above equation is customized to meet the standard equation shape of the pde tool in Matlab.

$$G\Delta\mathcal{E} + (\lambda + G)\nabla(\nabla.\mathcal{E}) + fB = \rho aL = \frac{\partial^2\mathcal{E}}{dt^2} \tag{27}$$

G: modulus of elasticity
λ: Poisson's ratio

The electromagnetic force in electric machines are mainly generated in the air gap and are acting on the iron part of the stator. In finite element modeling, this force can be represented by its

resultant at each teeth of the stator [85]. Accordingly, this force will be expressed in the model by the Neumann boundary condition, and it will be settled to zero in the elliptic equation of vibration.

Electromagnetic force calculation:

Electromagnetic force calculation can be realized using two methods: one based on Maxwell stress tensor and one based on the principle of the virtual work [86].
According to Maxwell stress tensor, the electromagnetic force can be obtained as a surface integral:

$$F = \oint_S \sigma \, dS \tag{28}$$

σ: Maxwell stress tensor (it is a surface force density; it's unit is N/m2)

There is a relation between the Maxwell stress tensor and the flux density. It is expressed as:

$$\sigma(x,t) = \frac{1}{2\mu 0} * \left(Br(x,t)\right) \tag{29}$$

Br: radial component of flux density

The electromagnetic force in the electrical machine is mainly the force in the air gap acting on the stator; Maxwell stress tensor in the air gap is generated from the electromagnetic finite element model. In electromagnetic FEM, the flux density is interpolated for each triangle; then, the Maxwell stress tensor and the electromagnetic force is generated for each finite element. Since the displacement due to vibration should be elaborated at each point in the electric machine, the magnetic force for each finite element, the triangle, will be distributed using a weighted function on the corners of the triangle.

The vibration model, needs to be built after the electromagnetic model, since the input of the vibration model, other than the physical characteristics of the material, is the radial electromagnetic force applied to the stator, especially on the teeth of the stator.
Since the vibration model is mainly impacted by the electromagnetic force applied on the teeth of the stator, no need to model the whole machine, the iron part of the stator is only considered as seen in figure 34.

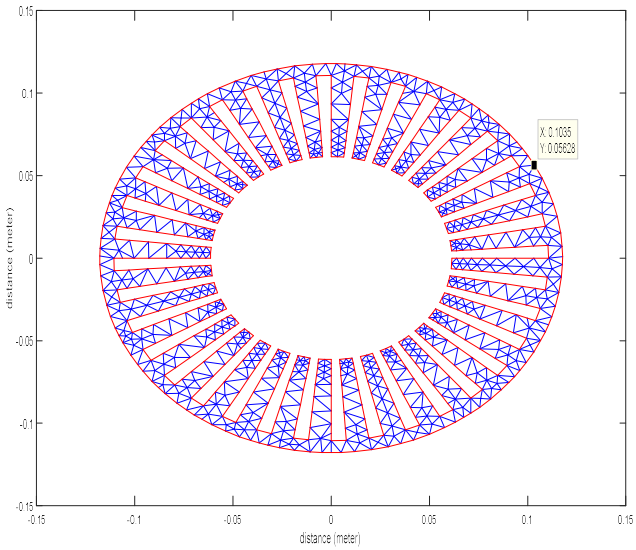

Figure 34: Stator's iron part of the laminated sheet

Figure 35 shows the distribution of electromagnetic forces in air gap. Figure 36 a zoomed view of figure 35. Figure 37 shows the vibration in space at the machine's boundary when nominal voltage is considered at the phases. Figure 38 is an illustration of the stator displacement.

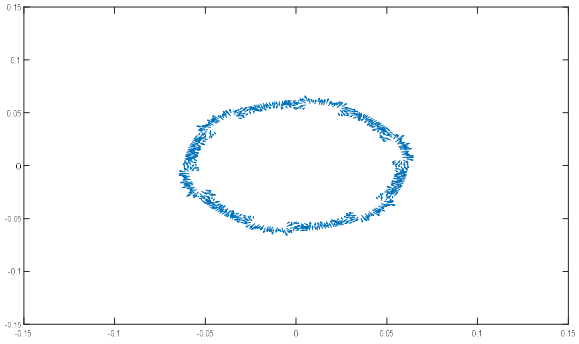

Figure 35: Distribution of electromagnetic forces in the air gap

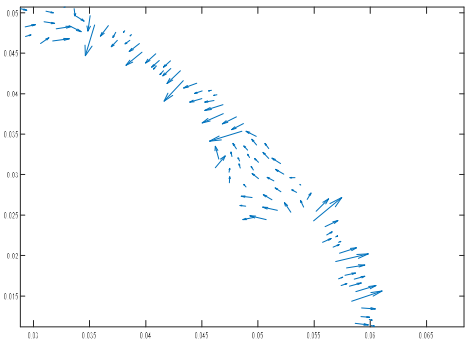

Figure 36: Zoom figure 35

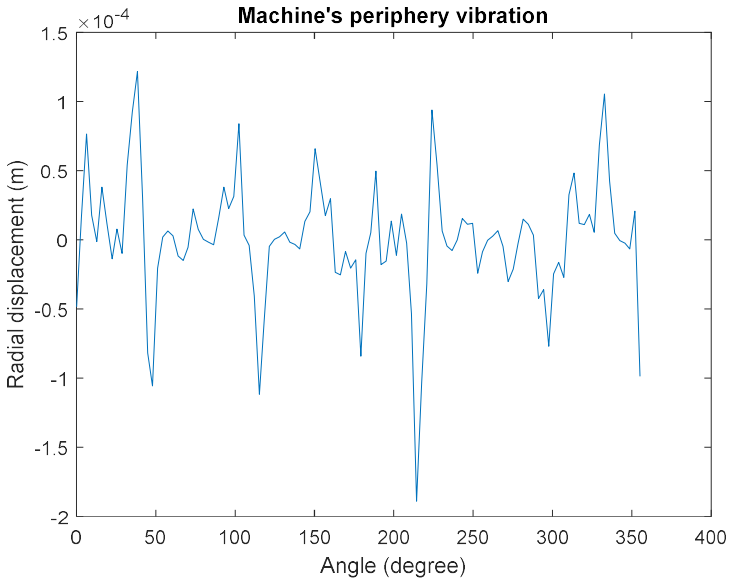

Figure 37: Vibration on the periphery of the SPMM

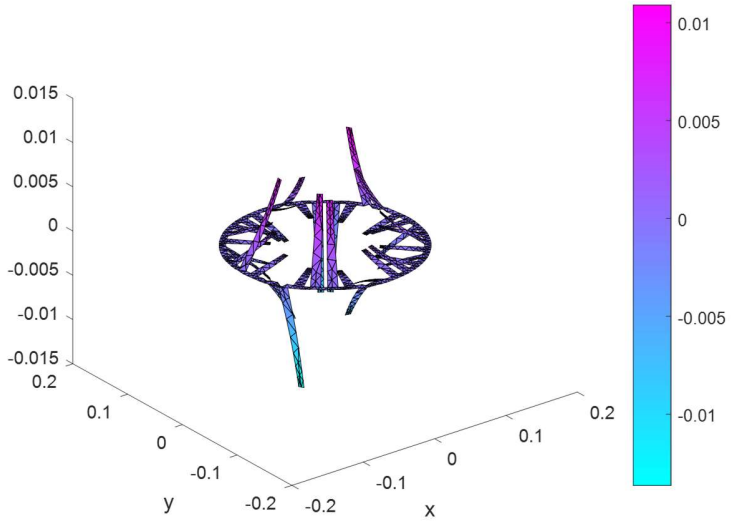

Figure 38: : Stator's displacement in mm (Healthy machine)

2.5 Integration of faults in FEM

In this section we will integrate the three selected types of faults in the FEM: demagnetization presented by a crack in one magnet, turn to turn short circuit fault and eccentricity fault. Some

simulation results concerning the electrical, thermal and vibration aspects of the machine are presented.

2.5.1 Demagnetization fault

A crack at the upper periphery of the magnet of the first pole is executed. Figure 39 is zoomed view of the meshed machine's laminated sheet when there is a crack on the upper periphery of the magnet. The red lines in the figure are the geometry of the machine and the blue lines are the mesh generated by the pde tool in Matlab.

The direction of the crack is radial, parallel to the flux lines. The crack is between 12 and 23 degrees. We can see that there is no flux leakage at the periphery of the magnet. However, due to the crack, the density of flux lines has increased at the two right and left side of the magnet. The flow of flux lines in this case is shown in figure 40. This has increased the flux focusing in the teeth of the laminated sheet where the maximum flux density reached 1.92 Tesla. This is an alarming value since the maximum permissible flux density in the core is 1.7 Tesla. At the health state, with no crack in the magnet, this value was 1.68 Tesla.

The air gap flux density in the area above the crack has almost conserved its shape but with lower values this means lower average air gap flux density, hence, lower torque and lower power as we will see later in the coming chapter.

Simulation has been done for two different radial depth of crack: 1 mm and 3 mm. figure 39 shows a zoomed view of the cracked magnet. Figure 40 shows the flux lines in this case; the black arrows point at the flux focusing on the right and left side of the crack. In figure 41, the air gap flux density for the two depths of cracks is elucidated.

Comparing the graphs in figure 41, we remark that the two air gaps have similar shape but different flux density values. As the crack deepen, the flux density above the interval of the crack decreases. However, the maximum flux density in the machine, due to flux focusing, remain the same whatever is the depth of the crack. This is convenient for this type of cracks (crack parallel to flux lines) because the flux lines tend to concentrate at the edges of the crack regardless its depth.
Yet, changing the interval of the crack will change the results.

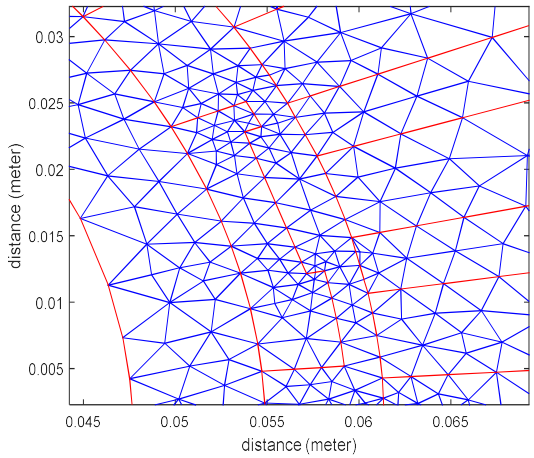

Figure 39: Crack in the magnet of pole 1

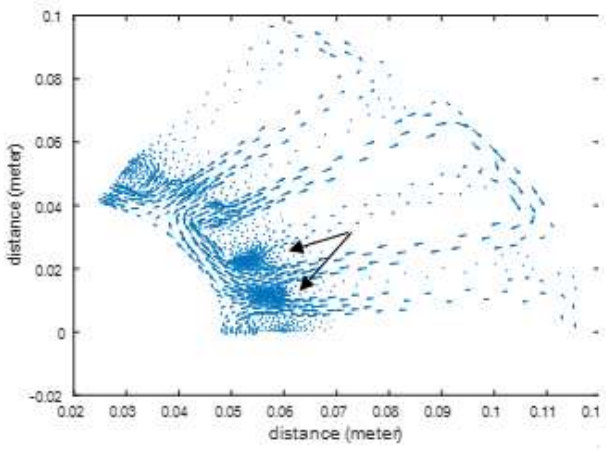

Figure 40: Flux focusing due to the crack

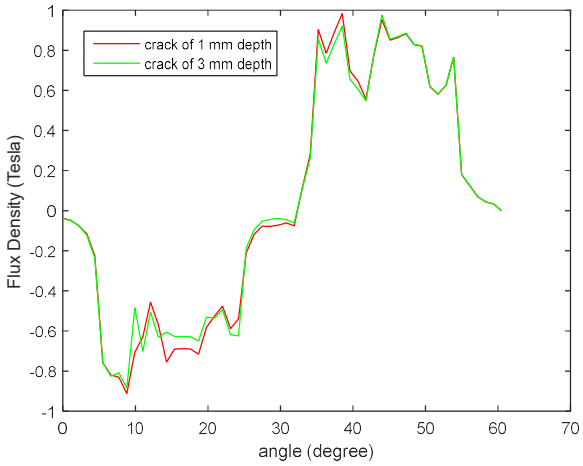

Figure 41: Air gap flux density for 1 and 3 mm crack

Moving to the thermal FEM, the distribution of temperature inside the machine in the case of healthy machine and machine with crack in one magnet is presented in figures 42 and 43 respectively. We mention that the 12 poles of the machine are modeled. We can see that the distribution of temperature in the two cases is almost similar. A miniature crack in the magnet change slightly the geometry of the machine and has no impact on the source of heats inside the machine which are the slots; that's why this fault has no impact on the distribution of temperature inside the machine.

The vibration in the iron part of the stator in the case of a crack in one magnet is illustrated in figure 44. Comparing figure 44 and figure 38 that illustrates the vibration in the healthy case, we can see that the displacement has decreased in the case of crack.

The presence of the crack in the magnet decrease the air gap flux density in the range of the crack. This decreases the electromagnetic force acting on the stator's teeth. The vibration is directly proportional to this electromagnetic force; hence, the displacement of the machine decreases in this type of fault.

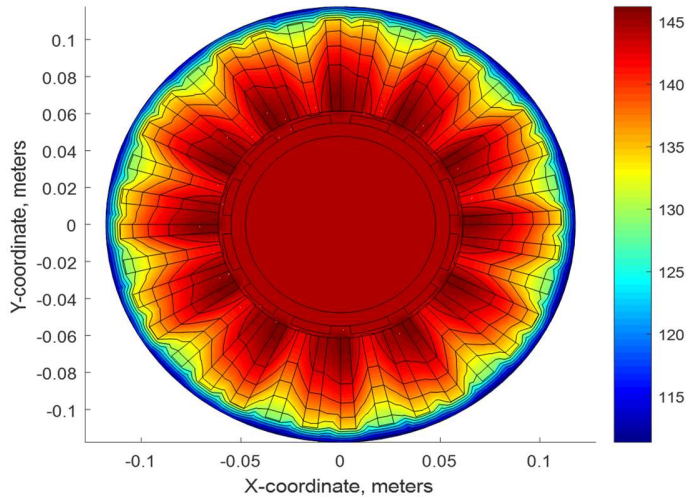

Figure 42: Distribution of temperature (°C) in the machine (Healthy case)

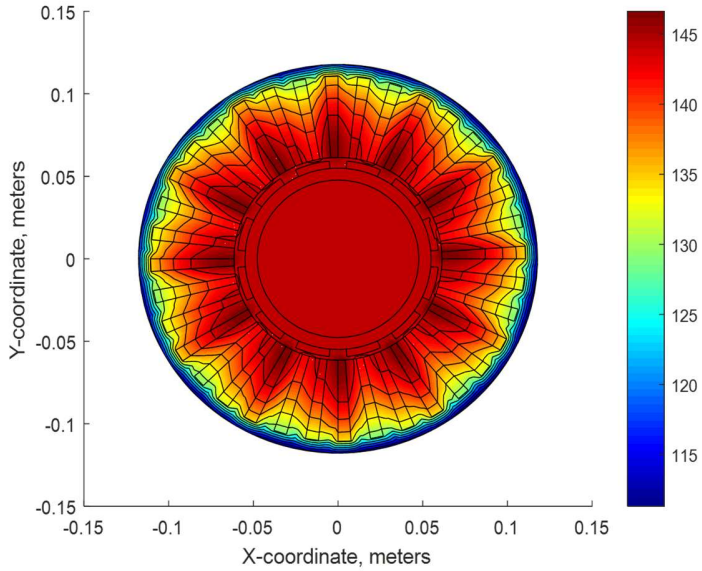

Figure 43: Distribution of temperature (°C) in the machine (in the case of crack)

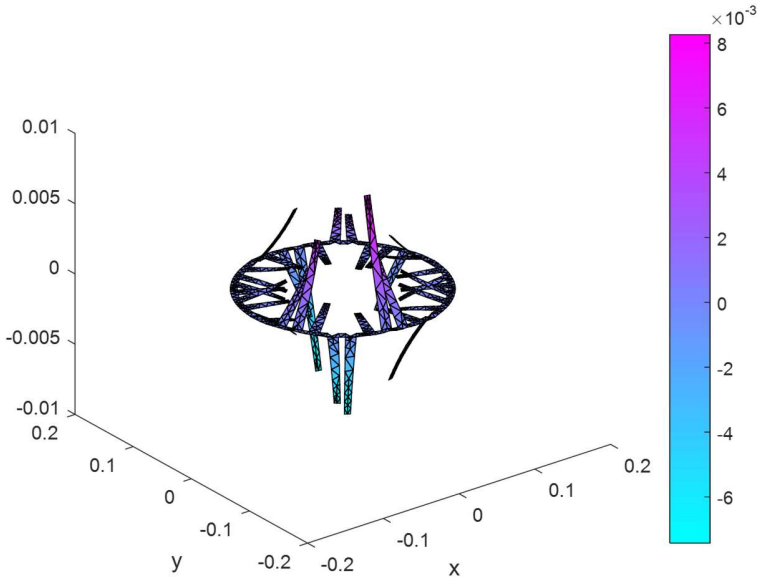

Figure 44: Vibration of the machine's stator in mm (in the case of crack)

2.5.2 Turn to turn short circuit fault

The second type of fault that will be tested and integrated in the machine's modeled is the turn to turn short circuit in one of the machine's slots.
The main causes of turn to turn short circuit are: thermal stress, mechanical stress and electrical stress. The sources of electrical stress are: supply voltage transient coming from line to line, line to ground or three phase fault, lightning, variable frequency drive, open and close of CB [87].

In the case of turn to turn short circuit the current in the faulted turns/coil increases. Its increase is expressed as following: [88]

$$Inew = \left(\frac{1}{1-\alpha\%}\right) * Irated \tag{30}$$

Inew is the value of current flowing in the turns after the fault.
Irated is the rated value of the current flowing in the coil or the value of the current at healthy case.

α is the ratio of the number of shorted turns to the number of total turns in the dedicated coil.
For example, in our machine, the number of turns per coil is 13. If one turn is shorted, the new current flowing in the coil became 1.09 times the old/rated current.
We mention that the turn to turn short circuit is a propagating fault. If it persists, it leads to total short circuit of the coil.

In table 9, the value of currents flowing in the faulty coil from the early stage of short circuit turns to the total short circuit of the coil is recorded.

TABLE 9: CURRENT VERSUS NUMBER OF SHORT CIRCUITED TURNS

Number of short circuited turns	**Inew/Irated**
1	1.1
2	1.2
3	1.3
4	1.4
5	1.6
6	1.9
7	2.2
8	2.6
9	3.3
10	4.3
11	6.5
12	13
13	infinity

Our aim is to detect the presence of faults at their native stage; hence, we will consider the case of one turn short circuited.

Figure 45 illustrates the flow of flux lines in the machine when a turn to turn short circuit occurs in the first slot of phase A. As remarked, there is increase in the density of flux lines near the relevant phase. Figure 46 shows the air gap flux density in this case. Comparing it to the healthy case in figure 19, it has different shape and a lowest maximum value that was near 1 in the healthy case and became near 0.7 in the case of turn to turn short circuit.

The short circuit in the stator has increased the temperature in the whole machine. The magnetic strength of the magnet is inversely proportional to the temperature. This increase in the temperature weakened the magnet; hence, the air gap flux density decrease.
In the other hand, the flux density in the machine increased and reach an alarming value 2 Tesla (figure 47).

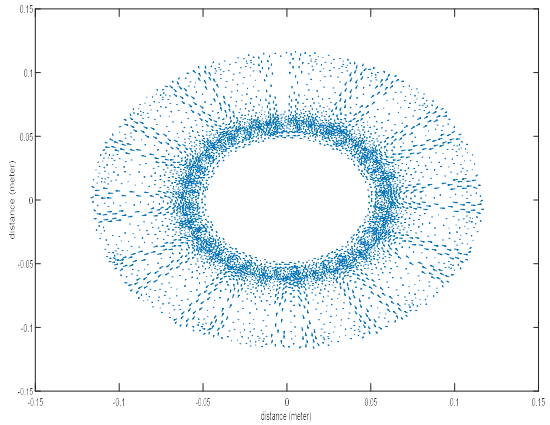

Figure 45: flow of flux lines in the machine with one turn short circuited

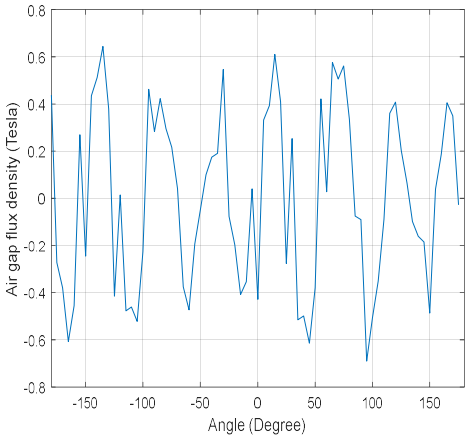

Figure 46: air gap flux density with one turn short circuited

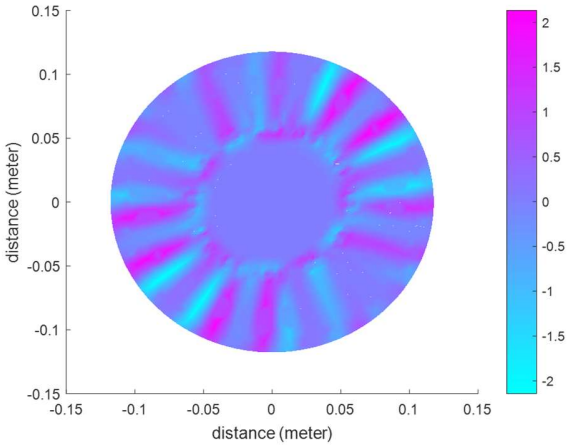

Figure 47: distribution of flux density inside the machine with one turn short circuited

Figure 48 shows the distribution of temperature inside the machine when there is turn to turn short circuit in one slot. Comparing it to the healthy case in figure 42, we remark the high increase in temperature. The presence of short circuit increases the temperature in the slots belonging to the faulty phase. This will impact the distribution of temperature in the while machine.

In this case of fault, the vibration is illustrated in figure 49 where we can see the decrease in the displacement when comparing the result with that of the healthy case.

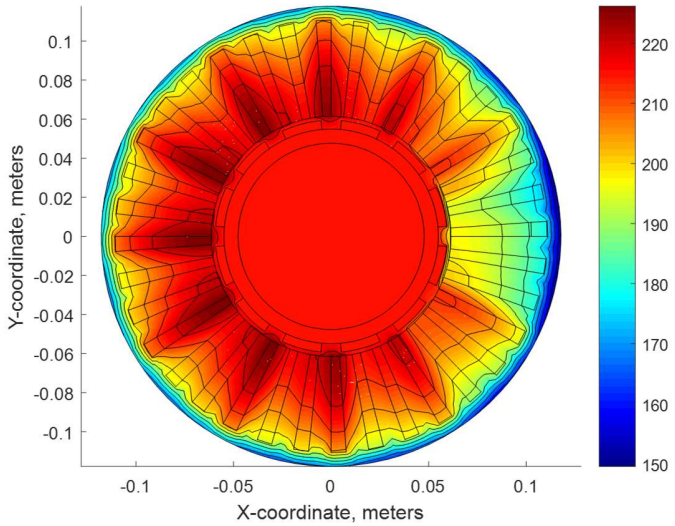

Figure 48: Distribution of temperature (°C) in the machine (in the case of short circuit turn in one slot)

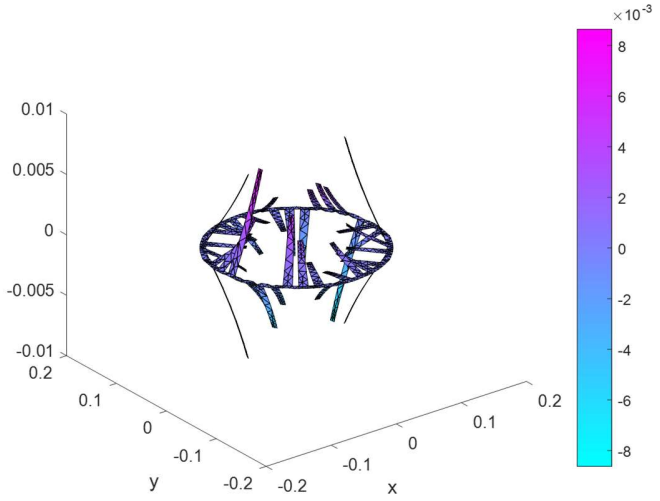

Figure 49: Vibration of the machine's stator in mm (in the case of short circuit turn in one slot)

2.5.3 Eccentricity

Eccentricity is one of the faults that may occur in the machine. It consists of non-uniformity in the rotor. In this analysis we will consider the dynamic eccentricity fault where all the rotor is moved to the right with a shift equal 10% of the air gap.

The machine's flux lines are illustrated in figure 50. We can realize a slight increase in the flux lines density, on the right side of the rotor where the air gap distance between the rotor and the

stator is minimum. Non-uniformity in the air gap flux density is also tracked in figure 51. It reaches a value near 1.5 Tesla in the area where the distance of air gap is least.

The eccentricity fault has increased the flux density in the laminated sheet where it reaches an alerting value of 3 Tesla (figure 52).

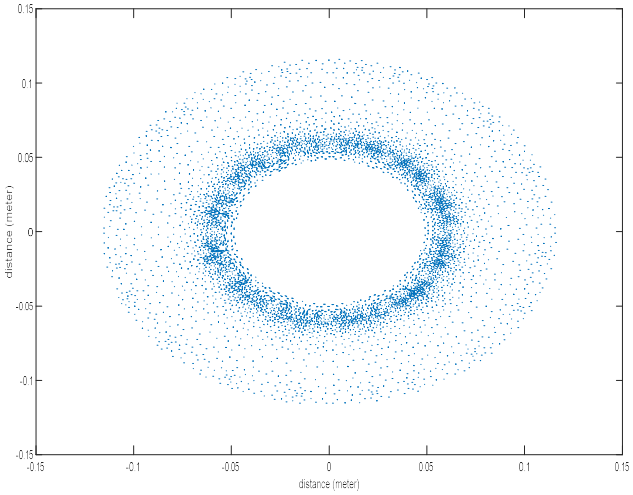

Figure 50: flux lines in the machine with 10% eccentricity fault

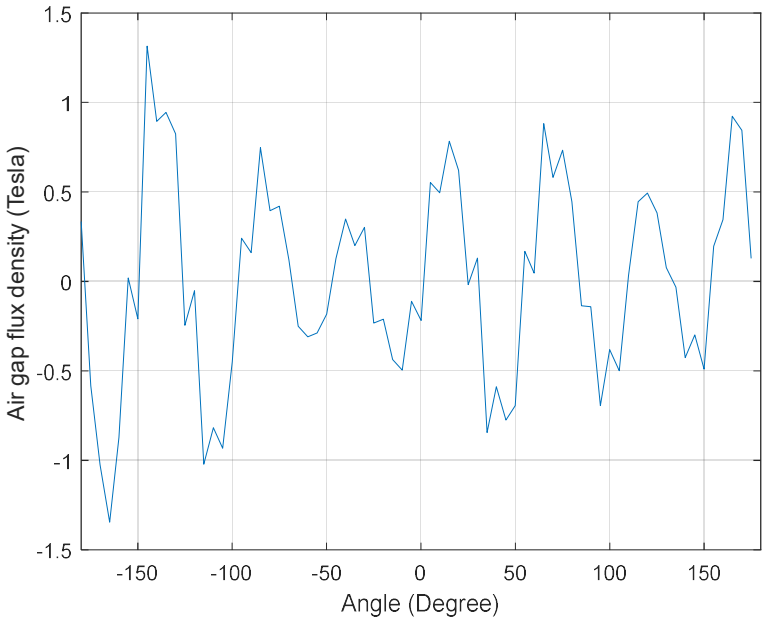

Figure 51: air gap flux density with 10% eccentricity fault

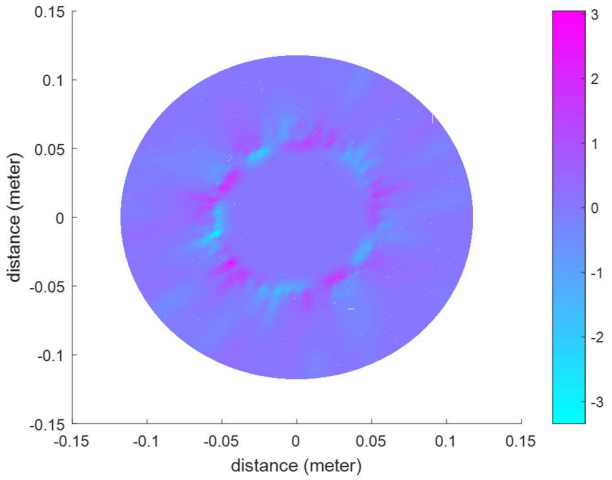

Figure 52: distribution of flux density inside the machine with 10% eccentricity fault

In the case of 10% eccentricity fault, the distribution of temperature in the laminated sheet of the machine and the vibration of its stator is illustrated in figures 53 and 54 respectively. Those results are almost the same as the healthy case. A 10% eccentricity fault change slightly the geometry of the figure and has no impact on the sources of heat in the machine; hence, this fault has no impact on the temperature distribution.

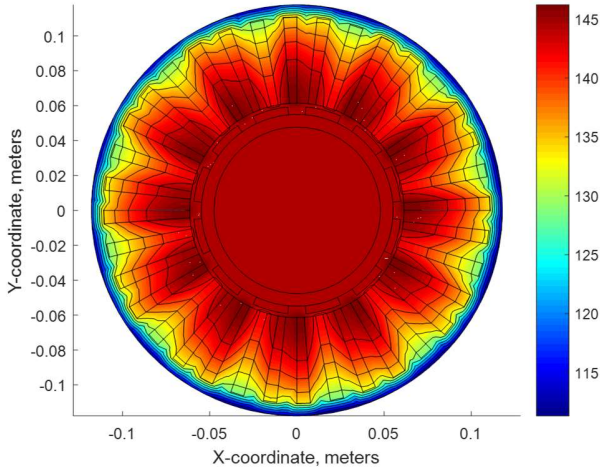

Figure 53: Distribution of temperature (°C) in the machine (in the case of 10% eccentricity fault)

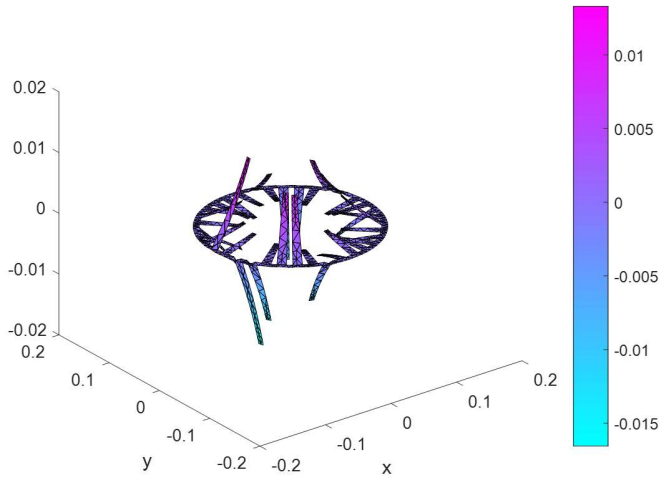

Figure 54: Vibration of the machine's stator in mm (in the case of 10% eccentricity fault)

2.6 Analytical analysis versus finite element Analysis

To compare and confront results between analytical and numerical method, the electrical machine will be modeled using the two methods while conserving the same specifications.
The considered cases are the healthy machine and the machine with crack in one magnet.
Analytically, the magnetic flux density is expressed as the product of the Magneto motive Force ($MMF_{s/r}$) produced by the rotor and the air-gap permeance (Λ_g) varying with time (t) and space (θ_s)[89].

$$B_{rad,s/r}(\theta_s, t) = \Lambda_g(\theta_s, t) \times MMF_{s/r}(\theta_s, t) \quad (31)$$

$\Lambda_g(\theta_s, t)$ is the air-gap permeance expressed by a Fourier series, in the non-saturated case [90]. In a healthy case, the permeance is constant in time and only depends on the space position θ_s.
The $MMF_r(\theta_s, t)$ is approximated by a rectangular function in the rotor-space (θ_r), function of magnetic and geometrical characteristics of the PMs [91].
In figure 55, a superposition of the air gap flux density due to the rotor contribution using FEM and Analytical method is showed. We remark the correspondence between the two results.

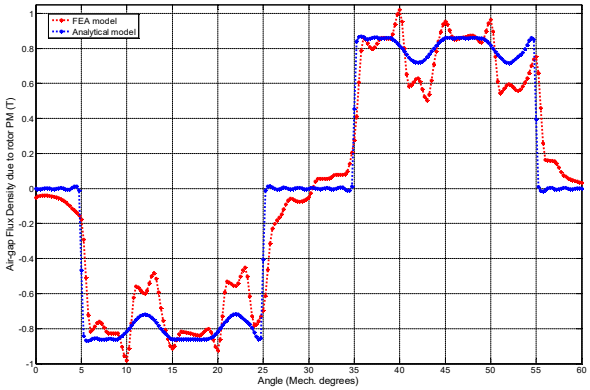

Figure 55: Air gap flux density using FEM and Analytical method

The same comparison is done when the PM crack is introduced in the machine. The modeling of the crack in the analytical model is executed by vanishing certain PM elements using a demagnetization signal added to the rotor magneto motive force [92]. The shape of the added signal in the rotor-space θ_r domain depends on the angular position and the depth of the crack in the faulty rotor pole. We mention that the analytical method doesn't take the radial position or the direction of the crack into consideration, like FEM do.

In figure 56, a superposition of the air gap flux density in the case of a crack using FEM and Analytical method is showed. The results of the two models are almost similar.

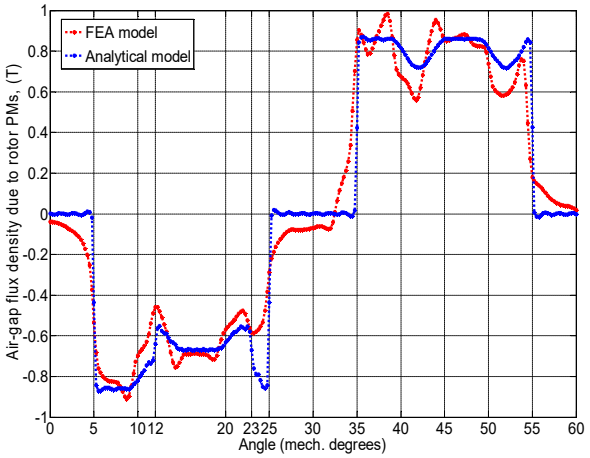

Figure 56: air gap flux density with 1 mm crack in the magnet of the first pole

2.7 Conclusion

Treating each model separately: electromagnetic, thermal and vibration, is important. However, building a complete model where the three previously mentioned models are integrated together is of big interest and is better for the machine's exemplification because, in real life, the three models are highly dependent.

A block diagram representing the combined model and their outcomes is presented in figure 57.

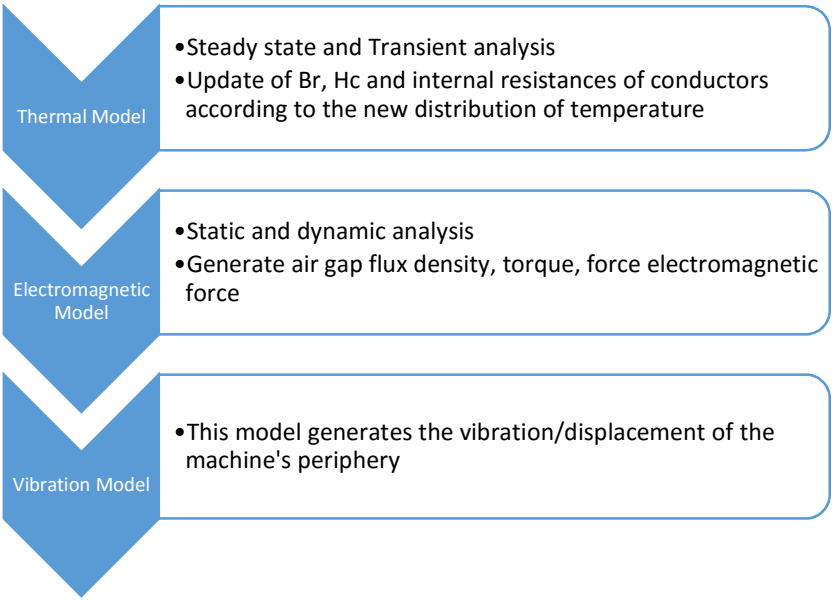

Figure 57: FEM's outcomes

At starting, a machine's position is selected. The execution of the thermal model will be implemented at each revolution, not at each time step to reduce the simulation time.
The thermal model generates the distribution of temperature in the whole machine. This model let us update the characteristic's parameters needed for the electromagnetic model, that are dependent on the temperature like the residual flux density of the magnet, the coercive force of the magnet, the internal resistance of the coil.

Then, the time stepping electromagnetic model is executed where the static electromagnetic model is the initial solution of this dynamic model. From the electromagnetic model, we get the flux density in the whole machine including the air gap flux density from which the Torque is calculated. Moreover, electromagnetic force acting on the teeth of the stator is deduced.
This force is the input of the vibration model that generates the displacement at the outer periphery of the machine.

The electrical, thermal and vibration aspects of the machine, in healthy and faulty case, was presented in this chapter. The three discussed FEM models will be applied to healthy and all types of faults in the machine.

The direct output of the discussed FEMs will form the base for the calculation and generation of other significant parameters aiming prognostic resolve. Hence, in chapter 3, a post processing analysis will be done where the extracted measurable parameters from the FEMs will be defined, they will be expressed in space, in time domain and in frequency domain. Moreover, features from these measureable parameters will be selected according to the need of the prognostic approach.

Chapter 3: Dynamic variable aspect for fault identification and detection

3.1 Introduction

The prognosis aims to detect a fault before it occurs; also, to detect faults of very tiny scale. Hence, the risk of false alarm is very high, especially that, consequences may be common for several type of faults. For this reason, it is convenient, when aiming to detect a specific fault, to detect more than one dynamic variable involved, during the occurrence of this fault.
In this chapter we will execute a post processing analysis of the FEMs' output. The resultant measured dynamic parameters will be presented. The parameter affected by each types of fault will be identified. The useful features for fault detection will be designated.

The investigated features will be the classical and mostly used in time domain and frequency domain signals; some are statistical indicators whereas the others spectral characteristics.

Those elaborated dynamic variables and signal features will be the input of the prognostic model.

3.2 Classical signal parameters and features

In this section we will enumerate, define and describe the different classical parameters and features that may be extracted from signals in the time and frequency domain.

3.2.1 Statistical parameters

Let's consider $xi(t)_{i=1,\dots,I}$, a discrete signal function of time. The main statistical parameters of this signal are: [166]

Peak to peak value

The peak to peak value of a signal represents the difference between its maximum value 'Xmax' and minimum value 'Xmin' expressed as [167]:

$$Peak\ to\ Peak = X_{max} - X_{min} \tag{32}$$

We mention that this value does not take into account the evolution of the signal function of time and consequently its practical utility is limited to the phenomena of short duration.

Mean

The mean, also called the average, indicates the average value of a data set. It is expressed as [168]:

$$Mean = \frac{1}{N} * \sum_{i=1}^{N} xi \tag{33}$$

It can detect the evolution of changes function of time.

RMS

RMS is the abbreviation of 'root mean square'. Its formula is [169]:

$$RMS = \sqrt{\frac{1}{N} * \sum_{i=1}^{N} (xi)^2} \tag{34}$$

$$E_x = \sum_{i=1}^{N} (xi)^2 \tag{35}$$

The RMS value depends strongly on the evolution of the signal as a function of time as it is directly related to its mean energy (E_X) expressed in equation (35). Hence, it can detect faults that cause an increase in the energy dissipated by the monitored system.

Kurtosis

The Kurtosis, also called the Pearson flattening coefficient, is defined as the moment of order 4 of the discrete signal as expressed in (36) [170]. It expresses the sharpness of the peak of a frequency-distribution curve. This indicator is typically used to detect the occurrence of impulsive type phenomena in the dataset.

$$Kurtosis = \frac{\frac{1}{N} * \sum_{i=1}^{N} (xi - Mean)^4}{\left(\frac{1}{N} * \sum_{i=1}^{N} (xi - Mean)^2\right)^2} \tag{36}$$

Skewness

The Skewness is based on the moment of order 3 as defined in (37). This indicator gives a measure of the asymmetry of the signal with respect to its average value, hence its effectiveness in detecting any change in this characteristic.

$$Skewness = \frac{\frac{1}{N} * \sum_{i=1}^{N} (xi - Mean)^3}{\left(\frac{1}{N} * \sum_{i=1}^{N} (xi - Mean)^2\right)^{\frac{3}{2}}} \tag{37}$$

A negative skewness means that the data are spread out more to the left of the mean than to the right.

Crest factor

The crest factor designates how extreme the peaks are in a signal; It is defined as the ratio of its peak level 'X_{max}' to RMS value as expressed in (36). For a purely sinusoidal signal, the crest value is √2 and will tend to increase when the signal becomes of pulse type [171].

$$Crest\ factor = \frac{X_{max}}{RMS} \tag{38}$$

Pulse factor

The pulse factor as expressed in (39), is the ratio of the maximum amplitude of a dataset to its mean absolute. For a simple sinusoidal signal, the absolute mean is $(2Xmax)$ / π and so the pulse factor is π / 2.

$$Pulse\ factor = \frac{X_{max}}{Mean} \tag{39}$$

Shape factor

The Shape factor is expressed in equation (40) as the ratio of the RMS value of a dataset to its absolute average. Like the case of the pulse factor, the shape factor is a function of the average of the rectified signal. For a simple sinusoidal signal, the value of the shape factor is π / (2√2).

$$Shape\ factor = \frac{RMS}{Mean} \tag{40}$$

Standard deviation

The Standard Deviation (SD) expresses how spread out numbers of a dataset are. Its formula is illustrated in equation (41).

$$SD = \sqrt{(\sum \frac{(xi - Mean)^2}{N}} \tag{41}$$

Variance

The Variance of a dataset is defined as the average of the squared deviation from its Mean. In other words, it expresses how spread are the elements of the data set from the Mean.

$$Variance = \sum \frac{(xi - Mean)^2}{N} \tag{42}$$

3.2.2 Spectral characteristics

The Fourier transform of $x(t)$ is $X_{s,f}(f)$. The main spectral parameters are [172]:

Power spectral density

The spectral power density PSD$_X$ (f) of a time-variable signal x (t) represents the distribution of its power over a certain frequency band. In the literature, several techniques for estimating this density exist, among which we can cite: parametric estimates based on the medializations of the process, the classical or non-parametric estimates based on the periodogram and those based on the variance of the periodogram. The second technique was adopted in this work using the appropriate Matlab periodogram function.

This feature is adequate for continuous signals. PSD is expressed in (43):

$$PSD_x(f) = \frac{\left|X_{s,f}(f,T)\right|^2}{T} \tag{43}$$

$X_{s,f}(f, T)$ is the Fourier transform of the time signal x (t) over one period 'T'.

Average spectral power

The average spectral power of a 2-D signal is calculated from its power density as illustrated in equation (44).

$$P_{fav} = \int_0^{fmax} PSD_x(f)\, df \tag{44}$$

Amplitudes of frequency components

A considered spectral indicators are the amplitudes A_{fk} of the complex Fourier transform $X_{s,f}$ (f) of the time domain signal x(t), at frequencies $f_k = kf_{mec}$ where k is an integer, as given by equation (45).

$$A_{fk} = |X_{s,f}(f)|_{f=fk} \tag{45}$$

3.3 Identify useful measured parameters for fault identification

3.3.1 Outcome of electromagnetic FEM

We started focusing on the demagnetization of the permanent magnet; in our selected machine, the Neodymium iron boron magnet is used. Demagnetization can arise due to several reasons: a crack

in the magnet, an increase of the temperature in the environment of the magnet, an increase in the level of vibration in the environment of the magnet.

The electromagnetic model computes the flux density in the whole machine. The air gap flux density will be used to calculate the torque.

Torque:

$$T = \frac{\Pi}{2} * \mathrm{D_r^2} * B_{gav} * Q_{rms} * l_a \tag{46}$$

Where, electric loading:

$$Q_{rms} = \frac{J * A_s * K_f * N_s}{\Pi * \mathrm{D_r}} \tag{47}$$

Bgav: average air gap flux density over one pole for an instant of time.
Dr: rotor's diameter
La is the axial length of the machine.
J: average current density
As: slot's area
Kf: slot's filing factor
Ns: number of slots in the stator

The average air gap flux density can be expressed as:

$$Bgav = \frac{2}{t}\int_0^{t/2} Bg(x)dx \tag{48}$$

Bg(x): the flux density at equidistant points in the air gap.
t: the tooth pitch.

In our model, the air gap region is considered to be moving as the rotor rotates.
The air gap flux density function of time for the healthy case, case of crack in a magnet, case of turn to turn short circuit in one stator's coil and case of eccentricity fault is illustrated in figures 58, 59, 60 and 61 respectively.

To draw the air gap flux density in the time domain an arbitrary point in the air gap is considered. This point has almost the same vertices for all the studied cases of the machine.

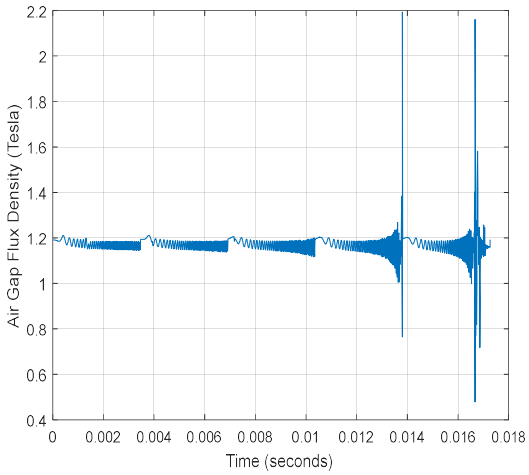

Figure 58: Air Gap Flux Density in time domain (Healthy machine)

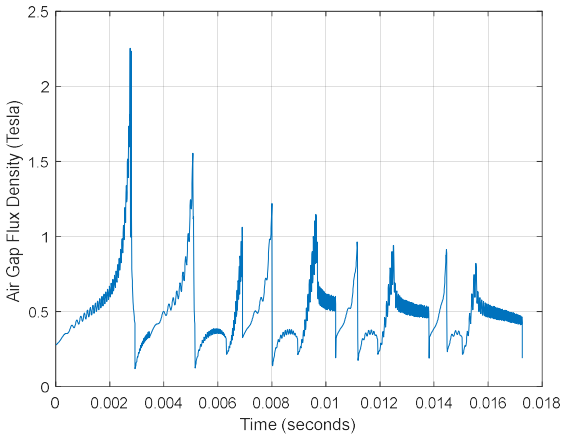

Figure 59: Air Gap Flux Density in time domain (Machine with 1 mm crack)

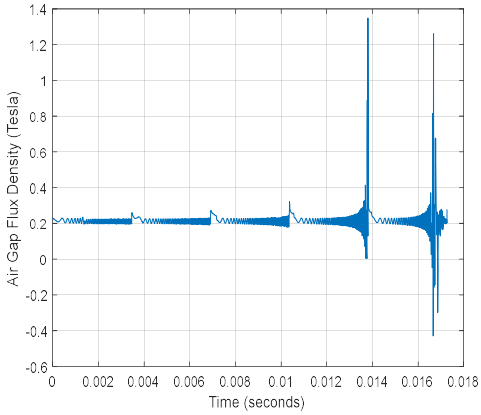

Figure 60: Air Gap Flux Density in time domain (Machine with 10 % eccentricity fault)

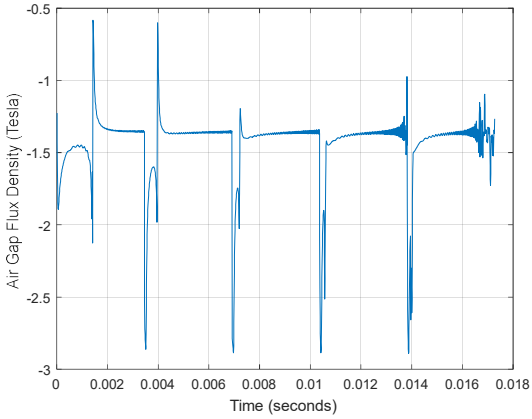

Figure 61: Air Gap Flux Density in time domain (Machine with turn to turn short circuit fault)

The analytical described equation to calculate the torque is integrated in the time stepping model of the machine which generates the torque function of time. This is the measurement that will sense a torque sensor located at the shaft of the machine. The simulation is done for the healthy and different types of fault previously mentioned. Figure 62 illustrates the torque for the healthy case, case of 10% eccentricity fault, turn to turn short circuit in one slot and 1 mm crack in one piece of magnet.

Contemplating figure 62, we can see the impact of the faults on the torque which shows that the torque is a good indicator for fault detection.
The transient part of the machines operation is clearly illustrated in the graph; this is the main advantageous of the time stepping dynamic model.

Comparing the graphs in figure 62, several notes can be recorded. The blue graph is the torque in the healthy case. The red graph is the torque in the case of 1 mm crack in one piece of magnet.

This graph is drawn near the one of the healthy case; however, this fault has impacted the torque with ripples clearly visualized on the graph. The yellow graph is the torque of the machine when a turn to turn short circuit occurred in one slot of phase A. In other types of electrical machine, like induction machine, when a short circuit occurs in the stator's windings, the air gap flux density increases and the torque increases accordingly. However, in our case where a permanent magnet is used, the torque has decreased in the case of turn to turn short circuit and this torque will continue decreasing as the number of short circuited turns increases. The cause is the high dependence of the magnet's electromagnetic performance on the operating temperature. The partial short circuit in one coil, in the stator, has increased the temperature at the magnet level. This has weakened the magnet; consequently, the air gap flux density decreases which leads to the drop in the torque.

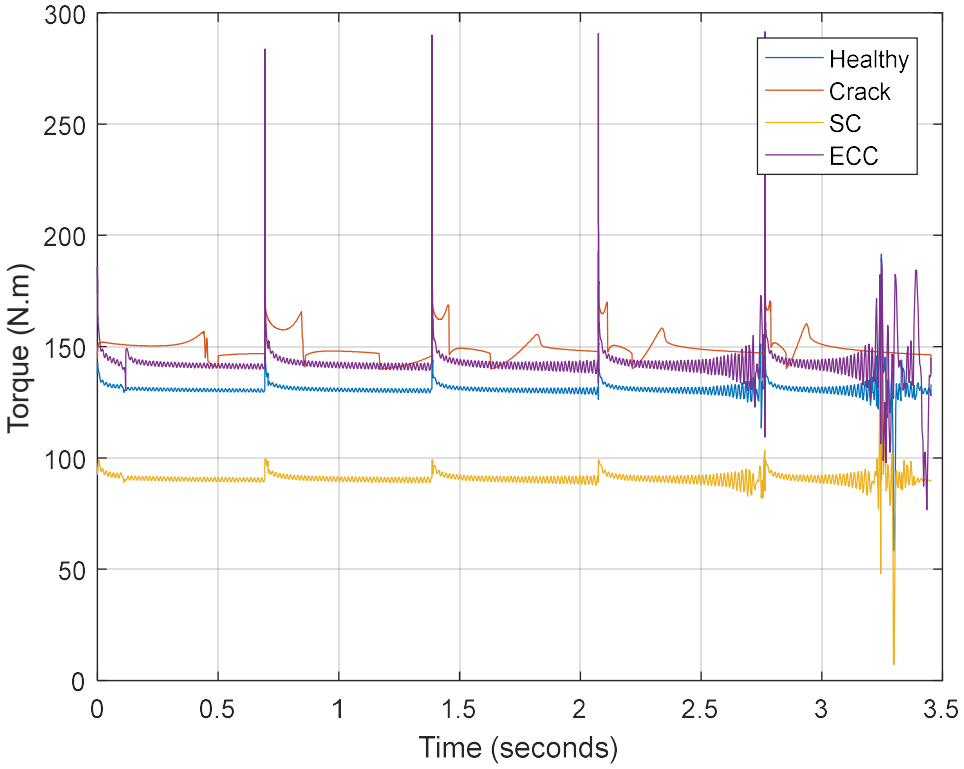

Figure 62: Torque versus time for the different states of the machine

We will examine the useful features of these signals, in the time and frequency domain, that will be beneficial for fault detection and machine prognosis. The transient period of the machine will be skipped. The treatment of the measured signal will be for the steady state region of the signal. To evaluate the impact of the designated faults on the machine's torque, a computation is conducted to calculate the different mentioned characteristics and features in the previous section.

New version of torque sensors is wireless, with no contact routine to measure the torque of machine's rotating part. It has an advantageous high optimistic accuracy of ±0.05% for measurements less than 10K N.m. This percentage error will be considered.

In table 10, an illustration of the previously mentioned signal statistical characteristics, are presented. The effect of sensor error on the features is encountered in the last column. The computation will be over one revolution.

TABLE 10: STATISTICAL FEATURES OF TORQUE SIGNAL

Machine's State / **Statistical feature**	**Healthy**	**Crack 1 mm in one magnet**	**10% eccentricity fault**	**Turn to turn short circuit fault**	**% change due to sensor error**
Peak to peak value	129.08	37.42	206.09	158.84	± 0.05%
Average	133.49	153.28	148.68	95.05	± 0.05%
RMS	128.11	146.76	143.58	90.72	± 0.05%
Kurtosis	18.97	3.11	17.56	52.84	± 0.05%
Skewness	0.23	1.15	3.12	-1.16	± 0.05%
Crest factor	1.44	1.16	1.95	1.83	0%
Pulse factor	1.44	1.16	1.97	1.83	0%
Shape factor	1	1	1.01	1.01	0%
Standard deviation	11.09	8.07	23.99	9.35	± 0.05%
Variance	60.4	58.24	404.09	23.5	± 0.05%

After examining table 10, the numbers show that some features are very good fault indicators due to their high disparity according to the machine state like peak to peak value, average…; few are bad fault indicator where they remain constant or almost constant for all the states like shape factor; others are partially indicative of fault occurrence where they are useful for some types of faults and not for others like variance.
In the other hand, some features are affected by the sensor error; others remain consistent.

In figure 63 we can see the spectral power density of the torque, in dB scale, for the different studied machine states. The graphs are distinct; which make the spectral power density a good fault indicator.

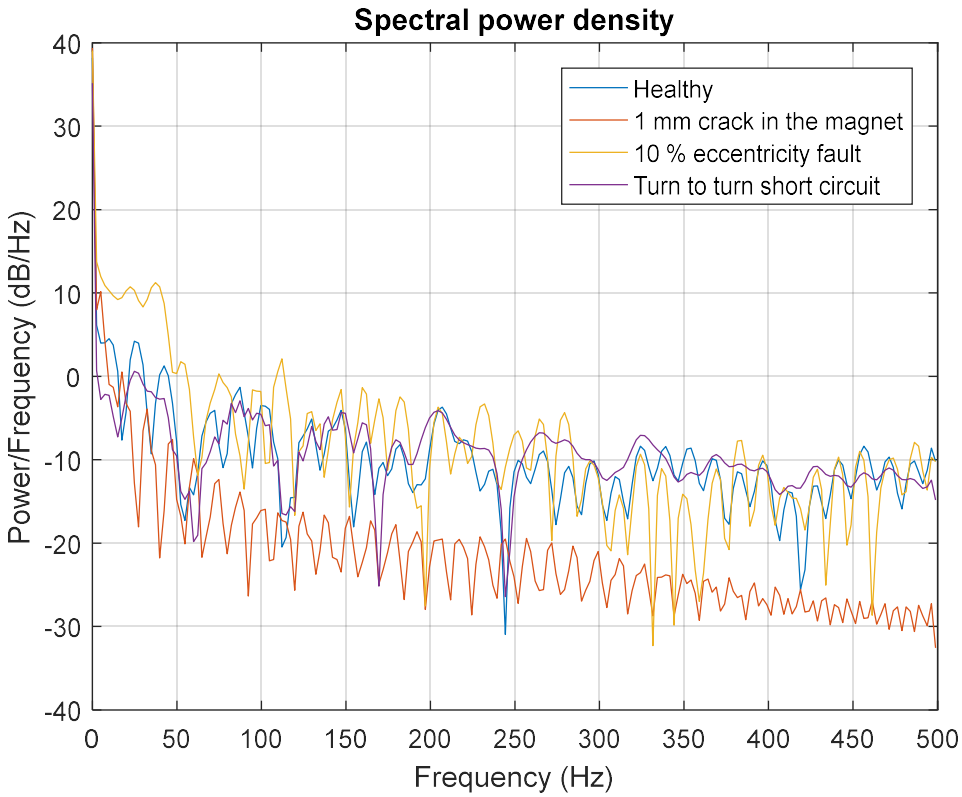

Figure 63: Spectral power density of the torque

The average spectral power is illustrated in table 11.

TABLE 11: AVERAGE SPECTRAL POWER DENSITY OF TORQUE

Machine's State	**Healthy**	**Crack 1 mm in one magnet**	**10% eccentricity fault**	**Turn to turn short circuit fault**
Average spectral power $(N.m)^2$	32.79	43.11	40.92	16.46

In figure 64, the Fourier transformation of torque is illustrated. We can see that the harmonics at frequencies higher than the fundamental has a very low amplitude, almost zero, common for all machine states. Hence, amplitudes of frequency components are not a good indicator for fault detection when interpreting torque signal.

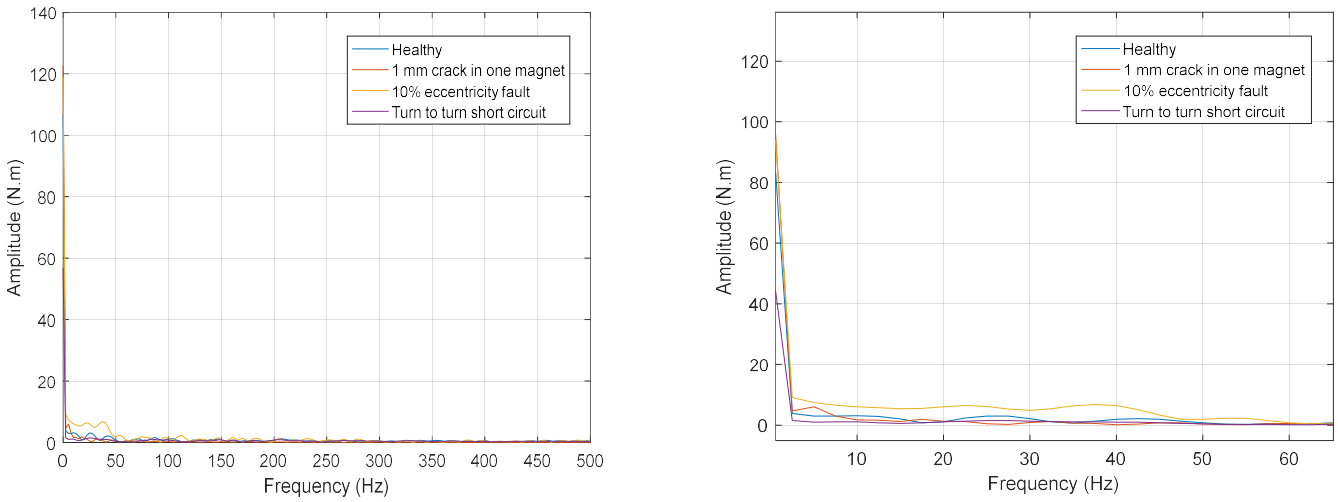

Figure 64: Fourier transformation of torque

As demonstrated, several features are useful for fault detection. One has to be chosen; no harm in choosing any of them. We selected the 'average' as fault indicator. The average and interval range recorded by the torque sensor when taking the error percentage into consideration is illustrated in table 12.

TABLE 12: AVERAGE TORQUE FOR THE DIFFERENT STATES OF THE MACHINE

Machine's State	**Average Torque (N.m)**	**Average Torque Range with ± 0.05% error**
Healthy	133.49	~= 133.4 133.6
Crack 1mm in one magnet	153.28	~= 153.2-153.4
10% eccentricity fault	148.68	~= 148.60-148.8
Turn to turn short circuit fault	95.05	~= 95.1-95

The average torque over one revolution is a good indicator for fault detection and identification. Since the values of the torques are distinct and the sensor error is very small, no need to take this error into consideration because it will not affect the diagnostic decision; the average torque intervals for each state does not overlap.

3.3.2 Outcomes of Thermal FEM model

In this section we will explore the thermal FEM model, investigate if temperature is a good indicator for fault detection and identify the best extracted feature from this measureable signal to track the presence of fault.

The thermal FEM model is capable of computing the temperature in the whole machine. As stated earlier, the aim of the model is to generate data that will record a temperature sensor if a prototype

is available. The most practical location of temperature sensor will be at the outer periphery of the machine. Hence, we will focus on the boundary temperature of the machine on all pre-mentioned cases to decide if temperature is a good fault detector, to be considered. To do so we only need the geometry of the machine, the physical characteristics of its parts, the sources of heat inside the machine and the boundary conditions.

Knowing the high impact of stator's short circuit on the distribution of temperature in the machine, we will start monitoring the boundary temperature of the machine's two poles laminated sheet in the case of turn to turn short circuit in the first slot. We will consider only small scale faults. The temperature at the left and right side of the laminated sheet is set to 40 °C. Figure 65 shows the machine's laminated sheet when the turn to turn short circuit is integrated in the first slot.

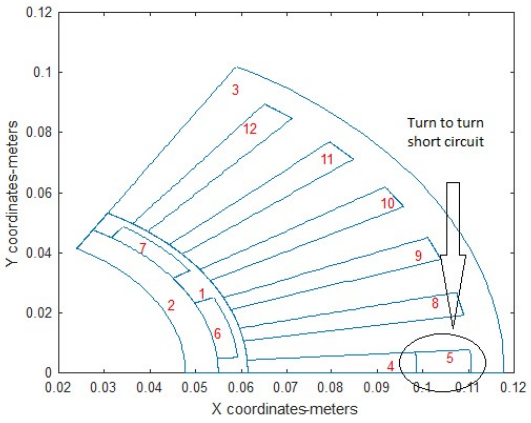

Figure 65: laminated sheet of the PMM with turn to turn fault integrated

The model of the machine with turn to turn short circuit is illustrated in figure 65. To execute the finite element modeling of this faulty case appropriately, a new domain is integrated in the faulty slot, in the laminated sheet, to designate the area occupied by the shorted turns where the current density is higher than the other part of the slot. This reflects the equivalent circuit of a coil containing short circuited turns.

As shown in figure 66, the coil of phase A containing turn to turn short circuit is divided into two parallel parts where a current divider occurs. A large current, the fault current, pass in "Rf" representing the shorted turns and a normal current pass in the healthy turns. The summation of the faulty current and healthy current will pass in the remaining coils forming the phase since the coils of the stator are connected in series. In other words, the highest current will pass in the healthy coils of phase A and not in the coil where the short circuit persist.

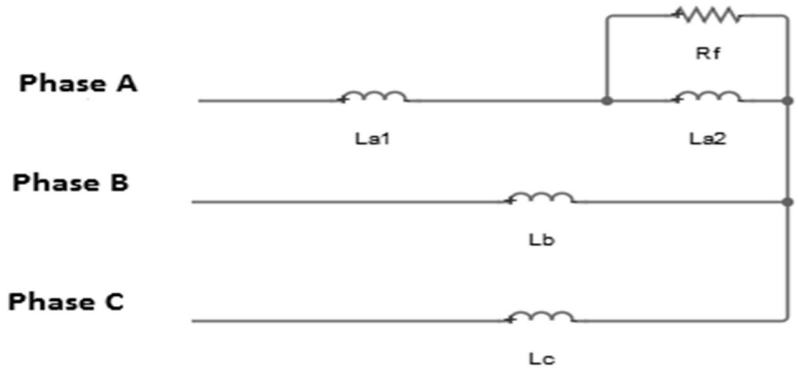

Figure 66: Equivalent circuit of turn to turn short circuit at phase A

The distribution of temperature in the laminated sheet of figure 65 is shown in figure 67.

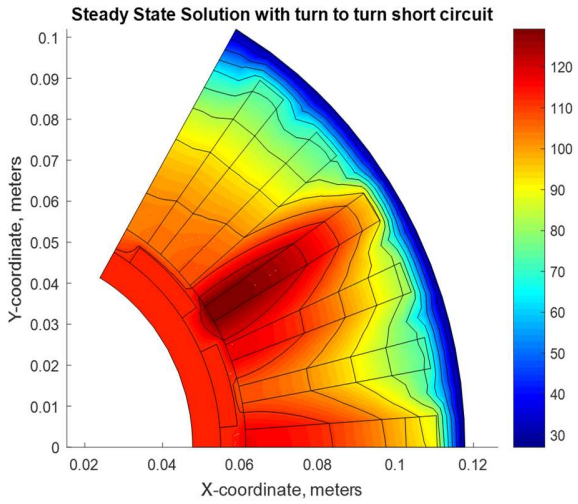

Figure 67: Distribution of temperature in the machine when a turn to turn short circuit occur in slot 1

Comparing the two slots of phase A, we observe that the temperature in the 4th slot is greater than the first slot where the short circuit occurs. This is expected since the current flowing in the 4th slot is the summation of current flowing in the faulty and healthy turns of the first coil in the first slot. The temperature at the top of the slot is less than the bottom because the top is nearer to machine's surrounding.

Figures 68 and 69 illustrates the temperature in degree Celsius versus the x coordinates of the points at the machine's boundary in the healthy case and in case of two turns short circuited respectively. The aim of this analysis is to make clear the relation between short circuit faults and temperature.

The points at the machine boundary are correlated with the meshing of the laminated sheet. After examining the below figures, we deduce that monitoring the boundary temperature of the machine is a helpful index for the detection and localization of an incepting fault like turn to turn short circuit. It will help in detecting the presence of turn to turn short circuit fault since the temperature will increase in the area above the phase containing the short circuit turns. Additionally, it will let us localize the fault because the temperature above the coil containing the short circuit has a temperature slightly lower than that of the healthy coils of the same phase as a result of the current divider that occurs in the faulty slot.

Comparing the results in the below three graphs, we remark that when a short circuit occurs, the temperature increases and reaches higher values as the number of short circuited turns augments. A maximum value of 102 °C is reached in the healthy case. In the case of turn to turn short circuit, the maximum detected temperature at the machines' boundary becomes 113 °C.

We mention that the input voltage in this analysis is the nominal voltage at all the phases.
In the same context, we remark that in the case of healthy machine, the distribution of temperature at the boundary is almost uniform. However, when the fault occurs, this uniformity stagger.

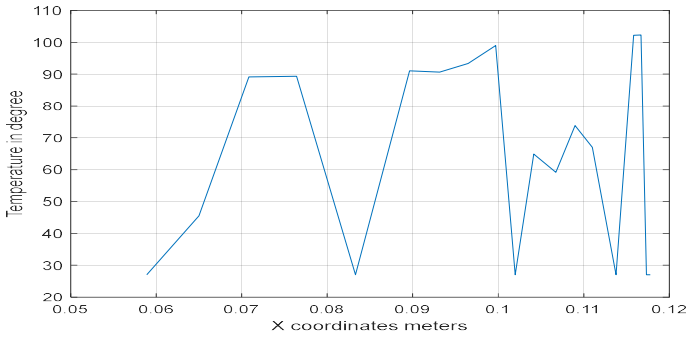

Figure 68: Boundary temperature in healthy case

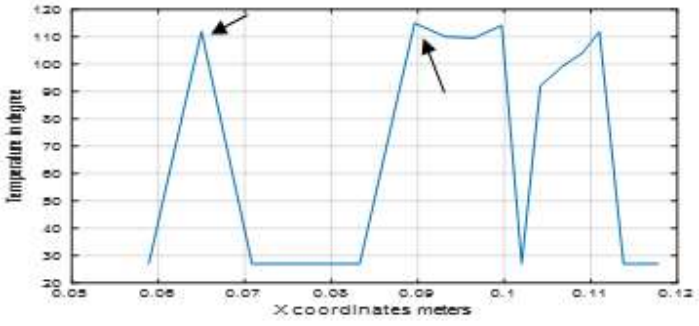

Figure 69: : Boundary temperature with turn to turn fault in the first slot (Phase A)

In figure 69, the first arrow indicates the temperature above the first slot where the fault persists. The second arrow indicates the temperature above the fourth slot that belongs to the same phase. The temperature above this slot is slightly higher than the temperature above the faulty slot, slot

1. Hence, monitoring boundary temperature is efficient to identify and localize native faults like turn to turn short circuit.

After clarifying the importance of monitoring the boundary temperature for fault detection and localization, a fictive temperature sensor will be located at the boundary of the machine, its readings for the different machine states is generated.
The location of temperature sensor at the machine's boundary is illustrated in figure 70.

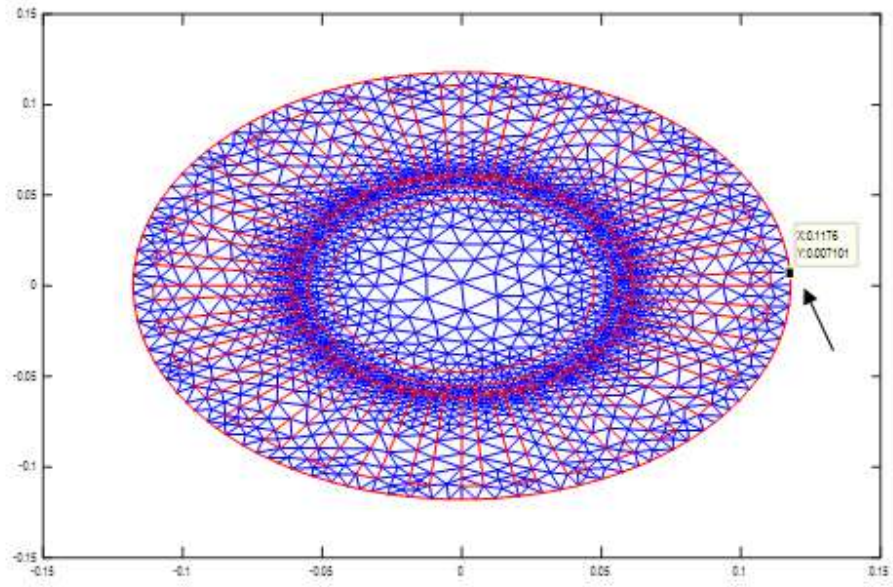

Figure 70: Location of temperature sensor

Temperature sensors provide an input to a system that is used to determine the temperature of a specific process or location. This requires that the sensor is connected to the instrument so that the signal can be received. This connection can be made by a prolonged cable from the sensor or by transmission via a wireless network.

Types of temperature sensors mostly used in automation applications are Resistance thermometers or resistance temperature detectors (RTDs) and Thermocouples.
Choice between them is usually determined by several factors. The table in annex A shows the difference between RTD and thermocouple sensors in term of temperature range, response time, size, accuracy, cost and physical aspect.

In [93] they showed that for direct measurement of temperature inside stator's coil, fiber optics temperature sensors are advantageous over RTDs. However, for our application and need to monitor the outer periphery, conventional sensors are sufficient.
The accuracy of this type of temperature sensors is ± 0.55 °C.

Figure 71 shows the temperature detected by this sensor for the case of healthy machine and faulty machine with short circuit in the first slot. We can remark the high difference between the sensed

temperature in the two cases. This is expected since the short circuit increases the value of current in the faulty phase; this increases the copper losses which will be expressed as heat.
In fact, the main sources of heat inside the electric machines are the copper windings.

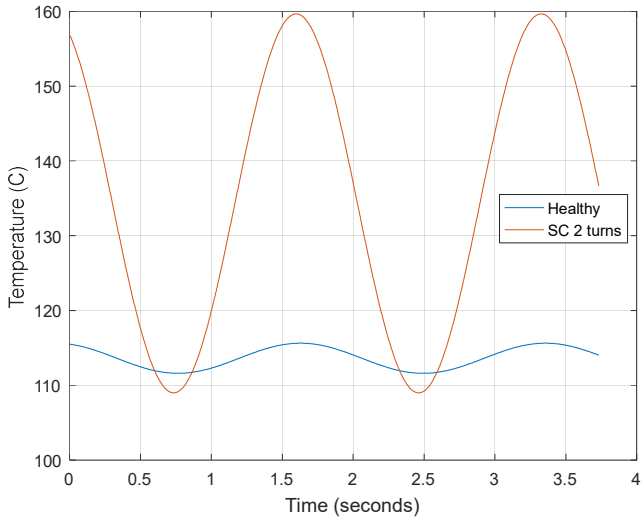

Figure 71: Sensor temperature for healthy machine and machine with turn to turn short circuit in slot 1

Figure 72 shows the sensor temperature when a turn to turn short circuit occurs in slot 1 and when it occurs in slot2. We can see that the temperature for the two cases is distinct. When the fault is in slot 1 the sensor temperature is higher since the location of the sensor is nearer to slot 1.

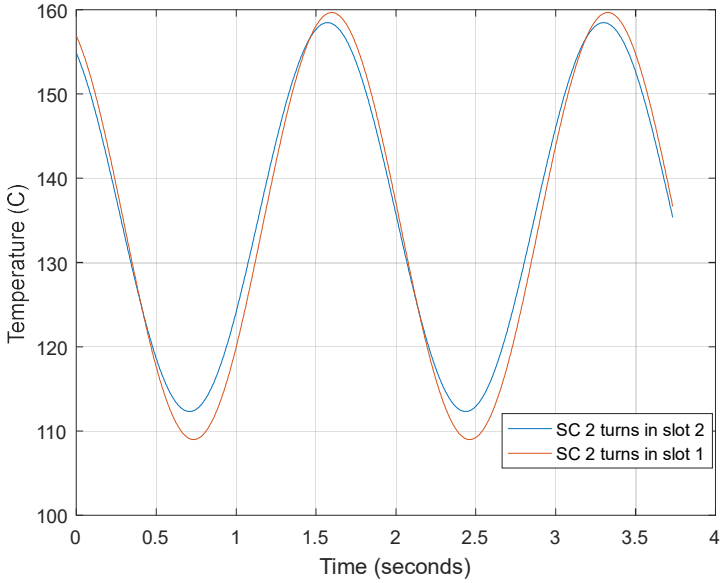

Figure 72: Sensor temperature for healthy machine and machine with turn to turn short circuit in slot 1

Since our goal is to detect the presence of turn to turn short circuit wherever it is located, the fault is moved each time to one of the 36 slots and the recorded data for each case, by the temperature senor, is illustrated in figure 73. Figure 74 is a zoomed view of figure 73.

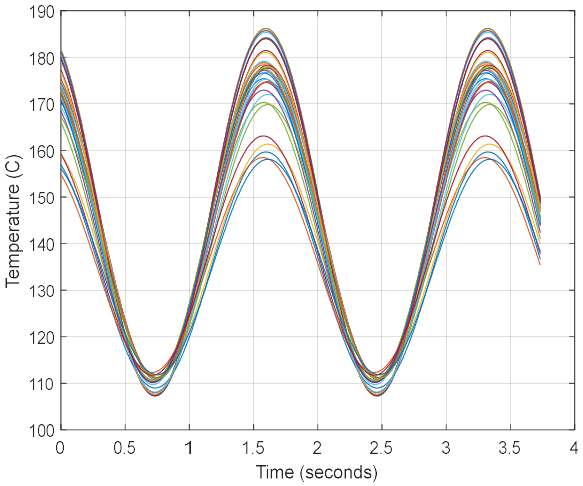

Figure 73: Sensor temperature for turn to turn short circuit in each slot

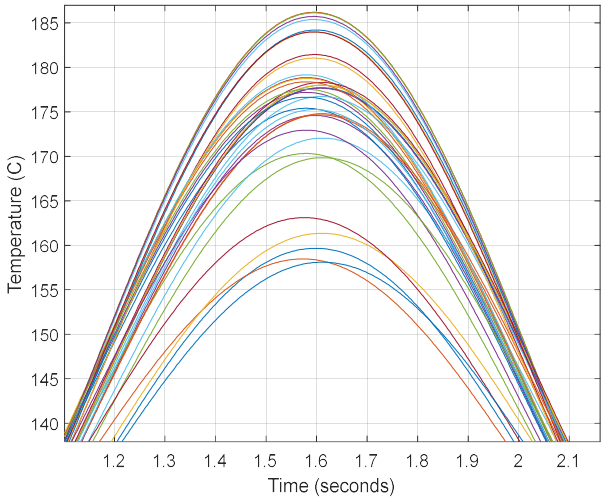

Figure 74: Zoom of figure 73

The same measurement is done for the case of 1 mm crack in one piece of magnet in the machine. Each time the crack is moved to one of the magnets and the sensor temperature is located. The position of the temperature sensor remains intact. The results are shown in figure 75.

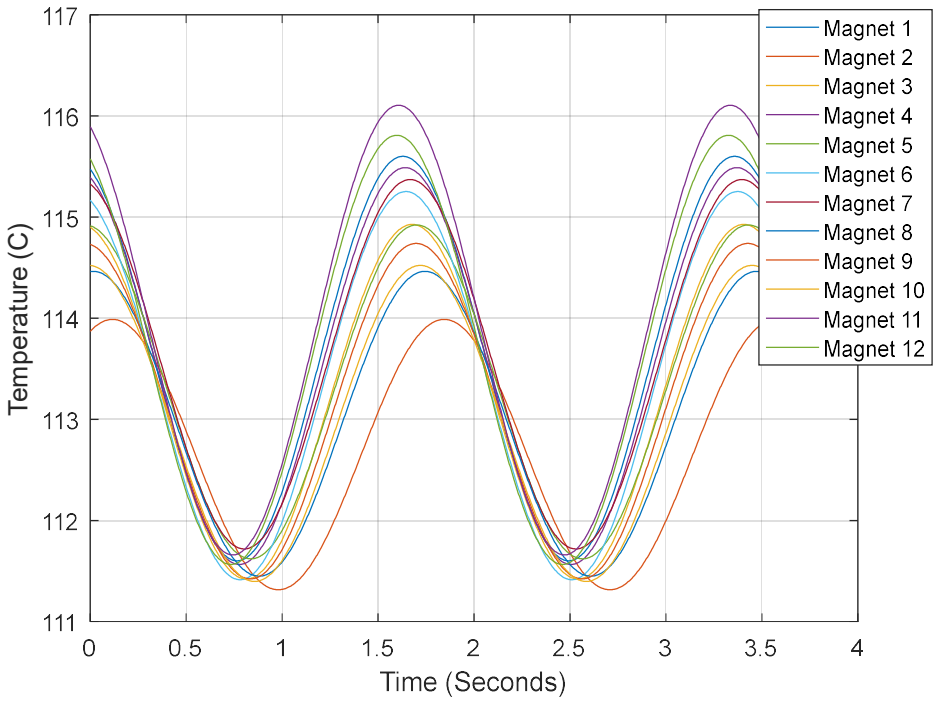

Figure 75: Sensor temperature for 1 mm crack in one magnet a time

For the state of 10% eccentricity fault in the machine, four cases are considered: rotor shifted to the right, rotor shifted to the left, rotor shifted upward and rotor shifted downward. The temperature results collected by the sensor is illustrated in figure 76.

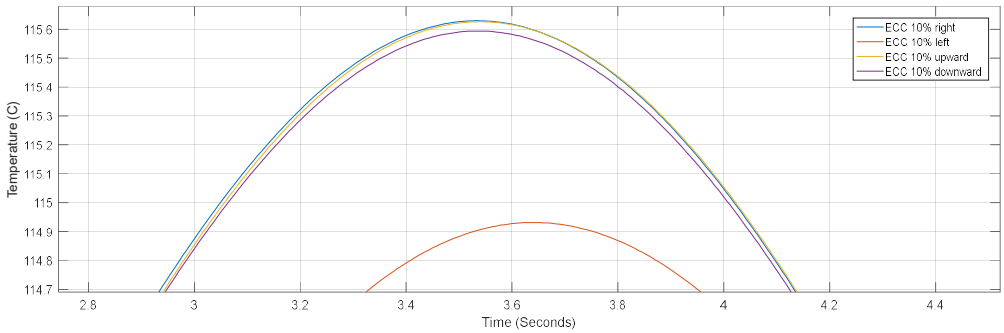

Figure 76: Sensor temperature for machine with 10 % eccentricity faults

For comparison purpose, figure 76 shows the temperature for the case of healthy machine, machine with an eccentricity fault and machine with a crack executed in one magnet.

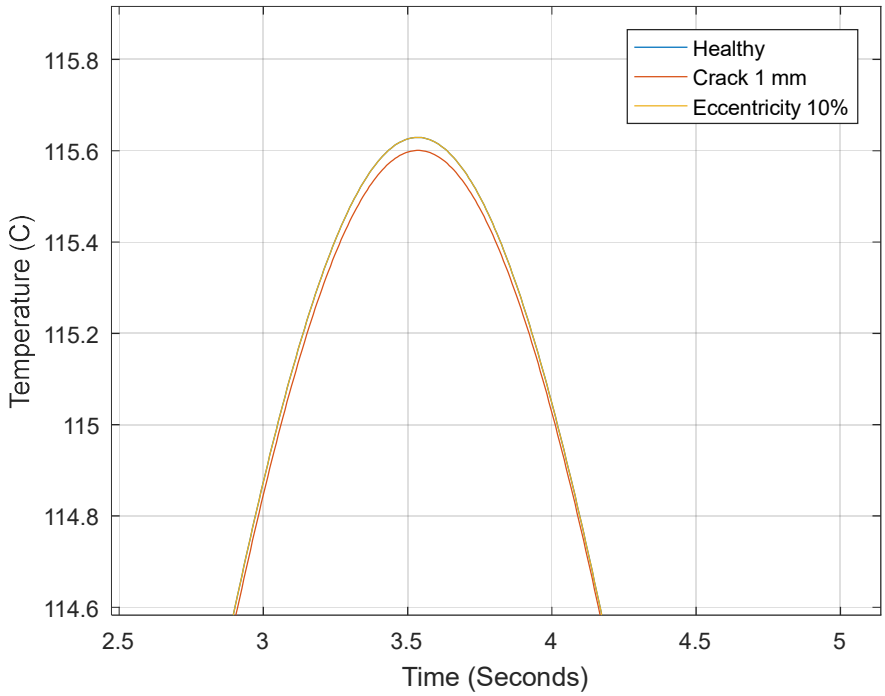

Figure 77: Sensor temperature for healthy machine, machine with eccentricity fault and machine with crack in the magnet

In figure 77, we remark that the sensor temperature for all the mentioned cases is almost the same. In other words, when an eccentricity fault or a demagnetization fault occurs in the machine, the data collected by the temperature sensor function of time is similar to that recorded in the case of healthy machine. Hence, the temperature is not a good indicator for eccentricity and demagnetization faults.

After collecting the temperature data for the different cases we need to analyze it; we should identify the useful features that should be extracted from this collected data to detect the presence of fault and elaborate the prognostic decision.

The illustration of the statistical features will be graphically since the number of temperature data sets is 53 (1 for healthy machine, 36 for turn to turn short circuit fault in 36 slots, 12 for crack in 12 magnets and 4 eccentricity fault); graphical representation of few data sets of each case will be more helpful and beneficial to visualize the disparity between the features and to select the best one.

The selected data sets that will be investigated will be the healthy state ‘Healthy’, the states with turn to turn short circuit in slot 1 ‘SC1’, in slot 13 ‘SC13’ and slot 25 ‘SC25’, the states with 1 mm crack in magnet 1 ‘M1’, in magnet 5 ‘M5’ and in magnet 9 ‘M9’, the states with 10% eccentricity fault on the right ‘ECC1’, on the left ‘ECC2’, upward ‘ECC3’ and downward ‘ECC4’.

The peak to peak, mean, rms, kurtosis, skewness, shape factor, pulse factor crest factor, standard deviation and variance of these data sets are respectively presented in figures 78, 79. 80, 81 82, 83, 84, 85 and 86.

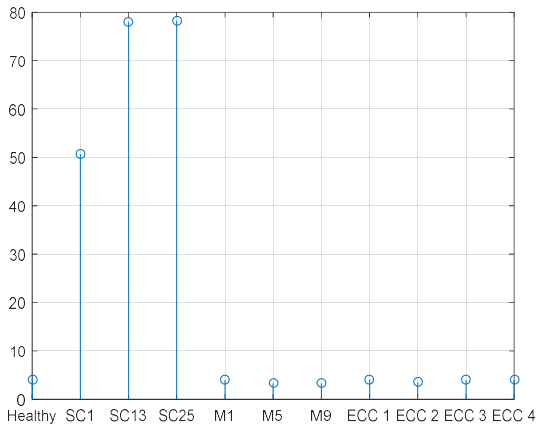

Figure 78: Peak to peak values of temperature data sets

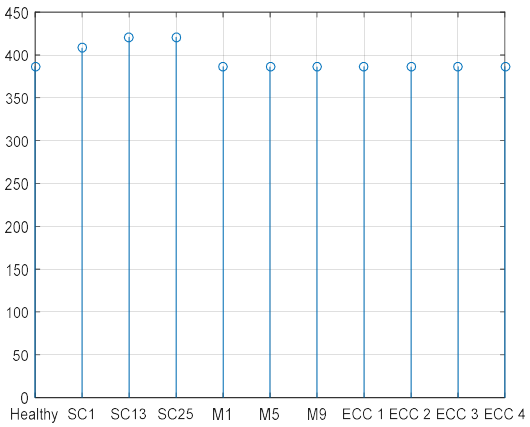

Figure 79: Mean values of temperature data sets

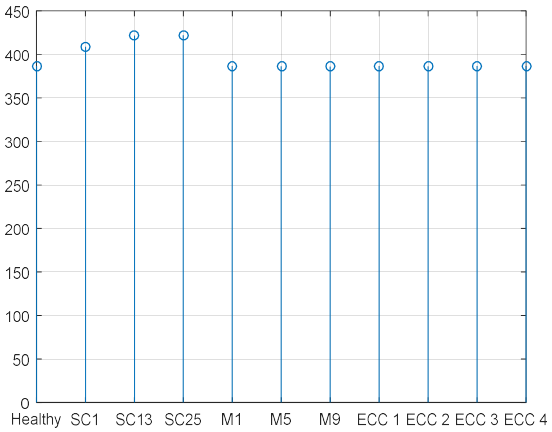

Figure 80: RMS values of temperature data sets

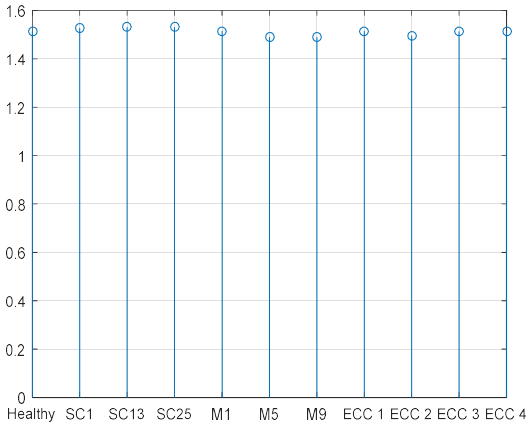

Figure 81: Kurtosis values of temperature data sets

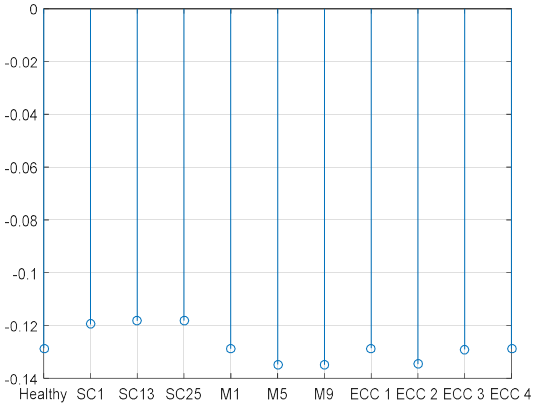

Figure 82: Skewness values of temperature data sets

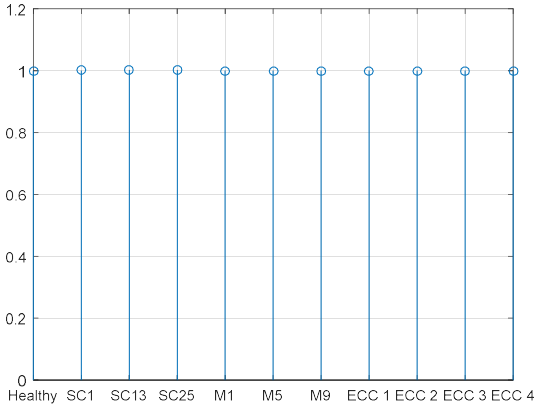

Figure 83: Shape factor values of temperature data sets

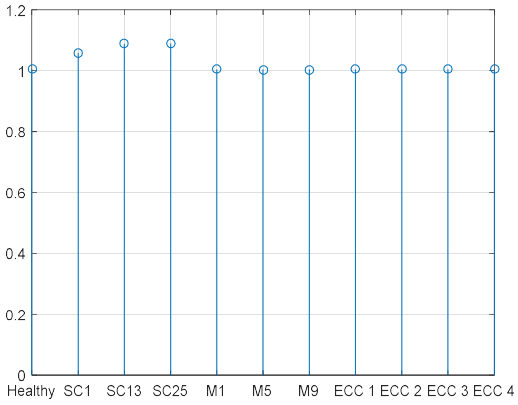

Figure 84: Pulse factor values of temperature data sets

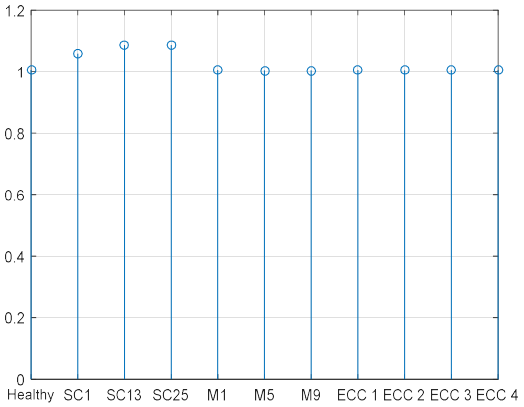

Figure 85: Crest factor values of temperature data sets

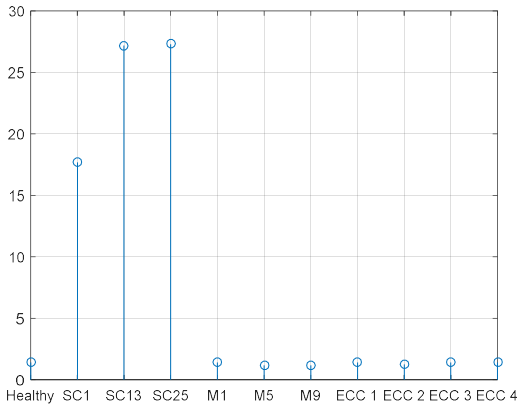

Figure 86: Standard deviation values of temperature data sets

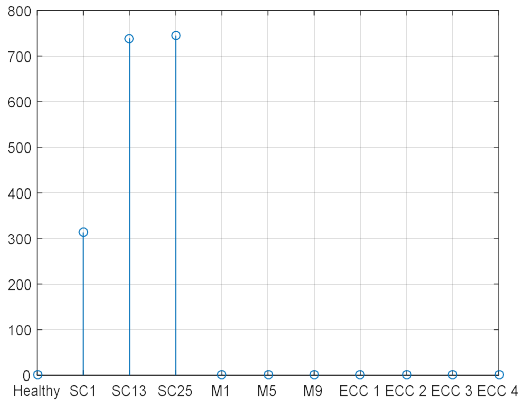

Figure 87: Variance values of temperature data sets

Several remarks can be noticed when observing the statistical parameters of the temperature signals:

- The 'peak to peak' values of data sets while the turn to turn short circuit occurs are widely distinct from the other data sets referring to healthy machine, machine with demagnetization fault and machine with eccentricity fault. However, the peak to peak value is the same when the turn to turn short circuit fault is in slot 13 or 25 because those two slots refers to the same phase.
- The 'mean' and the 'rms' values of data sets when there is turn to turn short circuit are distinct from the other sets referring to healthy machine, machine with demagnetization fault and machine with eccentricity fault. Comparing those referred to turn to turn short circuit, we remark a tiny distinction when the fault is in slots of same phase and a big distinction when the fault is slots of different phases.
- The 'kurtosis' and the 'skewness' values of the data sets shows distinctions in the case of healthy machine, demagnetization faults and eccentricity faults; however, those referred to turn to turn short circuit fault are similar, contrary to the 'peak to peak', 'mean' and 'rms' parameters. Yet, this distinction is very minute where stagger will be faced when the sensor error is considered.
- The shape factor remains constant over the different temperature data sets.
- The 'pulse factor' and 'crest factor' have the almost the same appearance of the 'mean' but we small differences in the values.
- The 'standard deviation' and 'variance' values shows distinction between the case of turn to turn short circuit and the other machine states; however, like 'means', 'rms' and 'peak to peak' values, when the turn to turn short circuit occurs in slots referring to similar phase, those values are almost constant.

To summarize the above, most of the statistical features are useful to detect the presence of turn to turn short circuit. confusion occurs when the machine state is healthy, contain demagnetization fault or eccentricity fault because the values are very near, almost constant. When coming to localize the presence of a fault ambiguity may occur specially when considering the sensor error.

To expand this observation, we will select the 'mean' feature where the mean of all the temperature data sets is evaluated in table 13; the accuracy of the temperature sensor will be taken into consideration. We will check if the average of the sensed temperature is efficient for fault detection.

Table 13 encounter the average sensor temperature for the case of healthy machine, machine with turn to turn short circuit in one of the 36 slots, machine with 1 mm crack in one piece of the 12 magnets and machine with 10% eccentricity fault. Column 3 and 4 illustrates the range of sensor measurement when an error of ±0.55 °C is considered.

TABLE 13: : AVERAGE SENSOR TEMPERATURE FOR DIFFERENT MACHINE STATE

Machine State	Average	Minimum	Maximum
Healthy	113.71	113.16	114.26
SC 1	135.34	134.79	135.89
SC 2	136.19	135.64	136.74
SC 3	137.61	137.06	138.16
SC 4	142.64	142.09	143.19
SC 5	141.43	140.88	141.98
SC 6	142.79	142.24	143.34
SC 7	146	145.45	146.55
SC 8	144.16	143.61	144.71
SC 9	144.12	143.57	144.67
SC 10	147.25	146.7	147.8
SC 11	144.94	144.39	145.49
SC 12	145.81	145.26	146.36
SC 13	147.94	147.39	148.49
SC 14	145.77	145.22	146.32
SC 15	145.71	145.16	146.26
SC 16	148.32	147.77	148.87
SC 17	145.9	145.35	146.45
SC 18	145.64	145.09	146.19
SC 19	148.32	147.77	148.87
SC 20	145.71	145.16	146.26
SC 21	146.15	145.6	146.7
SC 22	147.3	146.75	147.85
SC 23	145.57	145.02	146.12
SC 24	145.85	145.3	146.4
SC 25	148.14	147.59	148.69
SC 26	145.35	144.8	145.9
SC 27	145.26	144.71	145.81
SC 28	147.21	146.66	147.76
SC 29	144.63	144.08	145.18

SC 30	144.4	143.85	144.95
SC 31	145.79	145.24	146.34
SC 32	142.72	142.17	143.27
SC 33	141.72	141.17	142.27
SC 34	143.03	142.48	143.58
SC 35	138.33	137.78	138.88
SC 36	135.98	135.43	136.53
Crack magnet 1	113.69	113.14	114.24
Crack magnet 2	112.75	112.2	113.3
Crack magnet 3	113.27	112.72	113.82
Crack magnet 4	113.62	113.07	114.17
Crack magnet 5	113.37	112.82	113.92
Crack magnet 6	113.43	112.88	113.98
Crack magnet 7	113.64	113.09	114.19
Crack magnet 8	113.05	112.5	113.6
Crack magnet 9	113.18	112.63	113.73
Crack magnet 10	113.06	112.51	113.61
Crack magnet 11	113.98	113.43	114.53
Crack magnet 12	113.77	113.22	114.32
Eccentricity 10 % right	113.71	113.16	114.26
Eccentricity 10 % left	113.27	112.72	113.82
Eccentricity 10 % upward	113.7	113.15	114.25
Eccentricity 10 % downward	113.69	113.14	114.24

In fact, three observations have to be mentioned when examining the numbers in table 13.
First, there is a blatant temperature difference between the case of short circuit turns in stator windings and the three healthy, crack and eccentricity cases.

Second, the average temperature recorded by the sensor in the case of healthy machine, machine with magnet crack and machine with eccentricity fault is almost similar; hence, the average temperature of this sensor is not a good indicator for these types of faults. In other words, those three machine's states generate almost the same temperature distribution in the electric machine.
Third, the average temperature recorded for the case of turn to turn short circuit, each time occurring in one of the slots, is distinct. However, when the normal temperature sensor error is taken into consideration, there will be inconsistency and superposition in the expected measurement range which will lead to false alarm in the field of prognosis and fault detection.

Actually, simulation has shown that this indicator may generate 13 false alarm. The 13 false alarms came from the fact that temperature distribution inside the machine in the case of healthy machine and in the case of 1 mm crack in any of the 12 magnets is the same. Hence, the sensed temperature by the temperature sensor is almost the same in any of the previously mentioned machine states.

To overcome this problem, a second temperature sensor is added and located symmetrically to the first sensor. For each state of machine, temperature data will be collected from two sensors instead of one. The sensor error is also considered. This suggested solution has improved the results where the number of false alarm has decreased to 4. However, this is not satisfactory since our goal is to elaborate a definite result with no false alarms.

To solve this dilemma, two tracks appears: adding sensors at the boundary of the temperature till the number of false alarm suppress to zero or move to the frequency domain and extract useful characteristics from it.

Adding temperature sensors is not cost effective, hence, we will evaluate the frequency domain features hoping that it will elaborate the desired result.

The frequency spectral characteristics will be investigated for the temperature data sets. Figure 87 shows the spectral power density of several temperature data sets; a zoomed view is presented on the right. Some overlaps are clearly visualized.

The average spectral power density of those signals are illustrated in table 14. The numbers in this table shows distinction between turn to turn short circuit faults and all the other machine states similarly to the statistical parameters outcomes. The average spectral power density of temperature signals for healthy machine, machine with 1 mm crack in any of the magnets and machine with 10% eccentricity fault are all similar or almost similar. When it's a turn to turn short circuit fault, if the fault occurs in any of the slots referring to the same phase, the power spectral density is the same.
In other words, the spectral power density, like statistical parameters is useful for turn to turn short circuit fault detection and localization of the phase where the fault is occurring; however, it does not localize the slot where the fault is. It is not useful to detect the other types of fault.

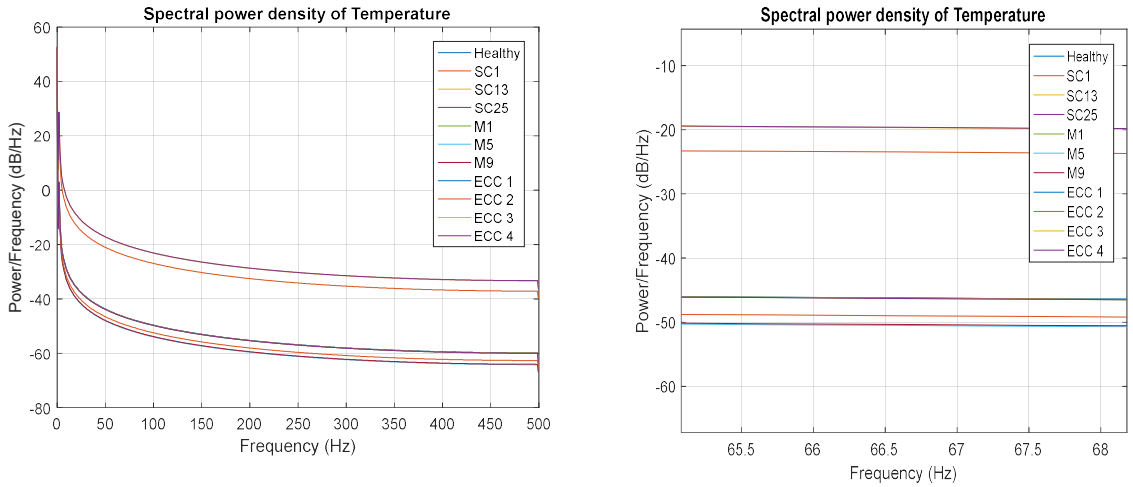

Figure 88: Spectral power density of temperature data sets (zoomed view on the right)

TABLE 14: : AVERAGE SPECTRAL POWER DENSITY OF TEMPERATURE

Machine's State	**Healthy**	**SC1**	**SC13**	**SC25**	**M1**	**M5**	**M9**	**ECC 1**	**ECC 2**	**ECC 3**	**ECC 4**
Average spectral power $(C°)^2$	25.81	60.49	81.79	82.13	25.79	25.29	24.99	25.81	25.14	25.8	25.78

Figure 89 illustrates the Fourier transformation of the collected temperature data for all the investigated states of the machine. Figure 90 is a zoomed view of figure 89. As we can see, a sharp peak is detected at the second harmonics of the spectrum where the frequency is equal ($2*f_{fundamental}$) where $f_{fundamental}$ is the fundamental frequency. A zoomed view on those sharp peaks in figure 89 shows distinction between the different machine states. We mention that the amplitude of this fourier transformation is not normalized.

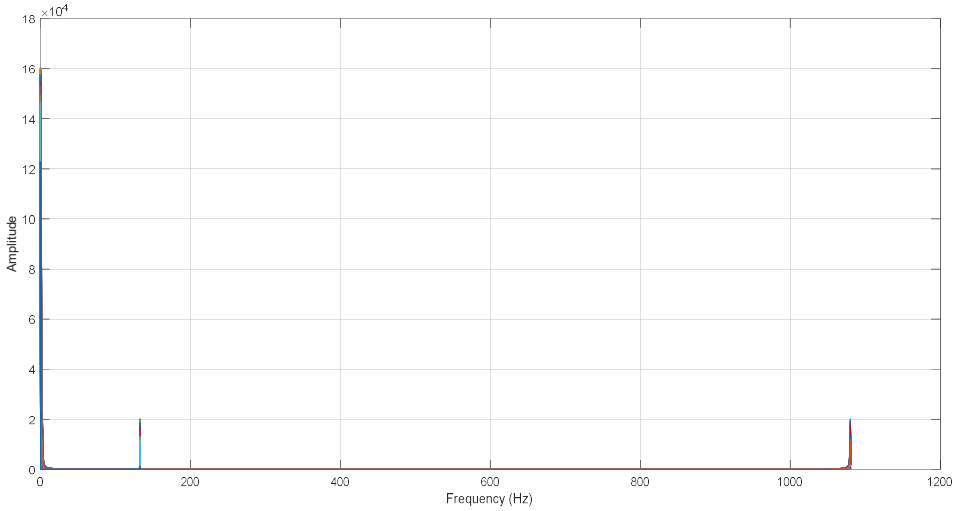

Figure 89: Fourier transformation of the collected temperature data for all the machine states

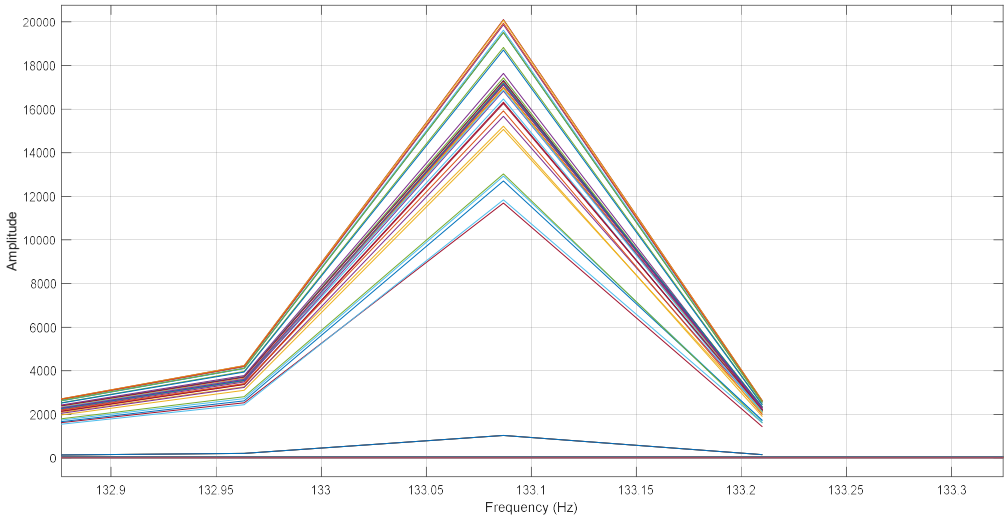

Figure 90: Zoom of figure 89

The graphs in figure 89 are distinct. Comparing the amplitudes, of the frequency domain, several false alarms are generated. Considering the data coming from the two sensors also didn't yield to the desired results. The proximity between temperature for the different cases and the prospected error of the sensor is causing this ambiguity.

To skip this problem, a synthetic index is introduced where the two set of temperature data coming from the two sensors are multiplied to form a new array of data for each case. This new set of data is treated in the frequency domain where it is proven to work well in most of the machine states. False alarm is faced only for the case of healthy machine and machine with 10% eccentricity fault.

Overcoming the confusion between healthy machine and machine with native eccentricity fault is impossible using the temperature aspect of the machine; this problem will be conquered with other dynamic indicators measurements.

3.3.3 Outcomes of Vibration FEM model

The same followed strategy for the thermal analysis will be applied for the vibration model in the aim of generating a useful database of vibration. Then, we will check if the vibration is a good indicator for fault prognosis.

The fictive vibration sensor will be located at the machine boundary, near the temperature sensor located in figure 70. According to [94], the percentage error of the vibration sensor is ±0.06%.
To understand and show the big impact of the different types of faults on the vibration at the machine periphery, the boundary vibration in space for each case is investigated.

In the presence of any type of fault, the distribution of flux density inside the electric machine changes, the distribution of air gap flux density changes, hence, the value of electromagnetic forces applied on the stator changes which leads to vibration variations at the machine's periphery.
We will start with the demagnetization fault where a crack is integrated in the upper periphery of one of the magnets. The vibration of the machine's periphery is generated in this case. For comparison purpose, different depths of crack are tried. The results are illustrated in figure 91.

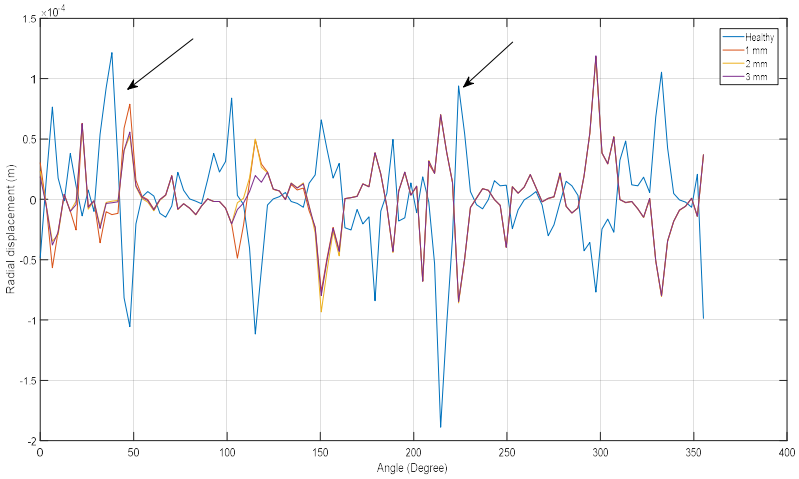

Figure 91: Vibration at machine's periphery in Healthy and demagnetization case

We Remarque in figure 91 that the vibration of the machine, radial displacement of the periphery, changes in the case of crack in one piece of magnet. The displacement on the whole periphery has switched to the opposite sense compared with the displacement in the healthy case. This is due to the new poles generated in the piece of magnet after the occurrence of the crack. We mention that the sense of the crack is parallel to the sense of magnetization and it's between 10 and 20 degrees; hence, the flux lines concentrates at the right and left side of the crack. This is why the electromagnetic force in the area above the crack decrease and the displacement in the machine's periphery directly above the crack decrease as indicated by the first arrow in figure 91.

However, in the second half of the machine, far away from the crack, pointed by the second arrow, the displacement is almost the same like that in the healthy case keeping the sense reversed.
This proofs that monitoring the vibration of the machine's periphery is a good indicator for the detection of demagnetization.

Figure 92 shows the machine's boundary vibration in healthy case and in case of eccentricity fault.
Figure 93 shows the machine's boundary vibration in healthy case and in case of turn to turn short circuit fault.

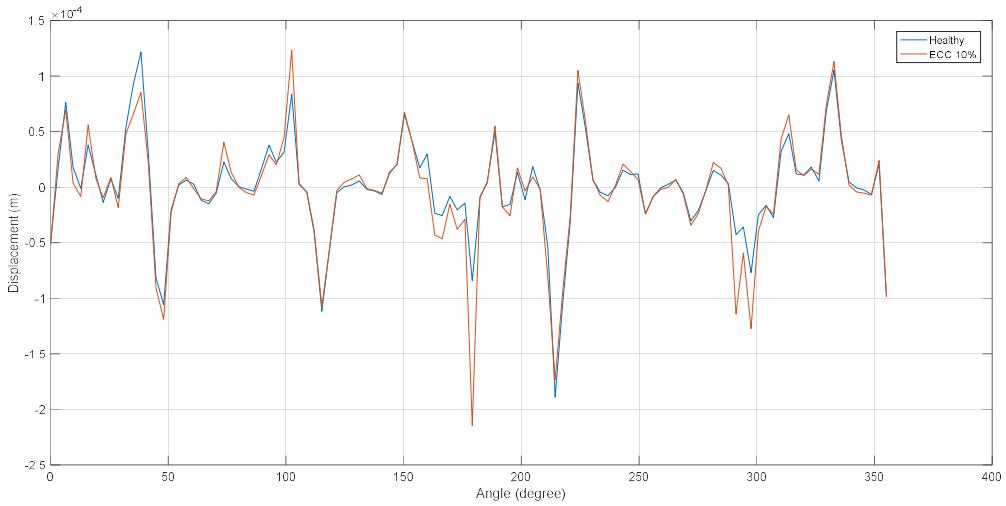

Figure 92: Vibration at machine's periphery in Healthy and eccentricity case

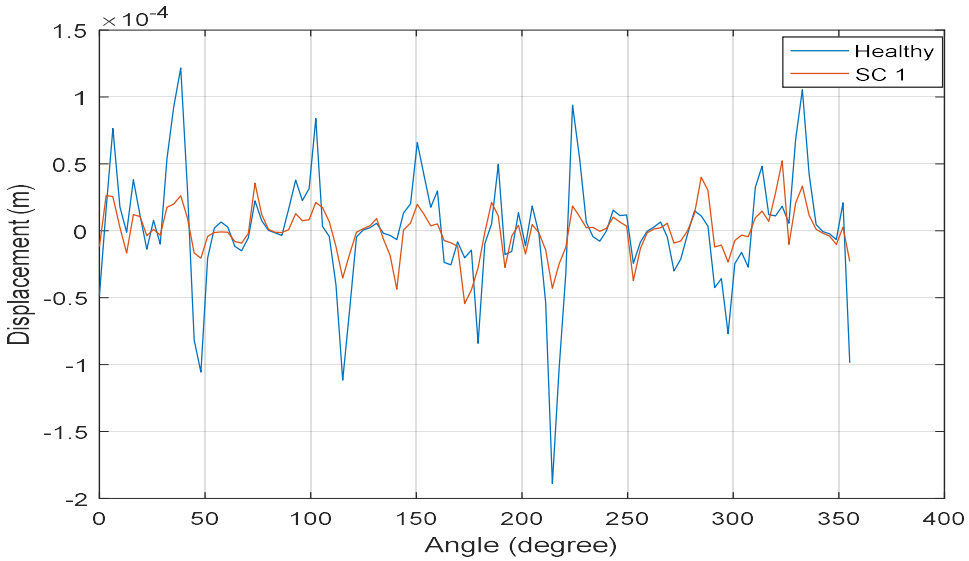

Figure 93: Vibration at machine's periphery in Healthy and turn to turn short circuit case

The graphs illustrated in figure 92 and figure 93 light on the importance of vibration as a fault indicator where it is clear the impact of machine's faults on the vibration of the machine's boundary.

In figure 92, the presence of the eccentricity fault and the non-uniformity in the air gap generates a non-uniformity in the air gap flux density. This non-consistency generates a flaw in the resultant electromagnetic force; which, in his turn, generates vibration defects in the whole machine in general and at the machine's boundary in specific.
In this faulty case, a higher value of boundary displacement is recorded compared with the case of healthy machine.

In figure 93 the presence of turn to turn short circuit in one coil reduce the machine's boundary displacement radically. The presence of short circuit increases the operating temperature of the magnet; hence, its coercive force decreases. This causes a reduction in the air gap flux density, a reduction in the electromagnetic force acting on the stator and a reduction in the boundary displacement of the machine.

After highlighting the efficiency of using vibration signal for fault detection, simulation is done to generate vibration database collected by the vibration sensor for the different states of the machine. Figures 94, 96, 98 and 100 are the vibration signals, in time domain, for the healthy machine, machine with 10 % eccentricity fault, machine with crack in one piece of magnet and machine with turn to turn short circuit in one slot respectively.
Figures 94, 96, 98 and 100 are a zoomed view of the above mentioned machine's vibration.

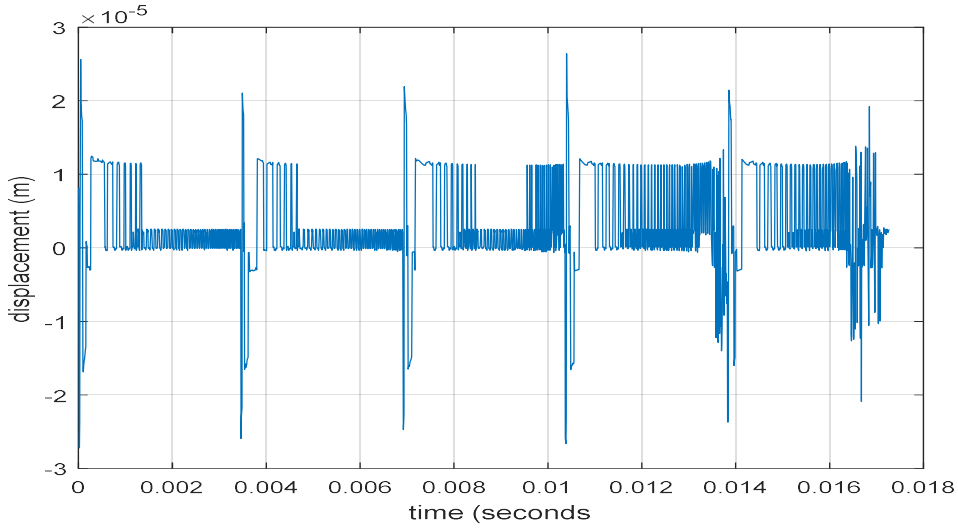

Figure 94: Vibration in time domain, Healthy machine

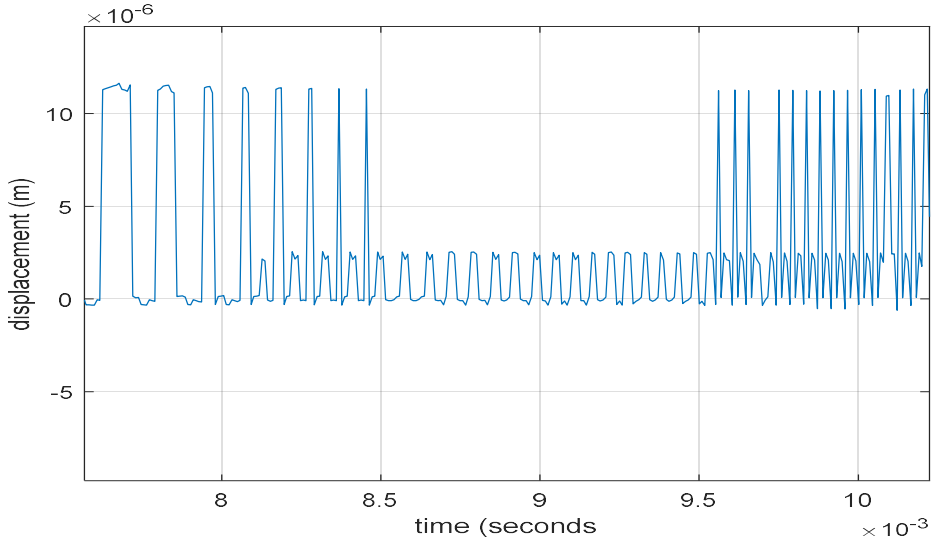

Figure 95: : Zoom figure 94

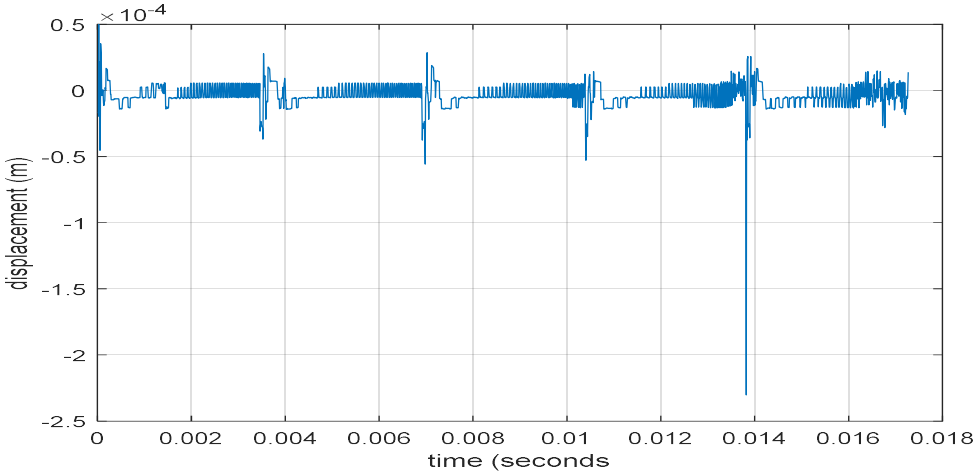

Figure 96: Vibration in time domain, Machine with eccentricity fault

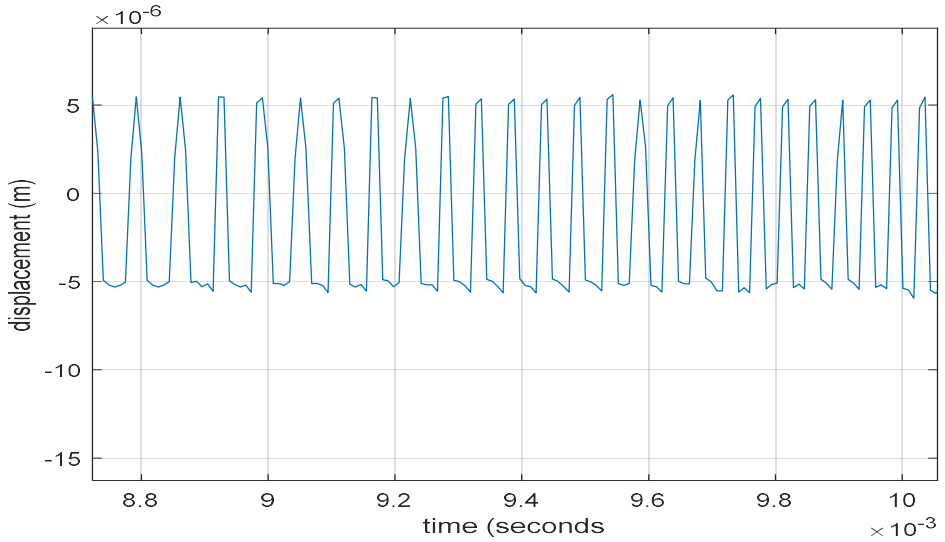

Figure 97: Zoom figure 95

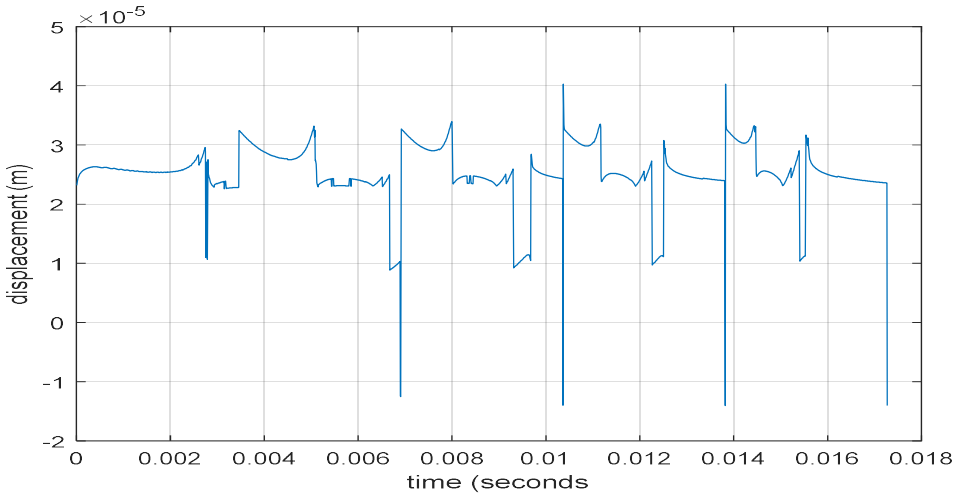

Figure 98: Vibration in time domain, Machine with demagnetization fault

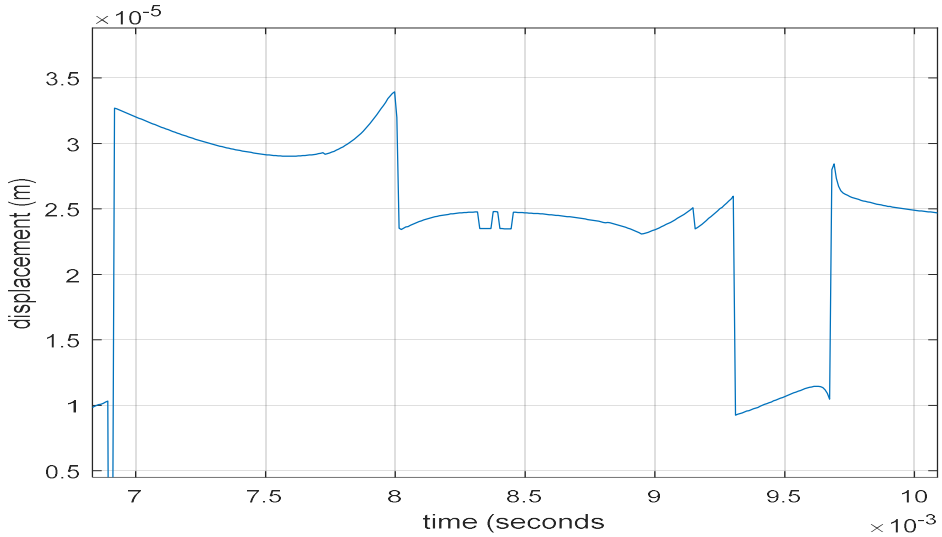

Figure 99: Zoom figure 98

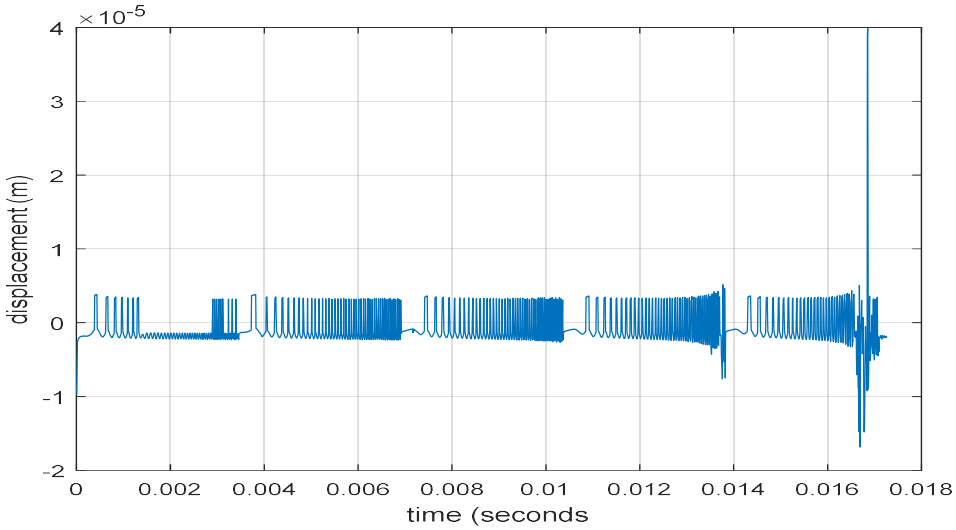

Figure 100: Vibration in time domain, machine with turn to turn short circuit in one slot

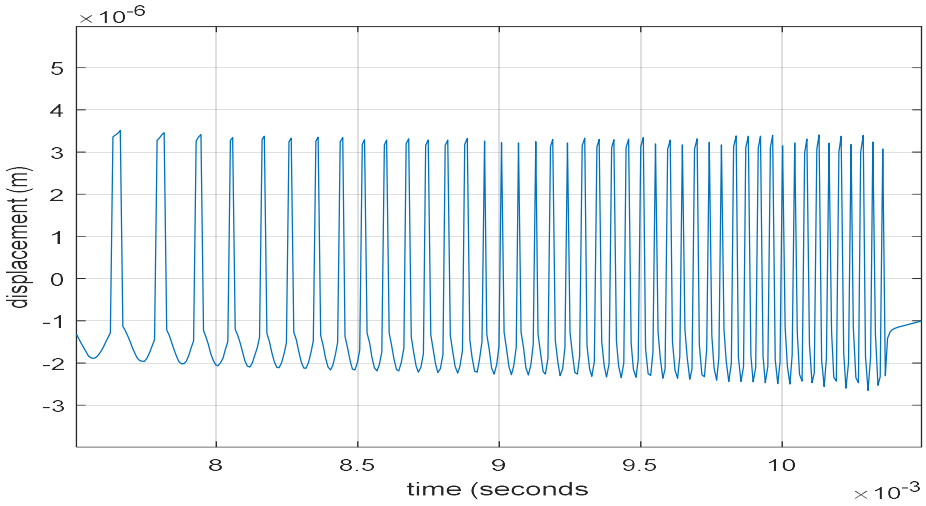

Figure 101: Zoom figure 100

Figure 98 illustrates the vibration result for the case of a crack integrated in magnet 1. However, cracks can occur in any of the 12 pieces of magnet. Hence, to be able to detect the presence of the crack wherever it is located, we conserved the position of the vibration sensor and we started moving the crack from magnet 1 to magnet 12 respectively, one at a time. The registered vibration, resulting from the executed simulation for each case, is illustrated in figure 102.

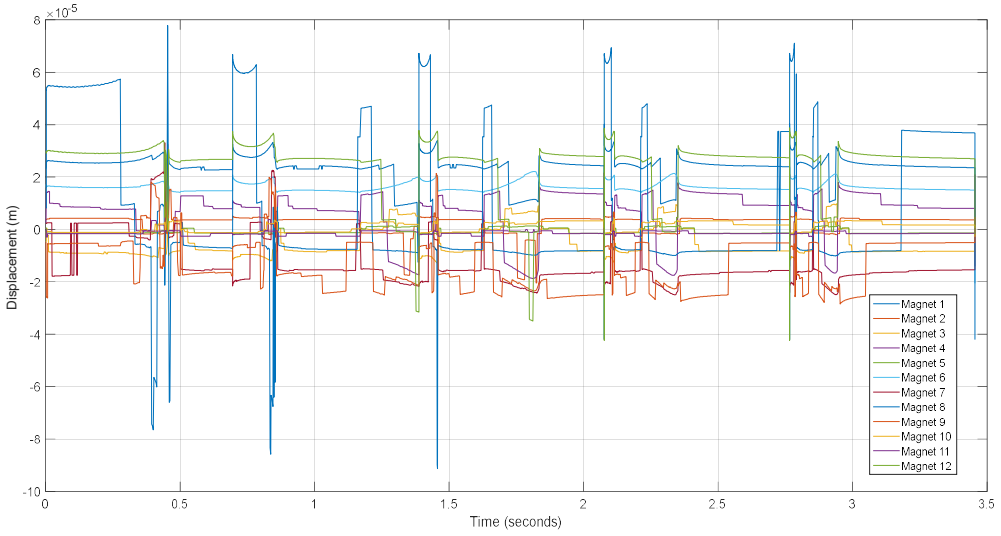

Figure 102: Vibration in time domain when a crack is integrated in one of the machine's magnet

In the same context, the turn to turn short circuit may occur in any coil in the stator. All the cases are to be encountered, hence, we will move the short circuit from slot 1 to slot 36 respectively and register the vibration detected by the sensor. The location of the sensor remains constant. Simulation shows that for each case, the sensor detects a distinct spectrum of vibration.

For illustration, the vibration in the case of turn to turn short circuit in slot 1, 4 and 7 respectively are shown in figure 103. Figure 104 is a zoomed view of figure 103.

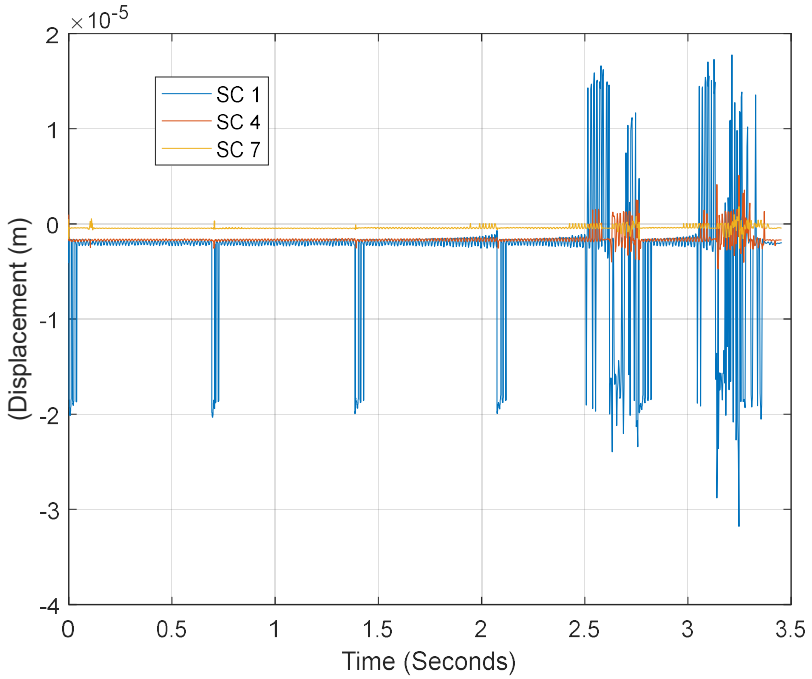

Figure 103: Vibration for the case of turn to turn short circuit in slot 1, 4 and 7

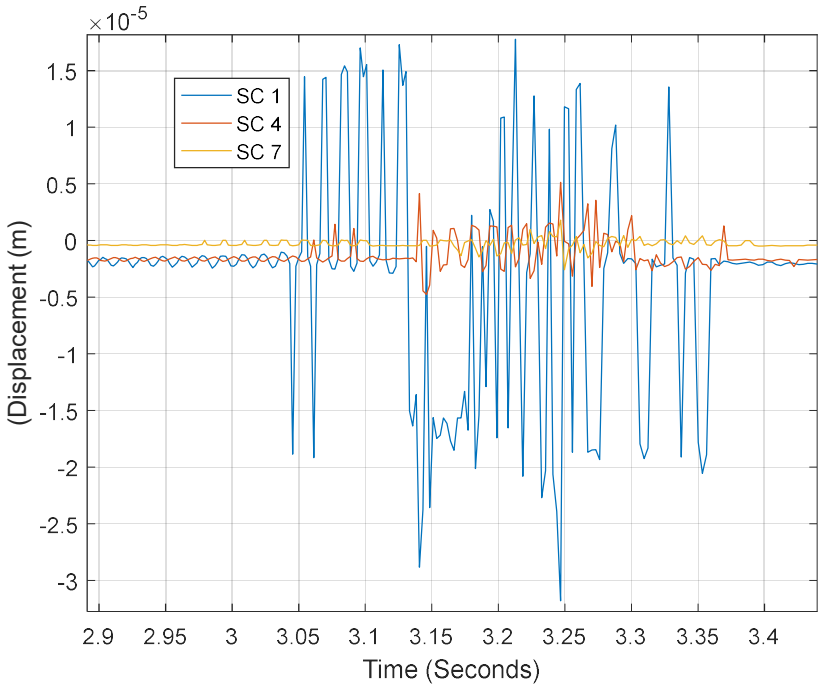

Figure 104: Zoomed view of figure 103

The previously introduced data features will be applied to those vibration signals. We will start with statistical parameters.

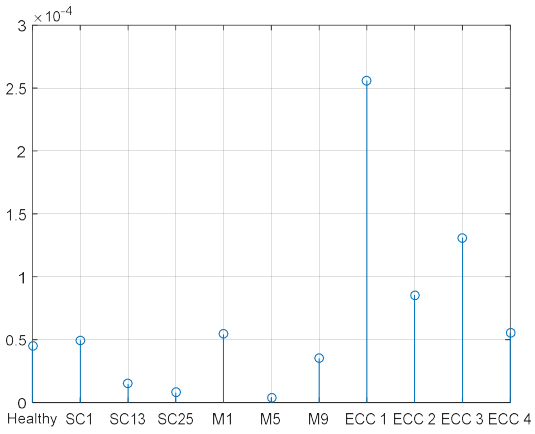

Figure 105: Peak to peak values of vibration data sets

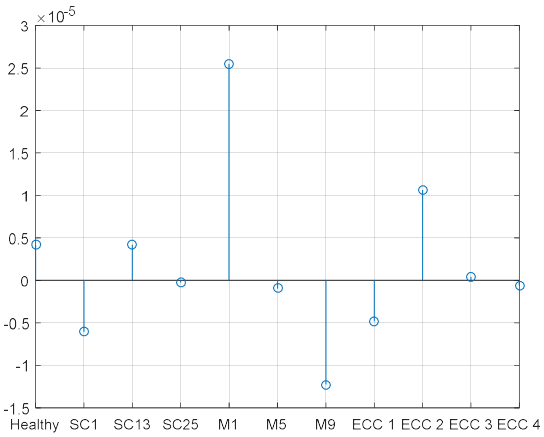

Figure 106: Mean values of vibration data sets

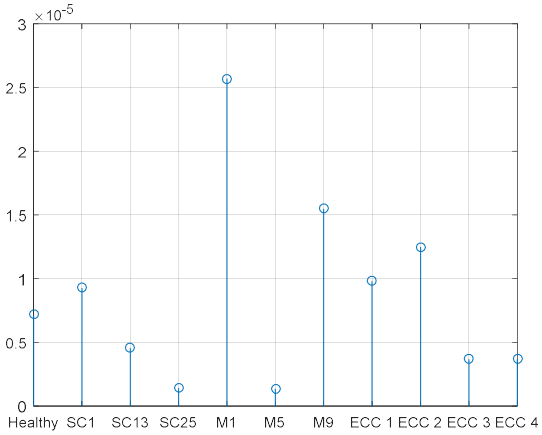

Figure 107: RMS values of vibration data sets

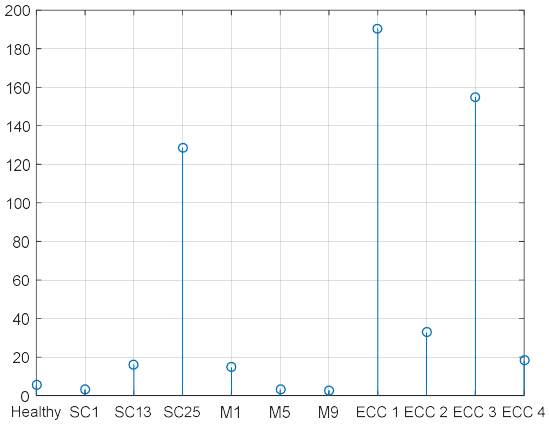

Figure 108: Kurtosis values of vibration data sets

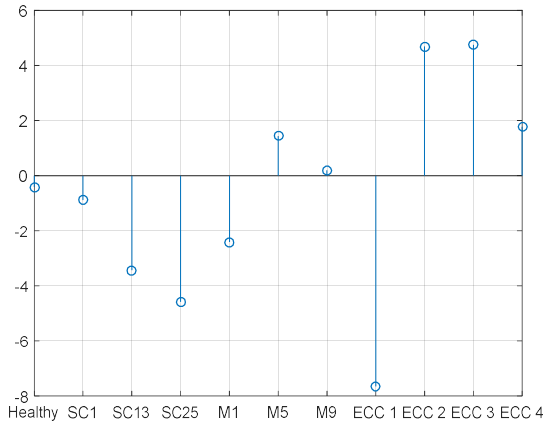

Figure 109: Skewness values of vibration data sets

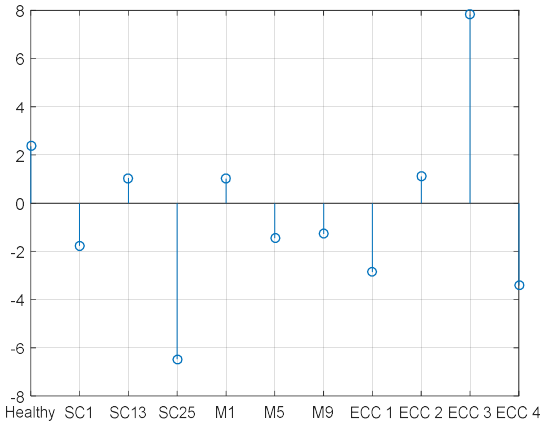

Figure 110: Shape factor values of vibration data sets

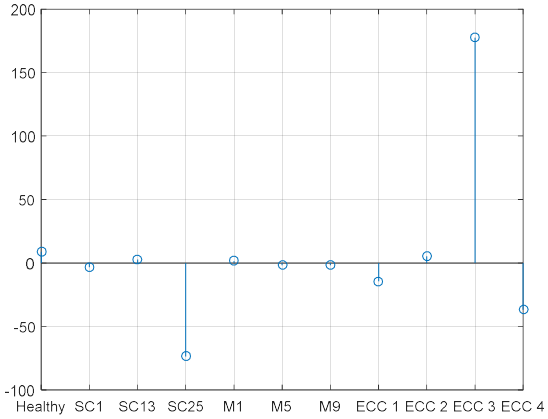

Figure 111: Pulse factor values of vibration data sets

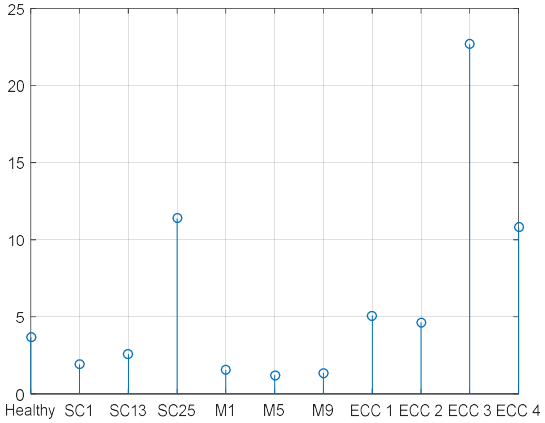

Figure 112: Crest values of vibration data sets

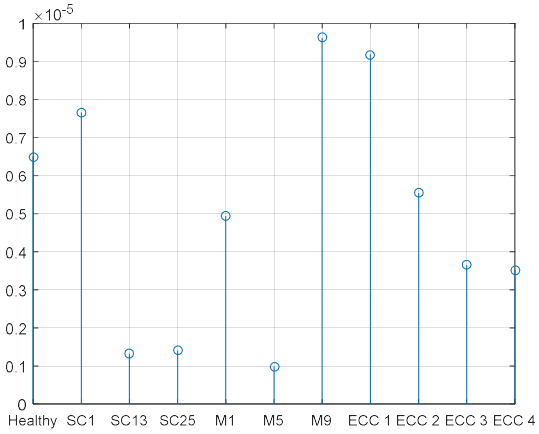

Figure 113: Standard deviation values of vibration data sets

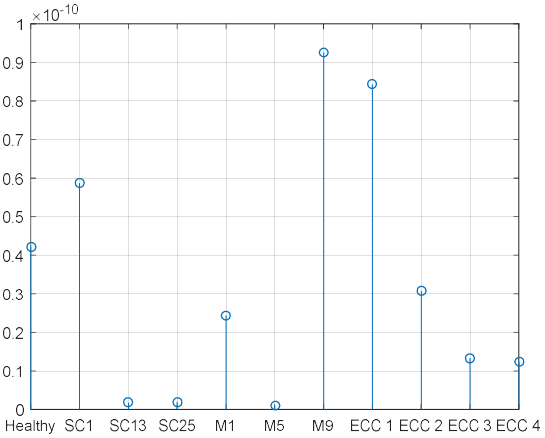

Figure 114: Variance values of vibration data sets

Observing the above statistical parameters of the vibration, we remark that most of them contains similarities in the values. The peak to peak, mean and RMS values contain less similarities and visible disparities.

The mean or average is selected to be evaluated for all the machine states. In table 15, the average displacement over one revolution after integrating different types of fault in the electric machine is noted.

TABLE 15: MACHINE VIBRATION FOR DIFFERENT TYPES OF FAULT

State of the machine	**Average displacement in meters (*10^-4)**	**Minimum sensor reading (*10^-4)**	**Maximum sensor reading (*10^-4)**
Healthy	0.0416	0.0416	0.0416
Crack magnet 1	0.255	0.255	0.255
Crack magnet 2	0.0314	0.029516	0.033284
Crack magnet 3	-0.065	-0.0611	-0.0689
Crack magnet 4	0.0799	0.075106	0.084694
Crack magnet 5	-0.0095	-0.00893	-0.01007
Crack magnet 6	0.1663	0.156322	0.176278
Crack magnet 7	-0.1666	-0.156604	-0.176596
Crack magnet 8	0.1544	0.145136	0.163664
Crack magnet 9	-0.1225	-0.11515	-0.12985
Crack magnet 10	0.0131	0.012314	0.013886
Crack magnet 11	-0.0145	-0.01363	-0.01537
Crack magnet 12	0.2675	0.25145	0.28355
Eccentricity fault (up)	-0.0481	-0.0481	-0.0482
Eccentricity fault (down)	0.1065	0.1064	0.1066
Eccentricity fault (right)	0.0043	0.0043	0.0043
Eccentricity fault (left)	-0.0058	-0.0058	-0.0058
SC1	-0.0607	-0.06066358	-0.06074
SC2	-0.0479	-0.04787126	-0.04793
SC3	-0.0127	-0.01269238	-0.01271
SC4	-0.0152	-0.01519088	-0.01521
SC5	-0.0614	-0.06136316	-0.06144
SC6	-0.0465	-0.0464721	-0.04653
SC7	-0.0036	-0.00359784	-0.0036
SC8	0.1594	0.15930436	0.159496
SC9	0.0661	0.06606034	0.06614
SC10	0.0064	0.00639616	0.006404
SC11	0.0196	0.01958824	0.019612

SC12	0.0251	0.02508494	0.025115
SC13	0.0419	0.04187486	0.041925
SC14	0.0314	0.03138116	0.031419
SC15	0.0235	0.0234859	0.023514
SC16	0.0089	0.00889466	0.008905
SC17	-0.0857	-0.08564858	-0.08575
SC18	-0.0306	-0.03058164	-0.03062
SC19	-0.0894	-0.08934636	-0.08945
SC20	-0.0497	-0.04967018	-0.04973
SC21	0.011	0.0109934	0.011007
SC22	-0.0405	-0.0404757	-0.04052
SC23	0.1388	0.13871672	0.138883
SC24	0.104	0.1039376	0.104062
SC25	-0.0024	-0.00239856	-0.0024
SC26	0.0502	0.05016988	0.05023
SC27	0.0084	0.00839496	0.008405
SC28	-0.0087	-0.00869478	-0.00871
SC29	-0.0185	-0.0184889	-0.01851
SC30	-0.0175	-0.0174895	-0.01751
SC31	-0.0028	-0.00279832	-0.0028
SC32	0.0016	0.00159904	0.001601
SC33	0.0114	0.01139316	0.011407
SC34	0.1931	0.19298414	0.193216
SC35	0.0478	0.04777132	0.047829
SC36	0.0723	0.07225662	0.072343

As shown in the graphs and tables above, the vibration sensed by the sensor is dissimilar for the different investigated machine states. This leads to admit the rightness of using vibration signal for prognosis and fault detection.

The suggested feature to be elaborated from the vibration signals is the average over one revolution. The average displacement in meters is illustrated in the second row of table 15. The minimum and maximum corresponding sensor reading for the different machine's states, when talking its percentage error (± 0.06%) into consideration, is illustrated in the third and fourth columns respectively.

We remark that the impact of the sensors error is almost negligible.
The average displacement for the different cases are widely dispersed; hence, vibration signal is a good indicator for fault detection and identification.

The frequency domain features will be checked also. Figure 115, 116 and 117 respectively illustrates the spectral power density of vibration in healthy machine and machine with eccentricity

fault, machine demagnetization fault and machine with turn to turn short circuit fault. The graphs show disparity between the signals.

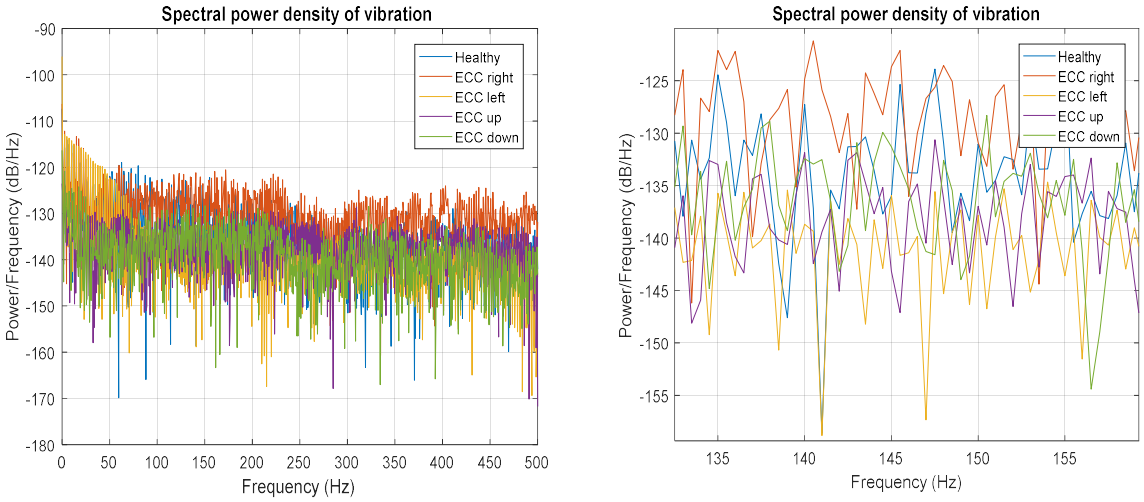

Figure 115: Spectral power density of vibration in case of healthy machine and machine with eccentricity fault (zoomed view on the right)

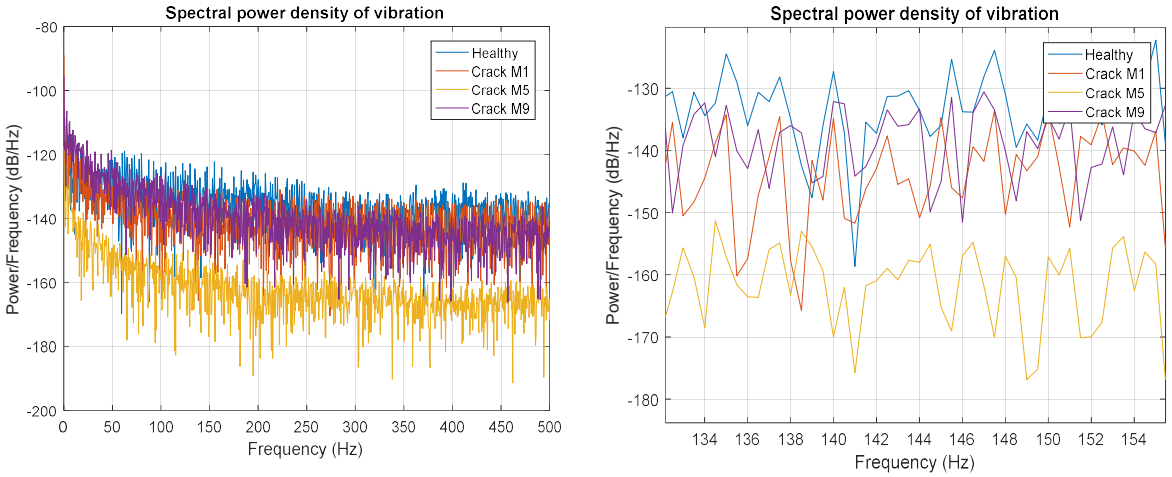

Figure 116: Spectral power density of vibration in case of healthy machine and machine with crack in one magnet (zoomed view on the right)

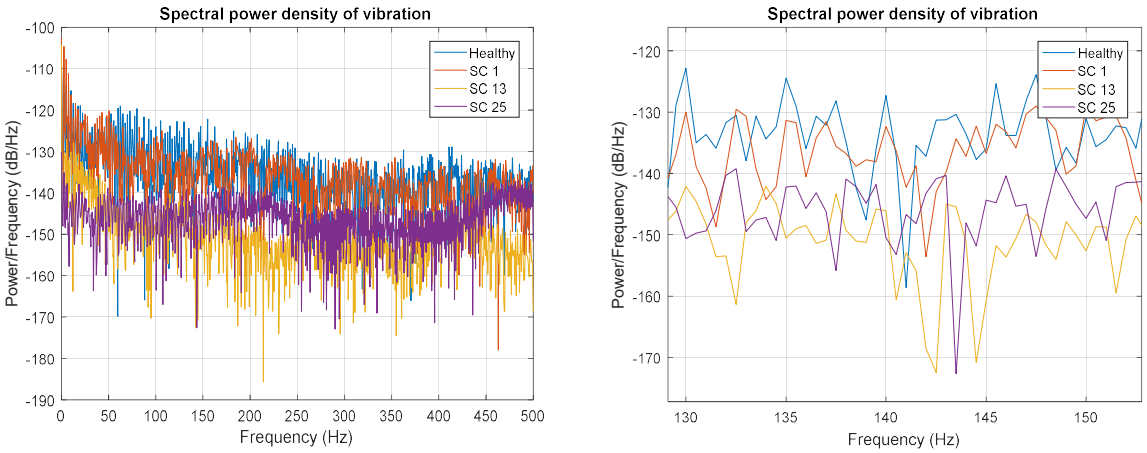

Figure 117: Spectral power density of vibration in case of healthy machine and machine with turn to turn short circuit (zoomed view on the right)

The average spectral power density of vibration/displacement is presented in table 16. The values are dispersing.

TABLE 16: AVERAGE SPECTRAL POWER DENSITY OF DISPLACEMENT

Machine's State	**Healthy**	**10% eccentricity right**	**10% eccentricity left**	**10% eccentricity up**	**10% eccentricity down**
Average spectral power of displacement $(m)^2$	6.0637e-14	1.0776e-13	2.8092e-13	1.3784e-14	1.4726e-14
Machine's State	**Healthy**	**1 mm crack in magnet 1**	**1 mm crack in magnet 5**	**1 mm crack in magnet 9**	
Average spectral power of displacement $(m)^2$	6.0637e-14	0.1295e-11	0.0003e-11	0.0387e-11	
Machine's State	**Healthy**	**Turn to turn short circuit in slot 1**	**Turn to turn short circuit in slot 13**	**Turn to turn short circuit in slot 25**	
Average spectral power of displacement $(m)^2$	6.0637e-14	0.1134e-12	0.0398 e-12	0.0021 e-12	

Like the torque and the temperature signals, the harmonics of the vibration signal will also be investigated. The Fourier transformation of several vibration data sets are illustrated in figure 118.

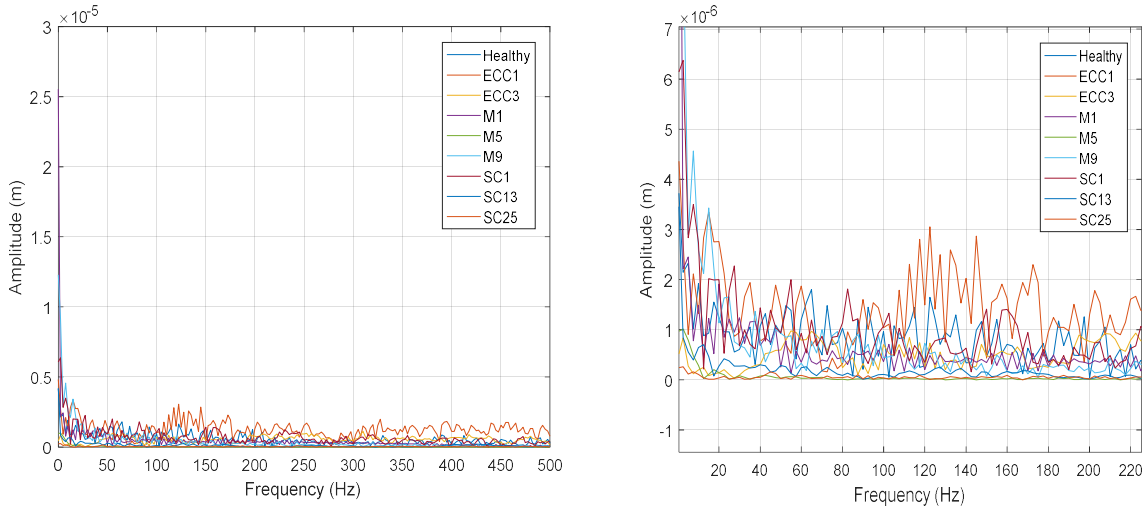

Figure 118: Fourier transformation of vibration (zoomed view on the right)

When observing the spectral Fourier transformations in figure 118, several peaks can be detected for some machine states. is However; those peaks are at all frequencies along the frequency axis; in other worlds, there is no privilege for a specific amplitude above the others. Hence, the amplitudes of frequency components are not good indicators for fault detection.

3.4 Priority between parameters' indicators for fault detection and localization

As we presented earlier, the three selected dynamic parameters: Torque, temperature and vibration are all affected, with uneven percentages and ranges for the different investigated machine's states and faults.
To decide which parameters are more likely to be a fault indicator for a specific fault, table 17 will illustrate the deviation of each parameter in the case of a specific fault, compared with the case of healthy machine. The comparison is of the average values of the signals.

TABLE 17: : PERCENTAGE OF PARAMETER DEVIATION FOR DIFFERENT TYPES OF FAULT

	Torque	**Temperature**	**Vibration displacement**
Machine with magnet crack	15 %	- 0.02%	± 384 %
Machine with SC in one slot	-28 %	27%	± 158 %
Machine with 10% eccentricity fault	11 %	0%	± 216 %

When dealing with fault detection, the vibration is the mostly and highly affected parameter after any of the mentioned types of fault is integrated in the electrical machine. The second affected parameter in the case of fault is the electric torque. The less affected parameter is the temperature. However, for fault localization, the temperature is useful to localize the slot where the turn to turn short circuit occurred. The vibration is useful to localize the magnet where the crack occurred.
For prognostic purpose, it is more likely to prevent false alarm by monitoring more than one dynamic parameter for each types of fault. Hence, all collected parameters are of big interest to assure safe and right prognostic decision.

3.5 Signature table for fault detection and localization

All the previously treated signals referred to the different dynamic machine parameters for the different types of investigated faults are summarized and illustrated in table 18. 'detection' designate the detection of the type of fault: demagnetization, turn to turn short circuit or eccentricity; 'localization' means specifying where the fault occurs: demagnetization of magnet 1, demagnetization of magnet 2, … or turn to turn short circuit fault in slot 1, torn to turn short circuit fault in slot 2, … etc.
In this table, the effect of those features on the detection and localization of turn to turn short circuit fault, demagnetization fault and eccentricity fault is designated by:

- 'Y' if **yes** the relevant feature is affected when the fault occurs.
- 'N" if **no** the relevant feature is not affected when the fault occurs.
- 'P' if the effect of the fault on the relevant feature is **partial**.

'Partial' for turn to turn short circuit fault indicates that the phase containing the shorted coil is detected and not the slot containing this shorted coil. 'Partial' for demagnetization and eccentricity fault means that some demagnetization or eccentricity types of fault are detected and not all of them. For example, the crest factor of vibration datasets shows similar results when there is crack in magnet 5 'M5' or 9 'M9' and distinct result when the crack is in magnet 1 'M1' (figure 112). Another example is in figure 111, the shape factor detects the right, up and down 10% eccentricity fault being distinct from the other vibration datasets; however, the shape factor of the 10% eccentricity fault to the left is similar to the healthy case.

As mentioned previously, the selected feature for 'Torque' and 'Vibration' datasets will be the 'Mean' and the selected feature for the 'Temperature' datasets will be the 'Amplitude of frequency component'.

TABLE 18: SIGNATURE TABLE FOR FAULT DETECTION AND LOCALIZATION

		Feature											
		Torque											
		PP	***Mean***	***RMS***	***Ku***	***Sk***	***SF***	***PF***	***CF***	***SD***	***V***	***APS***	***AFC***
Turn to turn short circuit	***Detection***	Y	Y	Y	Y	Y	N	Y	Y	Y	Y	Y	N
	Localization	N	N	N	N	N	N	N	N	N	N	N	N
Demagnetization	***Detection***	Y	Y	Y	Y	Y	N	Y	Y	Y	Y	Y	N
	Localization	N	N	N	N	N	N	N	N	N	N	N	N
Eccentricity	***Detection***	Y	Y	Y	Y	Y	N	Y	Y	Y	Y	Y	N
	Localization	N	N	N	N	N	N	N	N	N	N	N	N
		Temperature											
		PP	***Mean***	***RMS***	***Ku***	***Sk***	***SF***	***PF***	***CF***	***SD***	***V***	***APS***	***AFC***
Turn to turn short circuit	***Detection***	Y	Y	Y	Y	Y	N	Y	Y	Y	Y	Y	Y
	Localization	P	P	P	N	N	N	P	P	P	P	P	Y
Demagnetization	***Detection***	N	N	N	N	N	N	N	N	N	N	N	Y
	Localization	N	N	N	N	N	N	N	N	N	N	N	Y
Eccentricity	***Detection***	N	N	N	N	N	N	N	N	N	N	N	N
	Localization	N	N	N	N	N	N	N	N	N	N	N	N
		Vibration											
		PP	***Mean***	***RMS***	***Ku***	***Sk***	***SF***	***PF***	***CF***	***SD***	***V***	***APS***	***AFC***
Turn to turn short circuit	***Detection***	Y	Y	Y	Y	Y	P	P	P	Y	Y	Y	P
	Localization	Y	Y	Y	N	Y	P	P	P	P	P	Y	P
Demagnetization	***Detection***	Y	Y	Y	Y	Y	P	P	P	Y	Y	Y	P
	Localization	Y	Y	Y	N	Y	P	P	P	Y	Y	Y	P
Eccentricity	***Detection***	Y	Y	Y	Y	Y	P	P	P	Y	Y	Y	P
	Localization	Y	Y	Y	Y	N	P	P	P	Y	Y	Y	P

3.6 Conclusion

The followed strategy in this chapter is of big importance where we formed a database of suitable dynamic parameters for the different types of faults: demagnetization, turn to turn short circuit and eccentricity.

To do so, simulation is done for the machine during its healthy operation and after the integration of tiny faults in it. The goal was to generate parameter indices that are useful to detect and localize the presence of faults at its early stage.
Torque, temperature and vibration database is generated from electromagnetic, thermal and vibration finite element model respectively.

It has been proven that monitoring the outer temperature and vibration of the machine permits the detection and the localization of different types of faults. Some temperature features are partially useful in fault localization; where, for example, it may help in selecting the phase where a turn to turn short circuit fault occurs and not the specific slot containing this fault. Monitoring the torque will help only in detecting the presence of a specific type of fault; it's not helpful for fault localization.

The selected feature for torque data sets is the ‘mean’ of the signal; the selected feature for temperature data sets is the amplitude of frequency component; the selected feature for vibration data sets in the ‘mean’ of the signal. Since, the percentage error of the ‘Torque’, ‘Temperature’ and ‘Vibration’ sensors are taken into consideration, those features will be an interval rather than a discrete value.

The collected database and the extracted features in this chapter will form the essential platform where the prognostic strategy will be built.

Chapter 4: Prognostic Approach-Hidden Markov Model (HMM)

4.1 Introduction

In this chapter the prognostic approach will be presented.
The selected prognostic technique is the Hidden Markov Model (HMM). HMM is a data-driven prognostic approach since it tends to derive models directly from collected Condition Monitoring (CM) data; they get predictive output directly in terms of CM data. It's a stochastic signal model. It is called 'hidden' because the prediction current and future state of the investigated system is guaranteed by monitoring a sequence of features extracted from selected observable or observables only.
HMM should be built to fulfill three tasks: First detecting the presence of fault, second predicting the current state of the system, third predicting the future state of the system and calculate its remaining useful life (RUL), and this is the essence of prognosis.
In the following, the prognostic strategy, using HMM will be illustrated. The useful ways to express and calculate the remaining useful life (RUL) will be discussed.

4.2 Hidden Markov Model (HMM)

4.2.1 HMM strategy

A prognostic strategy, using HMM, will be developed to detect the presence of fault at its early stage. Extracted features of data coming from torque, temperature and vibration sensors will be the input of the prognostic model HMM. The output of the model will be the prognostic decision that will state if the machine is at its healthy or faulty state. If it's at a faulty state, it will precise the type of fault and its remaining useful life.

The chart in figure 118 represents the prognostic strategy and its tasks.

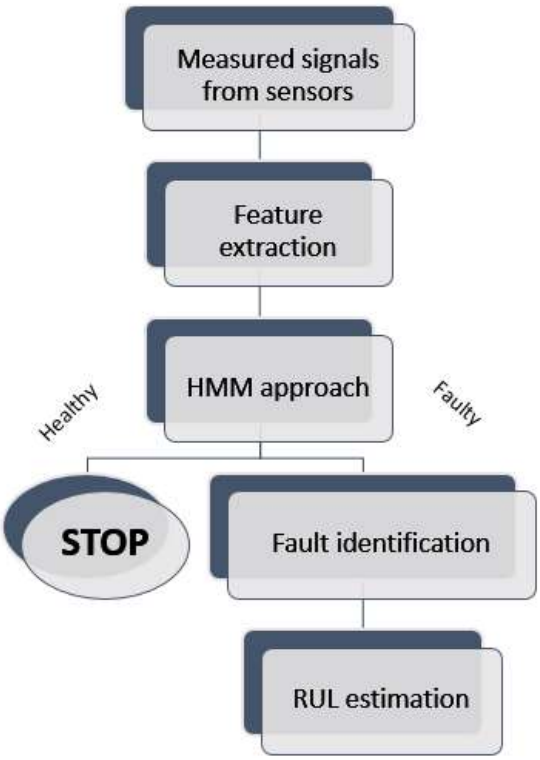

Figure 119: the prognostic strategy

In the beginning, the raw signal coming from torque, temperature and vibration sensors is collected. The selected features in chapter 3, for each dataset, will be extracted over one machine revolution. Those features will be the input of the prognostic model as will be explained in the following sections. This prognostic approach will answer the following question: 'what is the state of the machine?'. If the machine is Healthy, we stop. If the machine is faulty, the type of fault: demagnetization, eccentricity or turn to turn short circuit, will be identified and localized. Then, the remaining useful life of the damaged component will be estimated.

4.2.2 HMM: technical concept and model formulation

HMM consists of [95]:

- A set of states 'S': S= {S0, S1, S2, …, Sn} where 'S0' is the initial state of the system and S_i, i ϵ {1, 2,…,n} is the faulty state. In our application, the studied system is the permanent magnet machine; its initial state is the healthy machine and the faulty states are the machine with turn to turn short circuit, demagnetization fault or eccentricity fault. We mention that we will investigate system with single primitive fault.

- An initial probability value (π) for each state: it consists of a guess expressing the probability that initially the system is at a specific state

- A transition probability matrix (TM): this matrix represents the probability that the system, being at a certain current state, move to another state. The size of matrix (TM) is n by n where n is the number of available states.

- An output probability distribution matrix or emission matrix (EM): it expresses the likelihood that a certain measured sequence of values corresponds to a specific sequence of states. The size of matrix (EM) is n by m where m is the number of observables.

HMM can be generally expressed as: λ= (TM, EM, π).

In general, there is two main types of HMM: discrete and continuous [97].
The difference between the two types is the shape of input that accept the model.
Discrete hidden Markov model is suitable for examples containing limited number of observations.
Continuous hidden Markov model is suitable when the input is a real number. Unlike discrete HMM, the output probability (EM) must be calculated from a set of weighted probability using any type of probability distribution technique like “Gaussian Distribution”.

The elements needed to build a HMM are as follows [98]:

- The determination of ‘n’ number of distinct possible states in the model. They are expressed as:

S= {S_1, S_2, S_3, …, S_n}. The states are designated by {1, …, n}, each corresponding to a specific system’s condition.

The current and future states of the investigated system are the hidden or latent variables of the HMM.

- The determination of ‘n’ number of distinct observation sequences. They are expressed as:

O= {O_1, O_2, …, O_n}. The observations can be {discrete, R, $R^{d, \cdots}$}.

In our application, each observation O_i encounter more than one observable as will be explained later in figure 122.

The hidden variables and the observed data of the HMM can be illustrated by Trellis diagram in figure 119.

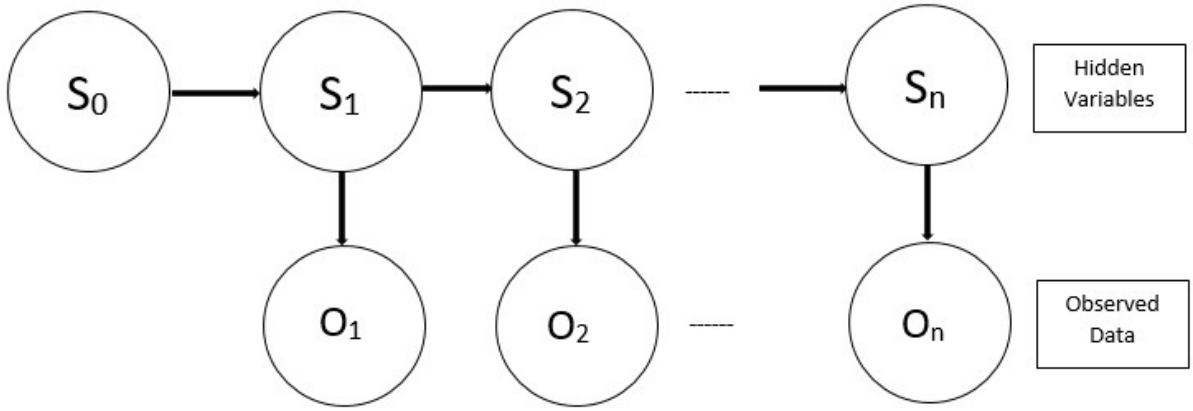

Figure 120: Trellis Diagram

S_0 is the initial state of the system.
The arrows directed from S_k to O_k indicates that they are conditionally dependent.
The S_k-O_k couple is independent of all the other state-observation couples.
At time t, to know the state S_t of the system, all we need is the relevant observation and the previous state S_{t-1}; the prediction of S_t is independent of all states prior to S_{t-1}.

The factorization or the joint probability distribution corresponding to the above Trellis model is expressed as [173] [174]:

$$P(O_1, \dots, O_n, S_1, \dots S_n) = P(S_1) * P(O_1|S_1) \ * \prod_{k=2}^{n} P(S_k|S_{k-1}) * P(O_k|S_k) \quad (49)$$

The parameters needed to build the HMM are as follows:

- An initial distribution probability which is an initial probability value (π) for each state. It is expressed as:

$$\{\pi_1, \dots, \pi_n\}$$

Where:

$$\pi_i = P(x_1 = S_i) \ where \ i \in \{1, \dots, n\} \quad (50)$$

x_1 is the system's state process at time t_1.

- TM which is the transition probability matrix. It is the probability of going from state 'i' to state 'j' and is expressed as:

$$TM(i,j) = P\left(S_{(k+1)=j} \,\middle|\, S_{(k)=i}\right) \ where \ i \ and \ j \in \{1, \dots, n\} \quad (51)$$

Equation 51 defines that: if the current state of the treated system S_k is 'i', the probability that the next state of the system S_{k+1} will be 'j' is TM(i,j). In other words, it represents the probability that the system moves from one state to another.
The size of the transition matrix is (n x n).

- EM which is the emission probability matrix. It is expressed as:

$$EM(O_k) = (P(O_k|S_{(k)=i}) \quad (52)$$

This definite how likely is a certain observable is generated by a specific state.
The emission probability matrix can be arbitrary.
When the observed data is continuous like temperature, vibration, or torque, Gaussian distribution is common.

After setting the above mentioned parameters for the HMM we are building, the next step will be training the model or decoding the model.
Algorithms like Viterbi and forward backward are suitable for this purpose. In fact, Viterbi algorithm was a replacement of "forward-backward method" introduced by Baum.
It has been shown in [165] that Baum-Welch algorithm, Viterbi algorithm and the classical methods are all applicable with left to right models. Those are the engines that drives the HMM.

In general, the model training is used if the set of state sequences that the system may follow are known, the decoding is used if the set of observations is known and we aim to know the most likely corresponding set of states to these observations.
When training data, Baum Welch (also called forward-backward algorithm) is used. When decoding data, Viterbi algorithm is used.

In our application, the Viterbi application will be used to drive the hidden Markov model after building it.

Viterbi Algorithm:

Viterbi is a dynamic programming algorithm discovered by 'Viterbi' in 1967. It follows the concept of minimizing the error probability by comparing the likelihoods of a set of possible state transitions that can occur, and decide which one has the highest probability to occur [96].
Its objective is to find the best path through the trellis diagram that is closest to the received observation sequence.

Before applying Viterbi algorithm, we assume that initial distribution, transition distribution and emission distribution are known.
The goal of the algorithm is to compute the maximum probability of states 'S' having a sequence of observations 'O'. where $O=O_{1:n,}$ a vector containing the observed data, and $S=S_{1:n}$, a vector containing the corresponding states [175] [176].

The goal of the algorithm is to assure:

$$S^* = \underset{S}{argmax} P(S|O) \quad (53)$$

Where S^* is the most likely sequence of states corresponding to the given sequence of observations.

We note that:

$$\underset{S}{argmax} P(S|O) = \underset{S}{argmax} P(S,O) \tag{54}$$

We will call the maximum likelihood of the occurrence of a state 'S_k', μ_k; it can be expressed as:

$$\mu_k(S_k) = \underset{S_{1:k-1}}{max} (P(S_{1:k}, O_{1:k})) = \underset{S_{1:k-1}}{max} (P(O_k|S_k) * P(S_k|S_{k-1}) * P(S_{1:k-1}, O_{1:k-1})) \tag{55}$$

We know that:
If f(a)> or = 0, for all a.
And g(a,b)> or = 0, for all a and b.

Then:

$$\underset{a,b}{max}(f(a) * g(a,b)) = \underset{a}{max}[f(a) * \underset{b}{max} (g(a,b))] \tag{56}$$

Let's consider:
$a = S_{k-1}$, $b = S_{1:k-2}$

Hence, equation (55) becomes:

$$\mu_k(S_k) = \underset{S_{k-1}}{max} [P(O_k|S_k) * P(S_k|S_{k-1}) * \underset{S_{1:k-2}}{max} (P(S_{1:k-1}, O_{1:k-1}))] \tag{57}$$

All the elements in equation (57) are known from the emission probability or and transition probability or can be calculated.

'$P(O_k|S_k)'$ is the emission probability.
'$P(S_k|S_{k-1})'$ is the transition probability.
From equation (55), $\mu_{k-1}(S_{k-1}) = \underset{S_{1:k-2}}{max} (P(S_{1:k-1}, O_{1:k-1}))$].

Accordingly, equation (57) can be written as:

$$\mu_k(S_k) = \underset{S_{k-1}}{max} [P(O_k|S_k) * P(S_k|S_{k-1}) * \mu_{k-1}(S_{k-1}) \tag{58}$$
(for k=2, …, n)

For k=1:

$$\mu_1(S_1) = P(S_1, O_1) = P(S_1) * P(O_1|S_1) \tag{59}$$

In general,

$$\max_{S_n}(\mu_n(S_n)) = \max_{S_{1:n}} P(O_{1:n}, S_{1:n}) \quad (60)$$

Equation (60) expresses the maximum value. Following the same logic, the maximum sequence is generated.

A graphical implementation of the above procedure is illustrated in figure 121. It's a kind of state diagram used for decoding a sequence of observable. The detection of the right track consists of finding the most probable path through the diagram. Each node represents a distinct state at a given time and designates a possible arrangement of the received data. Each branch represents the commute to a new state at the following time. When two paths are directed to the same state, the one having the higher weight is selected. This selected path is called the 'surviving path' [177].

The selection of surviving paths is achieved by all the states. Based on the observers, the most likely path is chosen and the least likely path is ignored

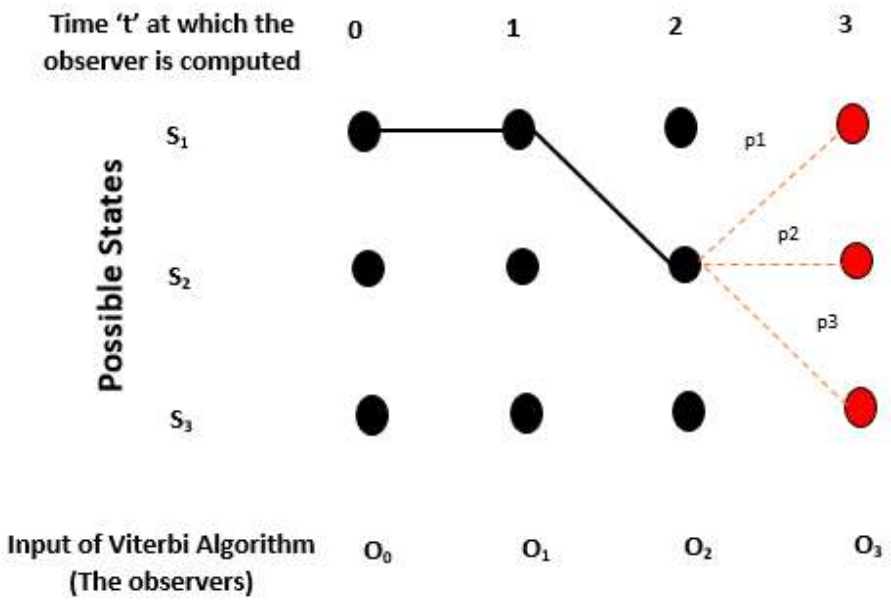

Figure 121: Viterbi diagram

In figure 121, an example of system with three possible states S_1, S_2 and S_3 is presented. The maximizing path till t=2, when the observation sequence (**input**) is O_0, O_1 and O_2, is traced in black; the sequence of states accordingly (**output**) is: S_1, S_1, S_2. We need to know the maximizing path till t=3; what will be the state of the system at this time. To answer this question, we will execute a probability step from t=2 to t=3 taking into account the maximizing path till t=2. The possible tracks are designated by red dotted lines in the diagram. The weight of those dotted lines (p1, p2 and p3), that expresses the possible next state, is calculated using equation (58); the path that has the maximum computed value will be part of the maximizer path that end up with the state of the system at t=3.

A numerical illustration of Viterbi algorithm for a specific sequence of observations will be presented in section 4.2.3.

A block diagram representing the strategy coupling the HMM with Viterbi algorithm is presented in figure 122.

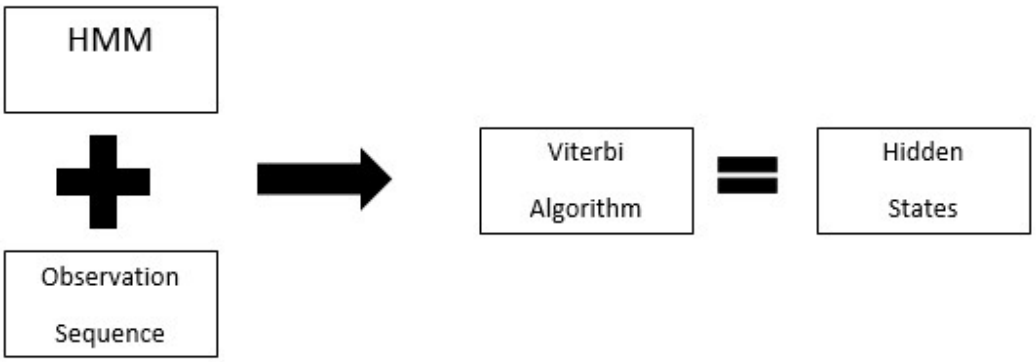

Figure 122: Block diagram combining HMM, Viterbi algorithm, observations and states

4.2.3 The HMM of our application

After illustrating the theory of HMM and Viterbi algorithm, in this section we will see how the theory will be applied to our application.
The first thing to think about is the number of considered machine states and the amount of data needed to build the model.

The elements of the HMM are as follows:

- 53 main states which encounter: the healthy state, 12 states where there is a 1 mm crack in one piece of the 12 magnets located on the machine's rotor, 36 states where there is a turn to turn short circuit in one slot of the 36 slots and 4 states where there is a 10% eccentricity fault on the left, right, upward and downward.

We mention that in this analysis, one type of fault is considered at a time; hence, there is no interrelation between the different types of faults.
Each of the above mentioned main states can propagate and reveal a new state. For example, let's consider a scenario where the machine moves from the healthy state to the state of a 1 mm crack in magnet 1. In this case, the set of states that may face the machine can be expressed as:

$S_1 = \{S_H, S_{F11}, S_{F12}, S_{F13}, S_{F14}, S_{F15}\}$

Where: S_H refers to the healthy state. S_{F11} refers to the faulty state with a 1 mm crack in magnet 1, S_{F12} refers to the faulty state where the 1 mm crack deepen and became 2 mm crack, S_{F13} refers to the faulty state where the 2 mm crack deepen and became 3 mm crack, S_{F14} refers to the faulty

state where the 3 mm crack deepen and became 4 mm crack, S_{F13} refers to the faulty state where the crack became a complete fracture.

- 3 distinct observations per state. It expresses the observed data. In our case the observation will be the measured values from the torque, temperature or vibration sensors. We mention that the raw data set, coming from the three sensors, is investigated over one machine revolution and the number of sampling points is 400.

Considering the above example of the 1 mm crack in magnet 1, the sequence of observation can be expressed as:

SO_1= {{SO_{11}}, {SO_{12}}, {SO_{13}}, {SO_{14}}, {SO_{15}}}

Where: {SO11} is a vector containing torque, temperature and vibration data in the case of 1 mm crack in magnet1, {SO12} is a vector containing torque, temperature and vibration data in the case of 2 mm crack in magnet1, …

The Trellis diagram representing this example is illustrated in figure 123.

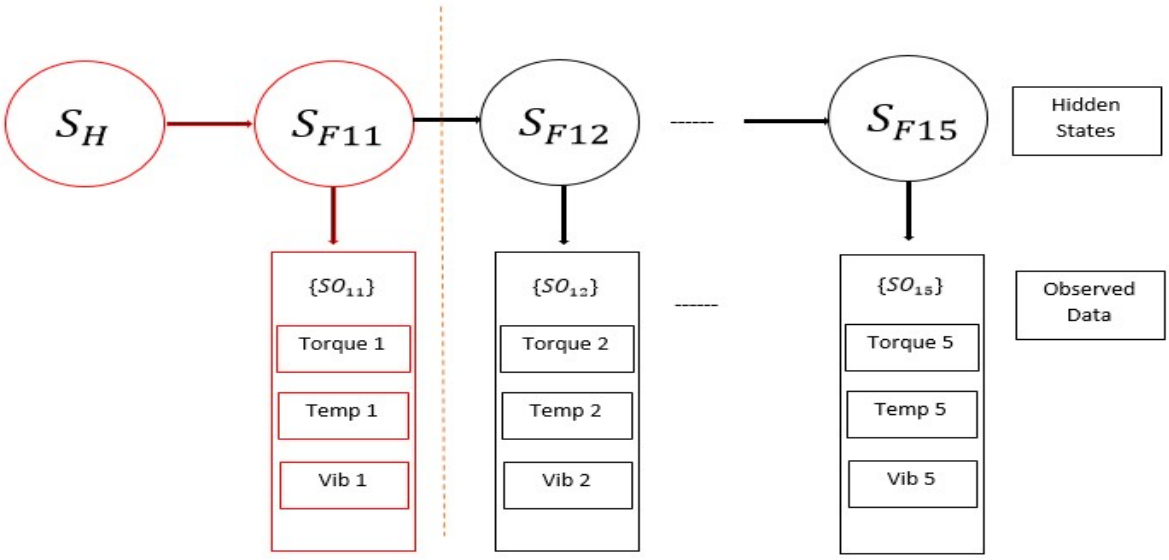

Figure 123: Trellis diagram example

In figure 123, 'Temp' is for temperature and 'Vib' is for vibration. The Trellis diagram in this figure illustrates the life cycle of the piece of magnet from the small scale fault until the complete deterioration. The radial length of the magnet in our machine is 4.5 mm. We considered the crack started with 1 mm radial length and it will propagate in incremental 1 mm length till complete deterioration. Accordingly, we got 5 states: SF_{11}, SF_{12}, SF_{13}, SF_{14}, SF_{15}, corresponding to 1 mm crack, 2 mm crack, 3 mm crack, 4 mm crack and the complete fracture at 4.5 mm. This corresponds to one of the 12 magnets of the machine; each piece of magnet can face the same dilemma.

Each type of fault has its own trellis diagram. In our model, we have three types of faults; each one encounters a number of states according to the number of faulty elements that can occur at a time in the machine. If we consider the case of turn to turn short circuit, the states of the trellis diagram, other than the initial healthy state, will be 13 where 13 is the number of turns per coil in the stator. This can occur in any of the 36 slots of the machine. If we consider the eccentricity fault, it starts at 10% and increases is step of 10% till it reaches the 100% which means a physical contact between the rotor and the stator; hence, we have 10 states. In this research, as we stated previously, the occurrence of the eccentricity fault can be at the right, left, up or down.

Hence, to generate one global model of our machine, all trellis diagrams representing the investigated faulty states are grouped together and illustrated in figure 124. In other words, we have a multilevel trellis diagram that is schematically represented in figure 124. The first 36 levels correspond to the turn to turn short circuit, the next 12 levels correspond to the demagnetization fault and the last 4 levels correspond to the eccentricity fault.

Each level in the diagram of figure 124 (the red and black parts) represents the life cycle of the faulty element in the machine starting with the healthy state, then the occurrence of primitive fault, the propagation of this fault till, finally, the deterioration of the defected element.

Since our purpose is to focus on the prognostic aspect, in our model the considered states are the healthy state and the faulty states with primitive fault; those are highlighted in red in the multilevel trellis diagram

The observations are a continuous signals function of time; however, we will take advantage of the extracted features, from this signals, in chapter 3, to be the input of the model.

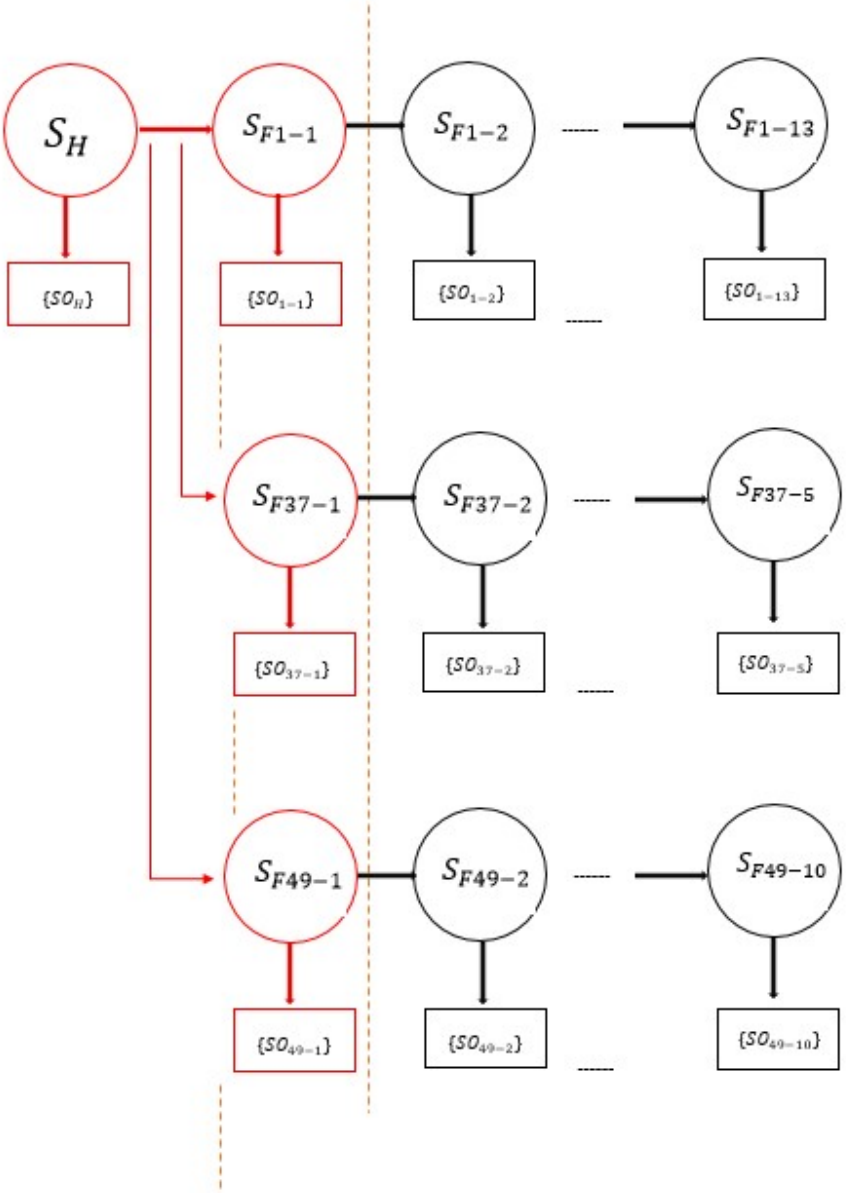

Figure 124: Multi level trellis diagram

A global HMM is built where all the states and observables highlighted in red are grouped in a single model. The observed features {{SO_H}, {SO_{1-1}}, {SO_{2-1}}, {SO_{3-1}} …} will be linked to the discrete states of HMM (S_H, S_{F1-1}, S_{F2-1}, S_{F3-1}…) where each number designate a pre-settled state. For example: state '0' designate the machine in the healthy case 'S_H ', state '1' designate the machine in the case of turn to turn short circuit in slot 1 'S_{F1-1}', …, state '37' designate the machine with crack in magnet 1 'S_{F37-1}', …, '49' designate the machine with eccentricity fault 'S_{F49-1}'…

In the same context, observation '0' is the range of average vibration detected by the vibration sensor when the machine is healthy 'SO_H', observation '1' is the range of average vibration detected by the vibration sensor when the machine has a turn to turn short circuit fault in slot 1

'$SO_{1\text{-}1}$', …, observation '53' is the range of average torque detected by the torque sensor when the machine is healthy…
To sum up, the constructed model will encounter the first layers highlighted in red in figure 124 because these layers represent the system with small scale faults we are interested in.

As we stated previously, the observations of the HMM will come from three observers: Torque, Vibration and Temperature sensors. The importance and cause of supervising three observers for each state is to prevent false alarm. When the three observers generate the same state sequence, the probability of error disappear.
For each state of the machine there is data coming from the three sensors. Features are extracted for every revolution. As clarified in chapter 3, some states share same observations. For example, the temperature of the machine remains almost the same in the healthy case, case of eccentricity fault or case of crack in one magnet. Torque in the case of turn to turn short circuit remains the same wherever the short circuit is. The same is applied for the case of crack in one magnet or eccentricity fault. Hence, the total number of observations will be 94 encountering 53 vibration ranges, 4 torque ranges and 37 temperature ranges.
Accordingly, the size of the Transition matrix is (53 x 53), the size of the emission matrix is (53 x 94), the initial state of the machine is considered to be healthy.

The below 'TM' matrix is a schematic presentation of the transmission matrix.

$$TM = \begin{bmatrix} 0.6 & 0.4*0.65/36 & \dots & 0.4*0.65/36 & 0.4*0.175/12 & \dots & 0.4*0.175/12 & 0.4*0.175/4 & \dots & 0.4*0.175/4 \\ 0 & 1 & 0 & 0 & 0 & 0 & 0 & 0 & 0 & 0 \\ \vdots & 0 & 1 & 0 & \vdots & \vdots & \vdots & \vdots & \vdots & \vdots \\ \vdots & \vdots & 0 & 1 & 0 & \vdots & \vdots & \vdots & \vdots & \vdots \\ \vdots & \vdots & \vdots & 0 & 1 & 0 & \vdots & \vdots & \vdots & \vdots \\ \vdots & \vdots & \vdots & \vdots & 0 & 1 & 0 & \vdots & \vdots & \vdots \\ \vdots & \vdots & \vdots & \vdots & \vdots & 0 & 1 & 0 & \vdots & \vdots \\ \vdots & \vdots & \vdots & \vdots & \vdots & \vdots & 0 & 1 & 0 & \vdots \\ \vdots & \vdots & \vdots & \vdots & \vdots & \vdots & \vdots & 0 & 1 & 0 \\ 0 & 0 & 0 & 0 & 0 & 0 & 0 & 0 & 0 & 1 \end{bmatrix} \quad (61)$$

The numbers expressing the probability of transition from healthy state to one of the faulty states is deduced from the percentage of fault occurrence illustrated in table 19. The percentage that the machine remains healthy is 60%. The percentage that the machine becomes faulty is 40%. This 40% was distributed among the different considered faulty states according to the percentage of fault occurrence.

TABLE 19: PERCENTAGE OF FAULT OCCURRENCE IN THE ELECTRICAL MACHINE

Fault type	**Bearing Failure**	**Stator Failure**	**Rotor Failure**	**Shaft Failure**	**Eccentricity failure and others**
% of occurrence	41	37	10	2	10

Since the only investigated faults are: stator failure, rotor failure and eccentricity faults, the percentage of fault occurrence of those three faults had been arranged to become: 65%, 17.5% and

17.5% respectively. Accordingly, for example, the probability of moving from healthy machine to machine with turn to turn short circuit in one of the 36 slots is (0.4*0.65/36). We mention that this is an analytical assumption and approach.

In the other hand, we remark that the probabilities in the diagonal are '1'. This is due to the fact that when a fault occurs in the machine it persists; and, it cannot return to its initial healthy state. Moreover, as we mentioned earlier, in this analysis we are considering one fault at a time and there is no correlation between faults.
This self-correlation of the states is very common in Hidden Markov models and it is always observed as a strong diagonal in the transition matrix.
We note also that faults of similar nature have similar probability of transition like crack in magnet 1 and crack in magnet 2 and crack in magnet 3 …

The below 'EM' matrix is a schematic presentation of the emission matrix.

$$EM = \begin{bmatrix} 0.6 & 0 & \dots & 0 & 0 & \dots & 0 & 0 & \dots & 0 & 0.2 & 0 & 0 & 0 & 0.2 & 0 & \dots & 0 \\ 0 & 0.8 & 0 & 0 & 0 & 0 & 0 & 0 & 0 & 0 & 0 & 0.1 & 0 & 0 & 0 & 0.1 & 0 & 0 \\ \vdots & 0 & 0.8 & 0 & \vdots & \vdots & \vdots & \vdots & \vdots & \vdots & \vdots & \vdots & \vdots & \vdots & \vdots & 0 & 0.1 & 0 \\ 0 & \vdots & 0 & 0.8 & 0 & \vdots & \vdots & \vdots & \vdots & \vdots & \vdots & 0.1 & 0 & 0 & 0 & 0 & 0 & 0.1 \\ 0 & \vdots & \vdots & 0 & 0.75 & 0 & \vdots & \vdots & \vdots & \vdots & \vdots & 0 & 0.125 & 0 & 0 & 0.125 & 0 & 0 \\ \vdots & \vdots & \vdots & \vdots & 0 & 0.75 & 0 & \vdots & \vdots & \vdots & \vdots & \vdots & \vdots & \vdots & \vdots & 0 & 0.125 & 0 \\ 0 & \vdots & \vdots & \vdots & \vdots & 0 & 0.75 & 0 & \vdots & \vdots & \vdots & 0 & 0.125 & 0 & 0 & 0 & 0 & 0.125 \\ 0 & \vdots & \vdots & \vdots & \vdots & \vdots & 0 & 0.8 & 0 & \vdots & \vdots & \vdots & 0 & 0.15 & 0 & 0.05 & 0 & 0 \\ \vdots & \vdots & \vdots & \vdots & \vdots & \vdots & \vdots & 0 & 0.8 & 0 & \vdots & \vdots & \vdots & \vdots & \vdots & 0 & 0.05 & 0 \\ 0 & 0 & 0 & 0 & 0 & 0 & 0 & 0 & 0 & 0.8 & 0 & 0 & 0 & 0.15 & 0 & 0 & 0 & 0.05 \end{bmatrix} \quad (62)$$

In our HMM model, the numbers expressing the probabilities of emission between the states and the observations are inspired from the percentage of observations' deviation between that of the healthy case and the faulty case. These percentages are illustrated in table 13 (chapter 3, page 120). For example, in the case of turn to turn short circuit in the stator's coil the absolute percentage change in the vibration compared to the healthy case is 158%, the percentage change in the temperature is 27% and the percentage change in the torque is 28%. Accordingly, the emission probabilities in this case is respectively, 0.75, 0.125 and 0.125.

The initial state probability, the TM and the EM constitutes the HMM of our model. The input sequence of observations will be vibration, torque and temperature data sensor. Viterbi will elaborate the appropriate sequence of states by calculating the likelihood probability.

For illustration, let's consider a simple example where the sequence of observations is {SO_H, SO_H, $SO_{F\text{-}1}$} that corresponds to the sequence of states {S_H, S_H, $SF_{1\text{-}1}$}. Figure 125 will show how this sequence will be decoded through Viterbi algorithm and the corresponding sequence of states is detected.

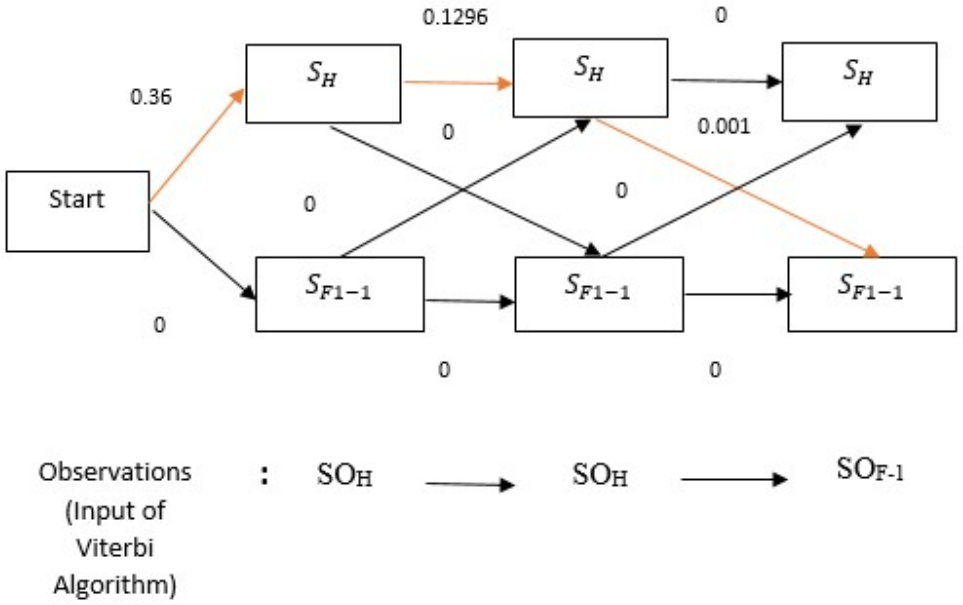

Figure 125: Example of Viterbi algorithm

At start, the probability that the system is healthy is '0.6' and the probability that the system is faulty is '0.4'. The probability that the system state is S_H if the observation is SO_H is '0.6' and the probability that the system state is S_{F1-1} if the observation is SO_H is '0'. Hence, the weight probability from 'Start' to S_H is 0.36 (0.6*0.6) and the weight probability from 'Start' to S_{F1-1} is 0 (0.4*0). Viterbi will choose the path having the highest probability which is in this case 0.36 and the selected path is highlighted in red. We mention that, for simplicity, we will consider the observation is from one sensor; we select the vibration sensor.

The second observation is also SO_H. The probability of remaining in state S_H is '0.6' (from the transition matrix). The probability of being in state S_H if the observation is SO_H is '0.6'. the probability from the previous state is 0.36. hence, the weight probability of remaining in state SH when the second observation is SO_H will be 0.1296 (0.36*0.6*0.6). Following the same logic calculation, we got the weighted probabilities of all the paths. The path of higher probability, at each observation time, is highlighted in red. Accordingly, the adequate sequence of states is {S_H, S_H, S_{F1-1}}. This path selected by Viterbi algorithm is called 'survivor path'.

These sequence of actions, represented in the block diagram of figure 125, elaborate the condition state of the PMM. The next and final step will be the calculation of the RUL.

4.3 Remaining useful life (RUL)

In fact, several papers and researches has defined the Remaining Useful Life (RUL). They all agreed that it is an estimation of the number of remaining years that an item, component, or system is expected to be able to function in accord with its envisioned purpose before a replacement alert knock due to a fault or the aging factor.

RUL can be calculated by three main approaches [99] [100] [101]:

- Model based approach where it utilizes the physical aspect of the failed model.
- Data driven approach where it utilizes the data coming from sensors and transform it to a model. The use of Bayesian approach is common in this field.
- Hybrid approach where the benefits of the model approach and the data approach is fused.

Data driven approach is adopted when no enough physical or specialists' knowledge is available for the studied model.
Calculation of RUL using model based approach is more accurate and precise.
It has been shown in [102] and [103] that combining different types of approaches: data driven and physics based, is beneficial to improve RUL accuracy and precision.
In our work, we will take advantage of the FEM and the well knowledge of the PMM's physical aspect and characteristics to calculate the RUL.
As stated previously, the degradation of the system may occur due to aging of the system's components or due to a fault. Hence, before presenting the 'RUL' predictive strategy, the matter of component aging is presented.

4.3.1 Aging of PMM's components

The components forming the electrical machine are: the core of the stator and rotor that is formed mainly from steel, the stator's coil that are made from copper, the magnet on the rotor in our machine it's a rare earth magnet called neodymium iron boron and the shaft constituted of aluminum.
They are all subject to aging.
The aging of the delicate components in the electrical machine is the major factor that intervene in the calculation of the RUL of the system after the prognostic decision is formulated.
The machine's components that are mostly subject to aging are: the coil and the magnet.

4.3.1.1 Aging of the stator's coil

The stator's coils are made of copper wire and its insulation. The main causes of wire's aging are temperature, humidity and corrosion.
The internal resistance of the wire is considered the parameter that impacted its age.
The aging equation of resistance is: [104]

$$\frac{\Delta R}{R^0} = A\, t^n\, e^{(-\frac{T0}{T})}\ \% \tag{63}$$

T: operating temperature of resistor in °C
t: time the resistor is operating at temperature T in hours
R0: initial value of the resistor in ohms
ΔR: increase in resistance of the resistor operating at temperature T for a time t, in ohms.
A: statistically independent random variables (the value of this variable can be taken as 1.51 x 1012.)
n: calibration parameter (it can be considered '0.610')

T0: initial temperature

According to [105], the ambient temperature of the machine is 293.15 K. As it operates, the temperature at the coils increases to reach 393.15 K. It decreases to reach 373.15 K, then, a lower value of 353.15 as the speed increases and the torque decreases.
The relation between Kelvin and Celsius is:

$$T(°K) = T(℃) + 273.15 \quad (64)$$

Hence, the three operating temperature of the machine are as follows: 120 °C, 100 °C and 80 °C. The type of copper used in the machine's coil is of class 200 °C, grade 2. The wire's diameter is 0.6 mm and its resistance is 0.05876-0.06222 ohm/m. At ambient temperature, 20 °C, the resistance of one phase is 0.42 ohm.

According to the copper development association, the lifetime of the conductor part of the wire is 100 years. The lifetime of the wire's insulation is 70 years. And this if no fault occurs and the normal environmental characteristics remain the same.
However, the average life cycle of permanent magnet machine is up to 14 years. Hence, it is useful to study the aging effect of copper resistance during the life time of the machine only, which is 14 years.

Table 20 shows the variation of the coil's resistance value due to aging, where no physical fault occurs in the machine.

TABLE 20: : VARIATION OF COIL'S RESISTANCE DUE TO AGING

Time (year)	ΔR/R0 (%)	ΔR	Rnew
1	7.622031	0.032013	0.452013
2	10.77918	0.045273	0.465273
3	13.20175	0.055447	0.475447
4	15.24406	0.064025	0.484025
5	17.04338	0.071582	0.491582
6	18.67009	0.078414	0.498414
7	20.166	0.084697	0.504697
8	21.55836	0.090545	0.510545
9	22.86609	0.096038	0.516038
10	24.10298	0.101233	0.521233
11	25.27942	0.106174	0.526174
12	26.40349	0.110895	0.530895
13	27.48162	0.115423	0.535423
14	28.51903	0.11978	0.53978

Although the resistance of the coil increases over the year, its impact is negligible on the operation of the machine. This fact remains true as long as no fault occurs and the temperature at the coil level is within the tolerated values.

Concerning the insulation, talking about its electrical and mechanical function, it is expected to resist voltage stress as well as to provide mechanical sustenance over a wide range of temperatures. Under normal condition, it's life cycle is 70 years. However, under abnormal conditions, mainly exposure to high operating temperature, its life cycle degrades radically.
According to [106], insulation's aging is directly related and inversely proportional to temperature (T). It is expressed as:

$$Insulation\ Aging = A * \exp\left(\frac{B}{T}\right) \tag{65}$$

A and B are constant characteristics of the insulation. The aging is in years and the temperature is in Celsius.
Insulation aging degradation function of temperature ranges that is suitable for electric machine application is illustrated in figure 126.
According to figure 126, if a normal operation of the electric machine is guaranteed, no need to worry about the insulation aging. However, when a fault occurs, the insulation aging becomes a huge concern; ignoring it will lead to catastrophic consequences.

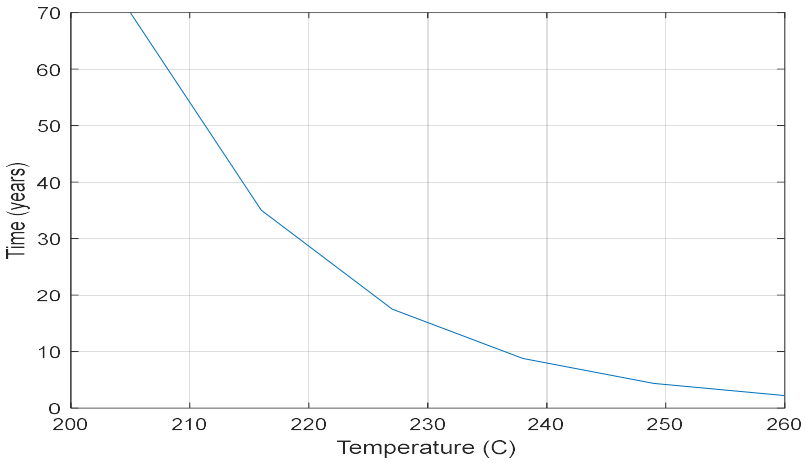

Figure 126: Aging graph of windings insulation

4.3.1.2 Aging of the magnet

Several factors affect the stability and performance of magnets: temperature, change in reluctance, external magnetic fields, radiation, and vibration.

Talking about temperature, diverse types of permanent magnets react differently to changes in operating temperature. For example, ferrite shows an increase in Hc as the temperature is increased

while the rest of the magnet types show decrease. All types show a decrease in Br as temperature increases, and all become non-magnetic ultimately when they reach their Curie temperature, Tc. The magnet used in our machine is neodymium iron boron. The most common temperature related parameters for the NdFeB are mentioned in table 21. [107]

TABLE 21: NDFEB TEMPERATURE RELATED PARAMETERS

Parameter	**NdFeB**
α, Temperature coefficient Br %/°C	0.11%
β, Temperature coefficient Hc %/°C	0.4%
Maximum operating temperature °C	180
Tc °C	300-400

NdFeB loses approximately 0.11 % of its Br and 0.4% of its Hc for every degree Celsius above 20°C. For example, a NdFeB magnet with a - 0.11 reversible loss will have 11% less magnetic flux at 120°C than at 20°C.

At 80 °C, the steady state temperature of the machine, Br became 1.11 Tesla and Hc became 649400 A/m. This is called the Reversible Temperature Coefficient.

Rare earth magnets may face three types of losses; each type moves the magnet to a specific phase.

- Reversible Losses

Reversible losses can be defined as temporary loss of the magnet's magnetic force. These losses can be reversed when the magnet returns to its normal original temperature. Reversible losses cannot be eliminated by magnet stabilization. Reversible losses are expressed by the Reversible Temperature Coefficient, -%Br/°C. The value of these losses differ according to the type of magnet used. We mention that they are not always linear as the temperature increases.

- Irreversible Losses

These losses are defined as a partial demagnetization of the magnet due to exposure to high or low temperatures or other demagnetizing stimuluses. These losses are only recoverable by re-magnetization and are not recovered when the temperature returns to its original value. This occurs when the magnets are operating at temperatures higher than the identified "maximum operating temperature" or when the operating temperature of the magnet reaches a minimal value, below the "knee" of the demagnetization curve. The range of maximum operating temperature of neodymium magnet is 80-140 °C.

- Permanent losses

Permanent losses occur when magnets are exposed to extremely high temperatures that are usually as high as the initial heat treatment when they were manufactured. This is called the magnet's Curie temperature. When a metallurgic change occurs, the magnetic properties are not recoverable to its initial state even after re-magnetization. The range of curie temperature of neodymium magnet is 310-400 °C.

Talking about time, the effect of time on modern permanent magnets is minimal. Figure 127 is a graph showing the percentage decrease of Br function of time when the maximum operating temperature of the magnet is 100 °C.

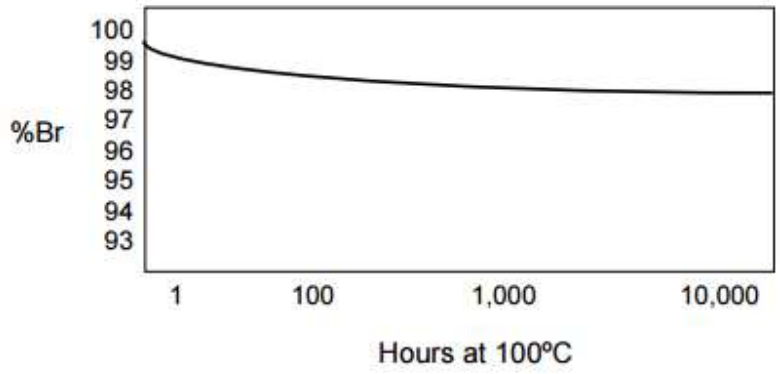

Figure 127: % Br versus operating hours

There is no aging equation for magnet relating its remanence flux density 'Br' to its temperature and operating time. However, approximate analytical equation can be deduced from experimental graphs like the one in figure 127. The curve is approximately a straight line; its equation is:

$$\%Br = \frac{98 - 100}{10000 - 1}\, t\ (hours) + 100 = \ -0.0002\, t(hours) + 100 \tag{66}$$

This is true if the operating temperature is 100 °C which coincide with our machine.
Table 22 below shows the effect of magnet aging on Br and Hc, under healthy conditions.

TABLE 22: EFFECT OF MAGNET AGING ON ITS BR AND HC

Time (year)	**Brnew (Tesla)**	**Hcnew (A/m)**
1	1.1052048	646594.592
2	1.1004096	643789.184
3	1.0956144	640983.776
4	1.0908192	638178.368
5	1.086024	635372.96
6	1.0812288	632567.552
7	1.0764336	629762.144
8	1.0716384	626956.736
9	1.0668432	624151.328
10	1.062048	621345.92
11	1.0572528	618540.512
12	1.0524576	615735.104
13	1.0476624	612929.696
14	1.0428672	610124.288

As we can see, there is small remarked degradation of Hc and Br with time.
The degradation worsens if the temperature at the magnet level increases where the flux losses increase as we can see in figure 128.

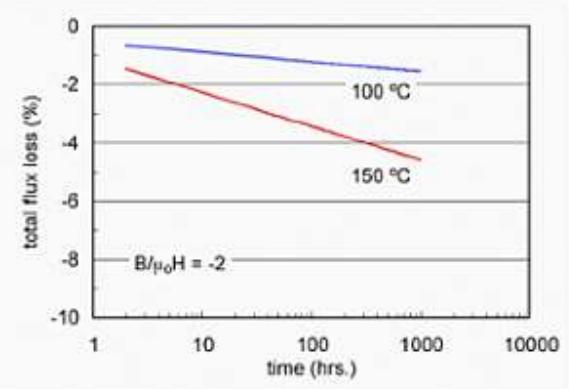

Figure 128: magnet's flux loss versus time at different temperatures

At 150 °C, the relation between the loss of Br and the time is:

$$\%\, Br\ loss = -0.0035 * time - 1 \quad (67)$$

If we consider the relation of loss in Hc is the same as Br. The new values of Br and Hc at 150°C with aging is presented in the following table 23.

TABLE 23: IMPACT OF MAGNET AGING ON BR AND HC WHEN THE OPERATING TEMPERATURE IS 150 CELSIUS

Time (year)	Machine's average operating hours	% loss Br	New Br	New Hc
1	2160	-8.56	0.92728	419161
2	4320	-16.12	0.83656	384505.9
3	6480	-23.68	0.74584	349850.9
4	8640	-31.24	0.65512	315195.8
5	10800	-38.8	0.5644	280540.8
6	12960	-46.36	0.47368	245885.8
7	15120	-53.92	0.38296	211230.7
8	17280	-61.48	0.29224	176575.7
9	19440	-69.04	0.20152	141920.6
10	21600	-76.6	0.1108	107265.6
11	23760	-84.16	0.02008	72610.56
12	25920	-91.72	-0.07064	37955.52
13	28080	-99.28	-0.16136	3300.48
14	30240	-106.84	-0.25208	-31354.6

The numbers in table 23 detect a pace acceleration in Br and Hc. The negative values indicate a complete deterioration of the magnet.

The impact of magnet losses due to aging is experimented for our PMM. Figures 129 shows the distribution of flux density inside the electric machine after 1 year, 5 years, 10 years and 14 years of aging.

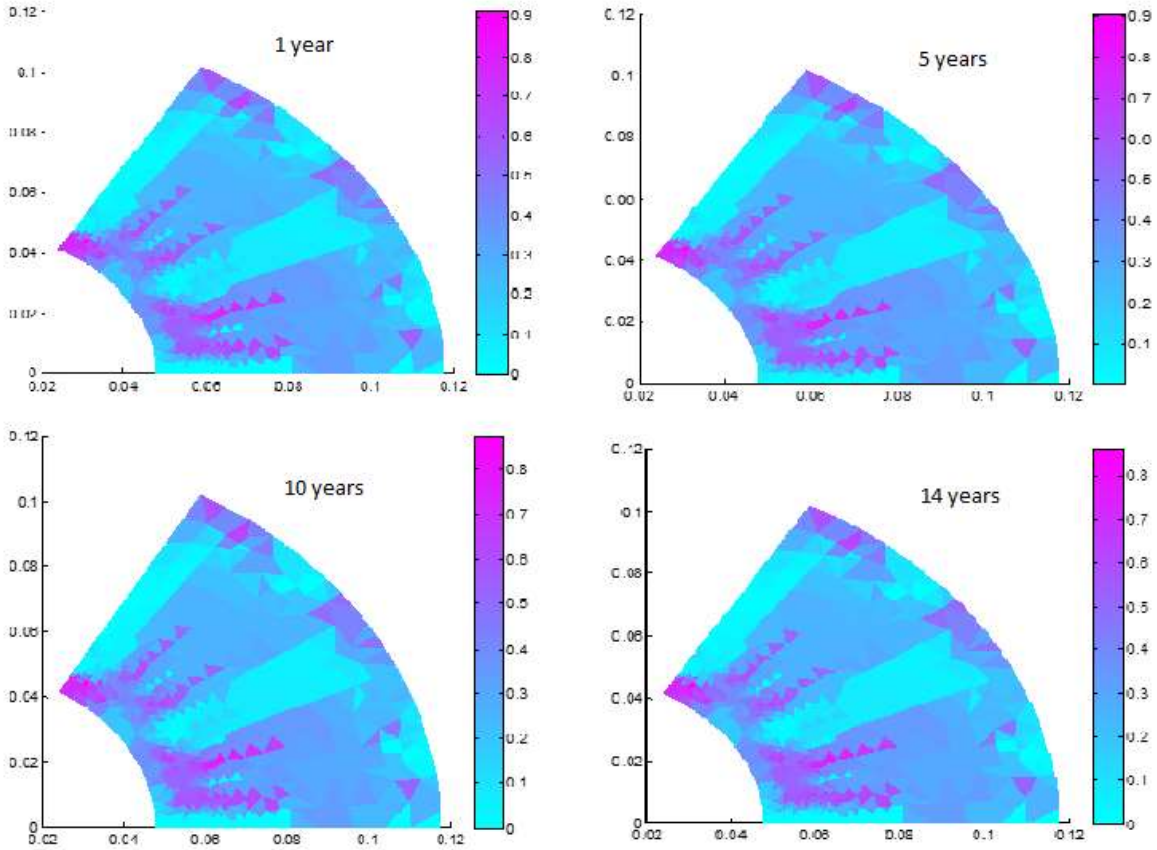

Figure 129: Distribution of flux density in the machine after 1 year, 5 years, 10 years and 14 years of aging

The air gap flux density of the machine function of aging is illustrated in figure 130.

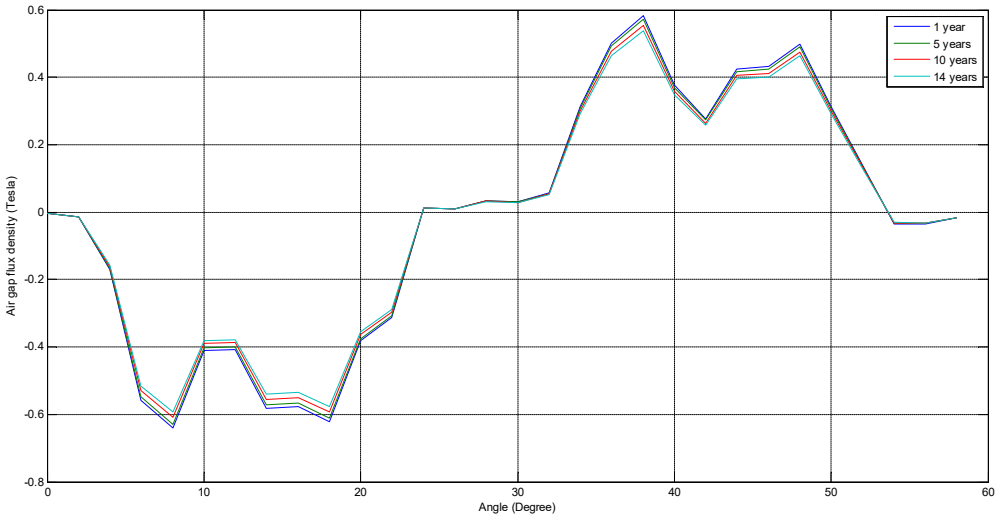

Figure 130: The change in air gap flux density with magnet aging (100 °C)

We can see that the impact of magnet aging is almost neglected on the machine's air gap flux density; hence, it has almost no effect on the machine performance.
However, in case of fault like turn to turn short circuit in one of the stator's coil, the temperature at magnet level may reach 150 °C. The change in the air gap flux density over years at 150°C is presented in figure 131.

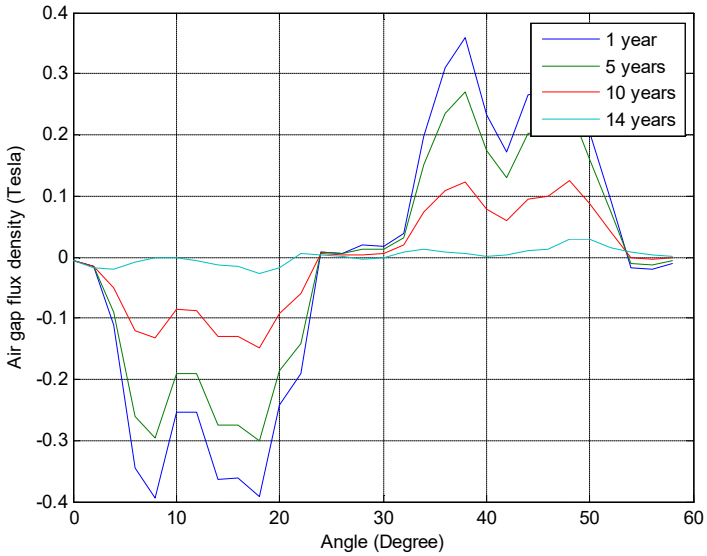

Figure 131: The change in air gap flux density with magnet aging (150 °C)

As we can see from figure 131, the air gap flux density degrades radically at 150 °C. this will affect largely the performance of the machine.
We will evaluate the magnet's aging impact, in this case, by calculating the machine's torque.

The impact of the change in temperature and aging on the torque is presented in table 24.

TABLE 24: IMPACT OF MAGNET AGING OVER YEARS AT TEMPERATURES 100 AND 150 CELSIUS

Year	**1**	**2**	**3**	**4**	**5**	**6**	**7**
		150 °C					
Bgav (Tesla)	0.27144	0.25146	0.23146	0.21148	0.19148	0.1715	0.15152
Torque	47.44733	43.95486	40.45888	36.96641	33.47044	29.97796	26.48548
		100 °C					
Bgav (Tesla)	0.4018	0.39938	0.39696	0.3945	0.39208	0.38968	0.38726
Torque	70.23408	69.81106	69.38805	68.95805	68.53504	68.11552	67.69251

Year	**8**	**9**	**10**	**11**	**12**	**13**	**14**
		150 °C					
Bgav (Tesla)	0.1315	0.11154	0.09154	0.07156	0.05158	0.03158	0.0116
Torque	22.98602	19.49704	16.00106	12.50859	9.016112	5.52014	2.027664
		100 °C					
Bgav (Tesla)	0.3848	0.38238	0.37994	0.37754	0.37508	0.37268	0.37026
Torque	67.2625	66.83949	66.41298	65.99346	65.56346	65.14394	64.72093

Figure 132 illustrates the degradation of the torque with aging when the operating temperature of the magnet is 150 °C versus the relative stability of the torque when this operating temperature is 100 °C.

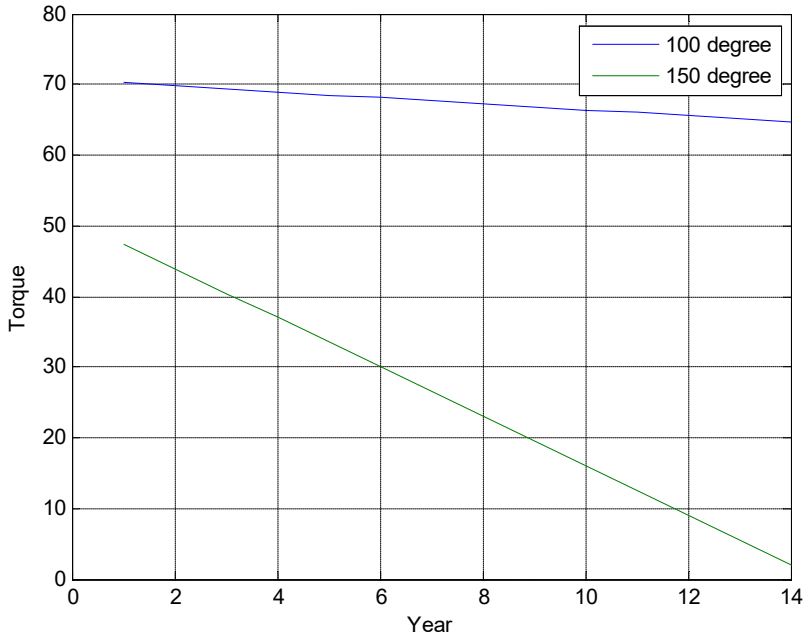

Figure 132: Torque with magnet aging at 100 and 150 degree of operation

In the end of this section, we conclude that tracking the aging of the dynamic and sensitive components inside the machine is not of big interest during normal operation because the life cycle of these components is much greater than that of the electric machine itself.
However, studying and considering this aging, when a fault occurs, is of very important because this will cause a big influence on the machine's health operation. Large degradation in the vital aspect of the machine is noticed and a significant deviation from the normal conditions is detected.

4.3.2 Estimation strategy of RUL calculation using thermal FEM in the case of turn to turn short circuit

As explained previously, the aging and performance of critical components in the PMM are highly affected by temperature.
Aging equation for the coil insulation is noted. The phases of the magnet, function of temperature, are noted. In this section, we will take advantage of the mature knowledge of the machine's thermal aspect and the well development of the thermal FEM, combine it with the aging equations and elaborate the appropriate insulation's RUL and magnet's phase in the case of turn to turn short circuit.

The proposed strategy will solve and answer two questions: what is the remaining useful life of insulation? And, where? In which slot? the next turn to turn short circuit fault will occur after the calculated time, RUL.
In other words, at the end of this analysis we will get the time we still have before insulation, in specific areas, deteriorates and cause a new turn to turn short circuit fault.

A block diagram presenting the steps of this strategy is illustrated in figure 133.

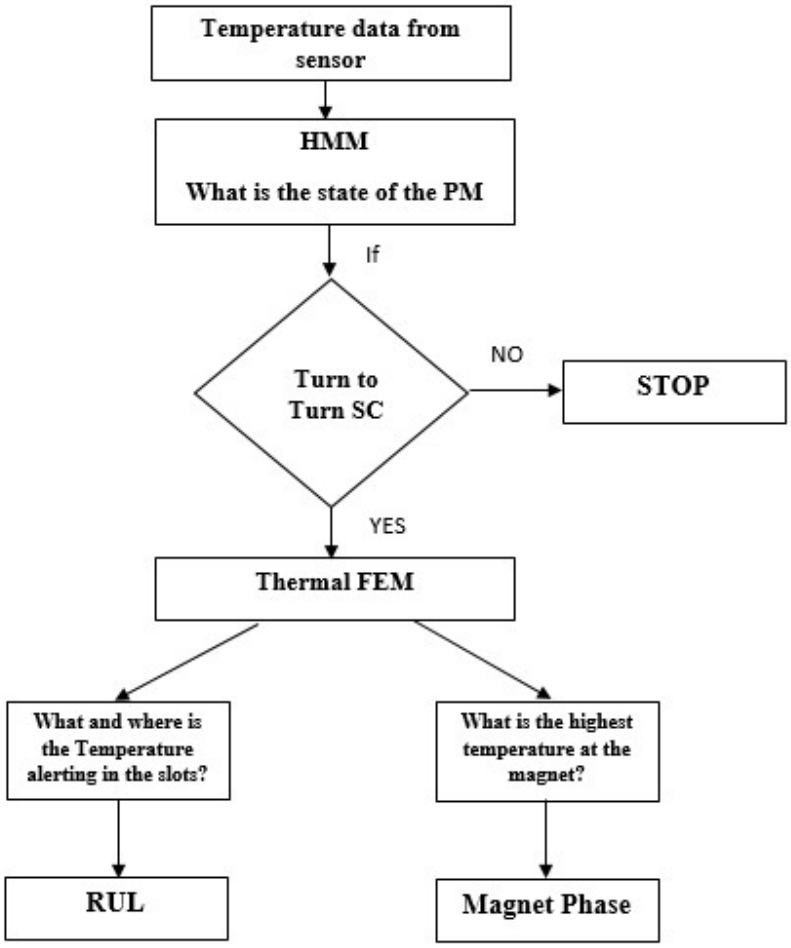

Figure 133: RUL calculation in the case of turn to turn short circuit

An illustrative example clarifying the prognostic approach and the RUL calculation in the case of turn to turn short circuit will be presented in figure 134.

The temperature data used as input for the HMM is coming from a temperature sensor located at the boundary of the machine. The prognostic approach (HMM) will investigate this data and the state of the machine is elaborated.

If a turn to turn short circuit is detected in the electric machine, the phase of the magnet and the remaining useful life of the insulation are calculated by means of the thermal FEM. The location of the next turn to turn short circuit that will occur in the machine, after the RUL flows, will be identified also.

The thermal FEM is capable of determining temperature in the whole machine. As stated in the previous section, the critical machine elements which performance is directly related to the

operating temperature are: the magnet and the stator coil. Hence, when a turn to turn short circuit fault occur, the higher temperature at the magnet and coil level is noted. The RUL of insulation is calculated by the insulation aging equation (65) from the previous section. The new 'Br' of the magnet due to the increase of its temperature is calculated from the aging magnet equation (66) and (67). According to the temperature of the magnet, its state is deduced as mentioned in section 4.3.1.2.

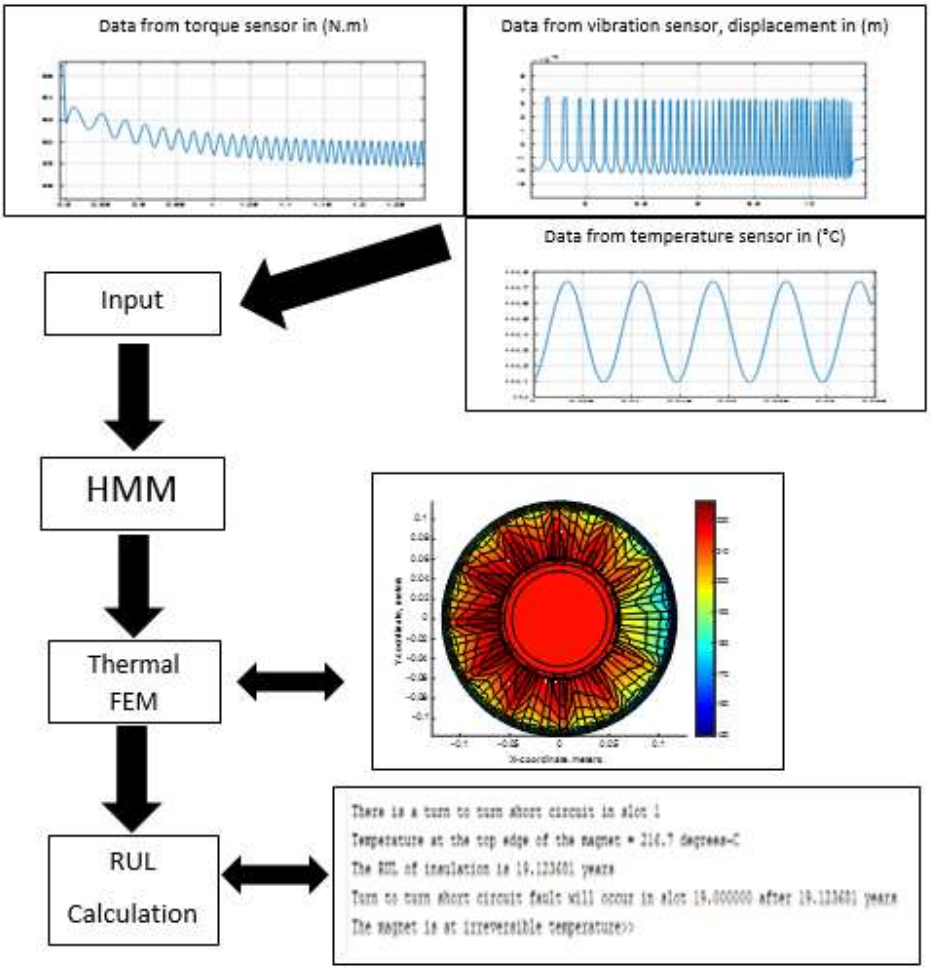

Figure 134: Illustrative example for RUL calculation

4.3.3 Estimation strategy of RUL calculation in the case of crack in the magnet

According to the literature, calculating RUL using data base models consists of the following steps:

- First, an offline database is prepared where data related to each phase of fault is encountered.
- Second, a health assessment of the machine is conducted. In our case, the HMM model is responsible of performing this assessment.
- Third, the RUL calculation or prediction is executed.

Previously, the offline database is elaborated. Then, during the condition monitoring of the system's operation, similarities between online and offline data sensor is tracked and detected. This is done by classification or regression [108].
Classification consists of matching data coming from sensors to one of the training data sets we already earned, where each set represents a specific state of the system.
Regression consists of predicting the real data from the sets of training data where a relation between these training data is created since the system phase of each set is known.

In our case we will use 'classification' because an online data coming from sensors can be generated from the developed dynamic FEM model of the machine.

Although dynamic FEM is the best real time representation of the machine performance during healthy and faulty operation; alone, it cannot generate online data useful for RUL calculation. Offline data sample can be generated for different machine states, as much as needed. For example, the model can generate data representing vibration detected by a vibration sensor when the machine is healthy, when the machine encounters a 1 mm crack in one magnet, when the machine encounters a 2 mm crack in one magnet… however, a sampling data representing this vibration when the machine moves from the healthy state to the state of 1 mm crack in one magnet, then the state where the crack worsens and became 2 mm is not possible. In other words, a model of the machine having any depth of the crack is possible using FEM; however, the time needed for the machine to shift from a faulty state with 'x' mm crack to a state with 'y' mm crack where y>x is not offered in FEM. In FEM, there is no representation of the fault propagation function of time.

Hence, many researches use to combine data base approach and model based approach to build a rugged strategy for RUL calculation. Data sets for the data base approach is generated from analytical analysis and numerical analysis like FEM. The model based method is formulated from the physical understanding of the system where a profound knowledge and an accurate representation of the fault propagation in it, function of time, is presented.

If an offline data corresponding to the machine life cycle starting with its healthy state, then during the existence of tiny crack in the magnet till the crack worsen and became a fracture was available, the RUL calculation becomes easy. Such offline data could've been represented in a data matrix ODM as follows:

$$ODM = \begin{bmatrix} DM01 & DM02 & \dots & DM0n \\ DM11 & DM12 & \dots & DM1n \\ DM21 & DM22 & \dots & DM2n \\ \vdots & \vdots & \ddots & \vdots \\ DMm1 & DMm2 & \dots & DMmn \end{bmatrix} \begin{matrix} \rightarrow data\ set\ observed\ at\ t = t0\ when\ the\ machine\ is\ healthy \\ \rightarrow data\ set\ observed\ at\ t = t1\ when\ there\ is\ 1\ mm\ crack\ in\ the\ magnet \\ \rightarrow data\ set\ observed\ at\ t = t2\ when\ there\ is\ 2\ mm\ crack\ in\ the\ magnet \\ \vdots \\ \rightarrow data\ set\ observed\ at\ t = tm\ when\ the\ magnet\ is\ completely\ fractured \end{matrix}$$

In the above matrix, 'n' is the number of sampling points and 'm' the number of times, during the life cycle of the machine, the data sets are recorded.

Different machine learning algorithm like K-NN and Gaussian process regression can be used to execute a health assessment of the system and then, calculate RUL as proofed in paper [108].

A comparison between the current measured data set and the offline data set will be conducted. The most similar offline data set refers to the current machine state. We assume that the future behavior of the current monitored system is the same as that acquired in the offline system.
The RUL is calculated:

$$RUL = EOL_{selected} - tm \tag{68}$$

'$EOL_{selected}$' is the end of life time of the system being in the current faulty phase identified by the health assessment already conducted.

Such offline data is not available since it needs a real monitored system that contains this propagating fault we are interested in. Hence, a suggested strategy, inspired from the above presented method, will be presented in the following to calculate the RUL.

First we will construct a synthetic offline database 'SODM'. SODM will have the form of a matrix as shown below:

$$SODM = \begin{bmatrix} DS01 & DS02 & \dots & DS0t \\ DS11 & DS12 & \dots & DS1t \\ DS21 & DS22 & \dots & DS2t \\ \vdots & \vdots & \ddots & \vdots \\ DSm1 & DSm2 & \dots & DSmt \end{bmatrix} \begin{matrix} \rightarrow data\ set\ for\ the\ case\ of\ 1\ mm\ crack\ in\ the\ magnet\ along\ t\ sampling\ time \\ \rightarrow data\ set\ for\ the\ case\ of\ 2\ mm\ crack\ in\ the\ magnet\ along\ t\ sampling\ time \\ \vdots \\ \rightarrow data\ set\ for\ the\ case\ of\ em\ mm\ crack\ in\ the\ magnet\ along\ t\ sampling\ time \end{matrix}$$

SODM represents sensor data in the healthy case and the case of crack in a magnet inside the PMM. Its size is (m x t) where: 'm' is the number of states representing the systematic propagation of the studied fault and 't' is the number of sampling points.

The difference between ODM and SODM is that the sets of data in ODM are extracted at a specific time during the life cycle of the machine; however, in SODM, the sets of data is extracted at an arbitrary time during a specific state of the machine.

In this section we will use this strategy to calculate the RUL in the case of crack in one magnet; the system we are investigating is the piece of magnet. The first detection of the fault will be when a crack of 1 mm depth is detected, which is compatible with the previous analysis's in chapter 3. In the other hand, since RUL calculation is mainly the time needed for the faulty system to deteriorate, the final set of data will be collected in the case of total fracture of the magnet.

Accordingly, each row of the SODM matrix is dedicated to sensor data at different depths of magnet's crack. We started with 1 mm crack depth and increment this depth, each time, by 1 mm till we reach e_m mm which is the radial width of the magnet. At this depth the magnet is fractured. We mention that the sampling time for all data sets are similar.

After constructing SODM, the first part of the suggested RUL calculation strategy is accomplished. The second part will be to find an appropriate equation that model the incremental growth of this fault, the crack, function of time.

One of the most important equations that models the growth and propagation of cracks is Paris equation.

The study of crack propagation is of big interest in many applications. Several researches used Paris equation to attribute this problem.

In [109], Paris law equation is used in aircraft application. They are concerned with aging of critical material in air craft function of time. Experimental testing of aircraft material is very important; however, constant material properties is not enough to evaluate materials in such critical application. Hence, they evaluate materials according to their dynamic capability to develop and propagate cracks.
Author in [110] used Paris equation to study crack growth and predict the remaining useful life of materials composing in magnet. In [111] the author uses it for crack propagation in microelectronic devices application.
A crack growth rate is assessed for magnet system in [112]. The paper was concerned of studying crack with different orientation and different shapes. To realize this delicate modeling, Dual Boundary Element Method and finite element method is coupled.

When applying Paris equation for crack growth prediction, some assumption needs to be made:

- the crack is not of constant amplitude, it's propagating function of time
- the crack is one dimensional
- the material, where the crack exists, has a certain elastic condition
- the load range is relatively constant
- sensor data and offline signals has similar time stamps
- the offline data set contains enough data that represents different degradation behavior

According to Paris law equation, the general fatigue crack growth model is:

$$\frac{da}{dNc} = C\ (\Delta K)^m \tag{69}$$

$$\Delta K = Kmax - Kop \tag{46}$$

$$Kop = \ Q * \sigma * \sqrt{(\pi \frac{a}{2})} \tag{71}$$

$$Q = \left(\cos\left(\frac{\pi * \ a}{2 * W}\right)\right)^{-\left(\frac{1}{2}\right)} \tag{72}$$

'$\frac{da}{dNc}$' is the crack growth rate.

'a' is the depth of the crack. 'Nc' is the number of cycle.

'C' and 'm' are calibration parameters dependent on the type of material where the crack is propagating. 'C' is called Paris equation parameter or crack growth coefficient, its unit is m/ (MN $m^{-3/2}$) ^{m} per cycle. 'm' is called Paris equation exponent or crack growth exponent, it is unit less.

‘ΔK’ is the effective stress intensity factor. ‘Kmax’ is the stress intensity factor at the peak load; it’s a critical or a threshold value before the occurrence of a fracture. ‘Kop’ is the operating stress intensity.

Maxwell stress tensor ‘σ’ will be calculated from the vibration FEM.

‘Q’ is a parameter dependent on the geometry of the system.

‘W’ is the radial length of the magnet.

A familiar relation between Nc and a is:

$$Nc = \frac{1}{\left(C\ \Delta\sigma\ \sqrt{\pi}\ Q\right)^{m}} * \frac{1}{\frac{m}{2} - 1} * \left(\frac{1}{a0^{\frac{m}{2}-1}} - \frac{1}{af^{\frac{m}{2}-1}} \right) \tag{73}$$

‘Nc’ is a cyclic loading, it is a cycle representation of repetitive or inconsistent stresses intensities on a certain location.
‘a0’ is the current depth of the crack. ‘af’ is the final depth will reach the crack at which the magnet is fractured.

Nc calculated according to the above equation is the RUL for the crack to move from a_0 to a_f depth. If we aim to calculate the time needed for the crack to propagate from 1 mm depth to a specific incremental depth, let’s say 2mm, the final state of the crack ‘f’ in this case will be 2 mm.

In this research we will consider a 4 mm depth as the final state of the magnet’s crack before fracture. Hence, we will run the FEM model with a 4 mm crack in one magnet to get the tensile stress ‘σ’ at this stage. Figure 135 is a section of the PMM’s laminated sheet with 4 mm crack in the magnet. Figure 136 is the air gap flux density and figure 137 is the boundary vibration in this case.

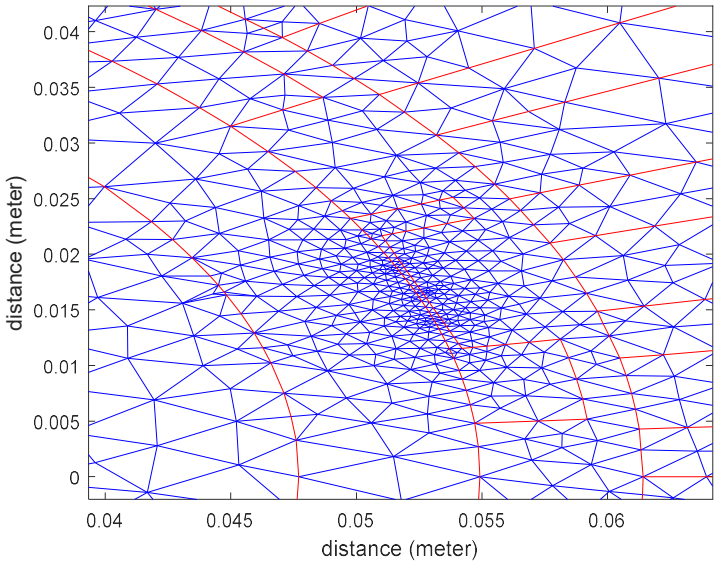

Figure 135: Meshed laminated sheet with 4 mm crack in the magnet

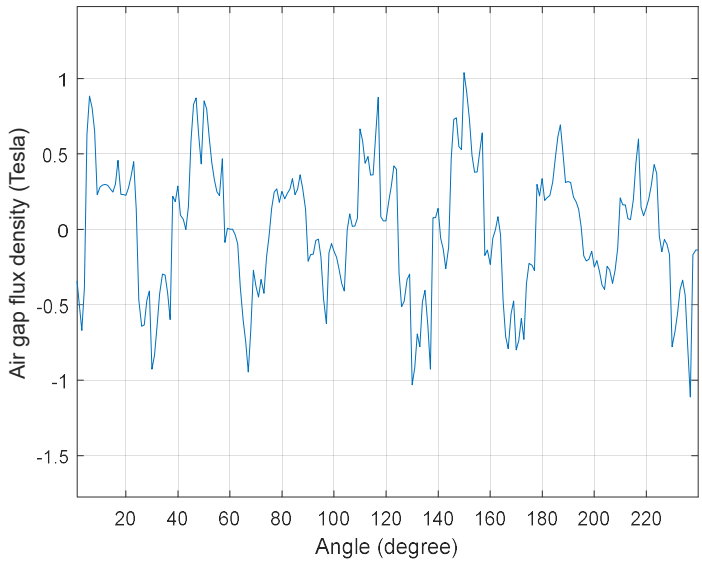

Figure 136: Air gap flux density in the case of 4 mm crack in the magnet

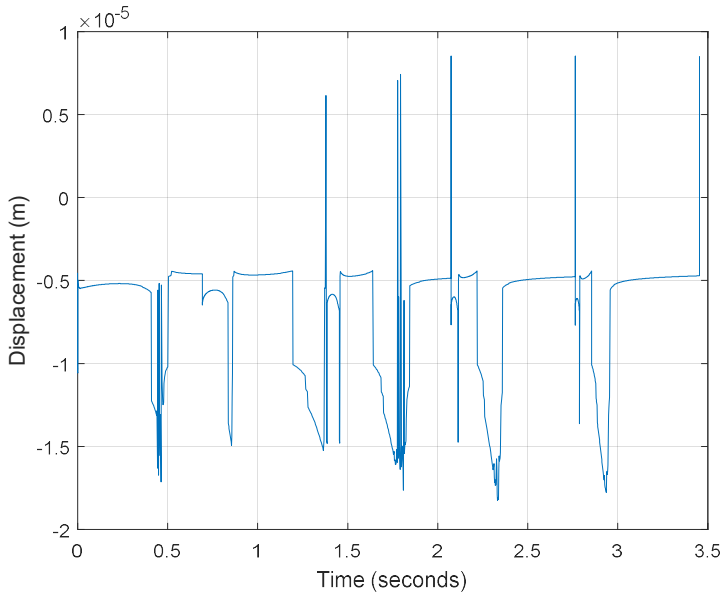

Figure 137: Vibration detected by the sensor in the case of 4 mm crack in the magnet

A block diagram illustrating the steps of the suggested strategy is illustrated in figure 138.

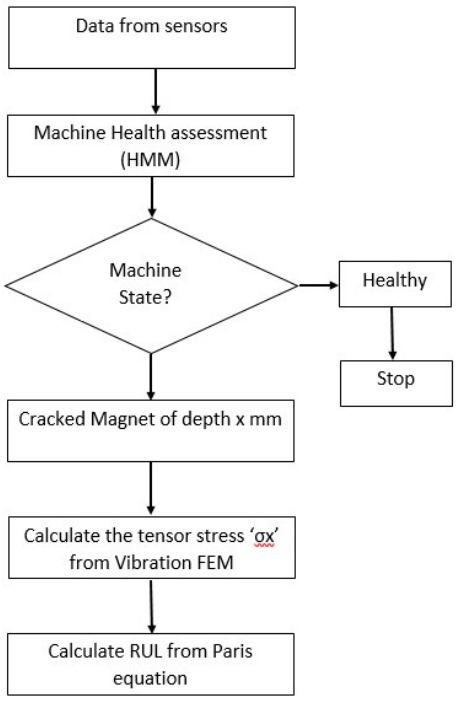

Figure 138: RUL calculation in the case of demagnetization fault

An illustrative example of RUL calculation in the case of demagnetization is presented in figure 139.

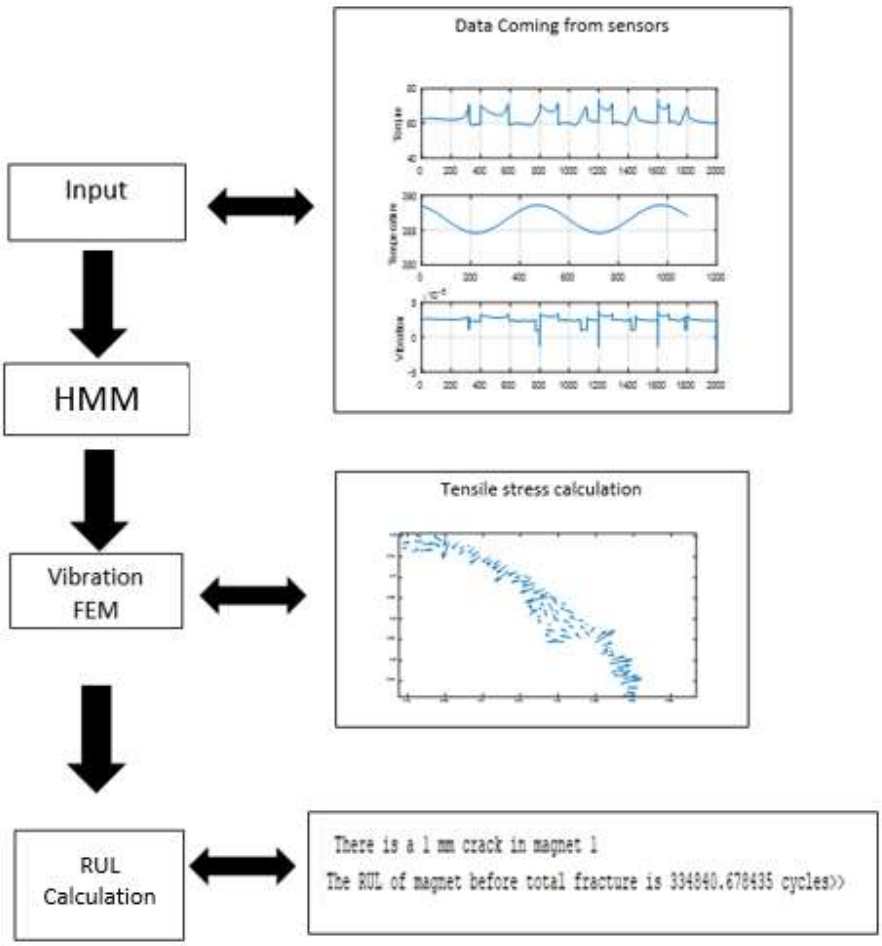

Figure 139: illustrative example of RUL calculation in the case of demagnetization

When the detected fault is a crack in one magnet, the vibration FEM is computed. Maxwell stress tensor is calculated from vibration FEM as stated in chapter 2 section 2.4. this calculated value is replaced in equation (73) to calculate the RUL.

Following the same logical reasoning serial, after detecting the presence of eccentricity fault by the prognostic approach HMM, a question is asked: what are the vital factors that will be affected in the machine? what are the critical components that will be affected accordingly?

According to the previous chapters, the main parameter affected in the case of eccentricity fault is the vibration where an increase in the vibration level is detected. However, its impact is inconspicuous on the critical machine elements we are considering and studying.
It has been stated that vibration and shocks have almost no harmful effect on modern magnet unless a severe physical damage exists.

Moreover, at low voltage the aging of machine's insulation in the case of mechanical stress due to fault that increase the machine's vibration like eccentricity fault is of no interest because the effect is negligible.

4.5 Conclusion

In this chapter, a Hidden Markov Model for prognostic purposes is developed, to detect the presence of short circuit, demagnetization and eccentricity faults. Prognosis aim to detect faults at its early stage or before it occurs; hence, the probability of false alarms is high. To avoid this problem and eliminate any possibility of ambiguity in the prognostic decision, we used three vital parameters that are useful for machine monitoring: torque, temperature and vibration to be input of the HMM. Then, RUL of critical components, magnet and wire's insulation, in the PMM is calculated. A suggested RUL calculation strategy that combines data base and model base approach is presented for different case of machine's fault. A global block diagram representing the HMM and the RUL calculation is illustrated in figure 140.

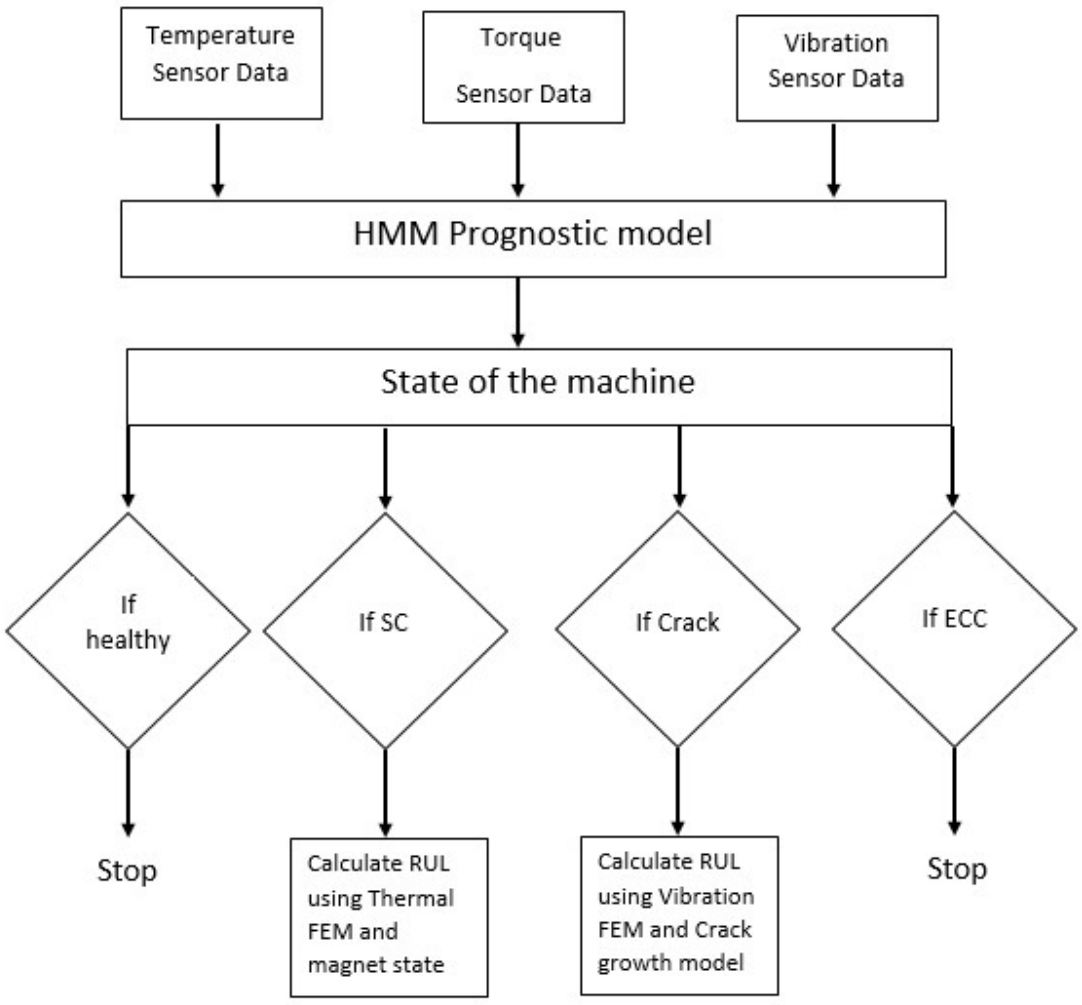

Figure 140: Global block diagram of the prognostic approach

Chapter 5: Closed loop system analysis

5.1 Introduction

In the previous chapters, the modeling and the prognosis strategy was applied on the open loop system. However, hybrid electric vehicle is an application where closed loop control system is widely applied for different purposes. In [113], a closed loop control system is implemented for speed torque control of surface permanent magnet machine in the HEV. In [114], the final goal of the implemented closed loop system is to manage the power transferred to vehicle's wheels in a way that meets the driver's demand within the rated limits of the powertrain and the battery.
The aim of this chapter is to show the impact of the closed system on the machine prognosis decision in the case of fault. Accordingly, a closed loop for the system combining the electrical machine and the inverter will be built. The control system will adjust the input power of the electric machine, coming from the battery, when working in the motor mode, to generate the required torque.
As illustrated in chapter 3, the different integrated faults in the machine has an obvious impact on its output torque. In the case of crack or eccentricity fault, the torque has increased; in the case of turn to turn short circuit the torque has decreased.
Hence, the act of the control system will be to adjust the input power of the electric machine to maintain the requested torque.
We will start by implementing the model of the inverter, coupling it to the machine and building the closed loop feedback system. For technique reasons, the simulation will be instantaneous where we will use the static electromagnetic model of the machine. The simulated system will be a combination of electromagnetic, vibration and thermal model of the machine with three phase Voltage Source Inverter and the control system.
This chapter will be divided into three main sections.
We will present:

- the inverter model and the technique used for the generation of its control signals in the first section.
- the fault interaction between inverter and machine in the second section.
- the feedback vector control of the machine, the impact of closed loop system on vital machine indicators and its influence on prognosis in the third section.

5.2 The inverter modeling

As stated previously, hybrid Electrical Vehicle is a combination between the conventional internal combustion system and an electric propulsion system. The combination between those two systems may be series, parallel or mixed [115], [116]. The electric propulsion system contains the electric machine, the controller and the inverter [117], [118]. Power switching devices are being intensively used in hybrid vehicles for their ability to drive various loads. In this section, the DC/AC power inverter system used as the interface between main hybrid energy storage system and the electrical machine will be described.

Being interested in building a closed loop system of the electric propulsion system, modeling the inverter became a necessity.

5.2.1 HEV's main power electronics elements

The main electric power train architecture of HEV application is illustrated in figure 141. Basically, a hybrid vehicle needs DC/DC choppers, DC/AC inverters and AC/ DC rectifier [117].

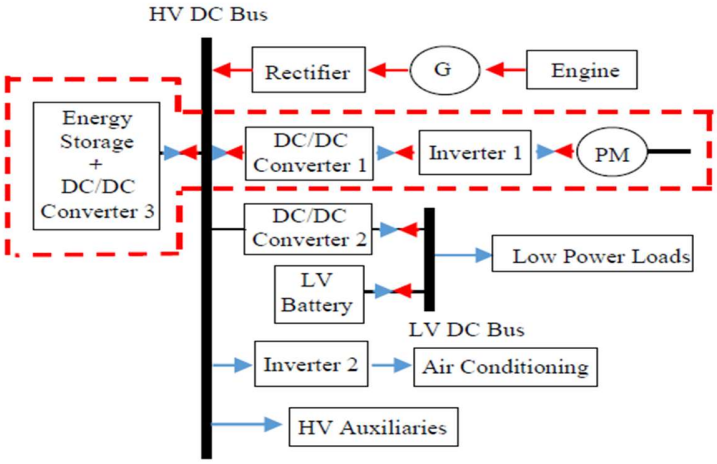

Figure 141: Main electric power train architecture for HEV [117]

A DC/AC inverter is commonly used as a power electronics interface between the main energy storage unit and the electric traction drive. In general, inverters are classified either as Voltage Source Inverters involving bidirectional current switches or Current Source Inverters consisting of bidirectional voltage switches. Most common automotive drives include VSIs where it has proven to be more efficient, cost effective, less space, faster dynamic response for rapid changes in speed or torque and be capable of running the motor without derating. Typically, a three-phase VSI consists of six bidirectional switches, each with a switch and an anti-parallel diode. By controlling these switches, the DC voltage at the input of the inverter is shaped into a balanced three-phase AC output voltage of desired magnitude and frequency.
Inverter 1 is used to convert the stiff battery DC voltage into the required variable voltage to be fed to the electric traction machine. The inverter subsystem consists of a power module made of high-power fast-acting semiconductor devices, DC link voltage, sensors, a filter and a control system as shown in Figure 142. The inverter is used as an AC drive and as a rectifier during regenerative braking when the electric motor acts as generator recharging the batteries. Therefore, to implement the motor and generator operation modes, this DC/AC converter has to be bidirectional.

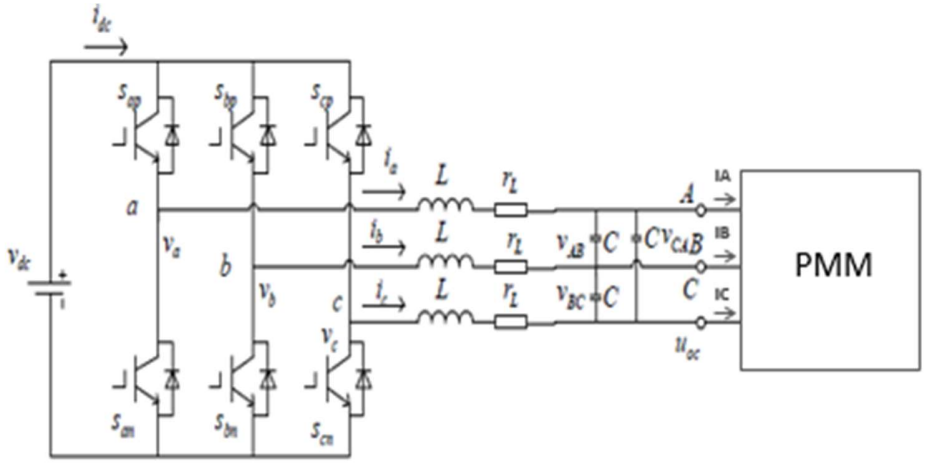

Figure 142: Standard two level three phase voltage source inverter

5.2.2 Power Inverter Modeling

The switched power inverter is nonlinear and time-varying due to the fact that it contains switches which alter the system topology with every commutation mode. However, during each switching mode the inverter subsystem is linear and possesses a linear piecewise-switched state space model. In fact, linear piecewise-switched system is a collection of linear subsystems along with a switching rule. Inverter or rectifier can be modeled using switched or averaged state space model. In [119] an average state space model of PWM three phases VSI is studied. The model is suitable for an input/output voltage waveform, regardless whether they are sinusoidal or non-sinusoidal, balanced or unbalanced, symmetrical or asymmetrical. In [120], a generalized state space averaging method is presented by using the proposed method. The calculating fundamental components of voltages and currents are in accord with the simulation and experiment of actual devices considerably compared with conventional state-space averaging method. Switch State matrix and switching functions for VSI are developed in[121] based on KCL and KVL. Paper [122] presents the analysis of a three-phase PWM inverter system including harmonic assessment of the inverter input current and output voltage with balanced and unbalanced loads. Analytical equation using the switching function approach is used to find the proper state equations to describe the power conversion circuit in MATLAB. The functional simulation model of a three-phase VSI using the switching function concept has been studied in [123]. The actual implementation of the model has been proposed with the help of MATLAB Simulink, and this concept was examined in other power conversion systems.

According to all the reviewed literature and based on the requirements of our application to have output voltage as dependent variables and load current as independent variables, we will develop a switched state space model with LC filter at the output as shown in Figure 142. In this model, the switching signals are used as a control variable that will appear inside the matrices of the state-space model; thus, we get a simple state space model instead of dividing the system into modes that make the model more complex [124], [125].

5.2.3 Switched state-space model and equations

Figure 143 shows the schematic of the power inverter. The system is driven by three inputs. The source voltage Vdc, the three phases stator current IA, IB, IC and the switching signals Sap, Sbp, Scp, San, Sbn, Scn. The inverter state variables are the voltages across the output capacitor VA, VB, VC, the inductor current ia, ib, ic (current across the three phases of the inverter). The dependent variables are the source current Idc and the three phases voltage feeding the machine VA, VB, VC which are usually measured in the drive for control purposes.

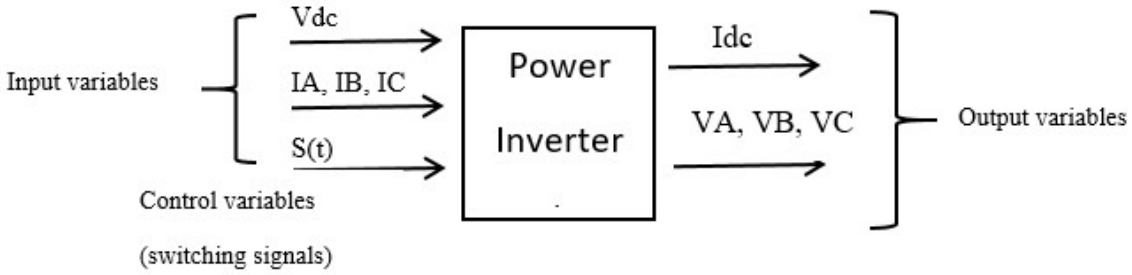

Figure 143: schematic of the power inverter

Accordingly, the inverter's dynamics can be described by the following switched linear state-space model.

$$\dot{x} = Ax + Bu \quad (74)$$

$$y = Cx + Du \quad (75)$$

Where $x = \begin{bmatrix} ia \\ ib \\ ic \\ VA \\ VB \\ VC \end{bmatrix}$ is the state vector , $\dot{x} = \frac{dx}{dt}$, $u = \begin{bmatrix} Vdc \\ IA \\ IB \\ IC \end{bmatrix}$ is the input vector, $y = \begin{bmatrix} VA \\ VB \\ VC \\ Idc \end{bmatrix}$ is the output vector and A, B, C and D are the state-space matrices using Kirchhoff's current and voltage law.

When applying Kirchhoff's current and voltage laws to the inverter's circuit in figure 142, we get the following equations:

$$ia = C\frac{dVAB}{dt} + C\frac{dVAC}{dt} + IA \quad (76)$$

$$ib = C\frac{dVBA}{dt} + C\frac{dVBC}{dt} + IB \quad (77)$$

$$ic = C\frac{dVCA}{dt} + C\frac{dVCB}{dt} + IC \quad (78)$$

$$Van = L\frac{dia}{dt} + Rl\,ia + VA \quad (79)$$

$$Vbn = L\frac{dib}{dt} + Rl\,ib + VB \quad (80)$$

$$Vcn = L\frac{dic}{dt} + Rl\, ic + VC \tag{81}$$

The three-phase inverter is composed of six switches distributed on three arms. The controls of the switches of the same arm are complementary to avoid a short circuit to the voltage source. This implies to express the switching system as shown below; moreover, each switch is replaced by its internal resistance RON.

$$Sap = 1 - San \tag{82}$$
$$Sbp = 1 - Sbn \tag{83}$$
$$Scp = 1 - Scn \tag{84}$$

Thus, we can write the following equations:

$$Vao = \frac{(Sap - San) * Vdc}{2} - (Sap + San) * RON * ia \tag{85}$$
$$Vbo = \frac{(Sbp - Sbn) * Vdc}{2} - (Sbp + Sbn) * RON * ib \tag{86}$$
$$Vao = \frac{(Scp - Scn) * Vdc}{2} - (Scp + Scn) * RON * ic \tag{87}$$

Load is balanced so we can consider the equation:

$$VA + VB + VC = 0 \tag{88}$$

Thus, the final state equations are as follows:

$$\frac{dia}{dt} = \frac{1}{L}(Van - VA - Rl * ia) \tag{89}$$
$$\frac{dib}{dt} = \frac{1}{L}(Vbn - VB - Rl * ib) \tag{90}$$
$$\frac{dic}{dt} = \frac{1}{L}(Vcn - VC - Rl * ic) \tag{91}$$
$$\frac{dVA}{dt} = \frac{1}{3C}(ia - IA) \tag{92}$$
$$\frac{dVB}{dt} = \frac{1}{3C}(ib - IB) \tag{93}$$
$$\frac{dVC}{dt} = \frac{1}{3C}(ic - IC) \tag{94}$$

Source current is function of switching signal and phases current.

$$Idc = Sap * ia + Sbp * ib + Scp * ic \tag{95}$$

5.2.4 Inverter Design Parameters

We sized the output filter in order to obtain minimum ripple in source current and minimum THD in output voltage. In practical, switching frequencies for power switching inverters used in HEVs fall in the range of 5-20 kHz [126]. Inverter design parameters are presented in table 19.

TABLE 19: INVERTER DESIGN PARAMETERS

Filter inductor	**0.14 mH**
ESR of filtering inductor	0.2 Ω
Filter capacitor	2.2 µf
Internal switch resistance	1 mΩ
Switching frequency	15KHz

5.2.5 Generation of control systems

Many techniques are used to generate the control signals to drive the three phases VSI. The adopted technique will be the space vector pulse width modulation (SVPWM). We will present results of this technique using MATLAB and Simulink. At this stage, to test and make sure that the model operates well, the load will be a simple resistance (R=10Ω, Vdc=250V, F=50Hz and Fs=1KHz) [129].

Figure 144 shows the SVPWM conduction mode of inverter's voltages and currents. Figure 145 shows the normalized harmonics of its output voltage.

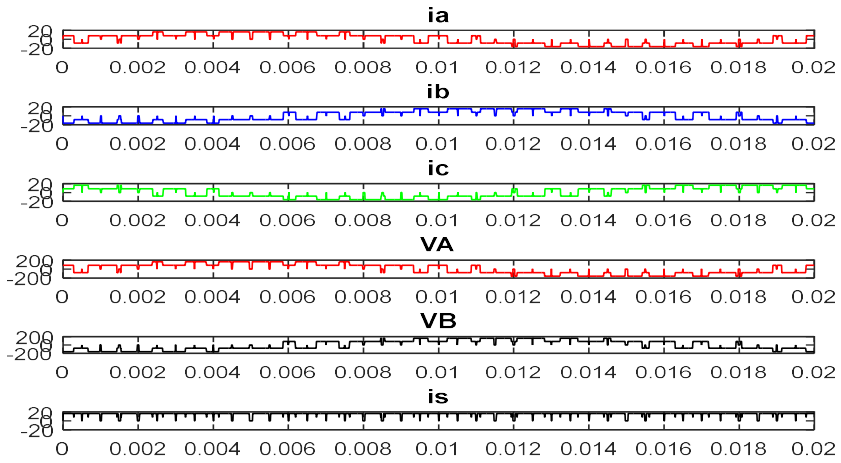

Figure 144: SVPWM conduction mode: electrical measurements

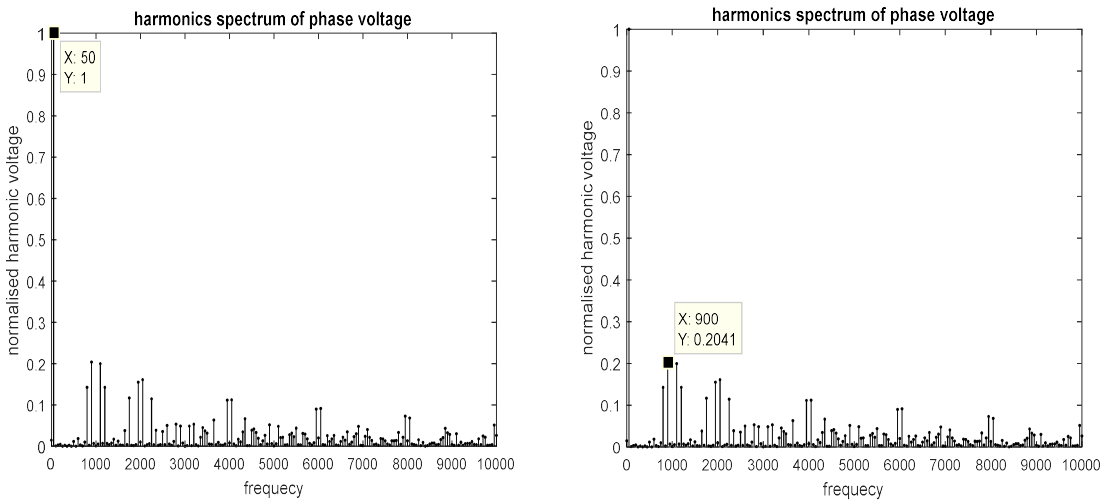

Figure 145: SVPWM conduction mode: normalized harmonics of output voltage

5.2.5.1 Theory Equations

1. Mean value of source current

$$I = \frac{3}{\pi}\, I'\sqrt{2}\, cos\alpha \tag{96}$$

2. Rms value of the source current

$$Ieff = I'\,\sqrt{2}\,\sqrt{\frac{1}{2} + (3\sqrt{3} * cos2\alpha)\;\;/(4\pi)} \tag{97}$$

3. RMS value of the fundamental line to neutral voltage

$$V'a = m\frac{Vdc}{\sqrt{2}} \tag{98}$$

5.2.5.2 Simulations Results

The simulation results are illustrated in table 25.

TABLE 25: SVPWM: SIMULATIONS RESULTS

Parameters	Code results	Theory results
VA_rms	112.7967	-
THD_VA	0.5322	-
Van_rms	114.9785	-
Van_rms_fund	101.5630	102.0621
ia_rms	11.2782	-
THD_ia	0.5319	-
Idc_rms	15.6496	15.2443
Idc_av	15.0543	15.2309

PWM techniques are useful in automotive applications due to their advantages.
Although SVPWM is more complicated than SPWM [129], the SVPWM technique gives higher level of fundamental voltage comparing it to SPWM. SVPWM is more reliable because it enables efficient use of DC voltages and smartly works with vector control thus, gives less Total Harmonic Distortion, better PF, and less switching losses at high frequencies[130].

5.3 Fault interaction between the inverter and the electric machine

In this section we will start by stating the faults that may occurs in the inverter. Then, threshold values of electrical, thermal and vibration parameters of power electronics will be highlighted. After that, the fault interaction between inverter and electric machine will be revealed.

5.3.1 Faults in the inverter

5.3.1.1 Electrical fault

Inverters used in automotive electric traction systems undergo some of the highest stresses due to their high power and relatively low voltage (hundreds of volts) which cause high currents (hundreds of amperes) and thus increase thermal and electric stresses in the inverter components and reduces the inverter efficiency.
Figure 146 shows the percentage of failure rates in the power electronics of the inverter.

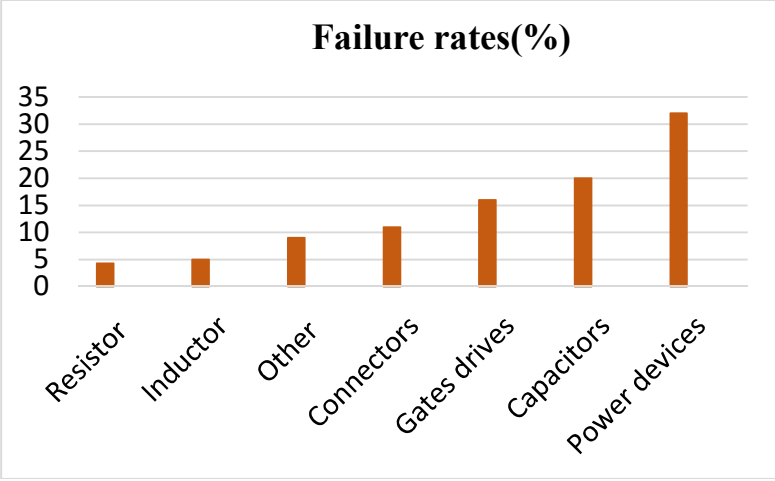

Figure 146: Rates of possible failures in power electronics of the inverter

As shown in Figure 146, the power devices are the weakest elements in the power electronic circuits. Power semiconductor faults are subdivided into open-transistor fault and short-transistor fault [117]. Open-transistor fault is usually a result of control failure, driver circuit failure, or physical damage in the transistor itself. Short-transistor fault is usually a result of high stresses on the device, error in circuit design or external causes such as a short circuit on the load side [131].

Thus, most common power inverter faults are: a single transistor short circuit, a phase-leg short circuit, single transistor open circuit, open-phase, a loss of driving signal, a capacitor short circuit fault, and a two or three phase short circuit [127]. In particular, open single switch, short circuit and open phase are mostly considered and studied.

In the other hand, the occurrence of electrical, thermal and mechanical phenomenon interactions leads to failure modes in the devices. Some failure modes have been observed on the bonded wires or on the interconnection elements. Others are linked with the metallization layer, whereas some crack propagation can be found inside the ceramic layer or in the silicon chip. The solder alloy join can also be damaged [132]. Consequently, there is a degradation of the semiconductor devices, which finally forces them into a failed state: short-circuit or open-circuit [133]. The typical power electronics package structure is shown in Figure 147 [134]. Paper [135] expresses that lifetime of IGBT module is affected by many failure modes such as material degradation, thermal cycling fatigue, power cycling fatigue and vibration fatigue.

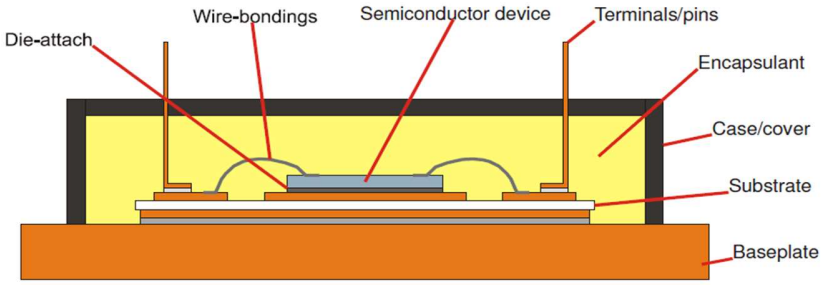

Figure 147: Typical power electronics package structure

5.3.1.2 Thermal stress

Many researches study thermal stress for power devices such as IGBT and estimate its lifetime based on swing temperature between junction and baseplate temperature. Paper [136] develops a 3D finite element model for IGBT module which indicates that the maximal stress is obtained at the heel of the bond wire. The author in [137] shows that lifetime of IGBT is limited when thermal resistance increases of 20%. Under thermal cycle range -40°C to 125°C lifetime is reduced to 1000 cycles and under power cycle with ΔTj =100°C lifetime down to 20000 cycles. Paper [138] shows that during vehicle acceleration the IGBTs are under a particularly high load and a 10°C increase in temperature rise reduces the number of load cycles by a factor of 3. Authors in [139] and [140] show that increase of junction temperature and collector to emitter voltage lead to deteriorate the solder layer of the bottom switch This increases the thermal resistance of the chip. The investigations on paper [141] proved that an IGBT module can handle 12.5% more output power if the maximum junction temperature rises from 150°C to 175°C. Paper [142] indicates that thermal stress can be induce by power and thermal cycling and temperature swing range is form 60°C to 100°C. Paper [143] presents a methodological study on power cycling stress in an active IGBT rectifier used in a Direct Wave Energy Converter. This model serves to evaluate the influence of IGBT rating over the IGBT lifetime. Authors in [144] develop a Physics-of-Failure lifetime modeling approaches that can be seen as a new methodology in power electronics that potentially can improve the lifetime estimation. A thermal model for VSI is created in [145], this model serves to predict the maximum switching frequency without violating thermal limits, and

to quantify the characteristics of the heat-sink needed to dissipate the heat under worst case conditions [146].

5.3.1.3 Vibration stress

Reliability of IGBT modules is highly affected by vibration. It is important to estimate power electronics systems reliability by taking into account their environment [147]. Papers [148], [149] and [150] determine that the operation and pulse frequency cause displacement on several component in IGBT module but the most affected is the short IGBT wire. Thus, they have influence on the lifetime of IGBT modules. Laser Doppler vibrometer and finite element analyses were conducted to obtain the strain values needed for lifetime assessments. These papers show that displacement of bonding wire of IGBT will increase with pulse frequency and decrease with operation frequency. Paper [151] compares reliability levels required for industrial-use and automotive-use. Results show that IGBT for automotive-use can support vibration stress till 20G. Paper [152] presents typical environmental conditions and operational requirements for automotive applications concerning vibration, humidity, junction and ambient air temperature. The environmental conditions and operational requirements of the IGBT are illustrated in table 26.
The fatigue life of aluminum wire under random vibration testing is evaluated in paper [153]. As a result, the appropriately designed aluminum wires with silicone gel can endure 18.4-Grms random vibration testing which is demanded for semiconductor devices for vehicle applications.

TABLE 26: ENVIRONMENTAL CONDITIONS AND OPERATIONAL REQUIREMENTS

Parameters	**Value**
Ambient air temperature	-40 to +135°C
Coolant water temperature	-40 to +105°C
Junction temperature	-40 to +175°C
Temperature cycling	1000 cycles @ ΔTj =165°C
Power cycling	30000 cycles @ ΔTj =100°C
Humidity	85%
Vibration test	10 G
Shock	50 G

After examining faults occurring in power inverter and permanent magnet machine each alone, a fault interaction between those two blocks should be built. Threshold value of useful parameters for the PMM were discussed previously; the same should be done for the power devices constituting the inverter before combining it with the FEM.

5.3.2 Threshold value of the inverter

In this section we will determine threshold value of power devices' parameters and make sure they are compatible with our HEV application; then, combine the finite element model of PMM with the state space model of VSI and show the simulation results of the whole system under normal and abnormal operation.

5.3.2.1 Electrical specifications of IGBT devices

The rated power of this machine is 15 KW, maximum current 29.3 A and maximum voltage 312 V which impose DC link voltage 590V and IGBT/DIODE module 1200V-50A. All specifications and electrical parameters of IGBT module are presented in the datasheet [154].

5.3.2.2 Thermal analysis of IGBT devices

The higher the maximum junction temperature Tjmax, the higher is the stress on the device which results in a reduced number of cycle. Therefore, the expected lifetime of the module decreases when the junction temperature increases. Paper [155] estimates the lifetime of the power module function of the chip temperature. It is expressed in the below equation:

$$Nf = 2.55 * 10^8 * e^{-0.127 * \Delta Tj} \quad (99)$$

Where ΔTj is the difference between junction temperature and reference temperature that should be 60˚C. Junction temperature will be calculated based on the Equation:

$$Tjunction = TAmbient + \Delta TAmbient\ to\ Heatsink + \Delta T\ case\ to\ junction \quad (100)$$

The ambient temperature is a constant, ΔTAmbient to Heatsink represents the temperature drop across the heatsink and it is calculated based on the total power losses from the IGBT and the diode. The ΔTIGBT module case to IGBT junction represents the temperature drop across the IGBT module case to the IGBT junction and it is calculated based on the total power losses from the IGBT as shown:

$$\Delta TAmbient\ to\ Heatsink = Ptotal * Rth\ Ambient\ to\ Heatsink \quad (101)$$

$$\Delta T\ IGBT\ case\ to\ junction = PIGBT * Rth\ case\ to\ jucntion \quad (102)$$

Where Rth Ambient to Heatsink is the thermal resistance from ambient to heat sink; $RthAmbient\ to\ Heatsink = 0.26\ K/W$ and Rth case to junction is the thermal resistance of IGBT from case to junction which is determined based on datasheet of IGBT.

During operation, the main losses in the converter are due to conduction and switching both in the transistor and the diode. Power losses calculation are represented in the following equation: [156] and [157].

$$Pcond.IGBT = \left(\frac{1}{2\pi} + \frac{m * \cos\alpha}{8}\right) * VCE0 * Is + \left(\frac{1}{8} + \frac{m * \cos\alpha}{3\pi}\right) RCE * Is\text{^}2 \quad (103)$$

$$Psw.IGBT = Fs * E(on + off) * \left(\frac{1}{\pi}\right) * \left(\frac{Is}{Iref}\right) * (\frac{Vdc}{Vref})^{Kv} \quad (104)$$

$$Pcond.diode = \left(\frac{1}{2\pi} - \frac{m * \cos\alpha}{8}\right) * VF0 * Is + \left(\frac{1}{8} - \frac{m * \cos\alpha}{3\pi}\right) RF * Is\text{^}2 \quad (105)$$

$$Psw.diode = Fs * Err * (\frac{Is}{Iref}\frac{1}{\pi})^{Kr} * (\frac{Vdc}{Vref})^{Kv} \quad (106)$$

Typically, Kv for IGBT losses is 1.3 to 1.4 and Kv and Kr for diode losses are 0.6 [156].

The thermal effect will be treated in two cases: first, when the inverter is near to the machine and second, when the inverter is at 176.002 cm from the machine (176.002 cm corresponds to the length of the front of the Toyota Prius 2017). Based on thermal degradation the below equation, the temperature will be calculated at 176.002 cm and study its impact on inverter to optimize at the end the minimum allowable distance between machine and inverter where the machine is considered the source of the heat.

$$Q = -K * S * \frac{\Delta T}{\Delta x} \quad (107)$$

Where $\frac{\Delta T}{\Delta x}$ is the temperature gradient.

5.3.2.3 Vibration analysis of IGBT devices

As mentioned in the literature review, during normal operation the IGBT module is exposed to displacement caused by operation and pulsing frequency. So, when IGBT module are integrated in circuit with 66.8Hz as operation frequency and 500Hz as switching frequency the normal vibration will be 0.06 µm [148]. This value is considered as threshold value for the IGBT module. The IGBT module are exposed to random vibration in paper [153]. The maximum value supported by the module is 18.4 Grms where 1Grms=9.88m/sec2, this value is considered as an acceleration and the vibration can be expressed as amplitude (acceleration, velocity or displacement) or as frequency. In order to be compatible with the vibration model of the used machine, the acceleration must be converted into displacement [158]. Since the vibration is a random signal it wasn't evident to do this conversion. Hence, according to the literature, we will consider the threshold vibration value of IGBT as 0.06 µm and the limited value as 957.75µm.
Like the temperature analysis, the vibration analysis will be considered in the two cases mentioned above based on vibration degradation presented as:

$$\text{Vib} = 20 \text{ Log D} \quad (108)$$

Where Vib is in dB. Accordingly, we will use the following equation to convert from µm to dB.

$$\text{dB} = 20 \log(\frac{meseaured\ displacement}{reference\ displacement}) \quad (109)$$

Where reference displacement is 10-6 µm based on norm ISO 1683.

5.3.3 Impact of machine performance on VSI

In this section we will study the impact of machine's faults on the power electronic devices of the VSI.
The importance of this section rises from the sensitivity of the electronic components forming the power inverter to vital features like temperature, current, voltage, vibration… Hence, three types of faults in the machine will be elaborated from the most to less severe: demagnetization, turn to turn short circuit and the eccentricity fault. Impact of each fault on power electronics will be treated in electrical, thermal and vibratory domains.

5.3.3.1 Healthy case

We consider a case study with maximum value of output voltage 312V, DC link voltage 590V, phase angle 0.483 rad, modulation index 0.92, operation frequency 66.8 Hz and small switching frequency 500Hz in order to reduce the time of simulation. We must take at least one fundamental period with step dt =1/(Fs*100) sec to simulate the results which correspond to 794 samples in one period, which is a long time simulation. Or, in healthy case the machine is symmetric; all poles are identical. The time needed for any point at the rotor to sweep one pole is 0.00288 sec. So, the simulation step will be 0.00288 sec.
Table 27 shows all measurements under normal case.

TABLE 27: MEASUREMENTS RESULTS UNDER NORMAL OPERATION

Measurements	Parameters	Value
Output Voltage	VA_rms_total	269.6688
	VA_rms_fundamental	231.6185
	THDVA	0.0266
	VB_rms_total	243.1782
	VB_rms_fundamental	204.1319
	THDVB	0.0306
	VC_rms_total	270.6204
	VC_rms_fundamental	231.6204
	THDVC	0.0268
Stator Current	IA_rms	12.7474
	IB_rms	11.4956
	IC_rms	12.7661
Source Current	is_rms	19.3490
	is_av	16.5125
Electromagnetic torque	Te	133.49
Air gap flux density	Bav	0.59
Max temperature at boundary	T°C	115.6005
Vibration	Displacement (m)	2.7195e-05

5.3.3.2 Demagnetization fault

The most sever fault in permanent magnet machine is demagnetization, that occur at magnet level due to a crack. However, due to the crack, the density of flux lines in the machine has increased at the two right and left side of the magnet; this will increase the flux focusing in the teeth of the laminated sheet.
The air gap flux density in the area above the crack has almost conserved its shape but it has slightly decreased. The air gap flux density, over the pole containing the crack, encountered a high flux density due to flux focusing and a slight decrease above the crack; this means higher average air gap flux density, hence, higher torque.
The electromagnetic force in the area above the crack decrease and the displacement in the machine's periphery directly above the crack decreases as indicated in Table 28.

TABLE 28: MEASUREMENTS RESULTS WITH DEMAGNETIZATION FAULT

	Parameters		**1 mm crack**	**3 mm crack**
Crack	Electromagnetic	Te(N.m)	153.28	132.25
		Bav(Tesla)	0.67	0.58
	Temperature	T˚C	115.5242	115.5242
	Vibration	displacement(m)	4.0281e-05	4.06e-05
	Electrical	Stator current (rms value)	12.3572	12.3572
		Source current (average value)	16.5406	16.5406
		Stator voltage (rms value)	261.4121	261.4121

It is noted that the displacement in case of crack increased compared with the healthy case; whereas the temperature remains the same. Hence, an analysis should be done, by mean of the analytical equations previously presented, to figure out the impact of the vibration increase on the inverter. The impact of this fault at the thermal level is nonexistent.

5.3.3.3 Turn to turn short circuit fault

Short circuit may occur at winding level. It may start as turn-to-turn short circuit and the number of shorted turns increases till all the coil is short circuited, if the cause of the fault persists [159]. Table 29 shows the measurement results of this case.

TABLE 29: MEASUREMENTS RESULTS WITH TURN TO TURN SHORT CIRCUIT FAULT

	Parameters		2 turn to turn	6 turn to turn
Short circuit	Electromagnetic	Te(N.m)	95.05	91.95
		Bav(Tesla)	0.41	0.35
	Temperature	T˚C	185.4478	217.8575
	Vibration	displacement(m)	3.9861e-05	8.8695e-05
	Electrical	Stator current in phase a (rms value)	2.1*Irated	2.9*Irated
		Source current (average value)	24.4812	28.1126
		Stator voltage Phase a (rms value)	270.0054	269.9830

Irated is the nominal value in healthy case.
As shown in table 29, temperature, stator current and vibration increase when short circuit fault occurs. The average air gap flux density and the torque decrease due to the weakening of the magnet caused by the high temperature. At six turns to turn SC, the current value will exceed the rated value of IGBT, this will induce damage in the power device. In this case, the protective device should be alerted and act to protect the system.
At six turns to turn SC, the maximum temperature at the boundary of the machine is 217.8575 ˚C, so, the T˚C at the encasement of the machine will be less than the maximum T˚C of the machine's boundary by 63.5˚C [158].
Thus, the ambient temperature around the inverter will increase to 154.357˚C. Based on Equations (94) to (101) the degradation of the lifetime function of junction temperature during turns to turn short circuit fault is calculated and illustrated in figure 148. At six turns to turns, lifetime of IGBT modules is 266.3560 cycles.

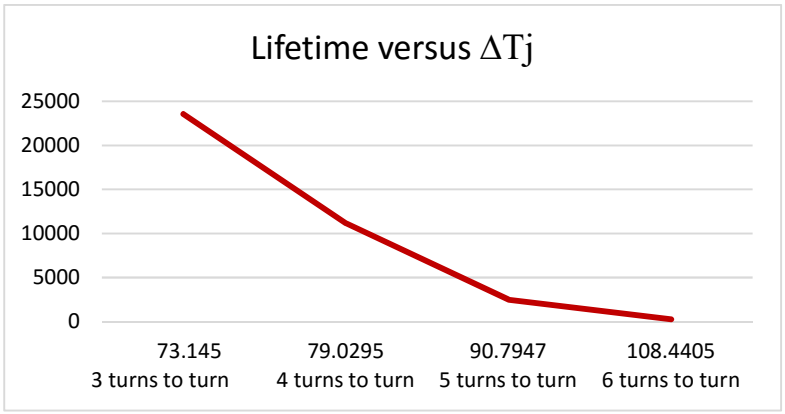

Figure 148: Lifetime of IGBT versus junction temperature

5.3.3.4 Eccentricity fault

The impact of the 10 % eccentricity fault on the machine and inverter parameters are illustrated in table 30.

TABLE 30: MEASUREMENTS RESULTS UNDER ECCENTRICITY FAULT

	Parameters		**value**
Eccentricity 10%	Electromagnetic	Te(N.m)	148.68
		Bav(Tesla)	0.65
	temperature	T°C	115.5242
	vibration	displacement(m)	4.7690e-05
	Electrical	Stator current (rms value)	11.1358
		Source current (average value)	12.0727
		Stator voltage (rms value)	227.1546

Compared to the healthy case, the displacement of the machine has increased in this faulty case, whereas the temperature remains intact. The impact of this increase in the machine's vibration level, on the inverter, will be analyzed in the following section.

5.3.3.5 Degradation of temperature and vibration during the three types of faults

Taking into account the distance between inverter and machine, the temperature and vibration will degrade between them. Table 31 illustrates the degradation of vibration and temperature at the inverter level.
The machine is considered as a heat source.
Temperature and vibration values will be calculated based on Equations (102) and (103). The distance between the machine and the inverter will be 1.76 m.

TABLE 31: DEGRADATION OF TEMPERATURE AND VIBRATION FROM THE MACHINE TO THE INVERTER

	Displacement (µm)	**Temperature (°C)**
Crack 1mm	69.18	103.0223
Crack 3mm	70.019	103.0225
2 turn to turn SC	108.5	147.8
6 turns to turn SC	241.43	158.78
Eccentricity 10%	126.42	103.0242

The calculated values, presented in table 26, and the threshold tolerated values of temperature and vibration of the inverter, mentioned previously, are compared. We conclude that, native faults in

the machine has no harmful impact on the inverter unless the fault worsen and reach an advanced stage.
However, some remarks that are useful for the optimization of machine and inverter location inside the vehicle are noted:

- The maximum temperature at six turns to turn short circuit doesn't exceed the maximum allowable junction temperature. The short circuit is assumed not to propagate more since the protective device should be sized to sense this fault. Thus, the efficiency of the cooling system can be reduced and designed accordingly.
- The location of the inverter can be optimized. No need to place it far from the electric machine where in many vehicles it's placed in the baggage and occupy a relevant volume, in the aim of protecting it from heat and vibration.

5.3.4 Impact of VSI's faults on PMM

Semiconductors are an important source of failure in traction systems. Failures occurring on power switches can affect the function of power converters and spread through the traction chain elements. Authors in [131] estimated that 40% of failures can be attributed to semiconductors faults and 39% to their auxiliary circuits. Driver circuits should be reliable enough, to prevent additional sources of failure.
Switch breakdown may result in switch open circuit or switch short-circuit.
In practice, the SC switch failure is most common compared to the OC failure (85% for SC and 15% for OC). In the coming sections the inverter switch faults, more precisely, open circuit and short circuit faults in IGBTs will be investigated. In addition to the open phase fault.

5.3.4.1 Single switch short circuit fault

Short-circuits are the most serious class of faults in power electronics converters. If a single switch is short-circuited, its phase pin is directly connected to the DC bus. When the lower switch is gated to be ON, the source will be shorted and a dangerous failure occurs. So, in this case the gate signal of the lower switch in the same branch must be immediately turned off to prevent critical situation.
Figure 149 shows the waveforms of phase currents when IGBT1 is shorted at 0.015 seconds, after one period of healthy operation. The spectrum of the output voltage presents a dc component.
The average output voltage, stator current, source current, torque and air gap flux density are illustrated in table 32.

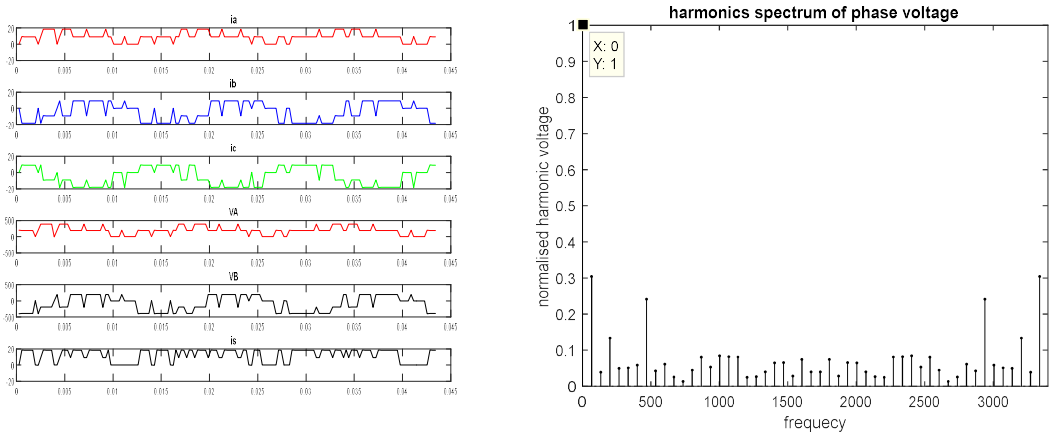

Figure 149: electrical measurements and harmonic spectrum of output voltage during IGBT1 short-circuit faulty

TABLE 32: MEASUREMENTS RESULTS IN IGBT1 SHORT-CIRCUIT FAULT

Measurements	Parameters	IGBT1 SC
Output Voltages	VA_rms_total	231.8209
	VA_rms_fundamental	82.1439
	THDVA	0.1489
	VB_rms_total	244.2722
	VB_rms_fundamental	179.2459
	THDVB	0.0450
	VC_rms_total	253.8740
	VC_rms_fundamental	200.6002
	THDVC	0.0364
Stator and Source current	IA_rms	10.9496
	IB_rms	11.5445
	IC_rms	11.9995
	is_rms	18.9955
	is_av	15.4281
Electromagnetic torque	Te	130.68
Average air gap flux density	Bav	0.59

The results in the above table shows that the impact of IGBT short circuit on the machine's performance is insignificant where a decrease of 2% in the electromagnetic torque is tracked.

5.3.4.2 Single switch open circuit fault

Open-circuits are the other serious class of faults in power electronics converters. If a single switch is open-circuited, its phase pin is not connected to the DC bus or to the machine and the delivered power from the inverter to the machine will be reduced.

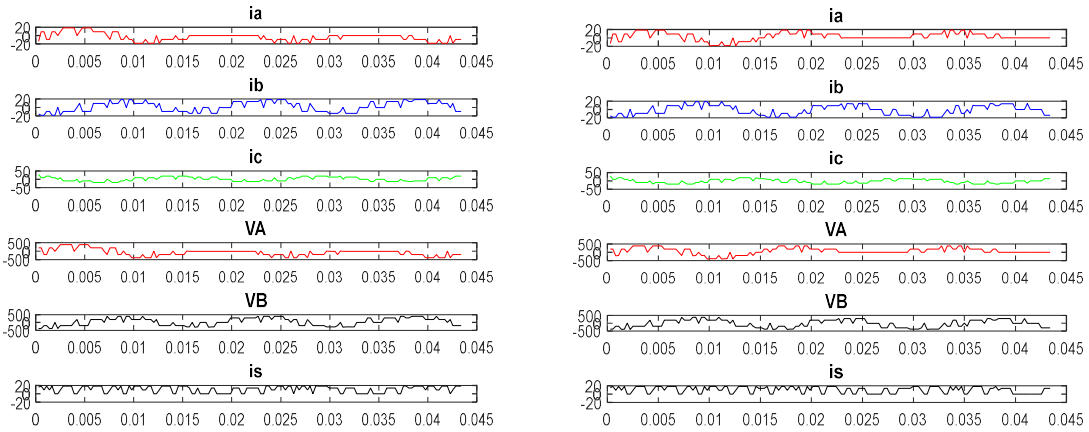

Figure 150: Electrical measurements when IGBT1 open-circuit (left) and IGBT2 open circuit (right)

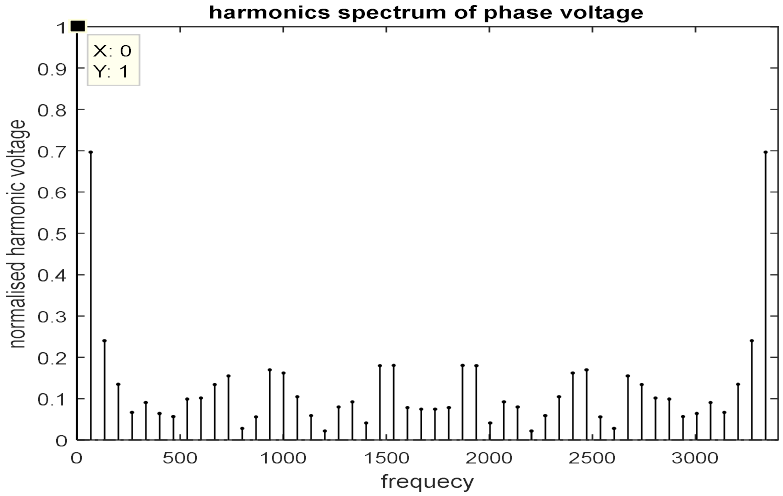

Figure 151: harmonic spectrum of output voltage in single open circuit fault

Figure 150 shows the waveforms during a single open-circuit fault in the upper power switch IGBT1 and lower power switch IGBT2 occurring at 0.015s. When an open-circuit occurs on IGBT1 at 0.015 s, current of phase a cannot be positive because the path through IGBT1 form the capacitor to winding a is open. Similarly, when IGBT2 is open-circuit, winding a current is non-negative under this fault. Once the open-switch faults appear, the current curve becomes unidirectional and asymmetric [160]. Also, the switch voltage cannot be described by the equations (110), (111), (112), (113), (114) and (115). As shown in figure 151, the spectrum of output voltage of phase a presents a dc component.

$$VT1 = (1 - Sap) * Vdc \quad (110)$$
$$VT2 = Sap * Vdc \quad (111)$$
$$VT3 = (1 - Sbp) * Vdc \quad (112)$$
$$VT4 = Sbp * Vdc \quad (113)$$

$$VT5 = (1 - Scp) * Vdc \quad (114)$$
$$VT6 = Scp * Vdc \quad (115)$$

The average output voltage, stator current, source current, torque and air gap flux density in this case are illustrated in table 33.

TABLE 33: RESULTS WHEN IGBT1 OR IGBT2 IS OPEN-CIRCUITED

Measurements	Parameters	IGBT1 Open	IGBT2 Open
Output Voltages	VA_rms_total	188.1346	193.2005
	VA_rms_fundamental	115.0120	116.6212
	THDVA	0.0754	0.0750
	VB_rms_total	232.1087	230.2512
	VB_rms_fundamental	186.1618	185.7714
	THDVB	0.0364	0.0359
	VC_rms_total	241.8622	249.5117
	VC_rms_fundamental	200.0118	202.9447
	THDVC	0.0323	0.0336
Stator and Source Current	IA_rms	8.9003	9.1258
	IB_rms	10.9743	10.8826
	IC_rms	11.4338	11.7938
	is_rms	14.2069	15.9919
	is_av	10.7018	12.2660
Electromagnetic torque	Te	98.28	125.29
Average air gap flux density	Bav	0.59	0.59

The occurrence of open circuit fault in one of the inverter's IGBTs has a negative impact on the machine's performance where its electromagnetic force decrease in a percentage between 6% and 27 %.

5.3.4.3 Open phase fault

When an open circuit fault occurs in a leg of the VSI no current will pass through this phase to the motor as shown in figure 152 where the current in the opened phase a becomes zero.
The average output voltage, stator current, source current, torque and air gap flux density in this case are illustrated in table 34.

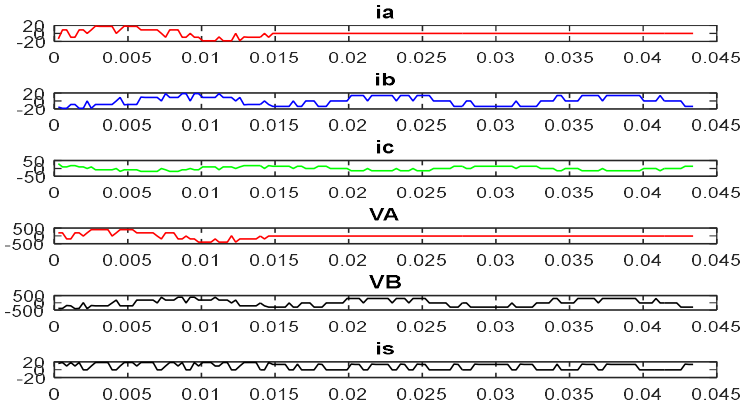

Figure 152: Electrical measurements in open leg faulty

TABLE 34: MEASUREMENTS RESULTS WHEN PHASE A IS OPEN

Measurements	Parameters	phase *a* open
Output Voltages	VA_rms_total	0.0054
	VA_rms_fundamental	0.0002875
	THDVA	7.3835
	VB_rms_total	218.5273
	VB_rms_fundamental	184.9293
	THDVB	0.0313
	VC_rms_total	218.6757
	VC_rms_fundamental	185.0858
	THDVC	0.0313
Stator and Source Current	IA_rms	0.0110
	IB_rms	10.3304
	IC_rms	10.3369
	is_rms	11.5118
	is_av	7.3702
Electromagnetic torque	Te	77.79
A average air gap flux density	Bav	0.588

The impact of the open phase fault on the machine's performance is flagrant where its electromagnetic fault decreased by 41% compared with the healthy case.

According to the results presented in the above tables, single switch open circuit, short circuit and open leg fault affects the operation of the machine in many ways:
- Current and voltage in all phases are affected under faulty operation. Voltage in phase a is -20% in case of SC, -31% in case of single OC, compared to the rated value; this reduces the power delivered to the machine.
- The power electronics circuit becomes unbalanced. This electrical unbalance fact leads to both electrical and mechanical damage to the electrical machine [161][162].

$$IA + IB + IC \neq 0 \quad (116)$$

$$VA + VB + VC \neq 0 \quad (117)$$

- THD of output voltage is greater than 3% (threshold value of harmonics for PMM)
- Torque is -26.39% of rated value in case of IGBT1 OC, - 41.7% in case of open leg fault and -2% in case of SC
- High oscillation in the torque
- Decrease in power factor

We note that, faults of small scale in the inverter have low impact on the air gap flux density. Study in [24] show that, in PMM, the main source of the flux in the air gap is the magnet, stator current don't have a big impact on the air gap flux density. This is validated by this chapter. When a single short circuit occurs in the VSI, the air gap flux density and the torque face a small variation; it remains almost intake. When an open circuit occurs in one IGBT of the VSI, the influence on the PMM depends on the location of IGBT. The influence on the torque can be 7% or 27 %.
In fact, this shows that the influence of relevant inverter's faults on PMM is not substantial. This can be interpreted when we recall that in PMM the main source of gap flux density comes from the magnets in the rotor. The investigated faults in this section affect the stator's involvement in the total air gap flux density in the machine which is relatively small.
This highlight the advantage of using permanent magnet machine in such application.

This interpretation is very logical since we are operating in open loop system; there is no feedback to upgrade the stator involvement in the air gap flux by increasing/decreasing the power coming from the source accordingly.

It is expected that the performance of the system will change in the case of closed loop, albeit in a small range. To clarify this matter, a closed loop system will be built in the next section. The case of machine demagnetization will be treated for demonstration.

5.4 Vector control for the PMSM

The most popular method used to control PMSM is vector control, which can be field oriented control or direct oriented control. Paper [163] proposes a new method for PMSM drive based on field-oriented control and space vector modulation. In this method, the reference currents of PMSM are calculated in terms of minimum torque ripples and reference speed operation. The machine is modeled in d-q axis. A DTC is presented in [164]. This paper shows that the DTC-SVM offers very good speed control performance. The analysis indicates that the increase of electromagnetic torque is proportional to the increase of the angle between the stator and rotor flux linkages. In our application, we need to keep the torque at reference value.
So, we will apply the DTC presented in this paper but the output will be the torque instead of the speed. In this approach, the output torque will be adjusted to a desired value by controlling the electrical power coming from the storage device (the battery) through the inverter. To increase or decrease the torque we will increase or decrease the intervention of the stator in the average air gap flux density knowing that the torque is directly proportional to it.

In figure 153, a block diagram representing the coupling between the PMM, the inverter and the closed loop control system is illustrated.

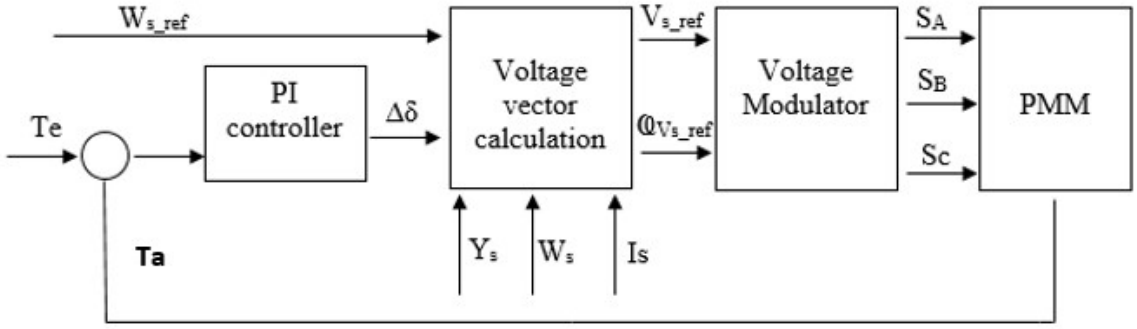

Figure 153: Direct torque control for PMSM

Where Δδ is the increment of load angle. Ys is rotor position. Ws is air gap flux density. Is is source output current. SA, SB and SC are the inverter switching vectors. Te is the desired torque. Ta is the actual torque.
Due to this direct torque control, the input power is no longer independent of the output power of the machine. Suppose that we desire to get a nominal output torque from the machine. In healthy case, the nominal input power of the machine will be enough to get this desired torque. However, the problem incarnates when a fault occurs.
As we clarified previously, faults like demagnetization and eccentricity increase the machine's torque; whereas others like turn to turn short circuit fault decrease the torque.

The governing analytical equations of the system are presented below.

The output of the PID controller Δδ is expressed as:

$$\Delta\delta(t) = kp * e(t) + ki * \int e(t)dt + kd * \frac{de}{dt} \tag{118}$$

e(t) represents the error.

$$\emptyset Vs_{ref} = \text{atan}\left(\frac{Vq}{Vd}\right) \tag{119}$$

Vq and Vd are the quadrature and direct machine voltage coming from Clark's transformation.

$$Vsref = \sqrt{(Vq^2 + Vd^2)} \tag{120}$$

$$Vq = rs * iq + (ws_{ref} * \sin(ys + \Delta\delta) - \text{ws} * \sin(ys))/\Delta t \tag{121}$$

$$Vd = rs * id + (ws_{ref} * \cos(ys + \Delta\delta) - \text{ws} * \cos(ys))/\Delta t \tag{122}$$

Δt is the sampling time.
wsref is the reference air gap flux density. ws is the simulated air gap flux density.
ys is the rotor position.
iq and id are the quadrature and direct current coming from Clark's transformation.
rs is the stator resistance.

The strategy followed to achieve the direct torque control of the PMM is illustrated in figure 154.

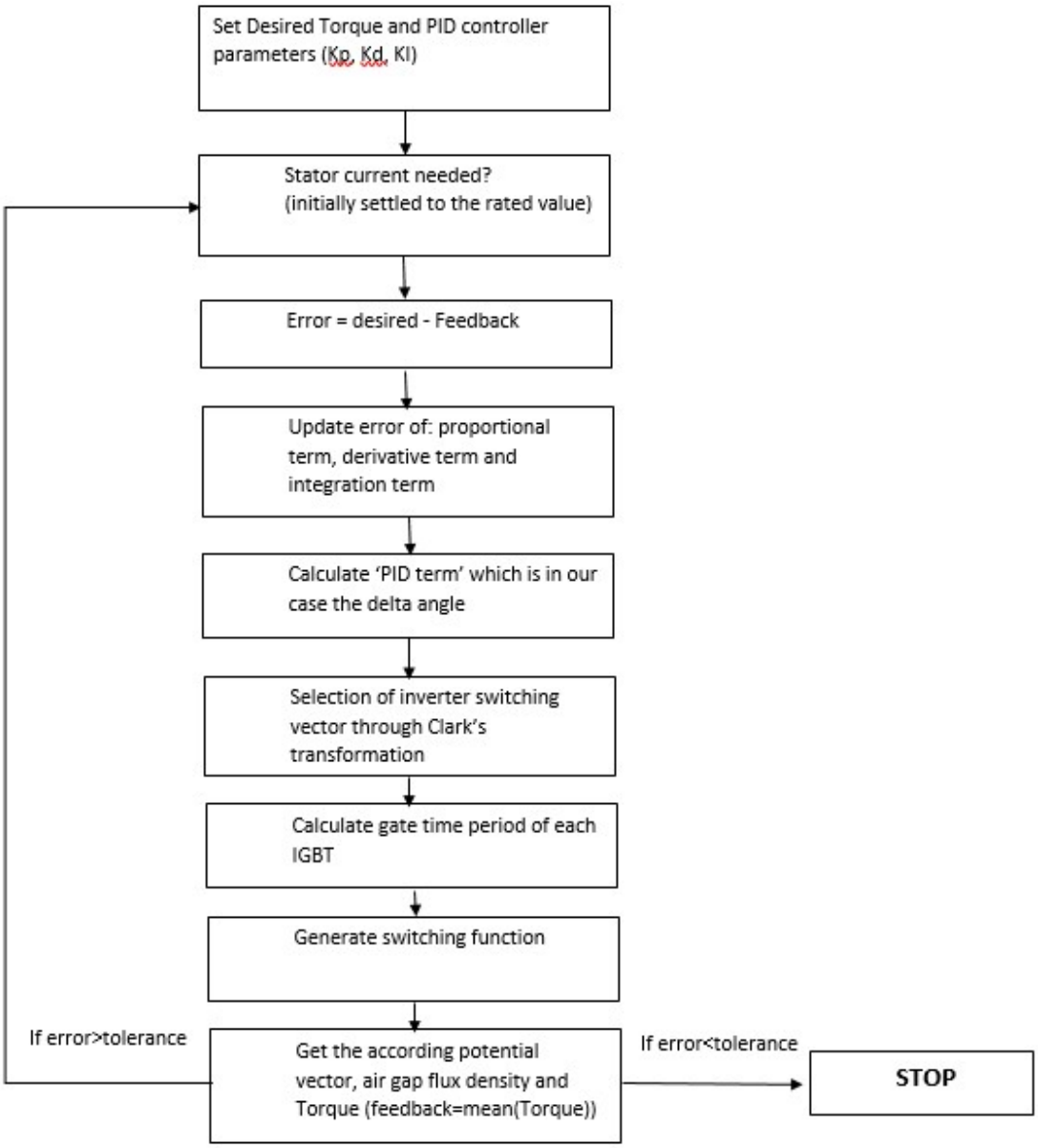

Figure 154: Block diagram of DTC strategy

To identify the effect of integrating a closed loop control system on the machine operation in the first stage and on the prognostic decision in the second stage, a comparison study between open loop system and closed loop system will be conducted.
A simulation for the case of 1 mm crack in one piece of magnet will be generated when the system is in open loop and when it is in close loop.
In chapter 3, we saw that the torque has increased in the case of crack in the magnet compared to the healthy case when using an open loop system. In open loop analysis, the input electric power is constant and independent of the output requirement.

We applied the closed loop system to control the output torque by adjusting the input power of the machine coming from the inverter side. Hence, in the case of 1 mm crack fault in the magnet, the controller will decrease the output torque by decreasing the input power. This will decrease the stator current which decrease the intervention of the stator in building the air gap flux density; in other words, this decrease the power of electromagnetic coupling between the stator and the rotor. To decrease simulation time, we used the static electromagnetic FEM that will be ran each machine revolution; hence the simulation step is 380°. At each instant of time 't', the thermal and vibration FEM models are computed too.
Figure 155 shows the block diagram of this combination.

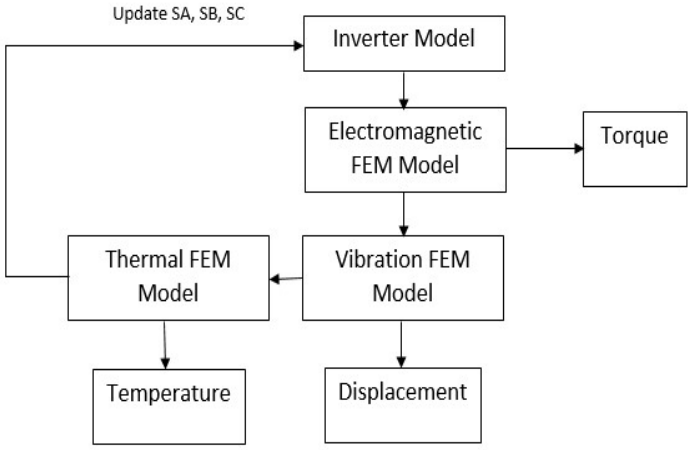

Figure 155: Block diagram of closed loop combined model

Figure 156, 157, 158 shows the difference between the healthy and faulty measurements of Torque, vibration and temperature in closed and open loop system; they are designated by ΔTorque, Δdisplacement and ΔTemperature respectively.

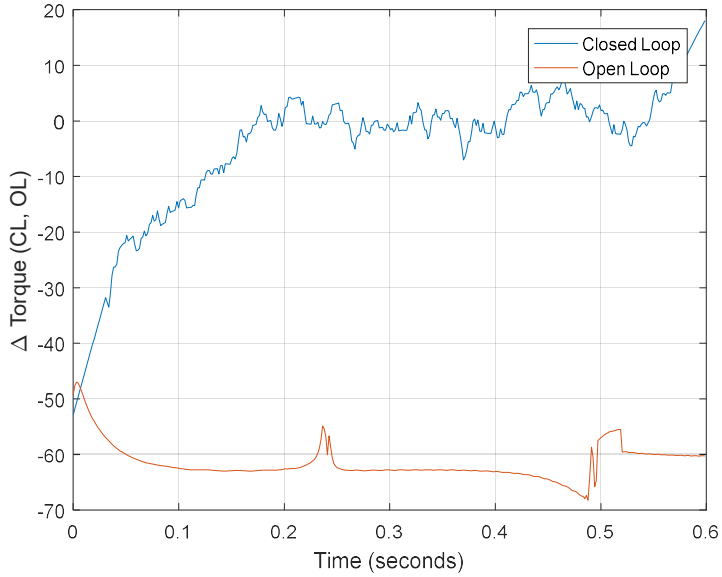

Figure 156: ΔTorque in case of 1 mm crack (Open and Closed loop)

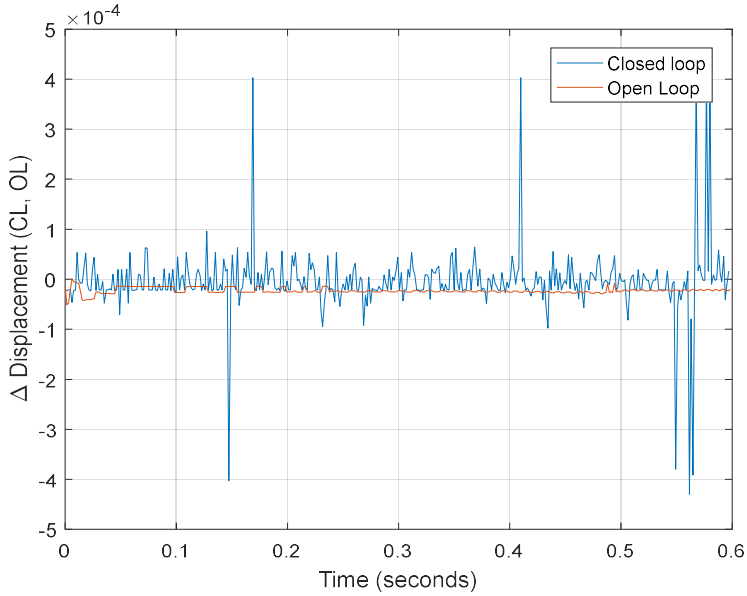

Figure 157: ΔDisplacement in case of 1 mm crack (Open and Closed loop)

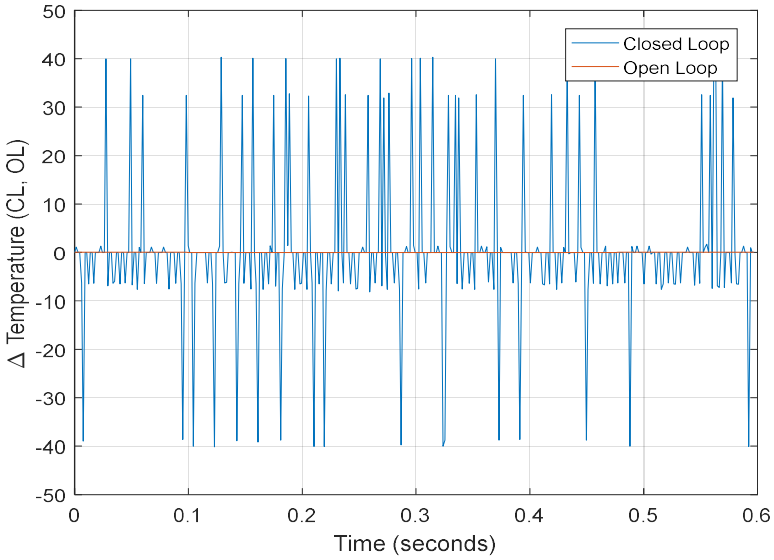

Figure 158: ΔTemperature in case of 1 mm crack (Open and Closed loop)

In the closed loop system, ΔTorque is around zero since we applied a vector control system with torque reference; however, in the open loop system, ΔTorque is high because the presence of crack in the magnet impacted the air gap flux density which in his turn impacted the torque knowing that the air gap flux density and the torque are directly proportional.
ΔDisplacement is detectable in the closed and open loop system; however, it is much higher in the closed loop system.
ΔTemperature is zero in the open loop system; as we stated in chapter 3, there is no change in the machine's temperature when a crack occurs in one piece of magnet. However, in the closed loop system, there is a detectable change in the machine's temperature; to adjust the machine's torque to the reference value, stator's current will be adjusted, which leads to changes in machine's temperature.
In the open loop system, there is no change in stator's current. However, in the closed loop system the difference is to be mentioned. Figures 159 and 160 shows the instantaneous current in phase A and the high envelope of this current respectively, for the open and close loop system.

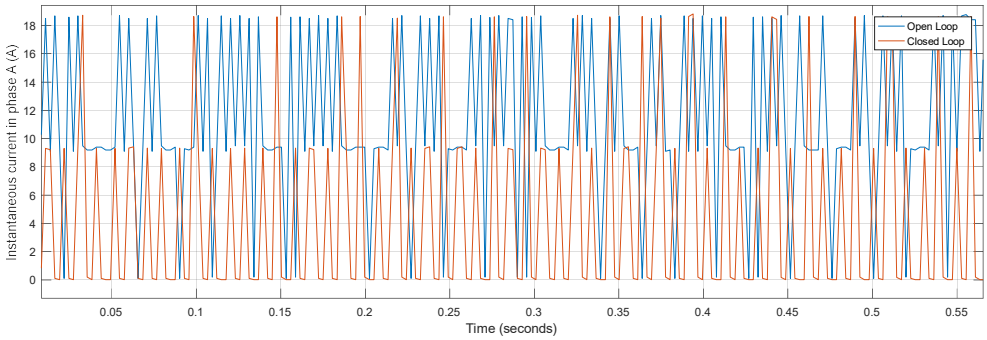

Figure 159: Instantaneous current in phase A in case of 1 mm crack (Open and Closed loop)

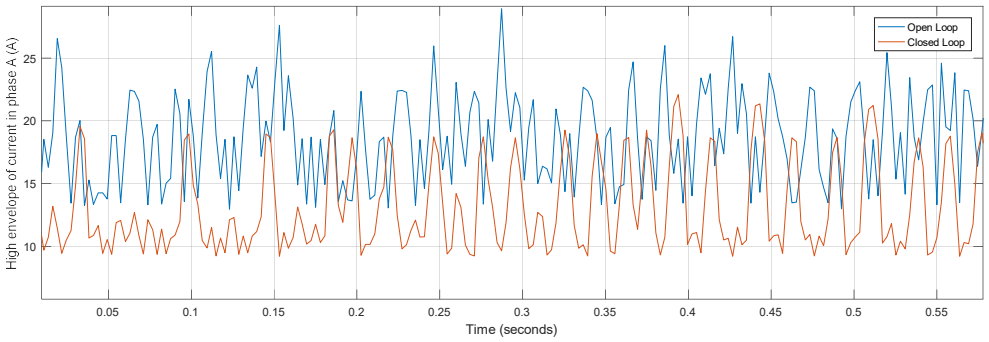

Figure 160: The high envelope of the signals in figure 159

Comparing the signals in the case of open and closed loop, we can see disparities in all system's aspects. This will surely affect the prognostic strategy. Table 35 will show comparison between machine's parameters in open and closed loop system.

TABLE 35: COMPARISON BETWEE MEASUREMENTS OF CLOSED LOOP AND OPEN LOOP SYSTEM-CASE OF CRACK IN THE MAGNET

Fault	Parameters	Open loop	Closed loop
Crack 1mm	Torque	151.39	128.96
	Stator current (average value)	18.66	13
	Source current (average value)	16.24	9.7
	Average boundary temperature	124.27	109.68
	Average boundary displacement	7.2216e-06	1.3882e-05

First, the torque should no longer be used as an input for the prognostic approach since the controller will tend to adjust it. The sensor will detect the same value wherever was the state of the machine. Second, temperature and vibration should be investigated again for all the machine fault cases where the extracted features in the open loop system may not be useful anymore for the closed loop system to achieve the right prognostic decision.

We note that the difference between the signals generated in open loop in this chapter and chapter 3 is due to the simulation step and electromagnetic FEM model used. In chapter 3, the dynamic electromagnetic finite element model is used where the rotor step is between 1 and 4 degrees. However, to minimize the time of simulation, in this chapter we used the static finite element; an instantaneous simulation is done every revolution where the rotor sweeps 360 degrees.

5.5 Features extracted from closed loop system data sets

In this section, useful features for fault identification, of the closed loop system, will be extracted.

In figures 161, 162 and 163 we can see closed loop torque, temperature and vibration data of the healthy machine and machine with 1 mm crack in one magnet.

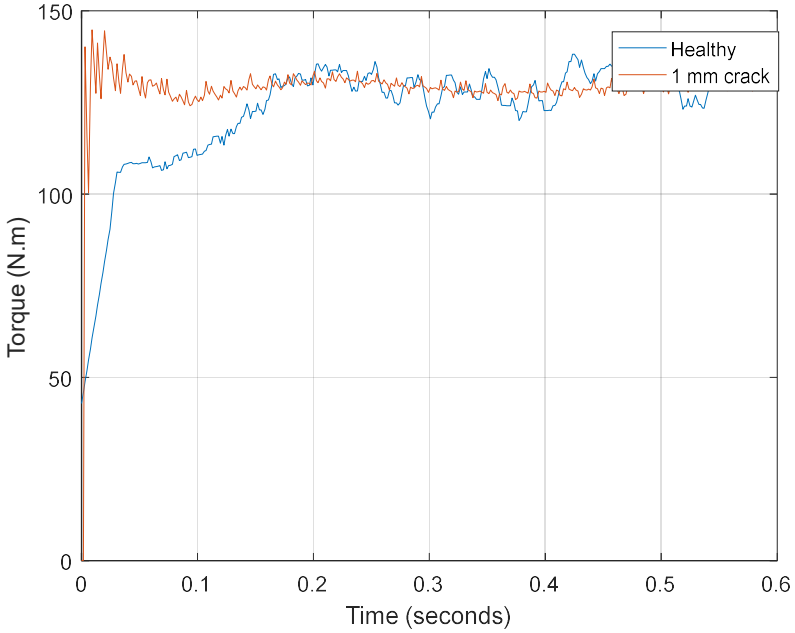

Figure 161: Torque of closed loop system of healthy machine and machine with 1 mm crack

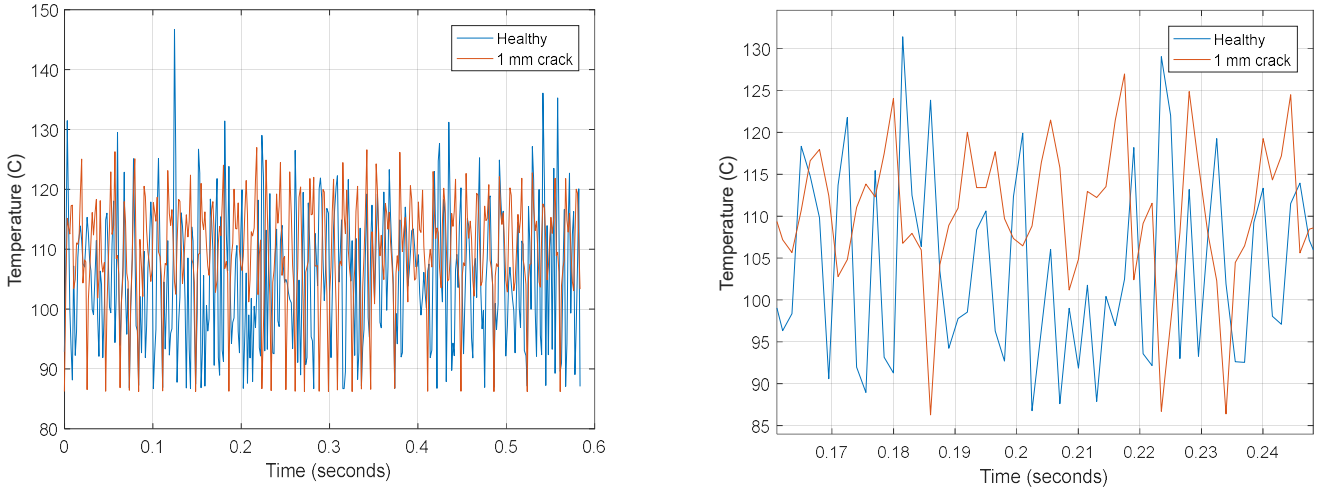

Figure 162: Temperature of closed loop system of healthy machine and machine with 1 mm crack (Zoom in at the right)

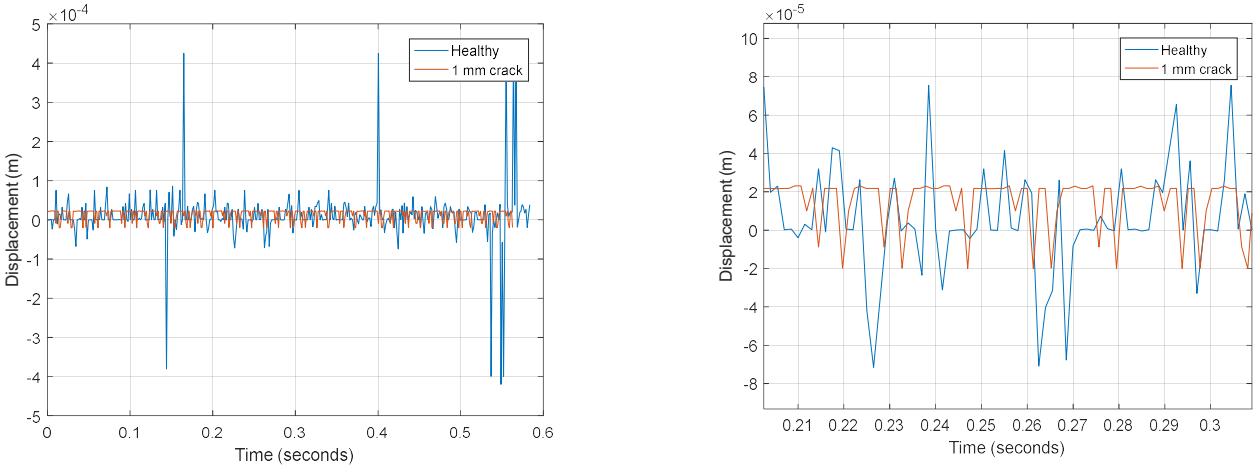

Figure 163: Vibration of closed loop system of healthy machine and machine with 1 mm crack (Zoom in at the right)

The classical introduced features in section 3.2 will be evaluated for the above data sets.

In table 35, an illustration of the previously mentioned signal statistical characteristics, are presented.

TABLE 36: STATISTICAL FEATURES OF CLOSED LOOP DATA SETS

Data	Torque		Temperature		Vibration	
Machine's State	**Healthy**	**Crack 1 mm**	**Healthy**	**Crack 1 mm**	**Healthy**	**Crack 1 mm**
Statistical feature						
Peak to peak value	198.42	144.82	80.64	80.64	8.4472e-04	4.3134e-05
Average	124.28	128.96	105.05	109.68	1.0379e-05	1.3882e-05
RMS	128.76	129.29	105.64	113.01	6.8310e-05	2.0318e-05
Kurtosis	3.7574	177.0935	4.32	2.71	32.3175	3.6031
Skewness	-0.0831	-12.6525	-0.8951	0.32	0.6461	-1.5183
Crest factor	1.5411	1.1202	1.6124	1.5784	6.2220	1.1402
Pulse factor	1.5966	1.1230	1.8935	1.9011	40.9505	1.6688
Shape factor	1.0360	1.0025	1.1743	1.2044	6.5815	1.4636
Standard deviation	33.6994	9.2157	35.0401	38.0505	6.7603e-05	1.4852e-05
Variance	1.1357e+03	0.0849e+03	1.2278e+03	1.4478e+03	4.5702e-09	2.2059e-10

For the torque data sets, all features except average and shape factor are good fault indicator. This is contrary to the open loop system where the average was one of the good fault indicator. This is expected since the controller tend to adjust the torque to a pre-settled normal value.
For temperature data sets, contrary to the open loop system, there is high disparity in the kurtosis and skewness and small disparity in the peak to peak and average value. A small difference is

detected in the standard variance and the variance. This is expected; the temperature is directly proportional to the current flowing in the stator's coil. The average current flowing in the stator's coil changes in the closed loop system (figure 159), hence the machine temperature changes too. For the vibration data sets, all the features are good fault indicator.

In figure 164, 165, 166 we can see the spectral power density in dB of the torque, temperature and vibration respectively, for the healthy machine and machine with 1 mm crack in one magnet.

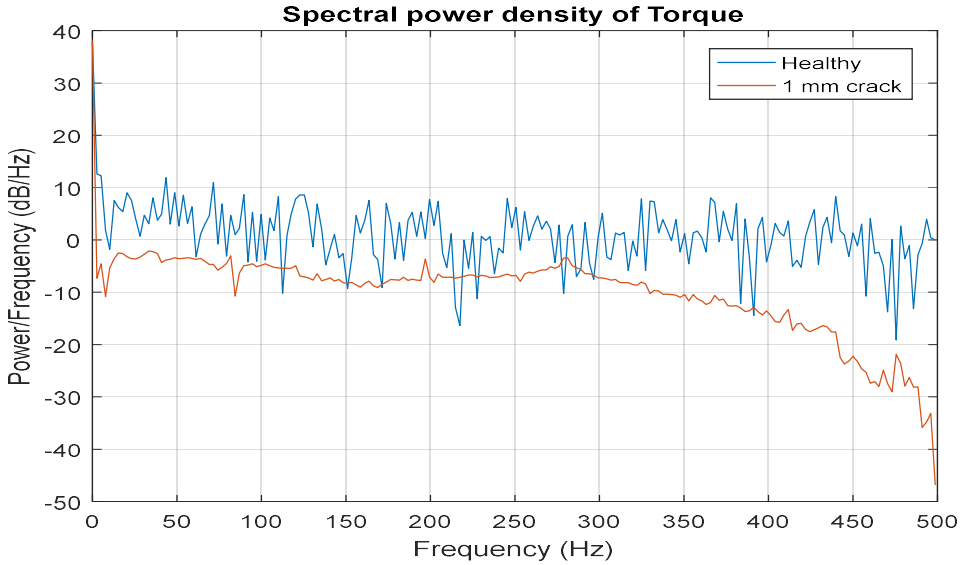

Figure 164: Torque spectral power density, closed loop, of healthy machine and machine with 1 mm crack

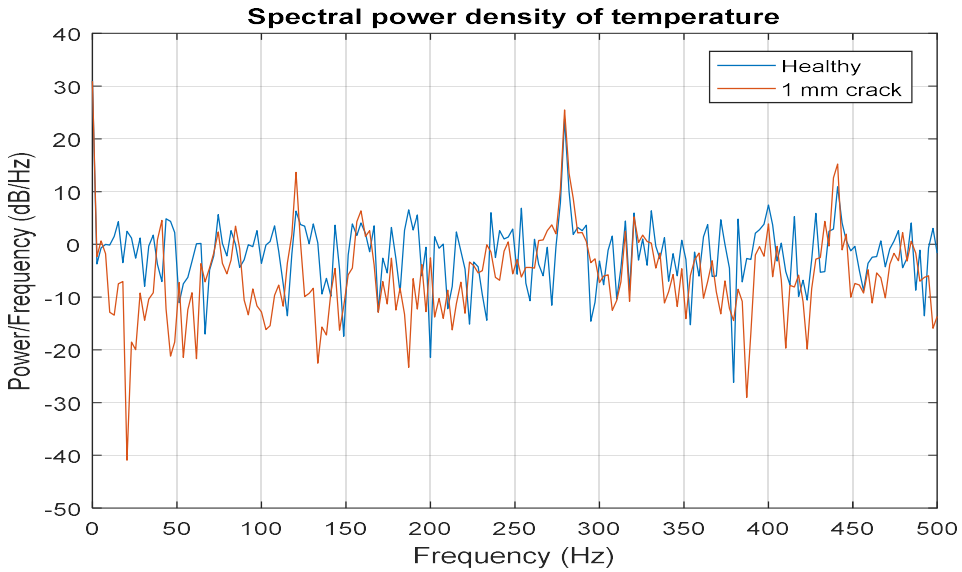

Figure 165: Temperature spectral power density, closed loop, of healthy machine and machine with 1 mm crack

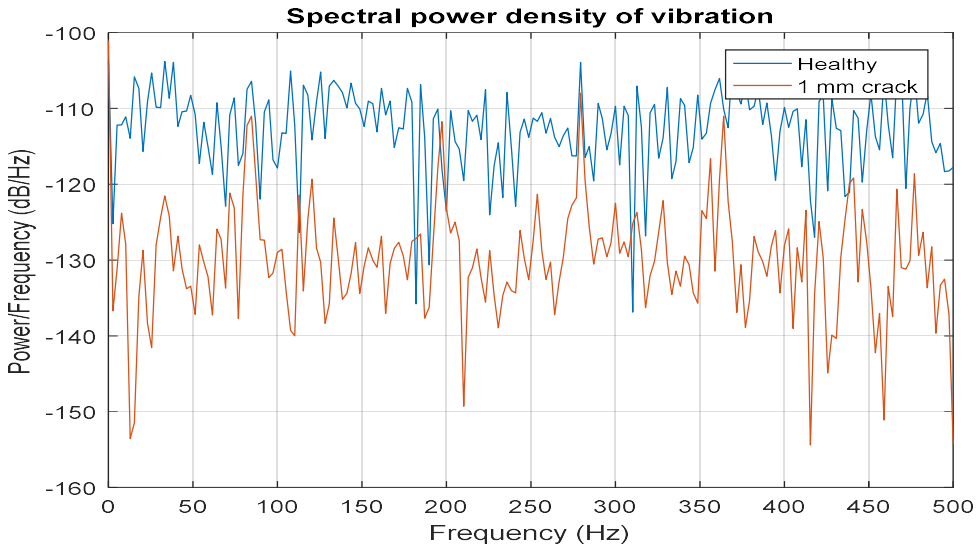

Figure 166: Vibration spectral power density, closed loop, of healthy machine and machine with 1 mm crack

The average spectral power of torque, temperature and vibration is illustrated in table 36.
There is disparity in the average spectral power density of the torque, however this disparity was much greater in the case of open loop system.
The average spectral power is the temperature data signal is the same; this similarity is like the open loop system.
For the vibration signal, there is disparity; however, this disparity was greater in the open loop system.

TABLE 37: AVERAGE SPECTRAL POWER DENSITY OF TORQUE

Data set	**Torque**		**Temperature**		**Vibration**	
Machine's State	**Healthy**	**Crack 1 mm**	**Healthy**	**Crack 1 mm**	**Healthy**	**Crack 1 mm**
Average spectral power $(N.m)^2$	31.94	33.16	7.65	7.75	0.4754e-11	0.0614e-11

The Fourier transformation of torque, temperature and vibration is illustrated in figures 167, 168, and 169 respectively.

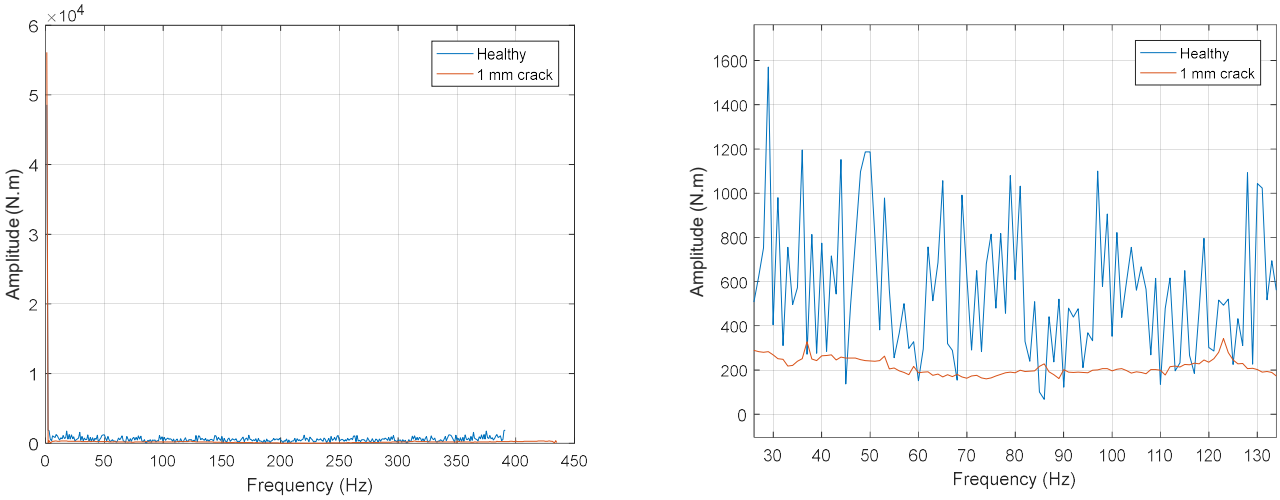

Figure 167: Fourier transformation of torque, Closed loop system

We can see that the harmonics at frequencies higher than the fundamental has no critical peaks, hence, amplitudes of frequency components are not a good indicator for fault detection when interpreting torque signal.

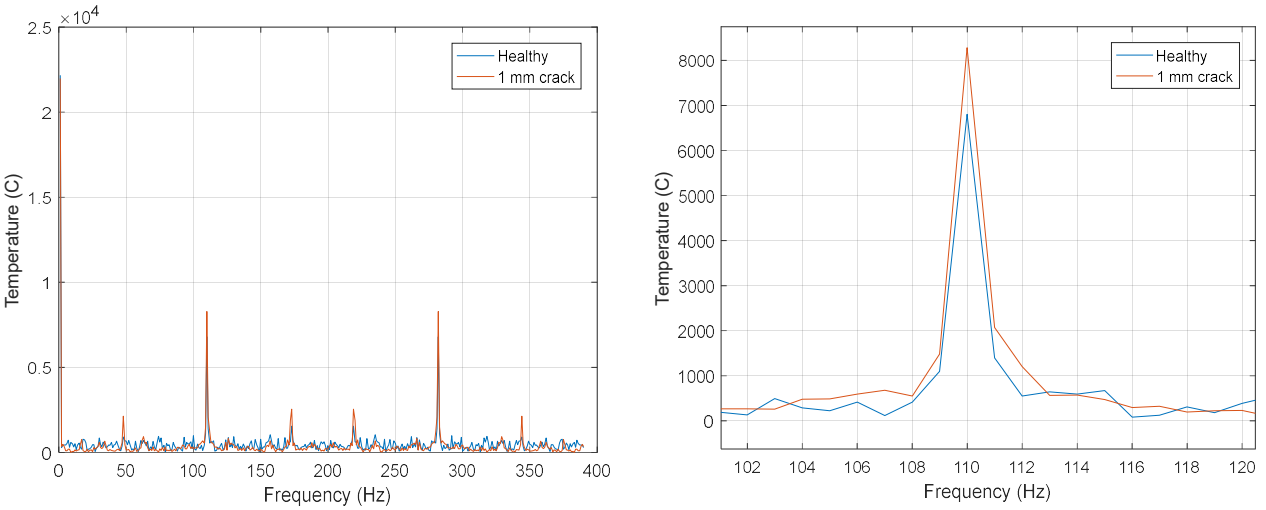

Figure 168: Fourier transformation of temperature, Closed loop system

Like the open loop system, a sharp peaks of distinct amplitudes are detected at the second harmonics of the spectrum which makes Fourier transformation and harmonics good fault indicator for temperature signal, in the case of closed loop system.

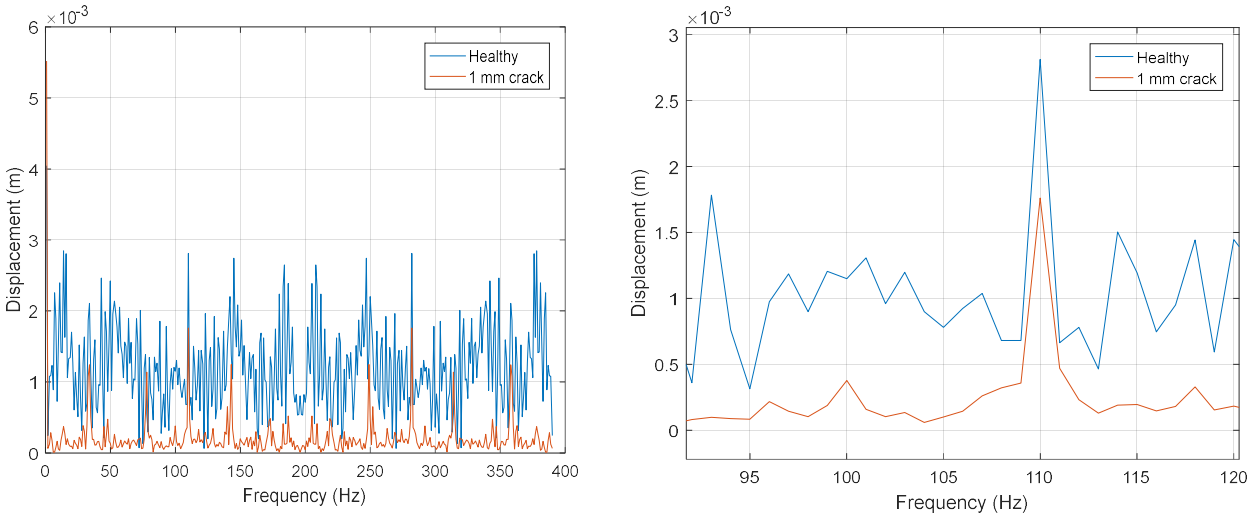

Figure 169: Fourier transformation of temperature, Closed loop system

In the closed loop system, unlike the open loop system, there is peaks of distinct amplitudes along Fourier spectrum; in specific, the peak at the second harmonic. Hence, this is a good fault indicator for the vibration signal.

After examining all the signal features of torque, temperature and vibration, a summary and a comparison between the effectiveness of these data features on fault detection in open loop and closed loop system is presented in table 38. We recall that 'Y' is for yes and 'N' is for no. the features nominated for the open loop system is designated in BOLD.

TABLE 38: COMPARISON BETWEEN THE EFFECTIVENESS OF DATA FEATURES ON FAULT DETECTION IN OPEN LOOP AND CLOSED LOOP SYSTEM

	Feature											
	Torque											
	PP	***Mean***	***RMS***	***Ku***	***Sk***	***SF***	***PF***	***CF***	***SD***	***V***	***APS***	***AFC***
Open Loop	Y	**Y**	Y	Y	Y	N	Y	Y	Y	Y	Y	N
Closed Loop	Y	N	N	Y	Y	Y	Y	N	Y	Y	Y	N
	Temperature											
Open Loop	N	N	N	N	N	N	N	N	N	N	N	**Y**
Closed Loop	N	Y	Y	Y	Y	N	N	N	Y	Y	N	Y
	Vibration											
Open Loop	Y	**Y**	Y	Y	Y	N	N	N	Y	Y	Y	N
Closed Loop	Y	Y	Y	Y	Y	Y	Y	Y	Y	Y	Y	Y

As we can see, the 'Mean' of the torque is no more efficient for fault detection in closed loop system. This was expected since the used controller is based on torque control. Some other features work well in closed loop system like kurtosis, skewness, shape factor … the kurtosis will be selected due to the high disparity between the healthy case and case with demagnetization fault.

In the open loop system, all the features except amplitude of frequency component are not good for fault detection when evaluating the temperature data set. However, in closed loop system, many

features work well for fault detection like mean, rms, kurtosis, etc, in addition to the amplitude of the frequency component. We will select the 'mean' of the temperature data set as fault detection feature since it has a computation time less than the 'amplitude of the frequency component'.

For the vibration data sets, some features were not useful for fault indication of open loop system like shape factor, Pulse factor and crest factor; however, for closed loop system, all the features show disparity between healthy machine and faulty machine. The selected feature will be the 'mean'.

The selected features for each data set will be the inputs/observers of the prognostic approach.

5.6 Impact of closed loop system on the prognostic model

The dynamic electrical, thermal and vibration behavior of the electrical machine is widely different if we are dealing with open loop system or closed loop system. Hence, the impact of those changes on the prognostic hidden Markov model should be evaluated.

As we mentioned previously, in chapter 4, the Hidden Markov Model is constituted of the transmission matrix and the emission matrix. The probabilities in those matrices will differ since the response of different machine parameters varied in the case of open loop and closed loop system. Moreover, the inputs, designated by observers, that drives the model are the selected features of torque, temperature and vibration; as we clarified in the previous section, the values of those features changes if we are operating an open loop system or a closed loop system. In other words, the percentages in the HMM's matrices and the inputs of the model will change in the case of closed loop system.

Concerning the output of the model and the prognostic decision, of course it will remain the same. Although the probabilities and inputs values changed, they are still designating the same machine state.

The percentage change in torque, temperature and vibration of the machine in the case of healthy machine and faulty machine with 1 mm crack in one magnet will be investigated in table 39. The data signals of the machine parameters in the case of open loop system and closed loop system differs widely. Table 39 shows the percentage changes in the average of those signals in the two cases.

TABLE 39: PERCENTAGE DIFFERENCE IN MACHINE'S PARAMETERS IN THE CASE OF OPEN LOOP AND CLOSED LOOP SYSTEM

	Open Loop	Closed Loop
Torque	+13.4 %	+3.6%
Temperature	0%	+4.2%
Vibration	±377 %	±236.2%
Stator current	0%	-23.33%

To illustrate the difference in the HMM in the case of open loop and closed loop, the transition and emission matrix will be implemented in the two cases following the same technical steps presented in chapter 4.

Since we are considering one type of fault which is the 1 mm crack in one magnet, the number of states is 13 encountering the healthy state and the states of a crack in one of the 12 magnets. The size of the transition matrix will be (13 x13). This is common for the open loop and closed loop system.

$$TM = \begin{bmatrix} 0.6 & \frac{0.4}{12} & \cdots & \frac{0.4}{12} \\ 0 & 1 & 0 & 0 \\ \vdots & 0 & \ddots & 0 \\ 0 & \cdots & 0 & 1 \end{bmatrix} \quad (123)$$

In the open loop system, the useful measurable parameters for crack detection is vibration and torque; we will eliminate the temperature since it shows no changes when a 1 mm crack fault occurs. Hence, the size of the emission matrix is (13 x 16); 13 is the number of states and 15 refers to 13 vibration ranges and two torque ranges.

$$EM = \begin{bmatrix} 0.6 & 0 & \cdots & 0 & 0.4 & 0 \\ 0 & 0.96 & 0 & \vdots & 0 & 0.04 \\ \vdots & 0 & \ddots & 0 & \vdots & \vdots \\ 0 & \cdots & 0 & 0.96 & 0 & 0.04 \end{bmatrix} \quad (124)$$

In the closed loop system, the useful parameters for crack detection is vibration and temperature; we eliminated the torque since we have torque vector control, the input power of the machine will be adjusted to maintain the value of the torque almost constant. The size of the emission matrix is (13 x 15); 13 is the number of states and 15 refers to 13 vibration range and two temperature ranges.

$$EM = \begin{bmatrix} 0.6 & 0 & \cdots & 0 & 0.4 & 0 \\ 0 & 0.98 & 0 & \vdots & 0 & 0.02 \\ \vdots & 0 & \ddots & 0 & \vdots & \vdots \\ 0 & \cdots & 0 & 0.98 & 0 & 0.02 \end{bmatrix} \quad (125)$$

Due to the high change in the machine vibration in the open and closed loop case, the probabilities in the emission matrices linked to torque and temperature is relatively small compared to the probabilities linked to the vibration. Moreover, the probabilities linked to vibration in the two systems are very near: 0.96 and 0.98; this indicates that, for the same type of fault, the response of the machine's vibration in the two systems is almost similar.

To proof that the different emission matrices for the open and closed loop system will generate the same state sequence having the same observation sequence, an example will be considered and treated for the two cases. Let's consider a sequence of observations $\{SO_H, SO_H, SO_C\}$, from vibration sensor, corresponding to the states $\{S_H, S_H, S_C\}$ respectively. SO_H designates the observer in healthy case. SO_C designates the observer in the case of 1 mm crack in magnet 1 of the

machine. S_H designates the state where the machine is healthy. S_C designates the state where the machine contains a 1 mm crack in magnet 1.

This sequence will be input for the HMM in the open and closed loop case. The trellis diagram of those two cases representing the Viterbi algorithm is illustrated in figure 170 and 171 respectively.

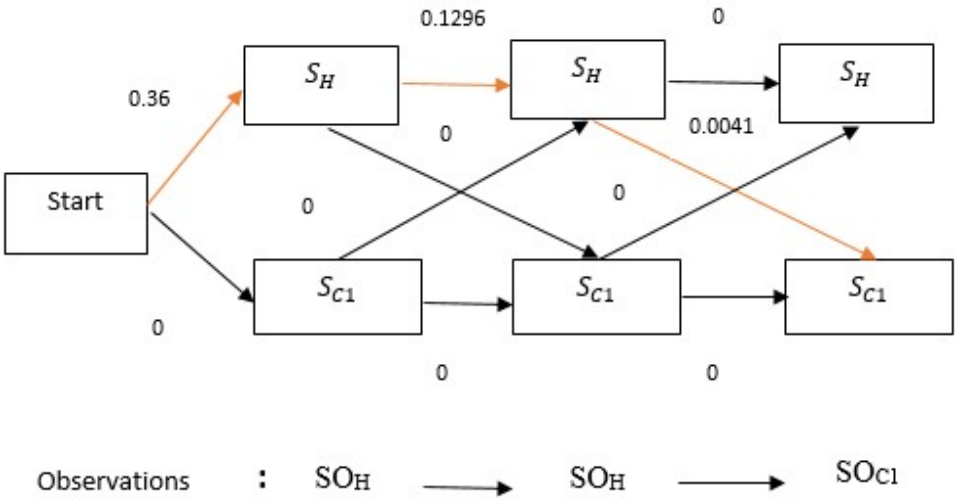

Figure 170: Viterbi algorithm for the open loop system

In figure 170, at start, the probability that the system is healthy is '0.6' and the probability that the system is faulty is '0.4'. The probability that the system state is S_H if the observation is SO_H is '0.6' and the probability that the system state is S_{C1} if the observation is SO_H is '0'. Hence, the weight probability from 'Start' to S_H is 0.36 (0.6*0.6) and the weight probability from 'Start' to S_{C1} is 0 (0.4*0). As we stated earlier in chapter 4, Viterbi will choose the path having the highest probability which is in this case 0.36 and the selected path is highlighted in red.
The second observation is also SO_H. The probability of remaining in state S_H is '0.6' (from the transition matrix). The probability of being in state S_H if the observation is SO_H is '0.6'. The probability from the previous state is 0.36. Hence, the weight probability of remaining in state SH when the second observation is SO_H will be 0.1296 (0.36*0.6*0.6).
The third observation is SO_{C1}. The probability of moving to state S_{C1} if the previous state is S_H is '0.4/12'. The probability from the previous state is '0.1296'. The probability of being in state S_{C1} if the observation is SO_{C1} is '0.96'. Hence, the weight probability of becoming in state S_{C1} is 0.0041 (0.1296*00.4/12*0.96).
Following the same logic calculation, we got the weighted probabilities of all the paths. The path of higher probability is highlighted in red. Accordingly, the adequate sequence of states is {S_H, S_H, S_{C1}}. This path selected by Viterbi algorithm is called 'survivor path'.

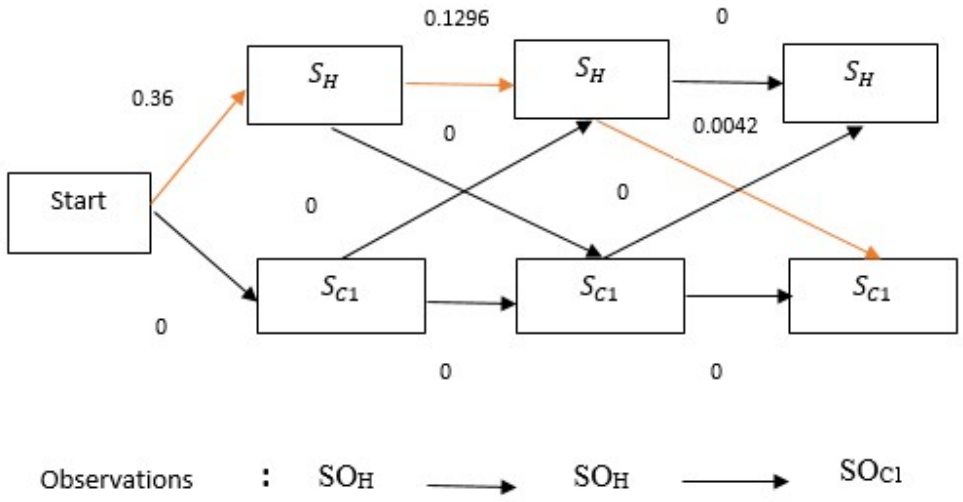

Figure 171: Viterbi algorithm for the closed loop system

Following the same logical calculation, the probability of the paths in figure 171 are calculated. We remark that the probability of the third path. It is calculated using the emission matrix of the closed loop system where 0.1296*(0.4/12) *0.98=0.0042.

Although different emission matrixes are used, the open and closed loop system generate the same sequence of states for the same sequence of observations. In figure 172, a diagram illustrating the prognostic response in the case of 1 mm crack in one magnet is presented.

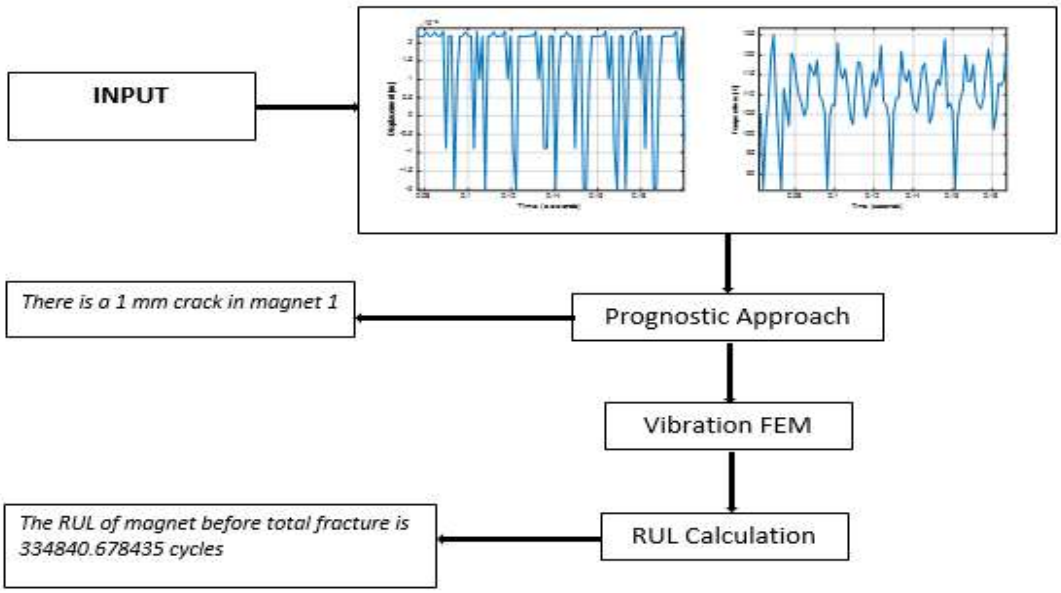

Figure 172: Diagram illustrating the prognostic approach in the case of closed loop system with 1 mm crack in one magnet

The input of the diagram in figure 172 is the features of the temperature and vibration data corresponding to a machine with 1 mm crack in magnet 1. The prognostic approach detects the presence of this fault. The RUL calculation of this type of fault is elaborated from the Maxwell stress tensor generated by the vibration FEM. Hence, the vibration FEM is conducted. This elaborated stress tensor will be the input of the RUL calculation equations that elaborate the time needed for the cracked magnet to fracture.

Although the emission matrix will change in the case of closed loop system, the fault detection, the prognostic decision and the RUL calculation will remain the same. In other words, the same prognostic decision, machine state and RUL calculation, in each case, is deduced using different HMM model and different measureable inputs.

5.7 Conclusion

This chapter describes the examined three phase Voltage Source Inverter and its principal components. A switched state space model of VSI is developed to be combined in the coming step with the FEM of the machine. Different types of faults occurring in VSI are represented. As a result, Single SC and OC and Open phase are the most interested when studying faults interaction between machine and inverter. Then, the different techniques used to generate control signal is examined [129] [131].

We illustrated the threshold values of temperature, current, voltage and vibration of the power electronics used in our HEV application.

Fault interaction between the electrical machine and the inverter was explored. The three types of faults, demagnetization, eccentricity and turn to turn short circuit are integrated in the machine to study their impact on the power devices; it has been shown that this impact is minor. Screw to that, switch short circuit and open circuit fault have been integrated in the inverter and results showed that they have a negative influence on the machine performance.

A closed loop system was built to adjust the output torque of the machine to a desired nominated value. The goal was to figure out the performance of the system in the case of fault, explore the change in the machine's measureable parameters and illuminate its impact on the prognostic model and prognostic decision.

General conclusion

Hybrid electric vehicle is leading technology and concept in the field of renewable propulsion system. The most worrying issue that faces this application is its availability and reliability. Hence, assuring the proper health operation of the vehicle is very important to increase its integration in the market.
To achieve this goal, a strategy is built to detect the primitive faults before it occurs or propagates. This is done by use of prognosis.
The most critical element in the propulsion system is the electrical machine. It is the main element of the traction system and the costliest. Permanent magnet machine is widely used in such application due to its high power density and low power to mass ratio. In this research, a surface permanent magnet machine, used in HEV application, is used. After examining the different types of fault that may occur in this machine, a fault index that take into consideration the percentage of fault occurrence and the cost of the defected element was introduced; it has been shown that demagnetization is the most severed fault.

The prognostic techniques, Hidden Markov Model, is used to detect faults in the electrical machine. The faults that mostly occur in the PMM are: demagnetization, turn to turn short circuit and eccentricity fault.

Three dynamic parameters are considered while building the prognostic approach: torque, temperature and vibration. Those parameters are the mostly affected when a fault occurs in the machine.

A prototype of the electrical machine where torque, temperature and vibration sensors are located to sense those parameters is not available. Hence, a correct and accurate model using electromagnetic, thermal and vibration finite element model is built for the machine in the case of normal operation and when a fault occurs. To precisely model the machine, those three finite element models are interrelated together to build a single model; since there is great interaction and dependency among them in reality, each one affects the other. Static and dynamic models are implemented. Fictive sensors are located at the boundary of the machine model and synthetic signals are collected. The change in parameters aspect at each type of fault is detected. The most appropriate features that point to the differences between those aspects are extracted.

Simulation showed that for all the types of faults investigated: the vibration of the machine is largely affected, the temperature is affected only if the fault is turn to turn short circuit and the torque is affected in a relatively small range compared to the vibration. It has been shown that the average of the vibration, temperature and torque signals over one machine revolution is a good feature for fault detection. The extracted features from the vibration, temperature and torque signals will be the input of the Hidden Markov Model. It has been shown that torque temperature and vibration are useful for fault detection; temperature and vibration are useful for fault localization.

A global Hidden Markov Model is built; its input is data coming from torque, temperature and vibration sensor. The prognostic strategy was able to detect the presence of fault at its early stage,

localize this fault and calculate the remaining useful life of faulty element. The remaining useful life of the machine in the case of crack in the magnet is based on the propagation analytical model of a longitudinal crack. The remaining useful life of the machine in the case of turn to turn short circuit is based on the aging equation of the stator coil's insulation.

After conducting this strategy for open loop system, a closed loop system is built. Modeling of the inverter is executed then coupled to the finite element model of the machine. The fault interaction between inverter and machine is showed. The encountered faults in the inverter are short switch, open switch and open phase. It has been shown that the impact of faults in the inverter are of small impact on the air gap flux density. After that, the closed loop feedback system is implemented. The impact of this controlled system on the measured parameters and on the prognostic model is illustrated.

Hybrid electric vehicle and prognosis are upcoming and flourishing subjects; this open the horizon broadly for further researches and studies in this field.

In the modeling domain

The system model can be expended to encounter the storage device and electronic equipment other than the inverter. This will enrich the analysis where the model become closer to the real electrical system inside the vehicle. This modeling can encounter the thermal and vibration aspect of the system.
Although two dimensional finite element model is enough for machine modeling since the electrical machine is similar along the shaft axes, in the case of fault, even in small case, this similarity is broken. Hence, a three dimensional finite element model will be a beneficial addition.

In the field of fault detection and localization

More than one fault can be integrated in a time where the impact of this multi fault on the vital machine parameters can be studied. Also multi fault can be integrated in the whole electrical system and the interaction between the elements of the propulsion system and its impact on the vehicle operation can be deliberated.
Three machine faults are considered in this thesis, other types of mechanical and electrical fault can be easily integrated in the finite element model, analyzed and treated.

In the prognostic axe

A data driven model is implemented, the Hidden Markov Model. Other prognostic techniques can be implemented and compared to the technique presented in this thesis. Model based prognostic technique can be also built.

Appendix A: DIFFERENCE BETWEEN RTD AND THERMOCOUPLE SENSOR

	RTDs (3-wire 100 ohm platinum probe is mostly used)	**Thermocouples (type J is mostly used for its temperature range)**
Temperature	between −200 and 500 °C	−180 to 2,320 °C
Response time	Lower	Faster
Size (Diameter)	3.175 to 6.35 mm	less than 1.6 mm
Accuracy and stability requirements	capable of higher accuracy and can maintain stability for many years	can drift within the first few hours of use
Cost	Less cost effective	More cost effective
Physical aspect	3-wire 100 ohm platinum probe	consist of two dissimilar metals – iron and constantan – soldered together at one end creating a measurement junction at the tip of the probe
Extension wire	Normal copper wire	Special wire

Reference

[1] Political Economist, World Energy 2016-2050: Annual Report, June 2016.
[2] J. Rogelj, M. Schaeffer, Bill Hare, Climate analytics, timetables for zero emissions and 2050 emissions reductions: state of the science for the ADP agreement, February 2015.
[3] H. Al-Sheikh, O. Bennouna, G. Hoblos and N. Moubayed, Condition Monitoring of Bidirectional DC-DC Converter for Hybrid Electric Vehicles, IEEE 22nd Mediterranean Conference on Control and Automation, pp. 97-102, 16-19 June 2014.
[4] H. Al-Sheikh, O. Bennouna, G. Hoblos and N. Moubayed, Study on power converters used in Hybrid Vehicules with Monitoring and Diagnostics Techniques,17th IEEE Mediterranean Conference (MELECON 2014), pp. 103-107, Beirut, Lebanon, 13-16 April 2014.
[5] M. Barcaro, N. Bianchi and F. Magnussen, PM Motors for Hybrid Electric Vehicles, The Open Fuels & Energy Science Journal, pp. 135-141, 2009.
[6] E. Odv´a and A. Mebarki, Electric motor-generator for a hybrid electric vehicle, Engineering MECHANICS Conference, p. 131–139, 23 March 2006.
[7] S. Moussaddy, A. Zgheib, H. Dernayka, M.H. El-Jamal, N. Moubayed et R. Outbib, Requirements change using product lifecycle management for manufacturing process in the hybrid vehicle context, SIELMEN 2009, 7th International Conference on Electromecanical and power systems, pp. 191-196, Romania, 8-9 October 2009,
[8] M. Yabumoto and C. Kaido, Electrical Steel Sheet for Traction Motors of Hybrid/Electric Vehicles, Nippon Steel technical report, no. 87, July 2003.
[9] T. Finken and M. Felden, Comparison and design of different electrical machine types regarding their applicability in hybrid electrical vehicles, international conference on electrical machines, pp. 1-5, 2008.
[10] A. Simpson, Cost-Benefit Analysis of Plug-In Hybrid Electric Vehicle Technology, 22nd International Battery, Hybrid and Fuel Cell Electric Vehicle Symposium and Exhibition, November 2006.
[11] B. Yang and A. Widodo, “Introduction of Intelligent Machine Fault Diagnosis and Prognosis”, Nova Science Publishers, 2009.
[12] D. Winkler and C. Gühmann, Modelling of Electrical Faults in Induction Machines Using Modelica, The 48th Scandinavian Conference on Simulation and Modeling, Särö - Dennemark, pp. 82-87, 30-31 October 2007.
[13] H. Al-Sheikh, O. Bennouna, G. Hoblos and N. Moubayed, Study on power converters used in Hybrid Vehicules with Monitoring and Diagnostics Techniques,17th IEEE Mediterranean Conference (MELECON 2014), pp. 103-107, Beirut, Lebanon, 13-16 April 2014.
[14] H. Al-Sheikh, O. Bennouna, G. Hoblos and N. Moubayed, Power Electronics Interface Configurations for Hybrid Energy Storage in Hybrid Electric Vehicles,17th IEEE Mediterranean Conference (MELECON 2014), pp. 122-126, Beirut, Lebanon, 13-16 April 2014.
[15] C. Sankavaram, A. Kodali, and K. Pattipati, An Integrated Health Management Process for Automotive Cyber-Physical Systems, IEEE International Conference on Computing, Networking and Communications, Workshops Cyber Physical System, 2013.
[16] A. Fuhs, Hybrid Vehicles and the Future of Personal Transportation, CRC Press, Taylor and Francis group, 2008.
[17] M. Barcaro, N. Bianchi and F. Magnussen, PM Motors for Hybrid Electric Vehicles, The Open Fuels & Energy Science Journal, vol. 2, pp. 135-141, 2009.

[18] C. Sankavaram, B. Pattipati, and A. Kodali, Model-based and data driven prognosis of automotive and electronic systems, IEEE Conference on Automation Science and Engineering, Bangalore, India, 22-25 August, 2011.
[19] D. Winkler, C. Gühmann, Modelling of Electrical Faults in Induction Machines Using Modelica, SIMS 2007.
[20] C. C. Chan, The state of the art of electric and hybrid vehicles, Proceedings of the IEEE, vol. 90, no. 2, pp. 247–275, 2002.
[21] A. Emadi, K. Rajashekara, S. S. Williamson, and S. M. Lukic, Topological overview of hybrid electric and fuel cell vehicular power system architectures and configurations, IEEE Transactions on Vehicular Technology, vol. 54, no. 3, pp. 763–770, 2005.
[22] O. D. Momoh and M. O. Omoigui, An overview of hybrid electric vehicle technology, in Proceedings of the 5th IEEE Vehicle Power and Propulsion Conference (VPPC '09), pp. 1286–1292, September 2009.
[23] T. Finken, M. Felden and K. Hameyer, Comparison and design of different electrical machine types regarding their applicability in hybrid electrical vehicles, international conference on electrical machines, 2008.
[24] M. Barcaro, N. Bianchi1 and F. Magnussen, PM Motors for Hybrid Electric Vehicles, the Open Fuels & Energy Science Journal, vol. 2, pp. 135-141, 2009.
[25] A. Simpson, Cost-Benefit Analysis of Plug-In Hybrid Electric Vehicle Technology, 22nd International Battery, Hybrid and Fuel Cell Electric Vehicle Symposium and Exhibition (EVS-22), Japan, November 2006.
[26] J. Zheng, W. Zhao, J. Hua Ji and G. Liu, Design and comparison of interior permanent-magnet machines for hybrid electric vehicles, IEEE International Conference on Applied Superconductivity and Electromagnetic Devices (ASEMD), Shanghai, China, 20-23 Nov. 2015.
[27] C. C. Chan, K. T. Chau, J. Z. Jiang, Novel Permanent Magnet Motor Drives for Electric Vehicles, IEEE transactions on industrial electronics, vol. 43, no. 2, April 1996.
[28] T. Schneider, A. Binder, Evaluation of new Surface Mounted Permanent Magnet Synchronous Machine with Finite Element Calculations, Computer Engineering in Applied Electromagnetism. Springer, Dordrecht, 2005.
[29] B. Li, M. Li, Calculation and Analysis of Permanent Magnet Eddy Current Loss Fault with Magnet Segmentation, Mathematical Problems in Engineering, 2016.
[30] J. Haataja, J. Pyrhönen, Permanent Magnet Assisted Synchronous Reluctance Motor: an Alternative Motor in Variable Speed Drives, Energy Efficiency in Motor Driven Systems. Springer, Berlin, Heidelberg, 2013.
[31] T. Hu, F. Lin, L. Cui, The Flux-Weakening Control of Interior Permanent Magnet Synchronous Traction Motors for High-Speed Train, proceedings of the 1st International Workshop on High-Speed and Intercity Railways, Lecture Notes in Electrical Engineering, vol. 147, Springer, Berlin, Heidelberg, 2012.
[32] A. Wang, D. Ma, and H. Wang, FEA-Based Calculation of Performances of IPM Machines with Five Topologies for Hybrid-Electric Vehicle Traction, World Academy of Science, Engineering and Technology International Journal of Electrical, Computer, Electronics and Communication Engineering, vol.7, no. 8, 2013.
[33] N. Babu T., H. S. Himamshu, P. Kumar N, Bearing Fault Detection Based on Daubechies Wavelet, archives of acoustics journal, vol. 42, no. 3, pp. 401–414, 2017.

[34] G. Henrique, B. Paulo, R. Scalassara, Stator fault analysis of three-phase induction motors using information measures and artificial neural networks, electric power system research, vol. 143, pp. 347-356, February 2017.
[35] F. Garcia-Guevara,F. J. Villalobos-Piña, R. Alvarez-Salas, Stator Fault Detection in Induction Motors by Autoregressive Modeling, Mathematical Problems in Engineering, 2016.
[36] J. Hong, D. Hyun, T. Kang, Detection and Classification of Rotor Demagnetization and Eccentricity Faults for PM Synchronous Motors, IEEE Transactions on Industry Applications 48, September 2011.
[37] A. Verma, S. Sarangi, M. Kolekar, Misalignment fault detection in induction motor using rotor shaft vibration and stator current signature analysis, International Journal of Mechatronics and Manufacturing Systems, January 2013.
[38] Ahmed, M. Ahmed, K. Imran, M. Shuja Khan, J. Akhtar, Detection of Eccentricity Faults in Machine Using Frequency Spectrum Technique, International Journal of Computer and Electrical Engineering, vol.3, no.1, February, 2011.
[39] K. Tian, T. Zhang, Y. Ai, W. Zhang, Induction Motors Dynamic Eccentricity Fault Diagnosis Based on the Combined Use of WPD and EMD-Simulation Study, applied science, 20 September 2018.
[40] G. Zanardelli, Elias G. Strangas, Hassan K. Khalil, Comparison of Wavelet-Based Methods for the Prognosis of Failures in Electric Motors, Power Electronics in Transportation, 2002.
[41] S. Nandi, H. A. Toliyat, Condition monitoring and fault diagnosis of electrical machines, IEEE Transactions on Energy Conversion, vol. 20, Issue: 4, December 2005.
[42] N. Hussein, D. Y. Mahmood, E. M. Abdul-Baki, 3-phase Induction Motor Bearing Fault Detection and Isolation using MCSA Technique based on neural network Algorithm, Journal of Engineering and Development, vol. 16, no. 3, September 2012.
[43]] W. T. Thomson, D. Rankin, on line current monitoring to diagnose airgap eccentricity histories verify the predictions in large three phase induction motors- industrial case, IEEE Transactions on Energy Conversion, vol. 14, no. 4, December 1999.
[44] S. Lee, T. G. Habetler, An online stator winding resistance estimation techniquefor temperature monitoring of line-connected inductionmachines, IEEE Industry Applications Conference, 2001.
[45] J.S. Hsu, Possible errors in measurement of air-gap torque pulsations of induction motors, IEEE Transactions on Energy Conversion, vol. 7, no.1, March 1992.
[46] J. S. Hsu, Monitoring of Defects in Induction Motors Through Air-Gap Torque Observation, IEEE transactions on industry applications, vol. 31, no. 5, September 1995.
[47] RS Mills, EY Avan and RS Dwyer-Joyce, Piezoelectric sensors to monitor lubricant film thickness at piston–cylinder contacts in a fired engine, Institution of Mechanical Engineers, Journal of Engineering Tribology, vol. 227, no. 2, pp. 100-111, February 2013.
[48] J. Yun, K. Lee, K. Lee, Detection and Classification of Stator Turn Faults and High-Resistance Electrical Connections for Induction Machines, IEEE transaction on industry applications, vol. 45, no. 2, March 2009.
[49] .H Dymond, N. Stranges, K. Younsi, Stator winding failures: contamination, surface discharge, tracking, IEEE transaction, 2002.

[50] P. Neti, P. Zhang, X. Qi, Online detection of end winding contamination in industrial motors, Electrical Insulation Conference (EIC), 2011.
[51] L. Enrique, C. Arroyo, Modeling and simulation of permanent magnet synchronous motor drive system, thesis submitted in partial fulfillment of the requirements for the degree of MASTER

OF SCIENCE in ELECTRICAL ENGINEERING UNIVERSITY OF PUERTO RICO, MAYAGÜEZ CAMPUS, 2006.
[52] W. T. Thomson, M. Fenger, Case Histories of Current Signature Analysis to Detect Faults in Induction Motor Drives, IEEE, 2003.
[53] The motor guide, ABB, second edition 2005.
[54] A. Wang, D. Ma, and H. Wang, FEA-Based Calculation of Performances of IPM Machines with Five Topologies for Hybrid-Electric Vehicle Traction, World Academy of Science, Engineering and Technology International Journal of Electrical, Computer, Electronics and Communication Engineering, vol. 7, no. 8, 2013.
[55] A. H. Bonnett, Root Cause AC Motor Failure Analysis with a Focus on Shaft Failures, IEEE transaction on industry applications, vol. 36, no. 5, September 2000.
[56] A. Simpson, "Cost-Benefit Analysis of Plug-In Hybrid Electric Vehicle Technology", November 2006.
[57] A. Yang, S. Widodo, Introduction of Intelligent Machine Fault Diagnosis and Prognosis, 2010.
[58] C. Pang, F. L. Lewis, T, Heng Lee, Z. Dong, Intelligent Diagnosis and Prognosis of Industrial Networked Systems, CRC press,2017.
[59] D. Galar, U. Kumar, R. Villarejo, C. Anders Johansson, Hybrid Prognosis for Railway Health Assessment: An Information Fusion Approach for PHM Deployment, 4th IEEE Conference on Prognostics and System Health Management (PHM), vol. 33, 2013.
[60] B.C. Mecrow, A.G. Jack, J.A. Haylock, J.Coles, Fault-tolerant permanent magnet machine drives, , IEE Proc -Electv. Power Appl, vol. 143, no. 6, November 1996.
[61] U. Fayyad, G. Piatetsky-Shapiro and P. Smyth. From data mining to knowledge discovery: an overview. Advances in Knowledge Discovery and Data Mining, pages 1-34. AAAI-Press, 1996.
[62] A. Lorton, Mitra Fouladirad, Antoine Grall, A methodology for probabilistic model-based prognosis, European Journal of Operational Research vol. 225, no. 3, pp. 443–454, March 2013.
[63] T. Xia, X. Jin, L. Xi, J. Ni, Operating load based real-time rolling grey forecasting for machine health prognosis in dynamic maintenance schedule, Journal of Intelligent Manufacturing, vol. 26, no. 2, February 2015.
[64] R. Xiong, F. Sun, Z. Chen, H. He, A data-driven multi-scale extended Kalman filtering based parameter and state estimation approach of lithium-ion polymer battery in electric vehicles, Elsevier, Applied energy, vol. 113, no. 1, January 2014.
[65] C. Sankavaram, A. Kodali, and K. Pattipati, An Integrated Health Management Process for Automotive Cyber-Physical Systems", IEEE International Conference on Computing, Networking and Communications, Workshops Cyber Physical System, 2013.
[66] M. Yu, D. Wang, Model-Based Health Monitoring for a Vehicle Steering System with Multiple Faults of Unknown Types, IEEE tractions on industrial electronics, vol. 61, no. 7, July 2014.
[67] Subhasis Nandi, Hamid A. Toliyat, condition monitoring and fault diagnosis of electrical machines, IEEE Transactions on Energy Conversion, vol. 20, issue: 4, December 20005.
[68] B. M. Ebrahimi, J. Faiz, M. J. Roshtkhari, Static-, Dynamic-, and Mixed-Eccentricity Fault Diagnoses in Permanent-Magnet Synchronous Motors, IEEE Transactions on Industrial Electronics, vol. 56, Issue: 11, November 2009.
[69] R. Brutsch, M. Tari, K. Frohlich, Insulation Failure Mechanisms of Power Generators, IEEE Electrical Insulation Magazine, vol. 24, Issue: 4, pp. 17 – 25, August 2008.

[70] Z. Wu, “Conception optimale d’un entrainement electrique pour la chaine de traction d’un vehicule hybride electrique”, 21 Mars 2012.
[71] J. Donea, A. Huerta, “Finite Element Methods for Flow Problems”, WILEY publisher, 2004.
[72] D. Ishak, Z. Q. Zhu, D. Howe, “Eddy-current loss in the rotor magnets of permanent-magnet brushless machines having a fractional number of slots per pole”, IEEE Transactions on Magnetics, vol. 41, Issue: 9, pp. 2462– 2469, 2005.
[73] S. J. Salon, Finite element analysis of electrical machines, Rensselaer Polytechnic Institute Troy, New York, 1995.
[74] Dimarogonas, D. Andrew, A. Stefanos, G. Thomas, Analytical Methods in Rotor Dynamics, Second Edition, 2013.
[75] D. Staton, A. Cavagnino, Convection Heat Transfer and Flow Calculations Suitable for Electric Machines Thermal Models, IEEE transaction on industrials of electronics, vol. 55, no. 10, October 2008.
[76] G. Dajaku, D. Gerling, An Improved Lumped Parameter Thermal Model for Electrical Machines, Institute for Electrical Drives, University of Federal Defense Munich.
[77] J. Shazly, S. Wahsh, A. Yassin. Author, Thermal modeling of an AFPMSM: A review, Journal of Electrical Systems and Information Technology, vol. 2, Issue 1, May 2015, Pages 18-26.
[78] V. Behjat, A Coupled Thermal-Electromagnetic FEM Model to Characterize the Thermal Behavior of Power Transformers Damaged by Short Circuit Faults, International Journal of Electrical Energy, vol. 1, no. 4, December 2013.
[79] B. Peter, W. Thomas, Heat Transfer Basics and Practice, Springer, 2012.
[80] S. Bhattacharya, F. Eckert, V. Boyko, A. Pich, Temperature□, pH□, and Magnetic□Field□ Sensitive Hybrid, Microgels, wiley, Online Library, 22 March 2007.
[81] S. Lee ; T.G. Habetler ; R.G. Harley ; D.J. Gritter , An evaluation of model-based stator resistance estimation for induction motor stator winding temperature monitoring, IEEE Transactions on Energy Conversion, vol. 17, Issue: 1 , Mar 2002.
[82] K. Hoffmann, S. Chiang, Computational fluid dynamics volume I, fourth edition, USA.
[83] B. Weilharter, Noise Computation of Induction Machines, thesis dissertation, 31 July 2012.
[84] R. Jazar, advanced vibrations, springer, 2013.
[85] A. Saito, M. Kuroishi and H Nakai, Vibration Prediction Method of Electric Machines by using Experimental Transfer Function and Magnetostatic Finite Element Analysis, iop science, 2016.
[86] J. Stratton, Electromagnetic theory, John Wiley & Sons, INC., Publication, 2007.
[87] D. A. Ghosh, G. Ledwich, Power Quality Enhancement Using Custom Power Devices, Springer, 2002.

[88] J. Pyrhönen, T. Jokinen, Design of Rotating Electrical Machines, Wiley, second edition, 16 December 2008.

[89] C. Madache, L. Clapham, “A model for magnetic flux leakage signal prediction”, Journal of physics, volume 36, number 20, 1 October 2003.

[90] J. F. Gieras, C. Wang and J.C. Lai, “Noise of polyphaser electric motors”, Taylor & Francis Group, LLC, 2006.

[91] J. L. Besnerais, “Reduction of magnetic noise in PWM-supplied induction machines-low-noise design rules and multi-objective optimization”, Ecole Central de Lille, Lille, 2008.

[92] A. B. Proca, A. Keyhani, A. El-Antably, Wenzhe Lu and Min Dai, "Analytical model for permanent magnet motors with surface mounted magnets," IEEE Transactions on Energy Conversion, vol. 18, no. 3, pp. 386-391, Sept. 2003.

[93] A. Mohammed, S. Djurovic, Stator Winding Internal Thermal Stress Monitoring and Analysis Using in-situ FBG Sensing Technology, IEEE Transactions on Energy Conversion, p. 99, April 2018

[94] A. Saha, FPGA based self-vibration compensated two dimensional non-contact vibration measurement using 2D position sensitive detector with remote monitoring, International Measurement Confederation; Institute of Measurement and Control, Elsevier, July 2017.

[95] L. Rabiner, a tutorial on hidden markov model and selected applications in speech recognition, proceedings of the IEEE, vol. 77, no. 2, 1989.

[96] G. Fettweis, H. Meyr, Feedforward Architectures for Parallel Viterbi Decoding,
Journal of VLSI Signal Processing, vol. 3, pp. 105 – 119, June 1991.
[97] A. Heng, S. Zhang, A. Tan, Rotating machinery prognostics: State of the art, challenges and opportunities”. Mechanical Systems and Signal Processing, vol. 23, Issue: 3, pp. 724–739, April 2009.
[98] S. Haider, W. Zanardelli, S. Aviyente, Prognosis of Electrical Faults in Permanent Magnet AC Machines using the Hidden Markov Model, IECON10, November 2010.
[99] A. Mosallam, Remaining useful life estimation of critical components based on Bayesian Approaches, thesis, Université de Franche-Comté, Submitted on 8 Dec 2016.
[100] K. Medjaher, D. Tobon-Mejia, N. Zerhouni. Remaining useful life estimation of critical components with application to bearings, IEEE Transactions on Reliability, Institute of Electrical and Electronics Engineers, vol. 61, Issue: 2, pp.292-302, 2012.
[101] M. Mishra, thesis: Model-based Prognostics for Prediction of Remaining Useful Life, Luleå University of Technology, December 2015
[102] L. Gang, A Study on Remaining Useful Life Prediction for Prognostic Applications, University of New Orleans Theses and Dissertations, 2011.
[103] Z. Chen, S. Cao and Z. Mao, Remaining Useful Life Estimation of Aircraft Engines Using a Modified Similarity and Supporting Vector Machine (SVM) Approach, 23 December 2017.
[104] E. L. Brancato, Insulation aging a historical and critical review, IEEE Trans. Electr. Insul, vol EI-13, no 4, August 1978.

[105] M. Hacen, H. Kamal eddin, stochastic estimation methods for induction motor transient thermal monitoring under nonlinear condition, Leonardo journal of sciences, Issue 20, pp. 95-108, 2012.
[106] N. Lahoud, J. Faucher, D. Malec, Electrical Aging of the Insulation of Low Voltage Machines: Model definition and test with the Design of Experiments, IEEE Transactions on Industrial Electronics, Institute of Electrical and Electronics Engineers, vol. 60, pp.4147-4155, 2013.
[107] Magnetic Products Online Brochure, Sagami Chemical Metal Co., Ltd., December 20, 2013.
[108] A. Mosallam, K. Medjaher, N. Zerhouni, Data-driven prognostic method based on Bayesian approaches for direct remaining useful life prediction, Journal of Intelligent Manufacturing, Springer Verlag, Germany, pp.1-20, 2014.
[109] S. Klysz, G. Gmurkzyk, J. Lisiecki, Fatigue of Aircraft Structures, Institute of Aviation Scientific Publications, pp.52-58, Warsaw, Poland, 2010.
[110] F.M.G. Wong, Fatigue, Fracture, and Life Prediction Criteria for Composite Materials in Magnets, Plasma Fusion Center Massachusetts Institute of Technology Cambridge, MA 02139 June 1990.
[111] R. Citarella, A. Frattura, Strutturale, Coupled FEM-DBEM method to assess crack growth in magnet system of Wendelstein, vol. 26, pp. 92-103, Germany, 2013.
[112] S. Jiang, W. Zhang, X. Li, An Analytical Model for Fatigue Crack Propagation Prediction with Overload Effect, Mathematical Problems in Engineering, vol. 2014, 23 July 2014.
[113] G. Sree Lakshmi ; S. Kamakshaiah ; T. Das, Closed loop PI control of PMSM for hybrid electric vehicle using three level diode clamped inverter for optimal efficiency, IEEE, India, 2013.

[114] M. Kuang, D. Smith, F. Syed, Closed-loop power control system for hybrid electric vehicles, Ford Global Technologies LLC, 2003.

[115] H. Al-Sheikh, et al. "Condition monitoring of bidirectional dc-dc converter for hybrid electric vehicles." Control and Automation (MED), 2014 22nd Mediterranean Conference of. IEEE, 2014

[116] H. Al-Sheikh, O. Bennouna, G. Hoblos, and N. Moubayed, Al-Sheikh, Hiba, et al. ‘Modeling, design and fault analysis of bidirectional dc-dc converter for hybrid electric vehicles.’ Industrial Electronics (ISIE), IEEE 23rd International Symposium, pp. 1689–1695, 2014.

[117] H. Al-Sheikh, G. Hoblos, N. Moubayed, Study on power converters used in hybrid vehicles with monitoring and diagnostics techniques, Electrotechnical Conference (MELECON), 2014 17th IEEE Mediterranean. IEEE, 2014.

[118] H. Al-Sheikh, G. Hoblos, N. Moubayed, Power electronics interface configurations for hybrid energy storage in hybrid electric vehicles, Electrotechnical Conference (MELECON), 17th IEEE Mediterranean. IEEE, 2014.

[119] W. Runxin, J. Liu. "Redefining a new-formed average model for threephase boost rectifiers/voltage source inverters." Applied Power Electronics Conference and Exposition, 2009. APEC 2009. Twenty-Fourth Annual IEEE. IEEE, 2009.

[120] L. Zhao, H. Ma. "Modeling and analysis of three-phase inverter based on generalized state space averaging method." Industrial Electronics Society, IECON 2013-39th Annual Conference of the IEEE. IEEE, 2013.

[121] Houldsworth, John A., and Duncan A. Grant. "The use of harmonic distortion to increase the output voltage of a three-phase PWM inverter." IEEE Transactions on Industry Applications 5 (1984): 1224-1228.

[122] L. Byoung-Kuk, M. Ehsami. "A simplified functional simulation model for three-phase voltage-source inverter using switching function concept." IEEE transactions on industrial electronics, pp. 309-321, 2011.

[123] M. Sébastien, M. Morari. "Explicit model-predictive control of a PWM inverter with an LCL filter." IEEE Transactions on Industrial Electronics pp. 389-399, 2009.

[124] M. Shahinur, N. Islam Raju, A. U. Ahmed, Sinusoidal PWM signal generation technique for three phase voltage source inverter with analog circuit & simulation of PWM inverter for standalone load & micro-grid system, International Journal of Renewable Energy Research (IJRER), pp. 647-658, 2013.

[125] Z. J. Shen and I. Omura, "Power Semiconductor Devices for Hybrid, Electric, and Fuel Cell Vehicles," Proc. IEEE, vol. 95, no. 4, pp. 778–789, 2007.

[126] A. Kontarček, M. Nemec, P. Bajec, and V. Ambrožič, "Single Open-phase Fault Detection with Fault-Tolerant Control of an Inverter-fed Permanent Magnet Synchronous Machine," Autom. – J. Control. Meas. Electron. Comput. Commun., vol. 55, no. 4, pp. 474–486, 2014.

[127] H. Saidi, N. Mansour, M. Abdelhamid, Electric Vehicle Speed Control using Three Phase Inverter operated by DSP-based Space Vector Pulse Width Modulation Technique, Proceeding of the International Conference on Energy System, Environmental Entrepreneurship and Innovation, vol. 32. Dubai, 2015.

[128] A. Waheed, M. Usman, Comparative study of SVPWM (space vector pulse width modulation) & SPWM (sinusoidal pulse width modulation) based three phase voltage source inverters for variable speed drive, IOP Conference Series: Materials Science and Engineering. vol. 51. no. 1. IOP Publishing, 2013.

[129] Z. Bin, Simulation Investigation of SPWM, THIPWM and SVPWM Techniques for Three Phase Voltage Source Inverter, International Journal of Power Electronics and Drive Systems (IJPEDS) pp. 223-240.

[130] P. Tripura, Y.S Kishore Babu, and Y. R. Tagore. Space vector pulse width modulation schemes for two-level voltage source inverter, ACEEE Int. J. on control system and instrumentation pp.34-38, 2011.

[131] A. Kolli, O. Bethoux, A. De Bernardinis, E. Laboure, and G. Coquery, Space Vector PWM Control Synthesis for a H-Bridge Drive in Electric Vehicles,"IEEE Trans. Veh. Technol., vol. 62, no. 6, pp. 1–12, 2013.

[132] B. Nagl, B. Czerny, M. Lederer, G. Khatibi, M. Thoben, and J. Nicolics, Electrothermal analysis of in situ vibration measurements on IGBT modules under operation conditions, 2012 4th Electron. Syst. Technol. Conf. ESTC 2012, pp. 3–8, 2012.
[133] K. LAKSHMI, S. REHANA BEGUM, Space Vector PWM Control Synthesis for a H-Bridge Drive in Electric Vehicles, International journal of innovative technologies, vol. 4, issue 3, pp. 588-596, March 2016.
[134] X. Perpiñà, L. Navarro, X. Jordà, M. Vellvehi, J.-F. Serviere, and M. MermetGuyennet, "Reliability and lifetime prediction for IGBT modules in railway traction chains," Reliab. Saf. Railw., pp. 193–222, 2012.
[135] B. Ji, X. Song, E. Sciberras, W. Cao, Y. Hu, and V. Pickert, Multi-Objective Design of IGBT Power Modules Considering Power Cycling and Thermal Cycling, IEEE Trans. Power Electron., vol. 8993, no. c, pp. 1–1, 2014.
[136] H. Medjahed, P. E. Vidal, and B. Nogarede, Thermo-mechanical stress of bonded wires used in high power modules with alternating and direct current modes, Microelectron. Reliab., vol. 52, no. 6, pp. 1099–1104, 2012.
[137] A. Note, Thermal resistance of IGBT Modules - specification and modelling, pp. 1– 14, 2014.
[138] V. Demuth, Power modules for hybrid and electric vehicles, October, 2010.
[139] M. Ikonen, Power cycling lifetime estimation of igbt power modules based on chip temperature modeling. 2012.
[140] R. John, O. Vermesan, and R. Bayerer, High temperature power electronics IGBT modules for electrical and hybrid vehicles, IMAPS High Temp. Electron. Netw. (HiTEN 2009), October, pp. 199–204, 2009.
[141] A. Vogel, K., Ciliox, A. and Schmal, IGBT with higher operation temperature - Power density, lifetime and impact on inverter design, Pcim, pp. 1–6, 2011.
[142] V. Smet et al., Ageing and failure modes of IGBT modules in high temperature power cycling, IEEE Trans. Ind. Electron., vol. 58, no. 10, pp. 4931–4941, 2011.
[143] T. Kovaltchouk, J. Aubry, B. Multon, and H. Ben Ahmed, Influence of IGBT current 65 rating on the thermal cycling lifetime of a power electronic active rectifier in a direct wave energy converter, 2013 15th Eur. Conf. Power Electron. Appl. EPE 2013, 2013.
[145] I. F. Kovacevic and J. W. Kolar, Modelling for the Lifetime Prediction of Power Semiconductor Modules, Reliab. Power Electron. Convert. Syst., pp. 103–140, 2015.
[146] J. M. Urrea, Naval Postgraduate,"Public Policy, no. Mar, p. 89, 2006.
[147] H. Abbad et al., A first approach on the failure mechanisms of IGBT inverters for aeronautical applications: Effect of humidity-pressure combination, 2010 Int. Power Electron. Conf. - ECCE Asia -, IPEC 2010, pp. 2450–2456, 2010.
[148] B. Czerny, M. Lederer, B. Nagl, A. Trnka, G. Khatibi, and M. Thoben, Thermo-mechanical analysis of bonding wires in IGBT modules under operating conditions, Microelectron. Reliab., vol. 52, no. 9–10, pp. 2353–2357, 2012.
[149] G. Khatibi, M. Lederer, B. Weiss, T. Licht, J. Bernardi, and H. Danninger, Accelerated mechanical fatigue testing and lifetime of interconnects in microelectronics, Procedia Eng., vol. 2, no. 1, pp. 511–519, 2010.
[150] M. T. B. Czerny", B. Naglb, M. Lederera, A. Trnkac, G. Khatibia, In situ vibration measurements on power modules under operating conditions, pp. 219–232, 2010.
[151] A. Nishiura, S. Soyano, and A. Morozumi, IGBT Modules for Electric Hybrid Vehicles, Fuji Electr. Rev., vol. 53, no. 3, pp. 65–69, 2007.

[152] W. C. B. Ji V. Pickert and B. Zahawi, In-Situ Diagnostics and Prognostics of Wire Bonding Faults in IGBT Modules forElectric Vehicle Drives, IEEE Trans. Power Electron. vol. 28, no. 12, pp. 5568-5577, pp. 1–10, 2013.
[153] K. Sasaki and N. Ohno, Fatigue life evaluation of aluminum bonding wire in silicone gel under random vibration testing, Microelectron. Reliab., vol. 53, no. 9–11, pp. 1766–1770, 2013.
[154] Grunditz, Emma. Design and assessment of battery electric vehicle powertrain, with respect to performance, energy consumption and electric motor thermal capability. Chalmers University of Technology, 2016.
[155] Thoben, M., et al. From vehicle drive cycle to reliability testing of power modules for hybrid vehicle inverter. PCIM Europe. 2008.
[156] "http://www.vibrationresearch.com/university/random-rms-calculator/.".
[157] F. B. Chaaban, R. Chedid, and R. Ginzarly, Impacts of Machine Configurations on the Penetration Rates of Small- Scale Wind Power Units 1- Introduction 2- Machine Configurations, no. April, pp. 1–9, 2013.
[158] S. C. Kim, Thermal performance of motor and inverter in an integrated starter generator system for a hybrid electric vehicle, Energies, vol. 6, no. 11, pp. 6102–6119, 2013.
[159] R. Ginzarly, G. Hoblos, and N. Moubayed, Faults in hybrid electric vehicles' permanent magnet machines, 2015 Third Int. Conf. Technol. Adv. Electr. Electron. Comput. Eng., pp. 169–174, 2015.
[160] M. Abul Masrur, Z. Chen, and Y. Murphey, Intelligent diagnosis of open and short circuit faults in electric drive inverters for real-time applications, IET Power Electron., vol. 3, no. 2, p. 279, 2010.
[161] M. B. B. Sharifian, T. Herizchi, and K. G. Firouzjah, Field oriented control of permanent magnet synchronous motor using predictive space vector modulation, Ind. Electron. Appl. 2009. ISIEA 2009. IEEE Symp., vol. 2, no. Isiea, pp. 574–579, 2009.
[162] D. Swierczynski and M. P. Kazmierkowski, Direct torque control of permanent magnet synchronous motor (PMSM) using space vector modulation (DTC-SVM)-simulation and experimental results, IEEE 28th Annual Conference of the Industrial Electronics Society. IECON 02, 2002.
[163] G. Sree Lakshmi, S. Kamakshaiah, T. Ram Das, Closed loop PI control of PMSM for hybrid electric vehicle using three level diode clamped inverter for optimal efficiency, International Conference on Energy Efficient Technologies for Sustainability, Nagercoil, India, 2013.
[164] M. Kuang, D. Smith, F. Syed, Closed-loop power control system for hybrid electric vehicles, Ford Global Technologies LLC, 2003.
[165] S. E. Levinson, L.R. Rabiner, M. M. Sondhi, an introduction to the application of the theory of probabilistic functions of a Markov process to automatic speech recognition, the bell system technical journal, vol. 62, no. 4, April 1983.
[166] B. Esmael, A. Arnaout, G. Thonhauser, A statistical feature-based approach for operations recognition in drilling time series, International Journal of Computer Information Systems and Industrial Management Applications, vol. 5, pp. 454-461, 2013.
[167] K. Alameh, N. Cité, G. Hoblos, and G. Barakat, "Feature extraction for vibration-based fault detection in Permanent Magnet Synchronous Motors," in Third International Conference on Technological Advances in Electrical, Electronics and Computer Engineering-TAEECE, 2015, pp. 163–168.

[168] K. Alameh, R. Ginzarly, G. Hoblos, and G. Barakat, “Modeling Approach and Fault Index Analysis of a Voltage-Source Brushless DC Motor,” in 3rd International Conference on Control and Fault-Tolerant Systems-SysTol’16, 2016.
[169] J. Antoni and M. Sidahmed, “Contrôle et diagnostic à partir des signaux acoustiques et vibratoires,” Acoust. Tech., vol. 38, pp. 9–15, 2004.
[170] D. Crombez, “Analyse de signaux vibratoires pour le diagnostic de défauts : Application sur les boîtes de vitesses automobiles,” Université de Rouen, 2011.
[171] D. Augeix, “Analyse vibratoire des machines tournantes,” 2013.
[172] “Spectral Estimation,” http://www.mathworks.com/help/signal/nonparametric-spectral-estimation.html.
[173] G. Cybenko, V. Crespi, Learning Hidden Markov Models using Non-Negative Matrix Factorization, IEEE transactions on information theory, September 2008.
[174] D. Ramage, Hidden Markov Models Fundamentals, December 2007.
[175] K. Katta, Design of Convolutional Encoder and Viterbi Decoder using MATLAB, international Journal for research in emerging science and technology, volume 1, issue 7, December 2014.
[176] G. W. Slade, The Viterbi algorithm demystified, January 2014.
[177] Z. Ghahramani, an introduction to Hidden Markov Models and Bayesian networks, international journal of pattern recognition and artificial intelligence, volume 15, pp 9-42, 2001.
[178] M. A. Djeziri, S. Benmoussa, M. Benbouzid. "Data-driven approach augmented in simulation for robust fault prognosis . " Engineering Applications of Artificial Intelligence 86 (2019) 154–164.
[179] M. A. Djeziri, S. Benmoussa, R. Sanshez. "Hybrid method for remaining useful life prediction in wind turbine systems. " Renewable Energy (2018). Renewable Energy. V. 116. pp. 173-187.
[180] S. Benmoussa, M. A. Djeziri . "Remaining Useful Life estimation without needing for prior knowledge of the degradation features . " IEEE IET Science, Measurement & Technology (2017). V. 11(8), pp. 1071-1078.
[181] L. Nguyen, M. A. Djeziri, B. Ananou, M. Ouladsine, J. Pinaton. "Fault prognosis for batch production based on percentile measure andgamma process: Application to semiconductor manufacturing". in Journal of Process Control, Vol.48. pp. 72-80 (2016).

Abstract: The core of the work is to build an accurate model of the electrical machine where the prognostic technique is applied. In this thesis we started by a literature review on hybrid electric vehicles (HEV), the different types of electrical machine used in HEV's and the different types of faults that may occur in those electrical machine. We also identify the useful monitoring parameters that are beneficial for those different types of faults. Then, a survey is presented where all the prognostic techniques that can be applied on this application are enumerated.

The electromagnetic, thermal and vibration finite element model (FEM) of the permanent magnet machine is presented. The model is built at healthy operation and when a fault is integrated. The considered types of faults are: demagnetization, turn to turn short circuit and eccentricity. A confrontation between analytical and FEM (numerical method) for electromagnetic machine modeling is illustrated. Fault indicators where useful measured parameters for fault identification are recognized and useful features from the measured parameters are extracted; torque, temperature and vibration signal are elaborated for healthy and faulty states.

The strategy of the adopted prognostic approach which is Hidden Markov Model (HMM) is explained. The technical aspect of the method is presented and the prognostic model is formulated. HMM is applied to detect and localize small scale fault small scale faults were where a systematic strategy is developed. The aging of the machine's equipment, specially the sensitive ones that are the stator coil's and the permanent magnet, is a very important matter for RUL calculation. An estimation strategy for RUL calculation is presented and discussed for those mentioned machine's components.

Closed loop configuration is very important; it is adopted by all available vehicle systems. Hence, the same previously mentioned steps are applied for a closed loop configuration too. A global model where the input of the machine's FEM comes from the modeled inverter is built.

Keywords: Hybrid electric vehicle, electrical machine, permanent magnet machine, finite element model, prognosis, hidden Markov model, remaining useful life, demagnetization, turn to turn short circuit, eccentricity.

Résumé : L'objectif de ce travail est d'élaborer un modèle performant/précis de la machine électrique permettant de proposer une technique de pronostic. Dans cette thèse, nous commençons par un état de l'art sur les véhicules électriques hybrides (VHE), les différents types de machines électriques utilisées dans les VHE ainsi que les différents types de défauts pouvant survenir dans ces machines électriques. Nous identifions également les indicateurs de défauts appropriés aux différents défauts considérés. Ensuite, une synthèse de techniques de pronostic pouvant être appliquées est proposée.

Le modèle à éléments finis électromagnétiques, thermiques et vibratoires (FEM) de la machine à aimants permanents est présenté. Le modèle est élaboré en fonctionnement normal et défaillant. Les types de défauts considérés sont : démagnétisation, court-circuit et excentricité. Une comparaison entre les deux approches analytique et FEM (méthode numérique) pour la modélisation de machines électromagnétiques est effectuée.

Les indicateurs de défauts analysés pour l'extraction les plus pertinents utilisent les différents signaux mesurées suivants : le couple, la température ainsi que les signaux vibratoires en états sains et défectueux.

L'approche de pronostic adoptée qui est le modèle de Markov caché (HMM) est développée. L'aspect technique de la méthode est présenté et le module du pronostic est formulé. La méthode de HMM est utilisée pour détecter et localiser les défauts à petites amplitudes. Une stratégie systématique a été développée. Le vieillissement de l'équipement de la machine, en particulier des éléments sensibles comme la bobine de stator et l'aimant permanent, est une question très importante pour le calcul du RUL (Remaining Useful Life). Une stratégie d'estimation pour le calcul RUL est présentée et discutée.

La configuration en boucle fermée est très importante. Elle est adoptée par tous les systèmes de véhicules disponibles. Par conséquent, les mêmes étapes mentionnées précédemment s'appliquent également à une configuration en boucle fermée. Un modèle global où l'entrée du FEM de la machine provient de l'onduleur modélisé est élaboré.

Mots-clés : Véhicule électrique hybride, machine électrique, machine à aimants permanents, modèle à éléments finis, pronostic, modèle de Markov caché, durée de vie restante, démagnétisation, court-circuit, excentricité.